Southward propagation of the Marlborough Fault System: Fault linkage and blind faults in North Canterbury

A thesis submitted in partial fulfilment of the requirements for the Degree

of Master of Science in Geology

in the University of Canterbury

by Jana Mittelstaedt

University of Canterbury

2011

Contents

Acknowledgments

I would like to express my gratitude to all those who gave me the possibility to complete this thesis. I want to thank the Department of Geology of the University of Canterbury for giving me permission to commence this thesis in the first instance, to do the necessary research work and to use departmental ressources. Furthermore I thank the Mason Trust for funding over the first year of my thesis making my many field trips possible and affordable.

I am deeply indebted to my supervisor Dr. Mark Quigley whose help, stimulating suggestions and encouragement from the initial to the final level enabled me to develop an understanding of the subject and finish my thesis. I would like to thank Dr. David Nobes for helping me out with my seismics work and Dr. Michael O'Neal from the University of Delaware for accompanying me in the field and mind opening discussions. I further like to thank Nicky Whitehouse and her team, especially Craig Woodward, for letting me use their Hawdon core data and help me with understanding of the core.

I am indebted to my many colleagues in the research group and beyond who supported me and where always willing to help me out and discuss my thesis with me. I am grateful to Tim Stahl and Sam McColl who in various instances reviewed my work and thus made it so much better. I also thank Duncan Noble and Sharon Hornblow for conducting field surveys when I was unable to go into the field myself.

I would like to show my gratitude to the landowners from the Mt White Station, Craigieburn and Flock Hill who gave me access to their land in order for me to complete my fieldwork and who were generally helpful.

This thesis would not have been possible without the support of my friends and family who always believed that I would do the best I can. Special thanks go to my husband Gerd who followed me here to New Zealand so I could advance my career and live my dream and lastly, my son, Fabian, who despite messing up my entire time plan (in cooperation with a couple of interruptive earthquakes) always managed to put a smile on my face.

Abstract

Geomorphological and paleoseismic studies provide insight into the fault geometry and kinematics of a series of dextral northeast striking faults, including the Porters Pass, Hawdon, Bullock Hill, and Esk faults, in the South Island of New Zealand. These faults show post-glacial offsets that are significantly larger than predicted from co-seismic displacement - surface rupture length regressions derived from empirical relationships. Geomorphological mapping reveals slip rates as high as 9 mm/year for the Hawdon fault and Bullock Hill fault over an expected fault length of c. 140 km. Surface expressions of some parts of the studied faults are obscured by glacial gravels, indicating that blind faults are present in parts of the Sourthern Alps and may be the source for a component of a reported slip deficit in North Canterbury. Concluding from comparing scaling relationship results for the individual faults I hypothesize that the Porters Pass, Hawdon, Bullock Hill and Esk faults are segments of an incipient fault system that stretches from the western tip of the Porters Pass fault to the Hope fault, east of Hanmer Springs. Considering the location, similar strike and dextral deformation mode, I suggest that this 140 km long dextral strike-slip fault system marks the southernmost extension of the Marlborough Fault System resulting from the ongoing southward propagation of the Pacific-Australian plate boundary in New Zealand's South Island.

1. Introduction

1.1 Thesis background

Large faults often evolve through linkage between smaller fault segments that strike similarly and rupture coseismically (Cartwright et al., 1995, Dawers & Anders, 1995). Segment lengthening can result in the coalescence of small separate segments at their tips and the formation of a larger fault. During this process the whole fault system can deform as if it were one single large fault with slip being partitioned among the different sections of the fault (Dawers & Anders, 1995). Examples of incipient faults that show fault linkage can be found in the Wasatch and Hurricane Fault Zones of the Basin and Range Province in the U.S. (e.g. Cartwright et al., 1995, Dawers & Anders, 1995), in the Statfjord East fault zone, northern North Sea (e.g. Gupta et al., 1998), and in North Canterbury, New Zealand (Fig. 1.1), where the deformation along the plate boundary is propagating southwards (e.g. Cowan et al., 1996, Walcott, 1998, Wallace et al., 2007, Wannamaker et al., 2009).

Studies of GPS and seismological data (Wallace et al., 2007) have revealed a slip deficit in North Canterbury with the estimated slip rate about two to three times higher than that shown by existing geological data. Most of the fault-slip is thought to occur in the Porters Pass Amberley Fault Zone (PPAFZ), which has been recognized by Cowan et al. (1996) as the southernmost extension of the dextral strike-slip Marlborough Fault System (MFS; Fig. 1.1). The PPAFZ does not exhibit a through-going fault trace but consists instead of a number of subparallel individual fault segments that total to a length of min. 32 km and max. 90 km (Howard et al., 2005). Based on scaling relationships from Wells & Coppersmith (1994), however, the measured coseismic offsets correlate to a fault length of 100-140 km (Howard et al., 2005) which may suggest that the PPAFZ is part of a larger fault zone. The observed slip deficit may be accounted for in hitherto undetected and unstudied faults in North Canterbury (Wallace et al., 2007).

In this thesis a number of smaller NE striking strike-slip faults in the vicinity of the southern Esk fault that may be an extension of the PPAFZ are examined. These faults, even more so than the PPAFZ, exhibit displacements that require significantly longer rupture lengths than inferred from surface rupture lengths. A second observation is that, in some places, these faults are inferred to pass through glacial outwash and till without any surface expression, which is interpreted to reflect refractive dissipation of seismic energy in the unconsolidated sediment. This indicates that some fault systems have "blind fault" segments. The short lengths of these faults and the blind nature of some sections may be why they have remained relatively unstudied prior to this investigation. Following closer analysis, these faults may account for the fault slip deficit in North Canterbury revealed in comparisons of geologic with GPS data (Wallace et al., 2007) as well as link up with the PPAFZ to form a major fault of the same scale as the MFS faults. I suggest that, contrary to existing interpretations, most fault-slip deformation in North Canterbury does not occur at the tip of the PPAFZ but further north-east in the centre of this

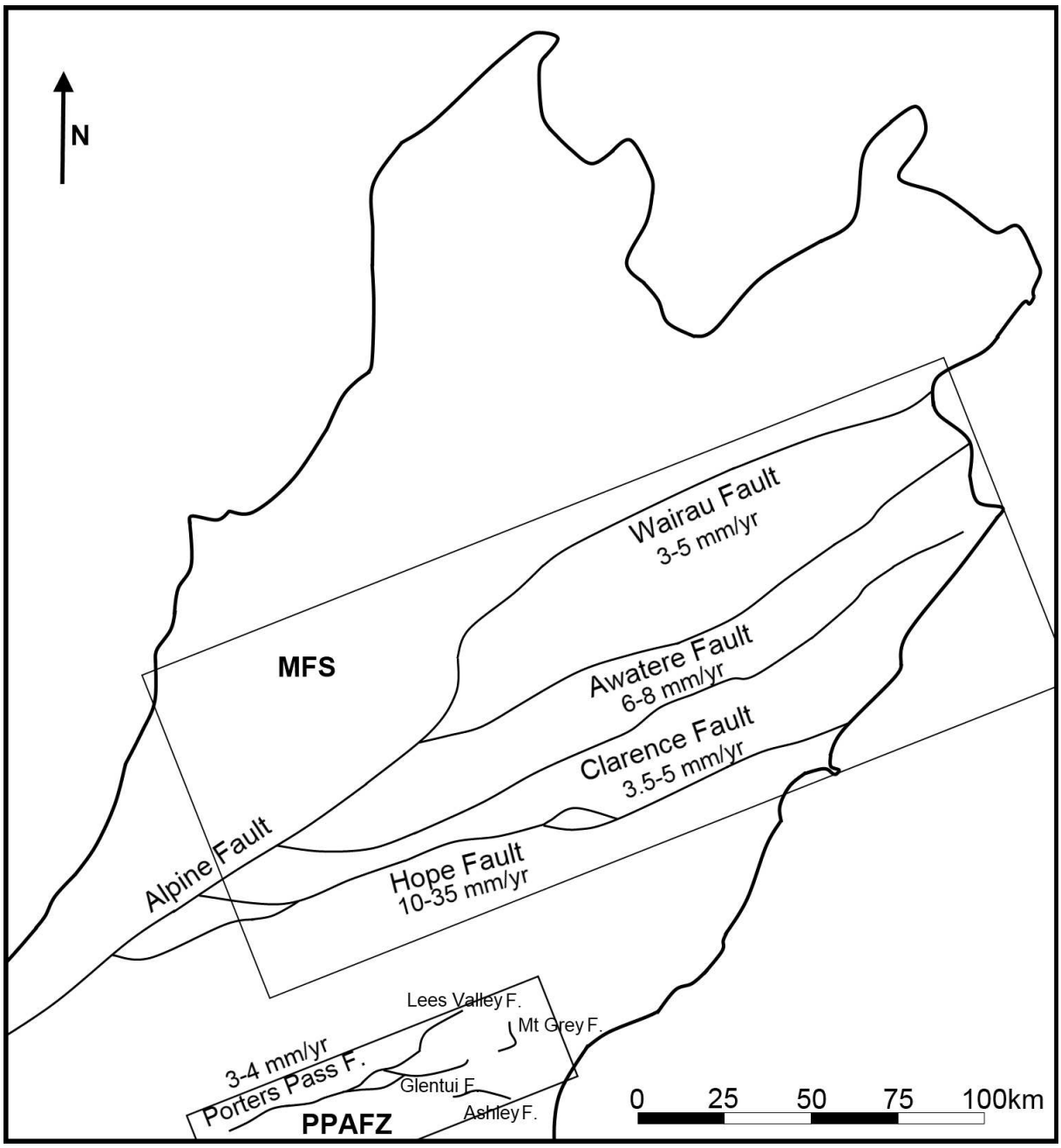

Figure 1.1.: Map view of the Marlborough Fault System (MFS) and the Porters Pass Amberley Fault Zone (PPAFZ) as mapped by Rattenbury et al. (1998), Begg & Johnston (2000), Nathan et al. (2002), Rattenbury et al. (2006), Cox & Barrell (2007), and Forsyth et al. (2008).

incipient fault system along the Hawdon and Bullock Hill faults. The study area includes the epicentre of the 1995 Cass M 6.2 earthquake (Gledhill et al., 2000).

1.2 Thesis scope and objectives

The rupture of the previously unknown Greendale fault on 4th September 2010 and the following aftershock sequence that uncovered further faults (Quigley et al., 2010) turned new attention to blind faults in the Canterbury region. Ten years prior Pettinga et al. (2001) divided the Canterbury region into nine domains ranging from strike-slip faulting to thrust faulting with only a couple of resolved and sufficiently studied faults. Pettinga et al. (2001) indicated that

the postglacial gravels covering the Canterbury Plains hid a number of blind faults which had the potential of causing major earthquakes as seen in the Darfield Earthquake (Quigley et al., 2010). Some recognized faults such as the Esk fault in North Canterbury were also understudied (Pettinga et al., 2001) despite contributing to regional seismic hazard.

On 24th November, 1995 an earthquake M_W 6.2 occurred in Cass, rupturing near the Esk fault, but could not be related to a known fault plane (Gledhill et al., 2000). Gledhill et al. (2000) reported an aftershock sequence rupturing along a NE-SW band, which followed the trend of the strike-slip faults to the south in the PPAFZ, although the focal mechanism of the mainshock was an oblique reverse one lying in the thrust wedge of domain 2 (Pettinga et al., 2001). An event of this size is indicative of an approximately 10 km long fault, moving 0.5-0.7 m and terminating within a few km on the surface (Stirling et al., 2008).

The objectives of this thesis are:

1. Recognition of active faults through detailed geological, structural and geomorphological field mapping.

2. Paleoseismic investigation of known and newly found faults in the field area to resolve postglacial activity.

3. Formulating the seismic hazard these faults pose to the Canterbury region.

4. Implications for the further tectonic and geomorphic development of the North Canterbury geology.

1.3 Methods

The field area is included in a series of maps (i.e. Gregg, 1964, Gage, 1970, Forsyth et al., 2008) that vary in their interpretation of the area. Therefore, detailed geological, structural, and geomorphological mapping in a high resolution of up 1:25000 was conducted in this study between 2010-2011. The aim of the mapping is to document the spatial extent of the geological structures and depict the Quaternary deformation. The map is then compiled and prepared for follow-up analysis in the georeferencing program ArcGIS. Particular sections are reprocessed in a simple picture editing program for visualisation.

The field mapping is complimented by surveying methods, such as real time kinematic satellite navigation (RTK) and ground penetrating radar (GPR) surveys that have been run over small fault sections. RTK resolves the surface elevation variations to centimeter-scale accuracy with the use of a base station, while GPR uses electromagnetic radiation to detect reflective surfaces underground. Additional measurements with the Laser Range Finder as an electronic distance metre (EDM) help defining displacements of geomorphic and geological structures.

To resolve fault activity and timing of last movement, optically stimulated luminescence (OSL) dating is used. For more general observations this study resorts to weathering rind dates reported by Fitzsimons (1997).

The geomorphology of an area provides valuable information on the activity of faults, be it distinctive displacement of geomorphic features or modification of a geomorphic landform that indicates tectonic activity, such as coseismic landslides, backtilting of terraces, or knickpoints in stream profiles. This information can even lead to the recognition of otherwise blind faults as

done by Litchfield et al. (2003) since the effects of a fault on the landscape are often much wider than the fault zone. A digital analysis in ArcGIS of all rivers and streams in the field area is conducted following the approach of Litchfield et al. (2003) to examine stream sinuosity indices and stream gradient indices for irregularities such as knick points.

Lastly logic trees are used where field data is not sufficient to establish faulting parameters or a range of scenarios is possible. Logic trees have been used in previous studies in NZ (e.g. Berryman et al., 2002), and use a weighing scheme to sample several choices of source parameters, demonstrating alternative scenerios and the related uncertainties, which are graphically depicted.

1.4 Characteristics of the study area

The study area extends from the Broken River in the South to Mt Binser in the North and Lake Pearson in the West to the Puketeraki Range in the East, encompassing the course of the Slovens Stream as well as parts of the Waimakariri, Poulter, and Esk Rivers (Fig. 1.2). The Esk fault lies along the east border of the study area, while the west part accommodates four smaller faults. Elevation ranges from 400 m in the river beds to 1680 m at the top of Purple Hill. While most of the study area is made of bedrock hills and glacial outwash plains, it also includes a variety of landmarks such as the Lakes Hawdon, Marymere, and Blackwater, bedrock and alluvial rivers, alluvial fans, terraces, landslides and swamps.

Most of the plains are used for pastures that provide good access on farm roads and sheep tracks with a 4WD vehicle. East of the Waimakariri and Esk River and north of the field area, however, access is limited. The Cass field station lies in the north-west of the field area and was used as the base station for the conducted field work.

1.5 Regional Geology

1.5.1 The Marlborough Fault System

The convergence component of transpressional deformation along the New Zealand plate boundary increased at ∼6.4 Ma (Walcott, 1998). Since then 90 km of shortening and 230 km of dextral strike-slip resulting from differential Australia-Pacific plate motions has been accommodated on the South Island (Walcott, 1998)). The Marlborough Fault System is a dextral strike-slip system that transfers oblique plate motion between the Alpine fault and the Hikurangi subduction zone (Fig. 1.1). The system consists of four mature NE striking faults (Wairau, Awatere, Clarence, and Hope fault) and an incipient fifth fault further to the south (PPAFZ). Deformation has propagated southward during the Quaternary as shown by the initiation age of faults within the MFS. The Awatere fault initiated between 5.5-6.2 Ma (Little & Jones, 1998), the Clarence fault at ∼3 Ma (Browne, 1992) and the Hope fault at ∼1 Ma (Wood et al., 1994), while the PPAFZ is just at the beginning of its formation (Cowan et al., 1996). The temporal relationships amongst fault "initiation" ages suggest that a "new" fault system initiates every 1.4-1.9 Ma further south (Wallace et al., 2007), although this is most probably a continuously southward evolving system of successive fault growth and maturity. While the Wairau, Awatere and Clarence faults display slip rates of ∼3-8 mm/year (e.g. Campbell, 1973, Little et al., 1998, van Dissen & Nicol, 1998) the Hope fault slips from 10-14 mm/year to as much as 11-35 mm/year on its various segments (e.g. Cowan, 1990, Knuepfer, 1992, van

Figure 1.2.: Map view of the study area including topography and landmarks. (43°03'S 171°47'E / 43°12'S 172°01'E)

Dissen et al., 2003) showing a progressive southward increase in slip rates. The Porters Pass fault has a Holocene slip rate of up to 3-4 mm/year (Howard et al., 2005).

At the current stage of deformation the zone between the Hope fault and the PPAFZ is a transition zone from oblique subduction to oblique continental collision with north-east trending hybrid strike-slip and thrust faulting (Pettinga et al., 2001). The major thrust faults, the Harper and Esk faults, are located slightly to the north-west of the strike-slip faults such as the Porters Pass and Torlesse faults and have not been studied in detail to assess their activity. Paleoseismicity and historical earthquakes show that North Canterbury is subject to intense deformation with the latest M>7 earthquake occurring on September, 4th, 2010 near Darfield (Quigley et al., 2010).

1.5.2 The Porters Pass fault

The Porters Pass Amberley Fault Zone is the deformation front of the subduction zone and has been thoroughly studied by Cowan et al. (1996) and Howard et al. (2005). A review of the Porters Pass fault is necessary in order to compare it to the faults in this thesis.

The PPAFZ extends from the Porters Pass fault in the west to a fold and thrust belt near the town of Amberley (Fig. 1.1), encompassing other segments such as the Lees Valley fault, Mt Grey fault, Cust anticline, Ashley fault and may even extend offshore to the Pegasus Bay fault zone (Cowan et al., 1996). All of these show evidence of Holocene deformation. The reverse Lees Valley fault shows 6 m high scarps on Holocene alluvial fans (Cowan et al., 1996). The Mt Grey fault is a oblique left-lateral tear fault that has ruptured twice in the last 2500 years (Cowan et al., 1996). The Ashley fault is a thrust fault with a minor dextral component, has a surface trace length of 4.5 km, and has ruptured at least twice since the formation of a late Pleistocene aggradation surface (Cowan et al., 1996).

The Porters Pass fault strikes between 058° and 098°, dipping steeply towards the south or north at 60-80° and featuring a scarp that is consistently up-hill facing (Howard et al., 2005). The fault extends from Lake Coleridge in the South to Mt Oxford in the North and has accumulated a total right-lateral offset of ∼2 km. Howard et al. (2005) identified six Holocene age earthquakes with a displacement of 5-7 m/event along the 40 km long discontinuous trace. These events were dated at 8400-9000 years BP, 5700-6700 years BP, 4500-6000 years BP, 2300-2500 years BP, 800-1100 years BP, and 500-600 years BP, producing a recurrence interval of roughly 1500 years. The slip rate of the fault is 3.2-4.1 mm/year on the eastern end and 0.3-0.9 mm/year on the western end, where the fault terminates against the NW striking Redcliffe fault (Howard et al., 2005). However, Wallace et al. (2007) argue that the PPAFZ could slip at as much as 6-8 mm/year or more according to the GPS data and Howard et al. (2005) note that the Porters Pass fault has a relatively short rupture length for its slip. The required length of the Porters Pass fault would be between 100-140 km based on regressions from Wells & Coppersmith (1994) that Howard et al. (2005) used for their estimation, but the fault can only be traced clearly for ∼40 km and the PPAFZ extends up to a maximum of 90 km.

1.5.3 The Waimakariri Valley

The geology and in particular the glaciology of the Waimakariri Valley was studied by Maxwell Gage throughout the 50s and 60s (i.e. Gage, 1958, Gage & Suggate, 1958, Gage, 1970). Further mapping projects include Gregg (1964) and the QMAP team in the last decade (Forsyth et al., 2008).

The geologic history of the Waimakariri Valley is one of transgression and regression, orogeny and glacial advances. The Esk fault is a prominent feature, which runs along the base of the Puketeraki Range starting at the tip of the Torlesse Fault. It is known to have been active during the Kaikoura orogeny, but its initiation is thought to be earlier than that, due to older pre-Kaikoura rocks being more deformed than younger rocks (Gage, 1970). Most of the field area is covered in massive, well indurated, strongly jointed greywacke of the Torlesse Group (T, Fig. 1.3A) dating back to the Triassic. The Tertiary rocks are exposed along the Broken River and Slovens Stream as well as at the south bank opposite the Esk River mouth. The Torlesse is unconformably overlain by the Late Cretaceous Broken River Coal Measures (B).

The Coal Measures are unevenly stratified, current-bedded, white quartz sandstones and dark grey, carbonaceous silt and sandstone with lensoid beds of coal (Gage, 1970). Between the Late Cretaceous and the Eocene the highly glauconitic sandstones of the Iron Creek Greensand Formation (I) as the inland continuation of the Waipara Greensand in North Canterbury were deposited (Gage, 1970). The Iron Creek Greensands are apparently conformable to the lower Coal Measures and the upper Porter Group. The lower half of the Greensand is composed of a massive, medium to coarse grained, green, grey, glauconitic quartz sandstone while the upper half is made of medium to fine grained, current-bedded glauconitic sandstone with prominent bands of dark greensand. In the Early Oligocene strongly jointed, moderately indurated, argillaceous limestone of the Puffer Formation (Pp) with noticeable quartz grains and glauconite was deposited (Fig. 1.3B), conformably overlain by the Thomas Formation (Pt) in the Late Oligocene (Gage, 1970). Basaltic eruptions occurred in the Mid Oligocene (Gage, 1970) and the Thomas Formation at Slovens Stream was close enough to the eruptive centres that no limestone deposition like elsewhere in the formation has occurred here. Instead coarse, poorly sorted, strongly current bedded, basaltic tuffs alternate with evenly bedded, finely laminated, greenish sands (Fig. 1.3C).

The Kaikoura Orogeny started in the Mid-Miocene followed by a regression facilitated by climate cooling and sea level drop in the early Pliocene (Gage, 1970). The Enys Formation (E) shows marine blue-grey silts grading into non-marine greenisch clays and sands at one point being eroded into a miniaturebadlands (Fig. 1.3D). The transgression was followed by the glacial advances of the Pleistocene, with thick moraines and extensive outwash plains covering the planar lower portions of the field area (Fig. 1.3E). A few glacial lake beds can be seen at the Esk River mouth and the Slovens Stream/Puffer Stream conjunction. The most recent deposits are of Holocene age and feature mostly river gravels and graded river beds (Fig. 1.3F).

1.6 Glacial History

The Waimakariri Valley has been covered by glaciers several times beginning in the Pliocene (Table 1.1, Fig. 1.4). Today remnants of the Avoca, Otarama, Blackwater and Poulter advances can be found. Ages (Table. 1.1) for the advances have been constrained by radiocarbon and weathering rinds dating thoughout the years and compiled by Fitzsimons (1997).

The Avoca Glaciation covered the whole of the Waimakariri Valley bound by the Puketeraki and Torlesse ranges (Gage, 1958). It is exposed at the Slovens Stream and Puffer Stream junction as thinly bedded silt under gravel outwash from the Blackwater II advance. The Otarama advance is exposed at the western base of Mt Rosa, reaching less than 300m (Gage,

Stage	**Glacial Advances**	**Age (ka)**
Aranuian Interglacial	Poulter	9.7±0.9 - 12.0±1.1
Otiran Glacial Stage	Blackwater III	18.4±1.8
	Blackwater II	21 - 23.3
	Blackwater I	29±8.9
	Otarama	56 - 70
Waimangau Glacial Stage	Avoca	ca. 128 - 300

Table 1.1.: Ages of the glacial advances in the Waimakariri Valley. Dates after Fitzsimons (1997).

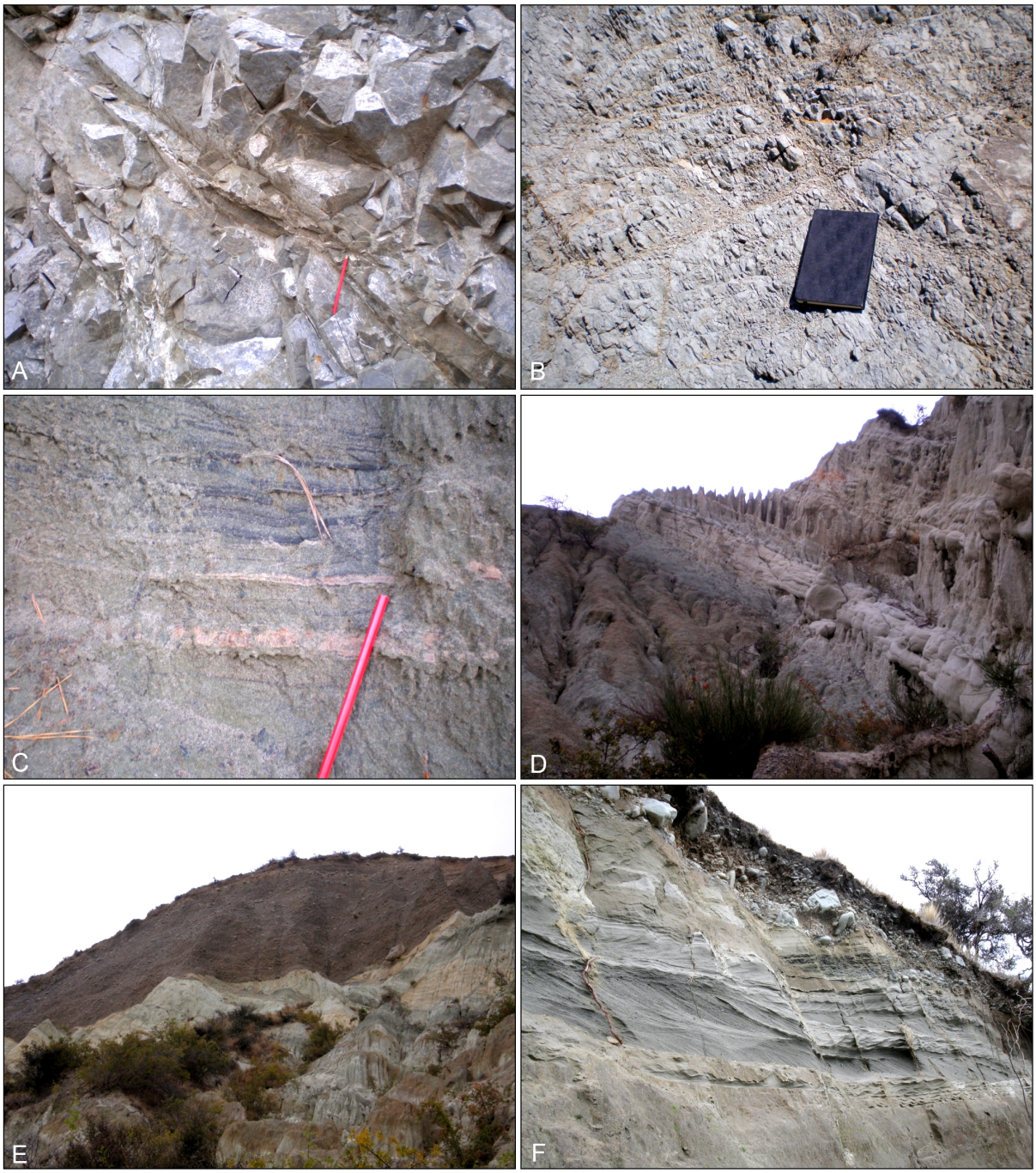

Figure 1.3.: Lithologies of the field area.(A) Greywacke of the Torlesse Group. (B) Limestone beds of the Puffer Formation. (C) Fine laminated sandstone of the Thomas Formation. (D) Eroded clays and sands of the Enys Formation. (E) Pleistocene till beds overlying the Enys Formation. (F) Holocene river sediments.

1958).

Three Blackwater advances followed, Blackwater I at 29±8.9ka, Blackwater II between 21 and 23.3ka, and Blackwater III at 18.4±1.8 with short interglacial periods (Fitzsimons, 1997). During the Blackwater advances the Waimakariri glacier completely filled the Waimakariri trough, flowing onto a broad terrace on the south bank of the Waimakariri River and depositing an extensive moraine on the north bank between Whale Hill and Mt White (Fig. 1.4). The moraines submerged the Og-Gog-Magog ridge and filled into the flat open floor of the upper part or the Slovens Creek, extending until the junction of Puffers Stream and Slovens Stream (Speight,

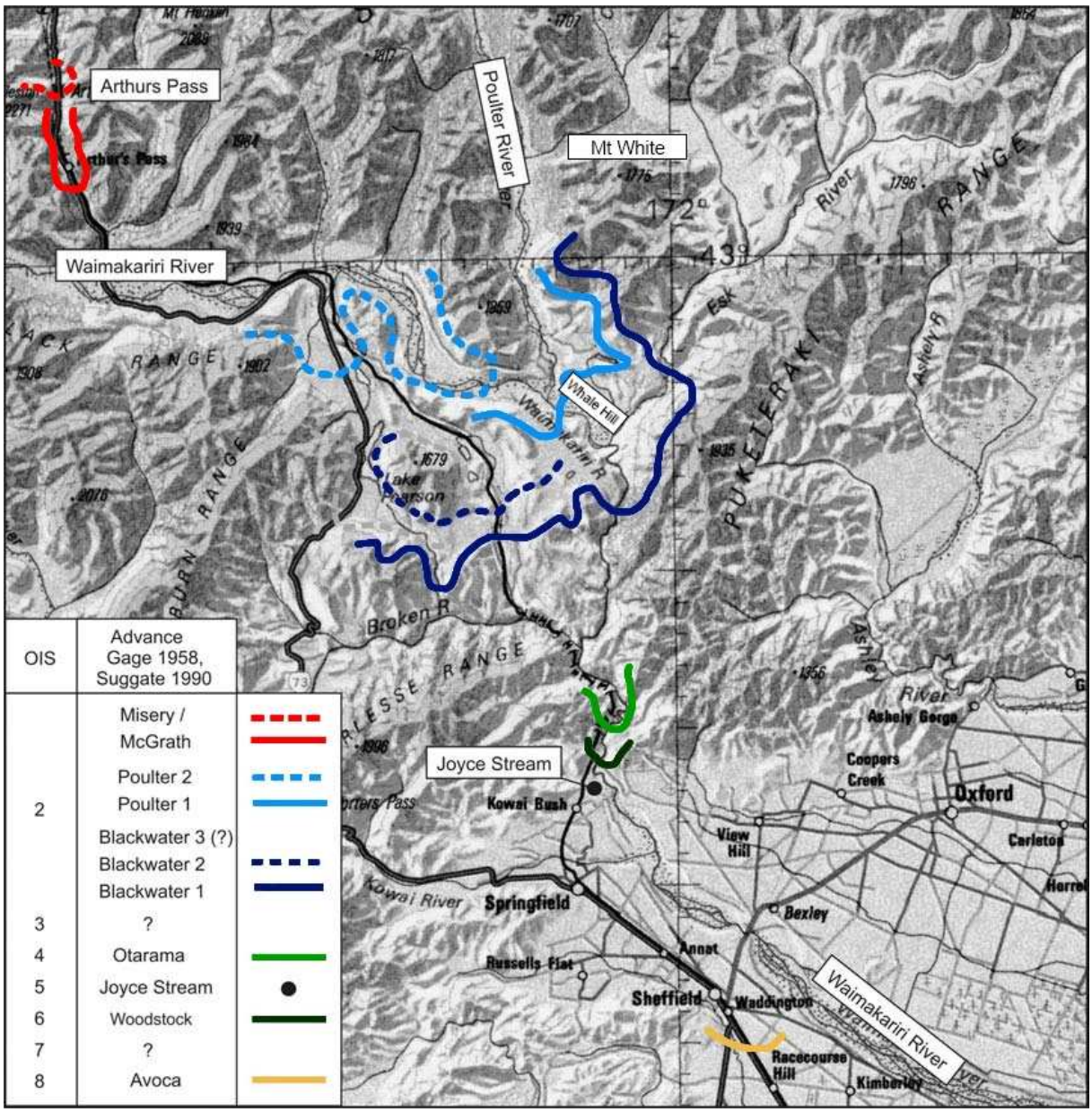

Figure 1.4.: A map showing the extent of the various glacier advances described in Gage (1958), Suggate (1990) and Fitzsimons (1997) after Rother (2006). (42°54'S 171°33'E / 43°27'S 172°14'E)

1938, Gage, 1958). When the ice retreated upstream, lakes formed at the Esk River and Slovens Stream mouths as seen by the exposure of varved silts, implying that the way downstream must have been blocked and the Puketeraki gorge only partly cut at that time. During the recession of the Blackwater advance Lake Hawdon formed between Mt St Bernard in the west and a low ridge in the east providing accommodation space (Moar, 1971). The Blackwater Lake and Lake Marymere are the largest of a number of kettle holes (Gage, 1958).

The Poulter advances between 9.7±0.9 and 12.0±1.1 ka BP (Fitzsimons, 1997) did not extend over the ridge of Og, Gog, and Magog, although the ice surface rose high enough in the adjacent Waimakariri valley to shed surface and melt water into the Slovens Stream valley (Gage, 1958). The Poulter moraine is exposed on the north and south bank of the Waimakariri River at the Poulter River mouth, near the bases of Mt Binser and the Bullock Hill respectively (Speight, 1938). The Poulter outwash is less abundant than that from earlier advances, implying a rapid

ice advance of short duration (Gage, 1958).

1.7 Vegetational History

Glacial retreat from the Blackwater advances caused a tundra-like grassland-shrubland with minor forest patches to establish in the region at 17,000 years BP (McGlone et al., 2004). After the Antarctic Cold Reversal at 13,600 years BP the stress-tolerant shrubland was mostly replaced by tall podocarp forest, indicating a sustained warming and increasing humidity (McGlone et al., 2004). Montane *Nothofagus* forest took over the podocarp forest at 7500 leading into the modern climate until the area was largely deforested by anthropogenic fires (McGlone et al., 2004). According to Moar (1971) the podocarp forest lingered longer at Lake Hawdon than in the nearby Cass Basin, on which McGlone et al. (2004) studies are based. The modern vegetational cover in the Waimakariri Valley consists of short-tussock grassland and shrubland with small patches of *Nothofagus* forest.

1.8 Thesis structure

Chapter 1 has presented the background, aim and scope of the thesis as well as giving a short overview of the regional geology, glacial and vegetational history.

Chapter 2 presents the data from mapping the field area and surveying the active faults. It describes the geomorphic expression and kinematic characteristics of each of the active faults and discusses the activity of these faults based on these results. Stream indices are also presented and discussed.

Chapter 3 encompasses the paleoseismology of the field area, presenting data from focal mechanisms, dating and scaling relationships. It discusses the relationship between moment magnitude and surface rupture length and the hazard these faults pose for North Canterbury.

Chapter 4 contains the synthesis of the previous data leading into a discussion of fault linkage and blind faults in North Canterbury, that culminates into the theory of an incipient fault system south of the Marlborough Faults.

2. Tectonic geomorphology of active faults

2.1 Introduction

The recognition and mapping of tectonic features such as faults and folds is the first step needed for any paleoseismological or hazard assessment work project. Potentially active structures have to be identified in the field and studied accordingly to collect the data necessary for follow-up work. In North Canterbury traditional field mapping often fails to produce adequate results as outcrops and subsurface data are few (Litchfield et al., 2003). The geomorphology, however, can give us much-needed information in order to not only recognise active faults but assess their activity level (e.g. Keller & Pinter, 2000, Litchfield et al., 2003).

The field area has previously drawn notice for its glacial deposits and landforms, first described by Speight (1938) and Gage (1958), while its tectonic structures are added to the many unstudied structures in New Zealand geology. Most faults in the area do appear in maps from Gregg (1964) and Forsyth et al. (2008), though at most only their slip sense is established or in case of the Esk Fault a recurrence interval is estimated but not backed up by actual geologic data (van Dissen et al., 2003). The vicinity to Christchurch of the PPAFZ and the MFS demands assessment of fault activity. In order to do so the faults and potential unmapped faults have to be recognised, mapped and surveyed.

This chapter describes the methods that have been used during field work and the outcome of this field work. Four faults have been studied in detail: the well-known southern Esk Fault, and the smaller Hawdon, Bullock Hill, and Og-Gog-Magog faults. Other faults with seemingly less impact on the area in the area are summarised and described in a similar but less extensive manner. The recognition of faults is followed by an exploration of the geomorphology of the area, examining rivers, terraces, and swamps and their possible response to the tectonic activity.

2.2 Methods

2.2.1 Mapping

The field area has previously been mapped by Gage (1958) to produce a detailed map of the Pleistocene deposits, and by Gregg (1964) and Forsyth et al. (2008) to generate regional geology maps of 1:250 000 scale. This study aims to produce a detailed structural and geomorphic map of the Waimakariri Valley (map pocket) which depicts the geometry and spatial extent of the faults in this area including the smaller faults that have been oppressed in previous studies for various reasons.

The mapping in the field was done on tracing paper on top of high resolution aerial photographs with scales of up to 1:1000 complimented by 1:50 000 topographical maps from Land Information New Zealand (LINZ). Another reference was the base map of the QMAP (Forsyth et al., 2008) and the map produced by Gage (1970) that present geological and lithological mapping that was only modified slightly where necessary. The final map utilises geographical features

as a reference, so that these features can be compared with other maps. Production of the map has been done in ArcGIS based on the elevation contours of the N.Z. Topographical series, sheet L34 (1:50 000). The colours used in the map represent the age of the formation and match with the international standard. A combination of textures and distinctive lines describe geomorphic features. Each unit is labelled with an acronym to help with identification.

The main objective was to recognise and illustrate the faults in the Waimakariri Valley. For this purpose the faults have been mapped to their true extent in the basement rocks and overlying Quaternary deposits and inferred where they could not been mapped in the field. For greater detail excerpts of the map have been enlarged and simplified to illustrate the fault extent and geometry more clearly. No elevation contours and lithologies are being used in these map figures.

2.2.2 Geographic Positioning

The Global Positioning Systems (GPS) were an invaluable asset to the mapping and survey process. Single points were recorded with a handheld Garmin eTrex, which like all GPS systems relies on the visibility of at least four satellites for 3D positioning. The more satellites are visible and the more impoved their angle is, the higher the accuracy of the measured point. This proved to be difficult in the field area at times, when a position had to be marked on a steep mountain site or cut river valley. The average horizontal accuracy of the handheld unit is ∼15 m. For specific surveys that needed a higher accuracy RTK has been used.

Real Time Kinematic (RTK) is a highly precise land survey technique based on GPS with a centimetre vertical accuracy. The RTK consists of two GPS receivers and two radios. One GPS receiver is set up on a known point as a stationary base station to provide a reference, while the other is the roving station, collecting topography data relative to the base station. Both stations receive GPS signals from the L2 Band satellites, which provides the high accuracy, and transmit the signals to each other via the radios. The roving station then collects data at a set increment, usually once a second or every 0.25 m. In the post-processing the signals are corrected to their absolute position compared to the relative position that is recorded. Therefore, the absolute accuracy depends on the correction of the base station, which is usually a couple of metres, while the internal accuracy is down to a few centimetres.

In the field a Leica SR530 was used for two separate surveys with different base stations, as the radio signals could not be transmitted. Both base stations have been corrected to the LINZ McQueens Valley site by using differential GPS, obtaining an absolute accuracy of ∼2m, while the internal accuracy is only a few centimetres. The same translation has been performed for the rest of the points through Microsoft Excel. Finally the points are being plotted using the "XYZ data to 3D polyline" conversion in ArcGIS.

2.2.3 Ground Penetrating Radar (GPR)

Ground Penetrating Radar (GPR) is a geophysical near-surface technique to obtain a profile of the subsurface to depths of <15 m. The technique uses the propagation of radio-frequency electromagnetic energy into the subsurface and measures the radar echoes, which then produce a radargram (Davis & Annan, 1989). The time that has passed between the transmission and reception of the signal gives information on the depth of the reflecting material, if the average radar velocity is known. The velocity, however, is dependant on the dielectric properties of the medium, in particular the dielectric permittivity, ϵ (Davis & Annan, 1989). The dielectric

Medium	velocity (m/s)
Air	300
Water (distilled)	33
Ice	160
Dry Sand	150
Saturated Sand	60
Shales	90
Silt	70
Clays	60

Table 2.1.: Typical velocities of a range of materials using 100MHz. Excerpted from Davis & Annan (1989)

permittivity in turn depends on the water content: The higher the water content, the slower the velocity of the radar.

In the survey two antennas are used, one that is transmitting the signal and one that is receiving the echoes. The two antennas have a set offset and should transmit a signal at a constant distance. These regular spatial increments, Δx, have to be less or equal to the minimum object size that is to be resolved. The resolution of a GPR instrument, R, is calculated using the following formula:

$$R \approx \lambda/4 = v/4f \tag{2.1}$$

In this λ is the wavelength, v the velocity and f the frequency. The unit used for surveys in this study is a Sensors & Software pulseEKKO 100A, with 100MHz antennas separated by 1m. The data was obtained by using spatial increments of 20cm, resulting in a resolution of 0.20-0.25m.

The subsequent echoes are recorded and visually displayed. The first signal to arrive is the direct airwave with a velocity of 300 m/μs which gives the time reference for the data (Davis & Annan, 1989). It is followed by the direct ground wave travelling at a speed of 40-200 m/μs producing a ground surface reference, before the echoes of reflecting mediums arrive (Davis & Annan, 1989). A few typical velocities for pure materials are given in Table 2.1, though materials are seldom pure in the field. A common feature in the radargrams are diffraction bends, which result from scattering of the GPR signal through features of the order but below the signal resolution such as boulders or truncated channels (Nobes, 2011). The shape of the diffraction hyperbole depends on the velocity between surface and diffracting feature: the flatter the diffraction hyperbole the faster the velocity and vice versa (Nobes, 2011).

In order to interpret the radargram successfully it has to be processed by migration. Migration is a mathematical inversion process which collapses the diffractions to their source and corrects the geometric position of the reflecting boundaries, i.e. dipping beds are usually steeper and deeper than they appear in the radargrams (Nobes, 2011). Finally the surface topography, from RTK or other surface surveys, is added to the top surface in order to focus the signal energy, assuming that the topography is small relative to the depth of the radargram. Thus, the radargram is ready for interpretation.

2.3 The Esk Fault

2.3.1 Characteristics of the Esk Fault

The Esk fault consists of two major strands that extend all the way from the Broken River to the Hurunui River (Fig. 2.1A). While the southern strand is rarely exposed in the field, the northern strand can be followed quite clearly (Noble, 2011).

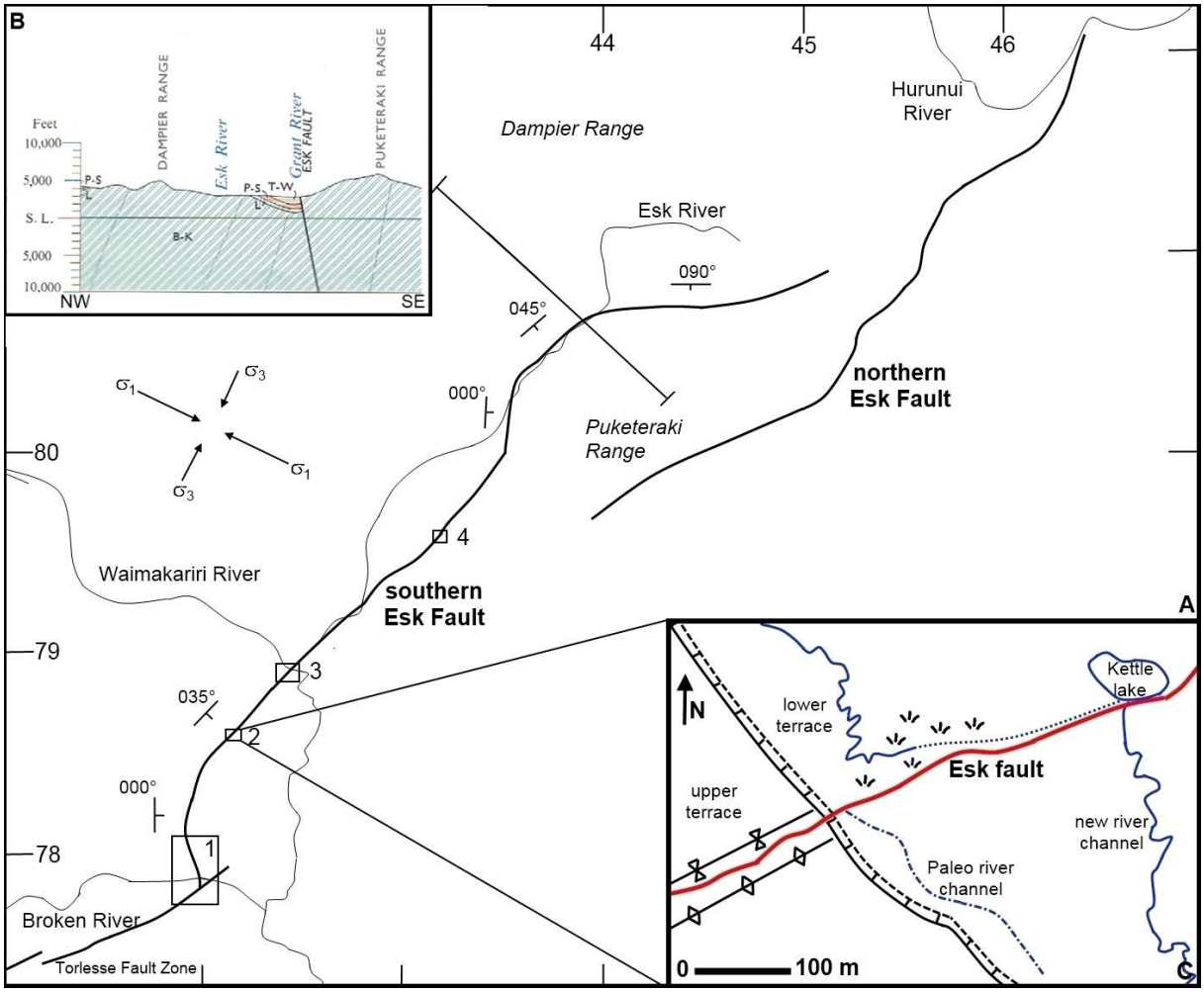

Figure 2.1.: A Map view in NZGM (New Zealand Map Grid - Geodetic Datum 1949) of the southern and northern Esk faults in New Zealand Map Grid (NZMG) showing strike measurements along the southern strand. Numbers 1-4 show the outcrops of the fault. No. 1 has been studied by Gage (1958) and depicts a major crushed fault zone with Pliocene rocks overthrust by the Torlesse Formation. No. 2 is a post-glacial surface rupture, shown in detail as C. No. 3 is similar to no. 1 showing a many faulted crushed fault zone with post-Pliocene deformation. No. 4 is a linear feature visible in the flank of the Lazyman in alignment with the fault trace. It has not been studied further, but is believed to be a fault scarp. Principal hoirzontal stress is oriented 115±5 (Sibson et al., 2011).**B** An excerpt of the geological cross section published by Gregg (1964) showing the Esk Fault dipping steeply to the Southeast. The line for the excerpt has been projected onto the Mapview (A). Unit abbreviations are as followed: B-K Torlesse Group, L Esk Formation, P-S Brechin Formation, T-W inland correlative of the Kowai Gravel (Gregg, 1964). **C)** Single displacement event on the southern Esk Fault. Two terraces of Blackwater outwash gravels have been offset by the Esk fault showing the same amount of displacement. The upper terrace shows significant anticlinal folding on the hanging wall and synclinal folding on the foot wall. A river has been diverted by the fault rupture and formed a swamp in the vicinity of the fault. (42°48'S 171°41'E / 43°19'S 172°30'E)

The southern strand trace has been observed from the Broken River to the Esk River over a length of 30±10 km striking between 000° and 090° dipping to the east into the Puketeraki Range (Fig. 2.1B). The Esk Fault dips 75° to the SE as determined from structure contours. Its southern tip terminates at the Torlesse fault aross the Broken River and the fault trace follows the Slovens Stream striking 000°, then up Puffers Stream changing its strike to 035° (Fig. 2.1A). It passes south of the Blackwater Lake up to the Esk River mouth where it follows the course of the river, running through the riverbed, roughly but cutting straight through the Lazyman before rejoining the Esk River and changing its strike once more to 090° before petering out in the Puketeraki Range (Fig. 2.1A). The Esk fault is clearly exposed in crushed bedrock at the Slovens Creek and Esk River mouths, thrusting Torlesse rocks over Miocene to early Pliocene cover deposits of the Enys Formation (Gage, 1970). Elsewhere, the Esk fault has been inferred through glacial gravels from the Blackwater advances and along the Esk River without appearing on the surface (Gregg, 1964, Forsyth et al., 2008). Only few places constrain the course of the Esk fault, an offset terrace south of Blackwater Lake, faults in the bedrock outcrop opposite of the Esk river mouth, and a scarp in the Lazyman (Fig. 2.1).

The northern strand of the Esk fault extends from the Okuhu River to the Hurunui River over a length of ∼20 km (Fig. 2.1A). The fault strikes from 005° to 057° and it dips 50°W. An advantage over its southern counterpart is that post-glacial sediments do not obscure the fault trace, therefore a multitude of scarps and offsets have been documented (Noble, 2011).

2.3.2 Activity of the Esk Fault

Since the fault is mostly hidden under glacial gravels as inferred by Gregg (1964) and Forsyth et al. (2008) two possibilities exist, a considerable part of the Esk fault shows blind faulting or no earthquakes have ruptured along the whole fault length since it was buried by glacial sediments, in contrast to the northern strand which has produced surface rupture during the Holocene (Noble, 2011). The southern part of the fault expresses itself mostly as crushed and many-faulted zone where it is impossible to get a general dip or displacement measurement. However, there is at least one post-glacial surface rupture along the fault near the Blackwater Lake (Fig. 2.1C). Here, glacial outwash terraces have been displaced vertically by 3.4±0.2 m with no distinguishable strike-slip offset.

A river that followed the terrace scarp has now ponded and diverted 230 m further north-east abandoning its former course. Anticlinal folding is observed on the hanging wall of the fault and is more pronounced on the older terrace. Despite the different amplitudes of the folding, the vertical displacement is the 3.4±0.2 m on both terraces, thus, displaying a single event. The folding is an indicator of reverse movement along the fault which is compliant with earlier observations (Gregg, 1964, Gage, 1970). No dextral displacement has been observed. The outwash terraces formed after the second Blackwater Advance, 21 - 23.3 ka (Fitzsimons, 1997, Forsyth et al., 2008), indicating that the southern Esk fault has ruptured at least once in the last 20 000 years.

The northern strand of the Esk fault exhibits primarily dextral-reverse movement. The fault displaces minor streams and ridges by 3.4 - 20 m laterally and 1 - 9.5 m vertically (Noble, 2011). Single event displacements show 5m dextral offset along the entire length of the fault and 2m vertical offset in addition where the fault displays reverse movement (Noble, 2011). Since these displacements have occurred mostly during the Holocene, the northern strand seems to be

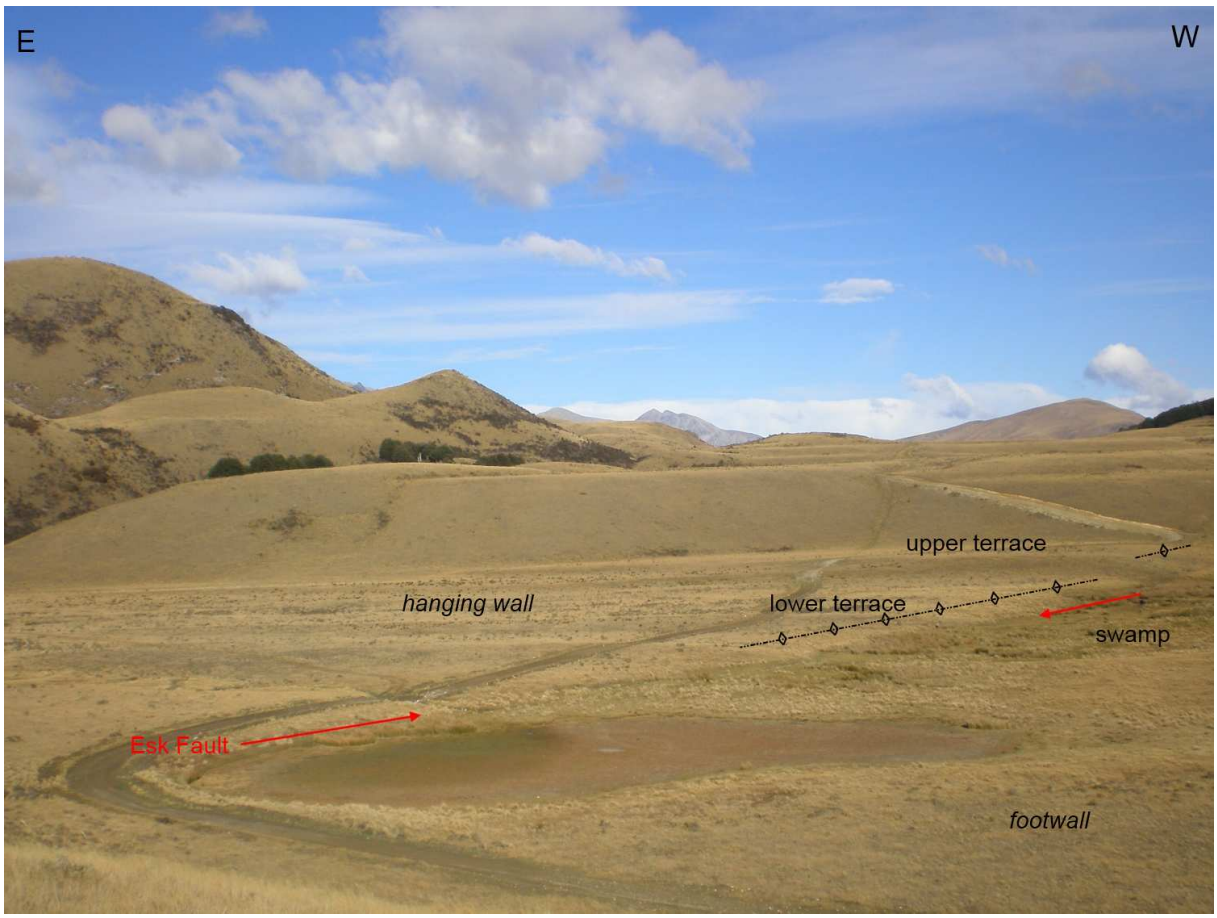

Figure 2.2.: The latest offset on the Esk Fault viewing SSW (Mapview in Fig. 2.1C). The Esk Fault runs across two terraces, a glacial till (upper terrace to the west) and a glacial outwash terrace (lower terrace in the centre) originating from the second Blackwater Advance (Gage, 1958). The northern side which is the footwall shows swampy terrain resulting of ponding. Folding is more prominent in the upper terrace with an anticline on the hanging wall and a syncline on the foot wall. It is the only place, where a Holocene surface rupture could be constrained.

more active than the southern Esk fault.

2.4 The Hawdon Fault

2.4.1 Characteristics of the Hawdon Fault

The Hawdon Fault is exposed over a length of 5 km in Torlesse bedrock on the slopes of Mt St Bernard and Purple Hill between Lake Hawdon and Lake Pearson (Fig. 2.3). The eastern end of the fault crops out in a small ridge of bedrock on the north-eastern shore of Lake Hawdon, though further exposure might be obscured by glacial gravels of the Blackwater advances. In the central portion of the fault it splits into three splays of the fault crops (Fig. 2.4). On the western end massive alluvial fans terminate the exposure of the fault.

On the slopes of Mt St Bernard the bedding of the bedrock dips 202/30 and shows a prominent joint set with a dip of 000/74, while further west the bedding changes to 150/55. The uphill facing scarp of the Hawdon Fault strikes roughly 080° and dips 47° to the south. Movement on the fault is predominantly dextral strike-slip, as shown by the offset of recent geomorphic features, with a minor normal component (Fig. 2.4).

Fig. 2.4 shows two chutes on the slopes of Mt St Bernard that are spaced 84±5 m apart and

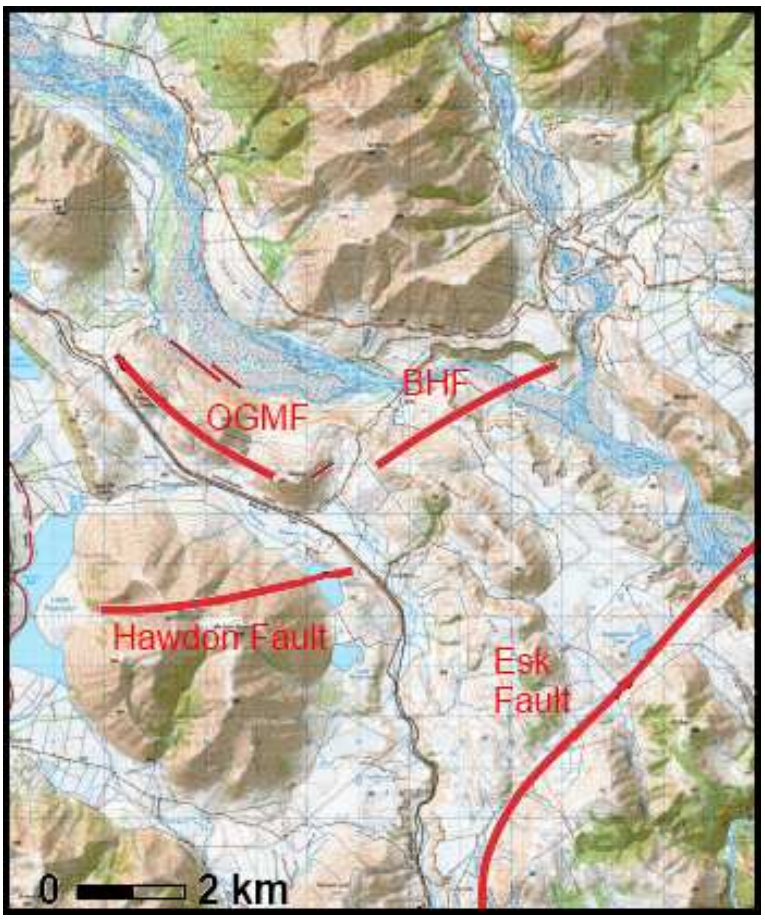

Figure 2.3.: A mapview of the smaller faults in the area, showing their extent in the field. BHF - Bullock Hill Fault, OGMF - Og-Gog-Magog Fault. (43°00'S 171°48'E / 43°09'S 171°57'E)

dextrally offset by 140±10 m, measured on aerial photographs and by EDM in the field. The down-faulted chutes extend all the way to the current base level and carry rain water down the slope, leading to a more intense plant cover along the channels. Below the cut-off chutes new channels are incising at the likely origin of the displaced chutes. Other chutes along that section that distribute sediment directly into Lake Hawdon seem to be unfaulted and are less deeply incised than the displaced channels. Further up the fault landslide deposits that eventually feed into the alluvial fan at the base of the slope cover a segment of the fault.

2.4.2 Activity of the Hawdon Fault

No dating has been done on the displaced chutes. However, they are almost certainly of post-glacial age, because they maintain a consistent cross-sectional geometry and extend all the way to the base level established after the retreat of the Blackwater glacier at 18.4±1.8 (Fitzsimons, 1997). There is a small possibility that the channels are inherited structures that persist through the glaciations and that they are much older. The existence of an accommodation space in the form of Lake Hawdon directly adjacent to the fault provides an excellent opportunity to examine the sediment deposits of the last 18.4 ka since the retreat of the Blackwater Advance and formation of the lake to obtain more information about the seismic activity of the fault. The number and timing of single earthquake events could be conserved in the sedimentary records providing no external distubances of the record and continuous sedimentation, which in turn can be used to further decipher the seismic history of the Hawdon Fault.

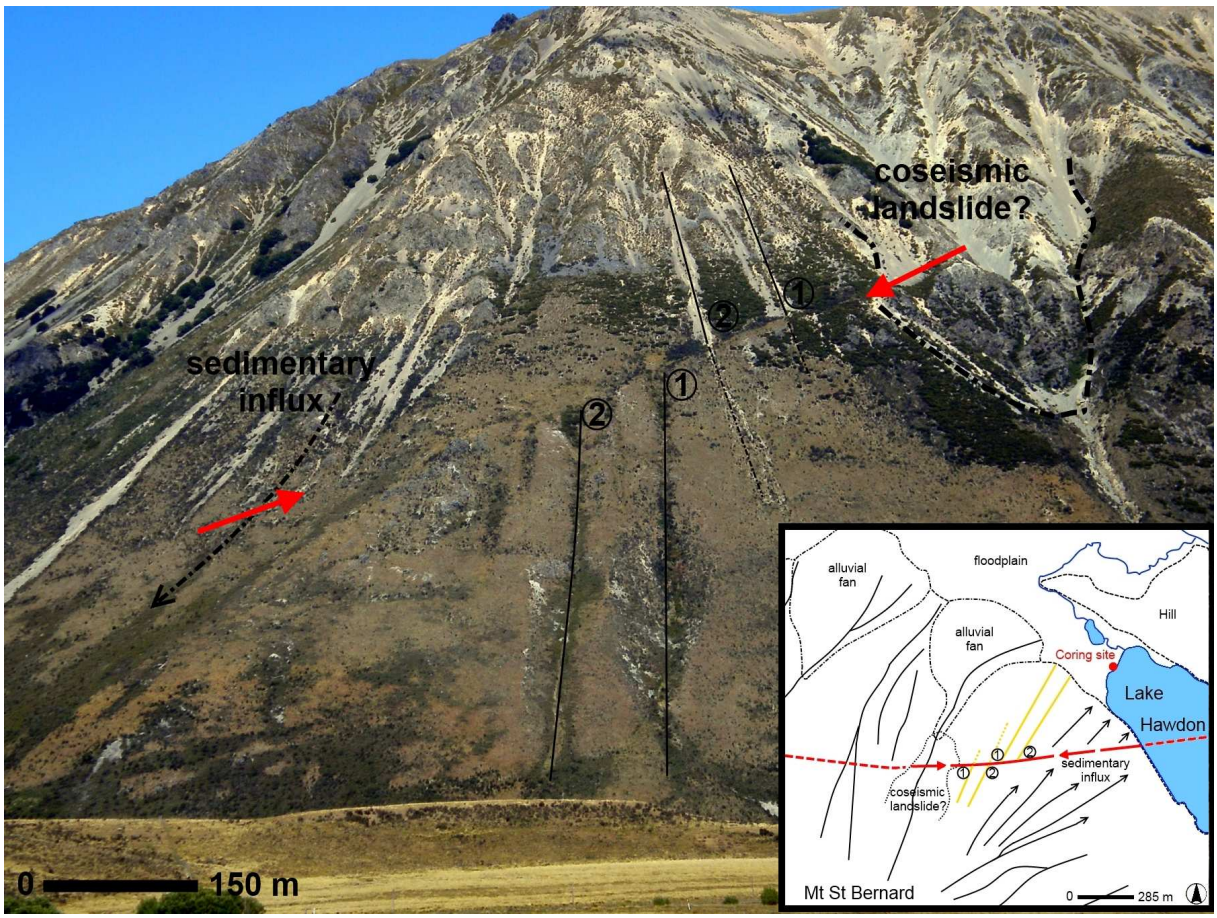

Figure 2.4.: South view of the E-W striking Hawdon Fault showing 150 m of dextral offset of two post-glacial chutes that are spaced roughly 84 m apart. Two new chutes are forming at the original position of the down-faulted chutes indicating relatively recent activity on the fault, while landslide deposits up the fault might have been coseismic. Chutes on the western side of the fault are transporting sediment into Lake Hawdon, where coring has been conducted on the northeastern shore by Nicky Whitehouse (pers. comm., September 2010)

In 2007 thirteen cores were taken from within a 5x5 m^2 grid at the north-eastern shore of Lake Hawdon by Nicky Whitehouse and her team (pers. comm., 2010) as part of paleo-climate studies (Fig. 2.5). C^{14} dating has been conducted by Whitehouse for the cores and used in conjunction with a deforestation signal (670 BP) at 160 cm depth by Moar (1971) to establish a general age-depth correlation (Fig. 2.5). As part of this study two of these (LH2-core, HZ-core) cores have been examined from high-resolution pictures in order to establish a rough core stratigraphy and identify sedimentary events (Fig. 2.5) following the example of Beck et al. (1996) who used the abundant occurrence of sedimentary events in post-glacial lake sediments to demonstrate enhanced seismicity in the European Alps in the early post-glacial period. The established core stratigraphy for the Hawdon Lake core is as follows:

Below 450 cm: Thinly laminated light grey clay with dark grey sand grains and black organic detritus. The top of this unit shows an increase in sand grains.

80 - 450 cm: Predominantly thinly bedded light brown silt that is intercalated with very thin (few mm) organic rich layers and up to 3 cm thick sand layers that are distributed unevenly through the core. The bedding is less pronounced than the bedding in the lower unit. The top of the unit incorporates gradually more unaltered organic material from approximately

140 cm.

0 - 80 cm: The top of the core consists of a thick peat layer without sedimentary disturbances.

Beck et al. (1996) described three events in their cores that they associated with seismic activity: 0.1-5 cm thick silt and sand layers with a sharp base and sometimes positive graded bedding that were interpreted as grain-flow deposits, debris-flow deposits containing 1-2 cm sized clasts of mud in a sandy-clayey matrix, and stratification disturbances with vertical flowage structures (ball-and-pillow type) and sets of inclined microfaults.

Following this description 17 sedimentary events were distinguished in the Hawdon core (Fig. 2.5). The most prominent event is a plume-shaped vertical disturbance (No. 4) in the LH2-core at 410 to 390 cm which correlates to an approximate age of 10000 BP (Fig. 2.5). The other sixteen events are dark sandy layers of up to 3 cm thickness with no visible grading, semi-irregular bases and irregular tops which are interpreted as grain-flow deposits. No grain flows, microfaults or flowage structures were identified in the core.

All events were assigned a quality class (Table 2.2): Class 1 holds those events that showed a disturbance of the layers and grain flow deposits visible in overlapping sections. Class 2 contains continuous features which span the whole width of the core and have a distinct base. The third class is assigned to features that are small, not continuous or very thin (1-2 mm). Event no. 4 is a feature in class 1. Eight of the events are width-spanning and assigned class 2, while seven are assigned class 3. The only event not clearly assigned is no. 14 which is a very thin, sandy layer (class 3) but appears in two overlapping core sections (class 1).

Since I could not find any clearly fault related events such as micro fracture and flowage structure, the seismic origin of the events is uncertain. However, there are a two observations that lead me to favour a seismic origin for theses features: the location of the drilling site is far from any river mouths avoiding coarser influx during floods and 8 events are continuous through the core. Thus, I assume that earthquakes have triggered these sedimentary events inside the

Figure 2.5. ***(following page)*:** Schematic core stratigraphy based on observations of the LH2 and HZ cores depicting 17 sedimentary events (16 grain flows, 1 vertical disturbance) that possibly originate from seismic activity on the Hawdon Fault. The ages (Table 2.2) have been retrieved from C$^{(}$14) dating in thirteen cores, including the LH2 and HZ cores, taken in a 5x5 m area (Whitehouse, pers. comm. September 2010) and a pollen signal (670 BP) for Polynesian deforestation at 160 cm depth (Moar, 1971). A-E show the characteristics of the observed cores.
A Gradual transition from silt to the concluding peat layer, which represents the most recent deposits.
B Exemplary 3 cm thick grain flow deposit (dark gray sand) in light brown silt/clay layer with organic detritus. Fifteen similar grain flows can be found throughout the core between 450-150 cm depth with a maximum occurence in the Early Holocene.
C Thinly bedded sandy silt with organic detritus makes up most of the Holocene part of the core and is intercalated with sandy grain flow deposits.
D Sedimentary disturbance composed of fine grained light sand disturbing a coarser grained dark gray sand layer with an approximate age of ∼10000 BP.
E Thinly laminated light gray clay alternating with dark gray sand layers makes up the Pleistocene part of the core and is predominantly undisturbed.

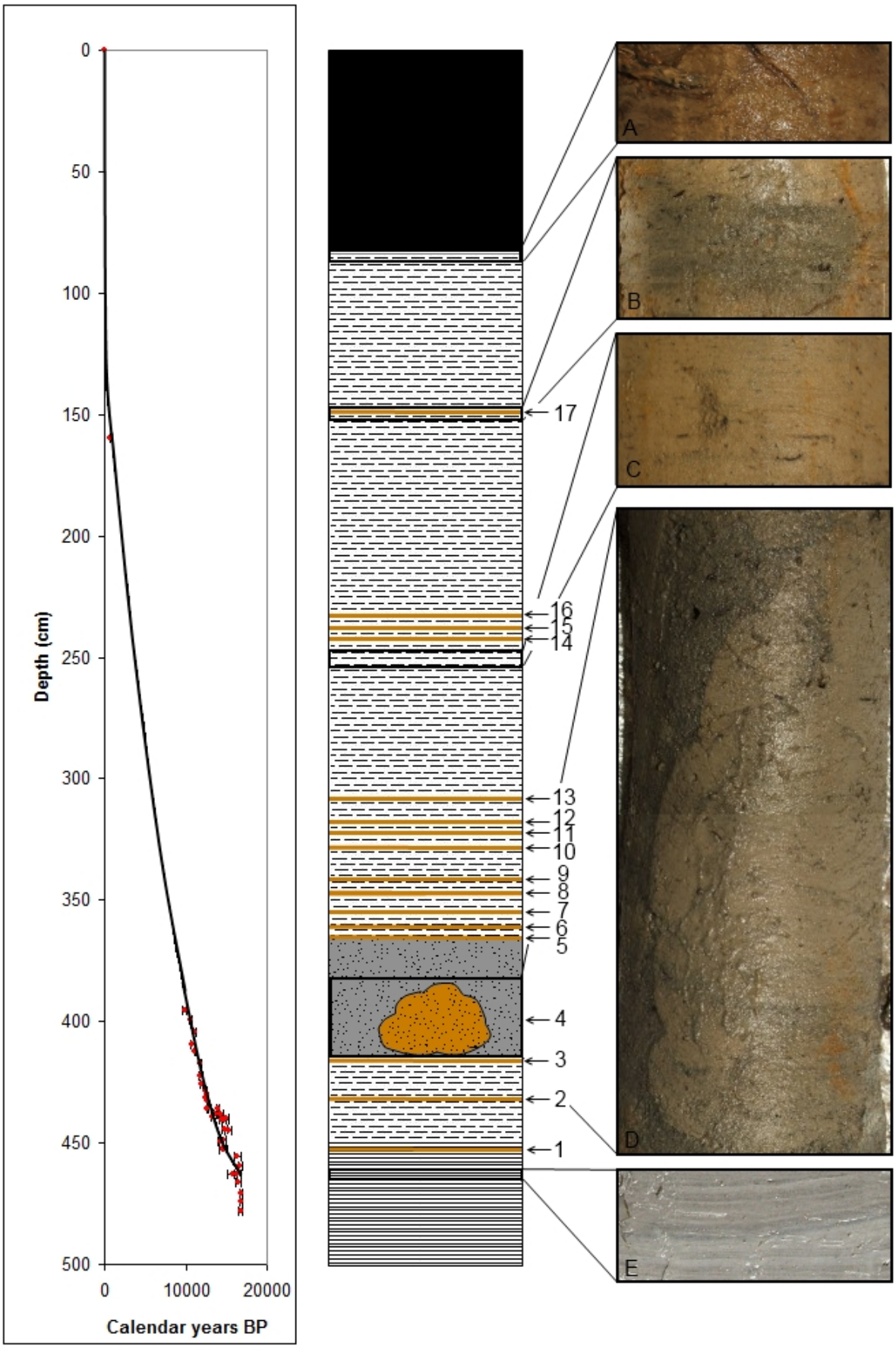
Depth (cm)
0
50
100
150
200
250
300
350
400
450
500
0
10000
20000
Calendar years BP
17
16
15
14
13
12
11
10
9
8
7
6
5
4
3
2
1
A
B
C
D
E

No.	Description	Depth (±1 cm)	Quality	correlated Age
1	Width-spanning, 2 cm thick, dark, coarse layer with distinct contacts	445	2	15226±34
2	small (quarter width) sandy deposit	420	3	12779±30
3	small (half width, 2 cm thick) sandy deposit	410	3	11879±
4	Sandy plume shaped vertical disturbance	390	1	10208±26
5	Width-spanning, 3 cm thick, dark, sandy to silty layer with irregular contacts	373	2	8919±24
6	Width-spanning, 3 cm thick, dark, sandy to silty layer with irregular contacts	360	2	8010±22
7	Width-spanning, 2 cm thick, dark, sandy to silty layer with irregular contacts	353	2	7547±21
8	Width-spanning, 1 cm thick, dark, sandy to silty layer with irregular contacts	345	2	7041±20
9	Width-spanning, 3 cm thick, dark, sandy layer with irregular contacts	335	2	6440±19
10	small (half width, thin) sandy deposit with sharp contacts	325	3	5875±18
11	Width-spanning, very thin (2 mm), broken, sandy layer	323	3	5712±18
12	Width-spanning, very thin (2 mm), broken, sandy layer	319	3	5552±17
13	Width-spanning, 2 cm thick, intercalation of sand and silt layers with sharp contacts	311	2	5141±17
14	Thin, not completely width-spanning, sandy layer, appearing in overlapping core sections	242	1 or 3	2404±10
15	3 cm thick, broken and intercalated, sandy layer	240	3	2344±10
16	3 cm thick, broken and intercalated, sandy layer	235	3	2199±9
17	Width-spanning, 3 cm thick, dark, sandy layer with sharp contacts	150	2	564±4

Table 2.2.: The table shows the number of identified sedimentary events. Quality class 1 is distinct disturbance and features visible in overlapping core sections. Class 2 includes continuous width-spanning features. Class 3 is assigned to very thin or non-continuous features. Event 14 is either a class 1 feature due to appearing in overlapping sections or class 3 for being not width-spanning. The ages (x) are based on the age model in fig. 2.5 and the resulting formula $f(x) = 18.54 * x^0.33$. Shown errors in age calculation are solely based on the correlation and error continuation. True errors are larger and depend on sedimentation rates, which are unknown to this study.

lake. Since the 8 non-continuous events should not be completely excluded I deduced a number of 13±4 single seismic events.

Using the age model derived from C(14) dating and the pollen signal, I find that the events can be divided into three clusters. The first group, event 1-3 (Fig. 2.5), between 410 and 450 cm depth correlates with an age of 10000 to 15000 years BP (Table 2.2). Event 4-13, found between 410 and 310 cm depth, occurred between 5000 and 10000 years BP (Table 2.2). A third cluster of three events (Nr. 14-16) can be found at 230 - 250 cm depth with an approximate age of 3000 BP (Table 2.2). However, these three are among those with a low certainty. Nr. 17 is a single clear event at 150 cm that must have occurred at ∼550 BP as it lies just above the deforestation signal of 670 BP. Recurrence intervals between consecutive events derived from the depth-age correlation of the events (Fig. 2.5) ranges from 70 - 2500 years with 10 events occuring within 1000 years of each other.

Considering that seismic activity began to be able to be recorded in the lake around 15000 BP, when the first sedimentary events have been distinguished in the core, the chutes had roughly 3000 years to form from the retreat of the Blackwater Advance at 18.4±1.8 (Fitzsimons, 1997) to the onset of activity. They have then been continuously displaced over a course of more than 10000 years, defined by either the end of the second cluster (5000 BP) or the end of the less certain third cluster (3000 BP). Evidence for the continuous displacement can be found by the complete lack of newer channels below the fault line but two which are right below the catchment chutes and, thus, are to be inferred of Late Holocene age. This is further indicated by the fact that these newly formed channels have not yet incised all the way down to the base level ending half way on the hillside or further up. The eastern channel has reached about half of the length of the displaced channel (Fig. 2.4). Assuming it takes 3000 years to form a mature chute that extends to the base level under comparable climatic factors, the incision of the most recent chute has a maximum age of 1500 years. The absence of any other half or fully formed channels suggests that the fault has moved continuously for almost 15000 years with the last event at ∼ 1500 years.

The factors that control the formation of these features, such as climate and vegetation cover, are likely to have differed from 18000-15000 BP to 1500-present. Therefore, the formation of the new feature may have been slower or faster than the early formation and these constraints are only rough estimates. The occurrence of another sedimentary event at ∼550 years (Nr. 17 in Fig. 2.5) hints on a much faster incision rate for the channel, however, the nature of the sedimentary event is unclear at this stage and the displacement of the channel could be minor enough to be negated by further incision over the following 550 years.

In summary the Hawdon Fault had a 140±10 m offset since 15±3.4 ka in 13±4 single events leading to a recurrence interval of 1154±617 years. This amounts to a post-glacialslip rate of 9.3±2.8 mm/yr, which is only slightly less than the slowest segment, 10-14 mm/y, and more than a quarter of the fastest moving segment, 11-35 mm/yr of the Hope Fault (e.g. Cowan, 1990, Knuepfer, 1992, van Dissen et al., 2003).

2.5 The Bullock Hill Fault

2.5.1 Characteristics of the Bullock Hill Fault

The Bullock Hill fault (BHF), first mapped by Gregg (1964), lies 1 km to the north of the Hawdon fault and strikes 055° (Fig. 2.3). Similar to the Hawdon fault, the trace length is ∼5 km, it displays dextral strike-slip with a normal dip-slip component, offsets Holocene landforms and both ends of the fault trace terminate in valley fill deposits. The trace extends across the northern flank of the Bullock Hill of Torlesse bedrock, but vanishes under glacial gravels in the Waimakariri valley for about 1 km, and is possibly exposed for another 500 metres on a Holocene river terrace on the far side of the valley (Fig. 2.6A-C). The regional principal stress of 115±5° (Sibson et al., 2011) favours reverse movement in a fault with this orientation. It is possible that the heightened topography of the area leads to a more or less equal distribution of vertical and horizontal stress, with the vertical stress being momentarily larger and causing the normal movement of the fault, e.g. Peru, Himalaya (Dalmayrac & Molnar, 1981, Burchfiel & Royden, 1985).

During its course through the hills the fault displaces four Holocene drainage channels filled with debris and may have controlled the development of two adjacent gravitational slope collapses. Offset of the channels ranges from 5 to 19 m measured by EDM, but could be as large as 110 metres as the easternmost channel (Table 2.3) below the fault (A in Fig. 2.6A) is much deeper incised than the closest offset channel above it (A' in Fig. 2.6A), indicating that its original source may have been the next channel along the fault (B' in Fig. 2.6A) which is similarly incised. Channel B (below the fault) would in this scenario have formed subsequent to channel A, before being displaced by more recent slip events. Sources of error in measurements include possible obscuring of the channel walls by accumulated debris and vegetation.

Continuing west of the displacement the fault runs through two collapsed slopes with edges that correlate with the fault trace that may relate to fault activity (Fig. 2.6C). These landslides led to exposure of Torlesse bedrock with six fracture sets (110/84, 048/74, 010/90, 110/41, 130/18, 310/67). Most of them are joints but the first set of 110/84 striations display fault movement.

Between the two collapses a swamp can be found lying to the north of the fault trace indicating possible fault-related ponding. The further trace westward through glacial gravels is unclear as there are no further offsets or possible fault related features.

The fault does not crop out in the glacial gravels between the foot of the Bullock Hill fault and the Waimakariri River. However, in a considerably younger fluvial terrace on the northern shore of the river a scarp stands out on a terrace as a very straight feature and in line with the projected fault trace (Fig. 2.6B). There are two possible explanations for this feature: The feature is a terrace riser caused by fluvial erosion or the feature is the fault scarp that does not disrupt the meandering channel around the terrace and would depict the last seismic event(s) on the fault. Atop the terrace the feature splays into three strands on the western side of the terrace, one (no. 2) of which evolves into a small anticline close to the main scarp (no. 1), and after being reduced to a single feature splits into two strands on the eastern side (Fig. 2.6C). The cumulative vertical displacement of the splays averages at 1.29±0.20 m compared to 1.24±0.15 m along the single scarp (Table 2.3). RTK and GPR surveys have been conducted to find out whether the feature is a terrace riser or fault scarp (see 2.5.2).

Site no	Distance along fault	Displaced feature	HD (m)	HD Error	VD (m)	VD Error	Movement sense
BHF 1	1405m	stream channel (D-D')	5.1	0.5	-	-	dextral/normal
BHF 2	1460m	stream channel (C-C')	14.4	0.5	-	-	dextral/normal
BHF 3	1556m	stream channel (B-B')	17.2	0.5	-	-	dextral/normal
BHF 3*	1595m	stream channel (A-B')	110.0	10	-	-	dextral/normal
BHF 4	1700m	stream channel (A-A')	19.0	0.5	-	-	dextral/normal
BHF 5	4260m	river terrace (splays 1,2)	-	-	1.23	0.1	-
BHF 6	4330m	river terrace (splays 1,2,3)	-	-	1.26	0.1	-
BHF 7	4375m	river terrace (splays 1,3)	-	-	1.49	0.1	-
BHF 8	4435m	river terrace (splay 1)	-	-	1.39	0.1	-
BHF 9	4470m	river terrace (splay 1)	-	-	1.09	0.1	-
BHF 10	4490m	river terrace (splays 1,2)	-	-	1.19	0.1	-

Table 2.3.: Displacement on the Bullock Hill and Hawdon Faults. HD - Horizontal displacement, VD - Vertical displacement. B* assumes B' is the origin of A instead of A'.

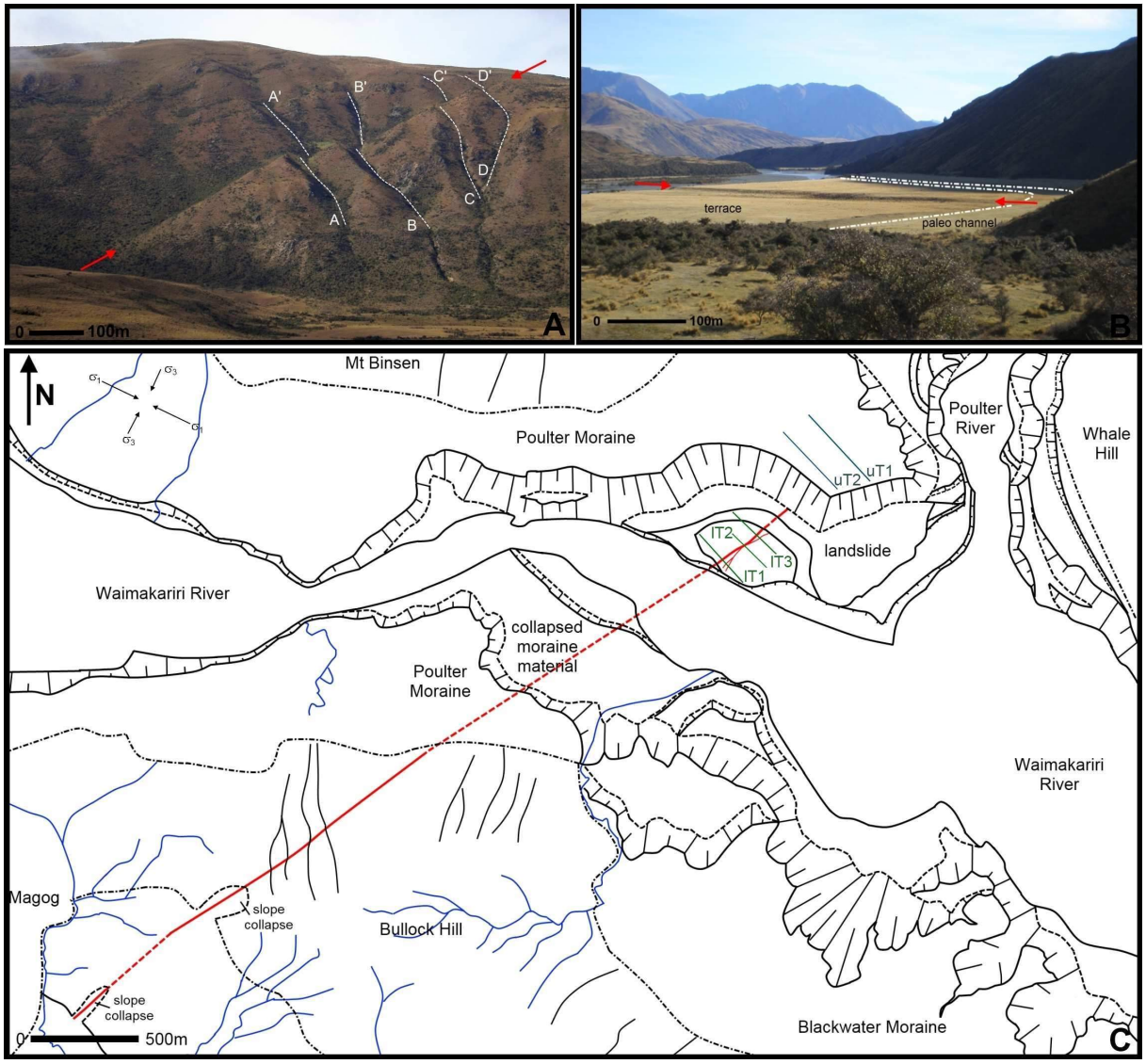

Figure 2.6.: South view of the Bullock Hill Fault (BHF) outcropping in the Bullock Hill. Shown is the dextral displacement of four channels (A-D). B) West view of the BHF offsetting an alluvial terrace and the surrounding undisturbed meander channel. C) Map view of the BHF. uT1 and uT2 depict the RTK runs on the upper terrace and lT1-3 show runs on the lower terrace. Both RTK results are described in section 2.5.2. Principal stress is reported at 115±5° (Sibson et al., 2011) though the normal movement of the fault makes indicates that the vertical stress might be larger than the horizontal stress. (43°03'S 171°52'E / 43°05'S 171°55'E)

A similar feature can be found on the other side of the meandering paleo-channel (Fig. 2.6B, C), but here dense vegetation makes interpretation difficult. However, the vegetation takes advantage of wetter soil conditions along the scarp in this part, suggesting ponding. There is no sign of the fault running through the older Pleistocene terrace on top of the river terraces and beyond the Poulter River, although the exposed Torlesse terrane bedrock along the river is highly crushed in places, suggestive of a fault zone. Another RTK survey was performed in order to detect the fault in the Pleistocene terrace as it may be obscured to the eye by the hummocky surface of the terrace (see 2.5.2). A post-glacial landslide on top of the lower river terrace formations (Fig. 2.6C) might have occurred coseismically with fault rupture. It does not appear to have resulted from undercutting by the river because, based on morphological evidence, it appears to post-date the time when the river flowed at this height.

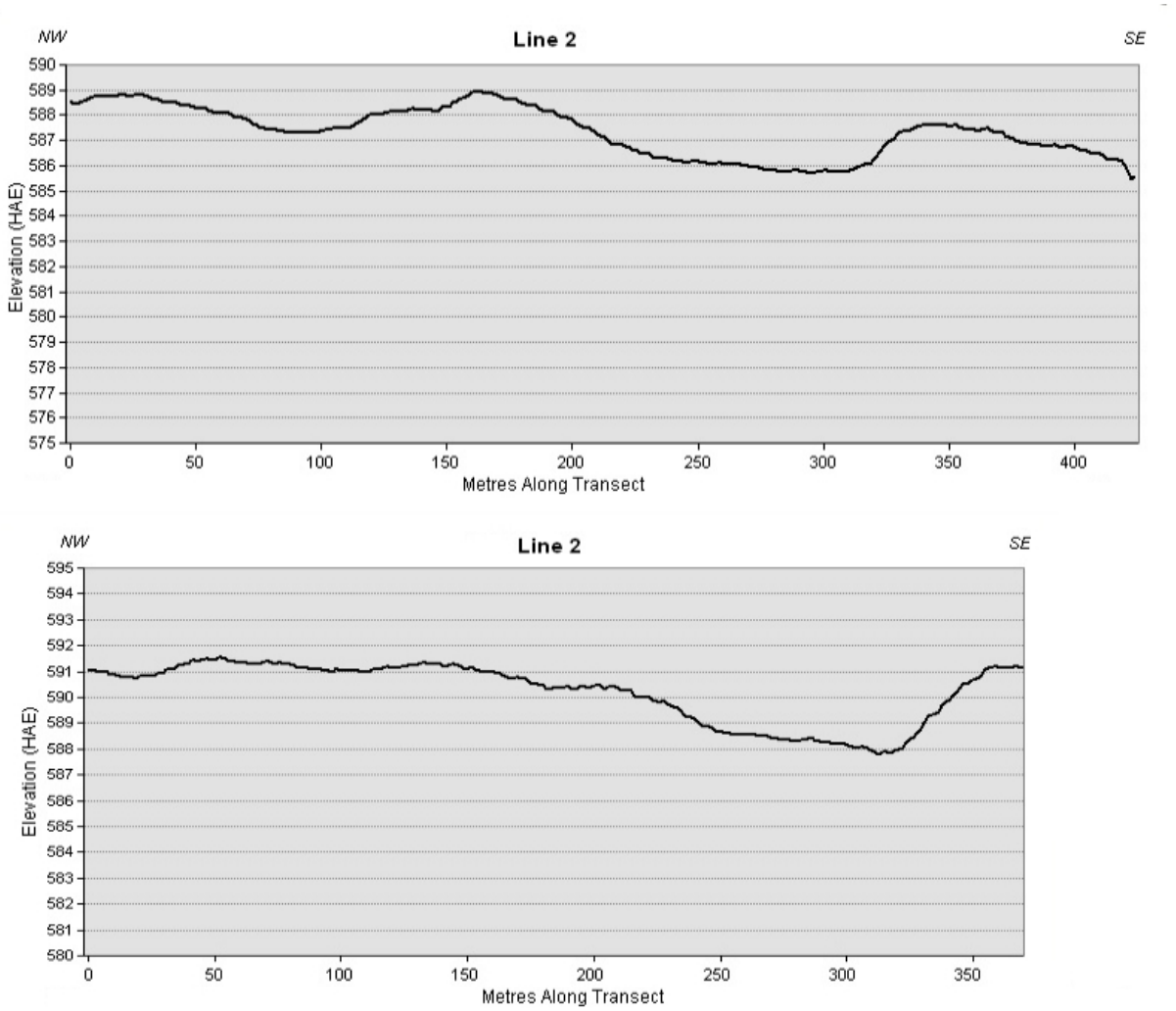

Figure 2.7.: Topography of the Poulter moraine surface at the Waimakariri/Poulter River junction by two RTK lines shown in mapview (Fig. 2.6) as uT1 (Line 1) and uT2 (Line 2). Depicts the typical hummocky surface of a moraine deposit. 10x vertical exaggeration.

2.5.2 RTK and GPR surveys

In order to get a better picture of the fault and its possible offsets after crossing the Waimakariri River two separate surveys have been undertaken. These include a RTK survey in the Poulter moraine material on top of the terraces and another one in the possibly fault-related displacment of a fluvial terrace below (see fig. 2.6 for lines), followed by a GPR survey on the same terrace. The RTKs delivered a better resolution of the topography in preparation of the GPR and can be used to detect warping and backtilting of the terraces. The GPR profiles, on the other hand, give insight into the subsurface of the terrace and help identifying faults and other buried features.

The RTK in the Poulter moraine features two lines run perpendicular to the inferred fault trace of the Bullock Hill Fault (uT1 and uT2 in fig. 2.6). The surface on top of the moraine is too hummocky to the naked eye to discern a clear fault trace. Assuming the fault offsets the moraine surface in a post-glacial earthquake a clear scarp, warping or backtilting should show up in the the profile. As one can see in fig. 2.7, no such features can be identified and the profiles look indeed just hummocky.

On the lower terrace three lines from west to east have been done perpendicular to the scarp, which can be seen in fig. 2.8 (lT1, lT2, and lT3 in fig. 2.6). Line 2 shows distinct backtilting on

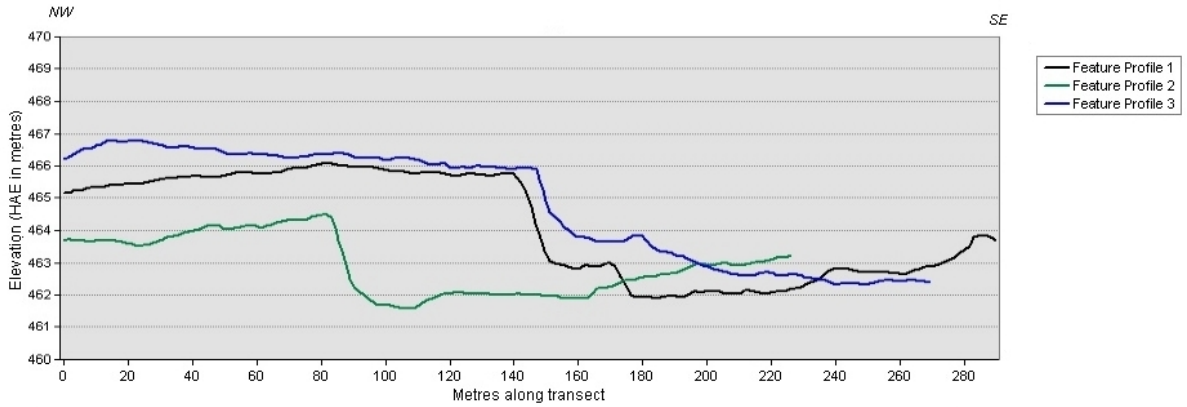

Figure 2.8.: Topography of a Holocene river terrace at the Waimakariri/Poulter River junction by three RTK lines shown in mapview (Fig. 2.6) as lT1 (Feature Profile 1), lT2 (Feature Profile 2), and lT3 (Feature Profile 3), and , crosscutting a potential terrace or fault scarp. The Profiles show the distinctive scarp and backtilting of the upper terrace. 10x vertical exaggeration.

the upper terrace. All three profiles feature a drop after the scarp and subsequent ridge. In line 1 and 3 the ridge is followed by a further lowering of the elevation, while line 2 does not feature such a step, but instead tilts northwest again. This observation coincides with the mapping of possible anticlines or paleo-channel walls that appear at the east and west of the scarp but not in the middle, were line 2 is situated (Fig. 2.6).

The RTK of the fluvial terrace was subsequently used as a focus for the GPR which has been conducted along the lines 1 and 3 of the RTK survey. The raw GPR profiles have been migrated with velocities of 80, 90 an 100 m/μs to collapse the diffractions, each time resulting in a smoother image (Fig. 2.9, fig. 2.10). According to the typical velocities in Table 2.1, a velocity of 80 - 100 mμs correlates to partially saturated sands and gravels. About two metres below the surface increased scattering suggests a boulder bed. Line 1 (Fig. 2.9) shows the features of a river channel just below the scarp, favouring a non-fault origin of the scarp. Another channel can be seen further SE of line 1. The channels are less clear in the second profile (Fig. 2.10), nevertheless, the scarp equally seems to be of a non-tectonic origin. At a closer look a thrust fault could possibly be interpreted in both profiles, less clear in line 1 than line 2 where two possible dicontinuities in layers appear. It is more likely that the scarp results from a really straight paleochannel with deeper incisions from time to time. However, the possible presence of a thrust fault in the critical position prohibits ruling out a tectonic origin. Trenching is needed to resolve this, but was beyond the scope of this study.

2.5.3 Activity of the Bullock Hill Fault

As the origin of the terrace scarp is inconclusive, only the offset channels are taken into account when defining the activity of the Bullock Hill Fault using a logic tree approach (Fig. 2.11). The ages of the channels extending to the current base level are probably no older than the first Poulter advance at 12.0±1.1 ka BP (Fitzsimons, 1997). Thus, channel age is weighted more heavily to <12 ka than > 12 ka. Total displacement can be 19 or 110 m, the great difference resulting from different correct channel correlations. The 110 m displacement seems more likely because of the degree of incision is more comparable between the further offset channels than the closer ones. Depending on whether a total displacement of 19±0.5 m or 110±10 m is used, the slip rate for the Bullock Hill fault is either 1.6±0.2 mm/year (cumulative weight of 0.14) or

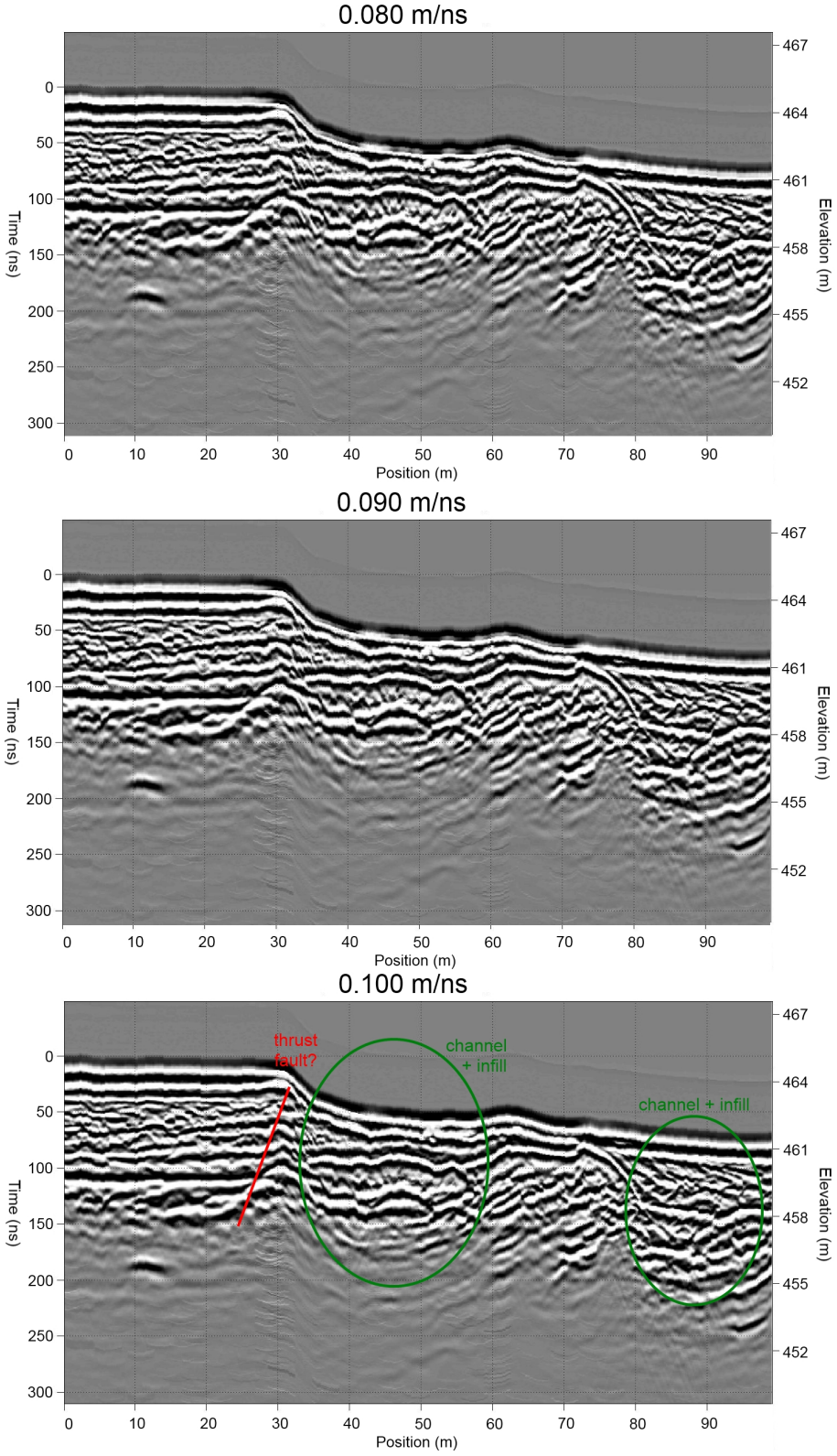

Figure 2.9.: Radargrams of the Holocene river terrace along the first RTK line (Fig. 2.8). The three profiles show the migration process from 80-100 m/μs, becoming increasingly smoother. All three show a channel including infill immediately next to the scarp and a second one further southeast. A possible thrust fault can be recognised under the terrace scarp.

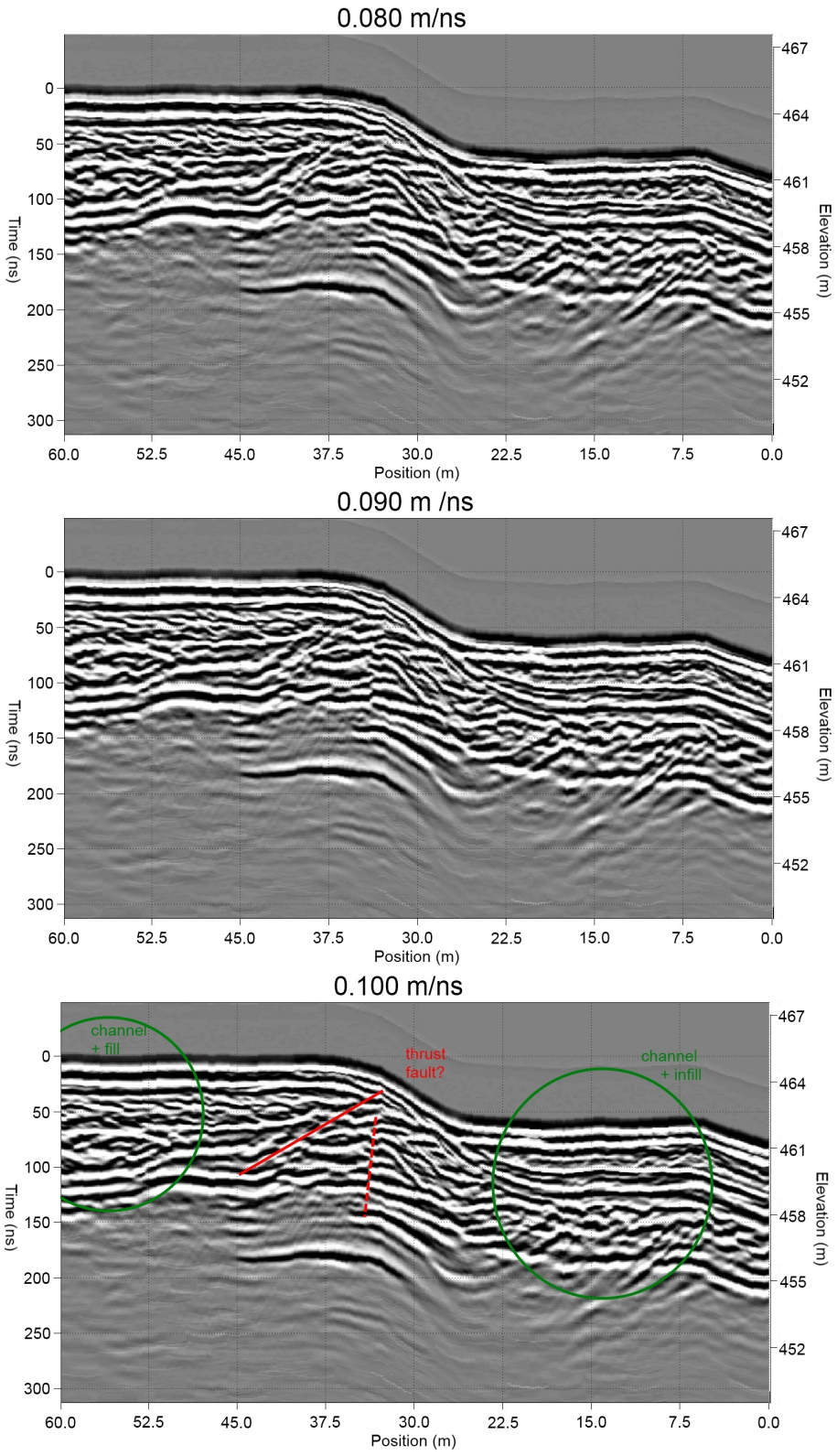

Figure 2.10.: Radargrams of the Holocene river terrace along the third RTK line (Fig. 2.8). The three profiles show the migration process from 80-100 m/μs, becoming increasingly smoother. All three show a channel including infill immediately next to the scarp and another one on the upper terrace. A disturbance under the terrace scarp is sharper than in the first radargram and might be a thrust fault although it is equally possible that it is just the edge of the nearby channel. A second steeper thrust was not reproduced in the first radargram.

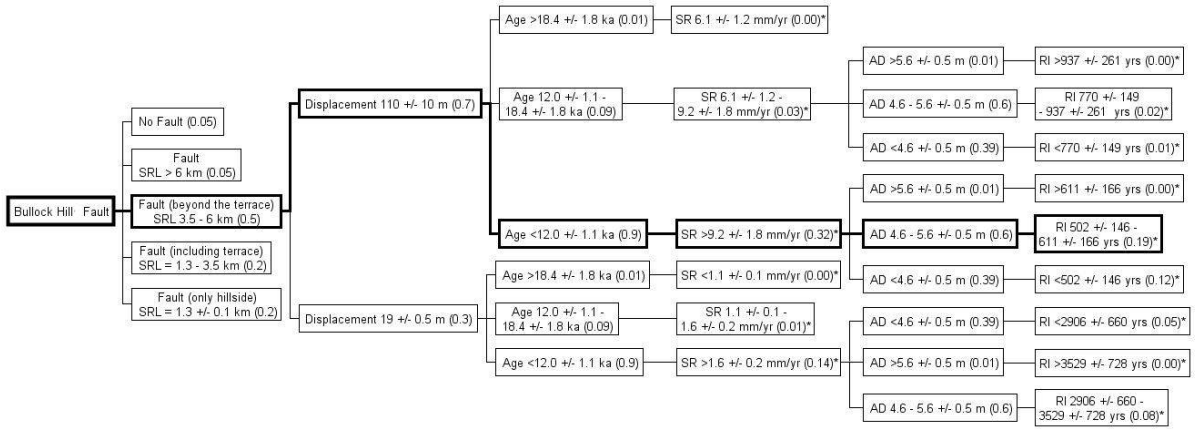

Figure 2.11.: Logic tree for the Bullock Hill fault. Weights are in brackets, * for cumulative weights. Parameters which are on the same level and are not subjected to further weighting, such as age and slip rate, and average displacement and recurrence interval show both, individual weighting of the branch and cumulative weight. The most likely scenario is emphasised. Values of 0.00 are possibilities of less than 0.5% probability.

9.2±1.8 mm/year (cumulative weight of 0.32). The first slip rate appears a very plausible value compared to other faults in the area, while the second is surprisingly high, but seems to the field observations better.

The offset of channel D is the best estimate for average displacement on the Bullock Hill Fault. This would lead to three events for channel C, four events for channel B and 22 events for channel A, assuming the total offset of 110±10 m and a recurrence interval of 502±146 - 611±166 yrs (cumulative weight of 0.19). In the case of the slower slip rate, channel A would only feature four events and the recurrence is much larger at 2906±660 - 3529±728 yrs (cumulative weight of 0.08).

Both the Bullock Hill and Hawdon Fault are very similar. They have the same length and show the same kinematics, are similarly orientated and in close proximity to each other. Thus, it is more likely that their slip rate is also similar adding to the observation that channels A and B' are a better match. This means, the Bullock Hill fault is again a small fault that appears to have had a rapid slip rate in the Holocene.

2.6 The Og-Gog-Magog Fault

The Og-Gog-Magog Fault is another short fault running along the southwestern slopes of the hills Magog, Gog, and Og for 3 km. The fault strikes 305° and dips NE into the hillside. It offsets channels on Og (Fig. 2.12A) and exhibits a clear fault scarp along Gog and Og (Fig. 2.12B) indicating the northern side has moved down in normal sense displacement. In Magog the fault is less visible but, nevertheless, produces a scarp before vanishing in a set of alluvial fans. The fault crosses a number of streams and alluvial fans in an irregular hillside with a number of small valleys and single hilltops south and north of the fault. It is hard to distinguish whether apparent stream and fan diversions in the hillside are related to fault activity or natural formations resulting from the existing landscape (Fig. 2.12C).

At Og a clear fault offset can be seen (Fig. 2.12A). A couple of minor run-off channels conspiciously start in a line at the same elevation without catchments to supply them. The line is visible by a change in hillside dip: the lower part with the incisions is steeper than the upper

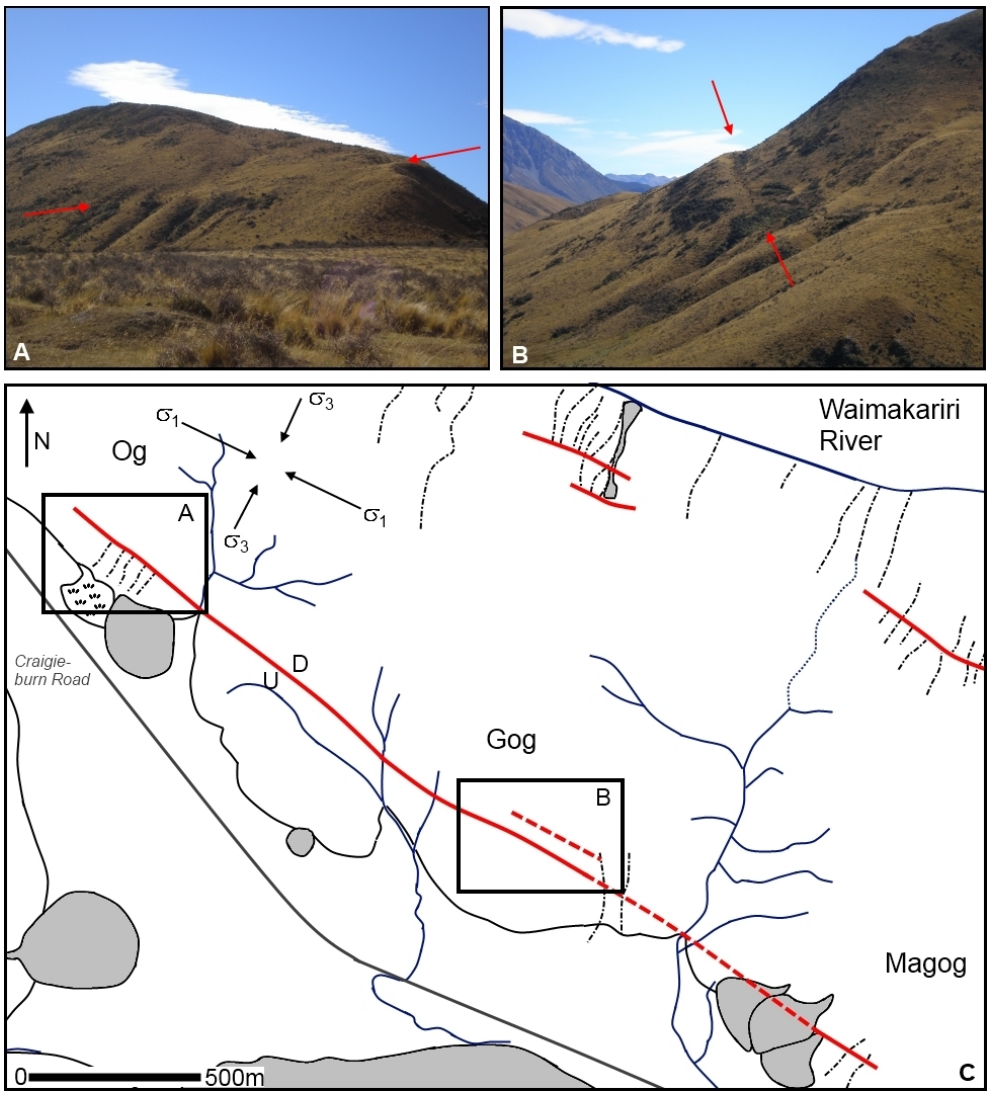

Figure 2.12.: **A** Four channels on the flanks of Og that start incision at the fault scarp (delineated by arrows) and have no upper counterpart indicating normal movement. Picture viewing north. **B** Fault scarp (delineated by arrows) running across the southern flank of Gog. Picture viewing NW from Magog. **C** Map view of the Og-Gog-Magog hills showing significant landmarks and fault exposure. Principal stress is 115±5 (Sibson et al., 2011). (43°03'S 171°48'E / 43°05'S 171°50'E)

part indicating a change in underground material, possibly from bedrock to morainic deposits. No displacements were measured since there are no recognizable features defining the original source for the streams. At the foot of the channels ponding occurs.

Across Gog the scarp is easily distinguishable (Fig. 2.12B) but has no obvious offsets beyond the 2-3 m wide scarp. The fault is invisible in the valley and runs through a complex alluvial fan on the slopes of Magog. The fan seems to split into three separate fans compared to the simple forms observed (Fig. 2.12C bottom right corner). It looks as if the main runoff-channel is diverted to the West, thus seemingly splitting the fan in two separate features. The fans lie on top of what appears to be older fan remnant indicating a change of the deposition area in the Holocene. Inferring the fault between the scarp in Gog and another scarp in Magog, the trace runs through the upper part of the fan where the channel bends SW again. Thus, it looks like the fault has caused the stream divergence and offset the fan during its formation, although no true offset could be observed. The scarp itself reappears covered by vegetation for 200 m before

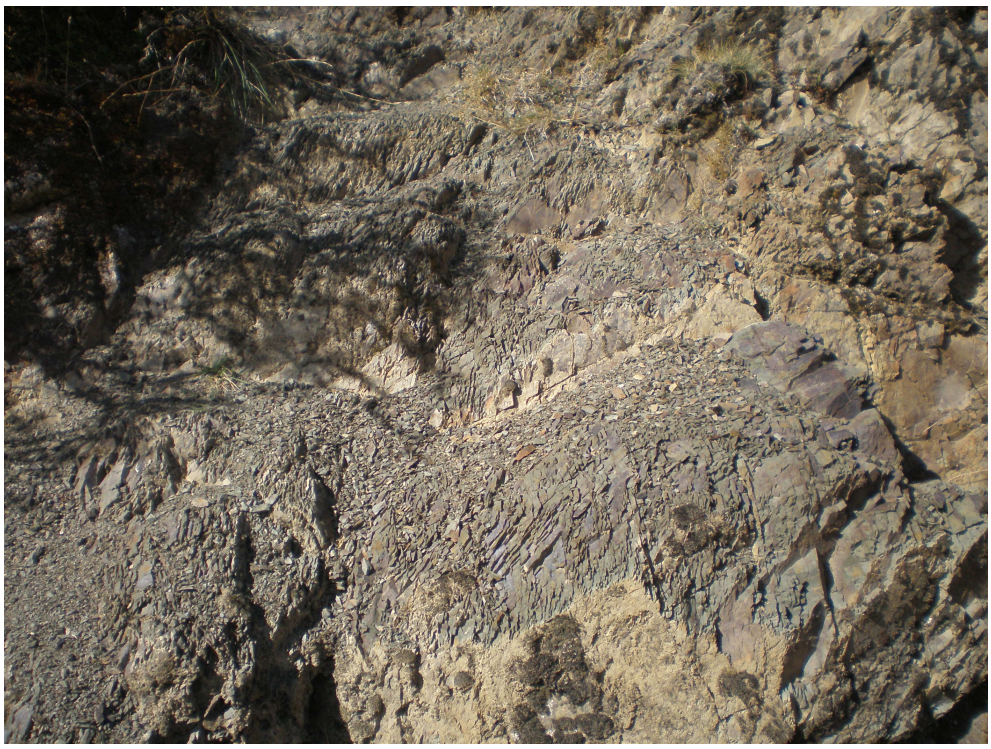

Figure 2.13.: Torlesse greywacke on the slopes of Magog being heavily sheared and partly transformed into schist, oriented at 310/70.

vanishing. Again, a swamp has formed at the foot of the hill. Outcrops atop the fault show heavily fractured and sheared bedrock with an internal foliation of 310/70 (Fig. 2.13).

All three hills were completely covered by ice during the Blackwater advances (Gage, 1958) and the valleys formed during the retreat, leading to the outwash plains south. Therefore, all channels and alluvial fans must have formed post-glacial and the fault has been active in the last 20 ka. The fault stands out as being a NW-SE orientated normal fault in an area full of NE-SW reverse strike-slip faults. Its normal movement are compliant with a regional stress field, where the maximum compressional stress is 115±5° (Sibson et al., 2011).

A similar configuration surfaced in the recent earthquake sequence in Canterbury. While the Greendale (mainshock 4/9/10) and Port Hills Fault (mainshock 22/2/11) are W-E/WSW-ENE trending showing some reverse and predominantly dextral movement (Quigley et al., 2010, GNS Science, 2011b), the June 13, 2011 earthquake occurred on a NW-SE trending fault at the eastern end of the Port Hills Fault and had sinistral movement (GNS Science, 2011a). Another NW-SE trending fault is the west segment of the Greendale Fault (Quigley et al., 2012). These provide potential analogues for the Og-Gog-Magog Fault.

2.7 Other faults

Beyond those four relatively large faults a number of smaller faults, unnamed in this study crop out in the field area. Many of them are less than 1 km of length and show no significant offset (less than 1 m), though, a couple of them seem to be active based on seemingly Holocene offsets.

The first set of fault comprises those that are associated with the Esk fault and probably less active as they show no offset of Quaternary features. The geological map of Gregg (1964) shows a second strand of the Esk fault (western Esk Fault) originating from the Torlesse Fault

west of the main strand that crosses the eastern flank of Broken Hill striking north. The fault then turns to strike NE at the foot of Mt St Bernard and crosses the Craigieburn Range parallel to the Esk fault. Reaching the Waimakariri River the two faults are only 700 metres apart and start connecting by a number of cross-cutting faults before becoming a single fault at Brechin Burn. However, these faults have not been thoroughly examined in this study and only the western Esk Fault has been observed once as a scarp in Broken Hill. Nevertheless, thrusting of post-Eocene age can be observed at the Broken and Waimakariri River, where Torlesse bedrock overrides Eocene Iron Creek Greensands. No recent offsets have been found while mapping the moraine deposits in the Winding Creek Valley.

Similar bigger faults (i.e. the Avoca Fault) have been described by Gage (1970) between the two Esk strands and are part of the wider fault zone at this locality since they do not extend beyond and are either similarly oriented or crosscutting. A similar scenario occurs at the shore of the Waimakariri River opposite of the Esk River mouth. A similar crush zone with a lesser extent than the one at Slovens Stream crops out on the shore displaying a number of small parallel faults within the bedrock.

The second set of faults contains a group of small-scale faults mostly visible through scarps in the hillside in the vicinity of the Hawdon and Bullock Hill faults. Three of them can be seen in Fig. 2.3 and Fig. 2.12. The hill Magog exhibits a second fault scarp of a 500±100 metres length on its eastern flank perpendicular to the Og-Gog-Magog Fault and possibly in connection with the Bullock Hill Fault. On the other side of Gog and Og, where the hills fall steeply along the shore of the Waimakariri River, two faults are dextrally offsetting runoff channels and landslide deposits. These faults might be connected to another fault on the northern flank of Magog. This second set seems to be active since they offset Holocene features, though to a lesser extent than the Hawdon and Bullock Hill faults.

2.8 Geomorphology

2.8.1 Rivers

A quantitative approach to the response of rivers tectonic activity are investigations of the Sinuosity Index and Stream Gradient Index. The Sinuosity Index (SI) is the ratio of the stream length between two points and the linear distance between the points. The increase and decrease of the SI along an axis of uplift can be attributed to tectonic activity. It has been used to detect folds, in which case the SI increases on the side, where the slope gradient decreases, and decreases distinctly, where the slope gradient increases again (Litchfield et al., 2003). In this study the Slovens Stream is analysed as its course runs by all the major faults in the area, crossing some and being possibly diverted by others (Fig. 2.14). Intervals for the SI were 1, 2, and 3 km, however, none of them show any anomality in their sinuosity. The SI of the whole stream is 1.3 and related to the pre-existing landforms. No fault-related folding seems to be apparent from the Slovens Stream's sinuosity.

The Stream Gradient Index describes the longitudinal profile of a stream and its changes in slope (Hack, 1973). It is used to identify knickpoints in the system, which can result from climate, sediment load, entry of large tributaries, lithology and tectonics (Bull, 1991). The Stream Gradient Index in this study is a ratio of the Gradient Index of each individual segment (GI) and gradient of the whole stream (K), using the formulas of Hack (1973):

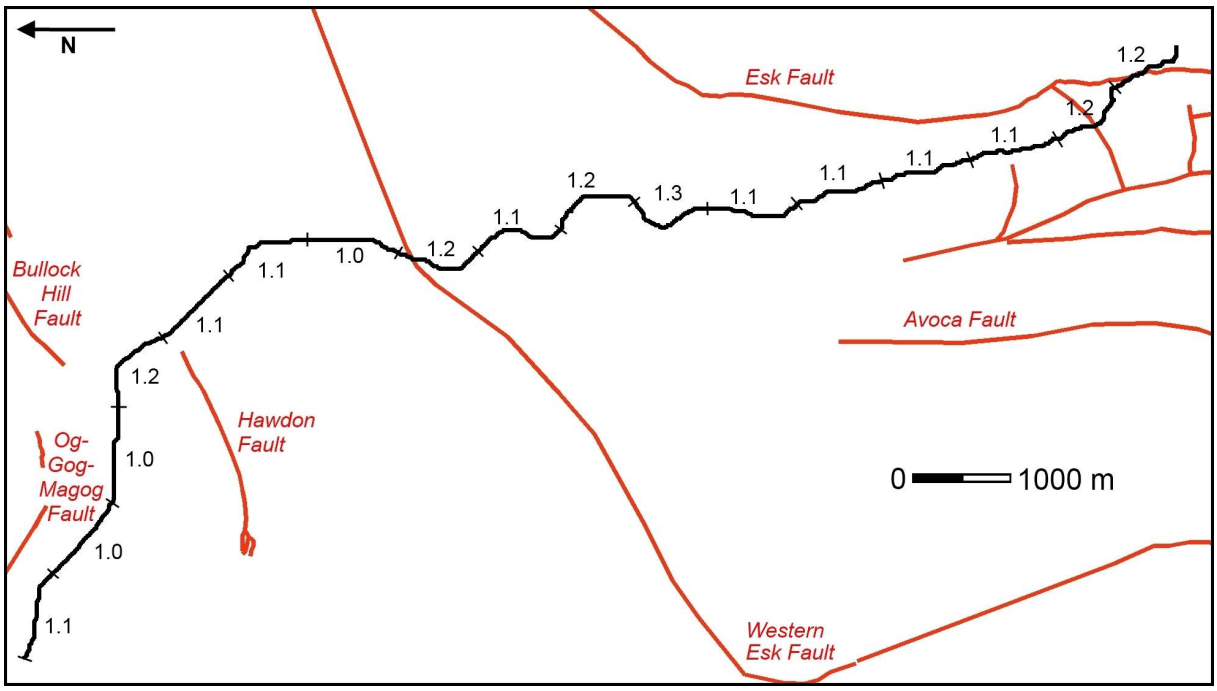

Figure 2.14.: The course of the Slovens Stream and its corresponding Sinuosity Index along each kilometre of the stream. All SI values are below 1.3 and there is no marked anomality. (43°05'S 171°52'E / 43°12'S 171°48'E)

$$GI = \frac{\Delta H * L}{\Delta L} \tag{2.2}$$

$$K = \frac{\Delta H_T}{\ln L_j - \ln L_i} \tag{2.3}$$

ΔH is the difference in elevation between the segment ends, while ΔL is the length between the two ends and L is the length of the stream from the drainage divide to the centre of the segment as seen in Fig. 2.15A. ΔH_T is the difference of elevation of the whole river with L_i being the length of the stream from the drainage divide to the centre of the segment and $L_j$being the length of the stream from the centre of the segment to the mouth (Fig. 2.15A). The knickpoints can be identified by sudden changes in gradient, that are generally above 0.5 but can be lower depending on the profile. An example of the gradient indices and identified knickpoints of the central Slovens Stream can be seen in Fig. 2.15B. The stream profile is rather atypically convex due to the abrupt change from glacial gravels to crushed and faulted bedrock in the lower reach.

In this study the profiles of nine streams (Broken River, Winding Creek, Slovens Stream, Broadleaf Stream, Poulter River, Boundary Stream, Esk River, Grant Stream, Brechin Burn) that run through the field area and across the identified faults have been examined after being extracted from a digital elevation model (DEM) in ArcGIS. The horizontal accuracy of the DEM was 25 m. From all elevation points I extracted the ones at twenty metre intervals as if using contour lines with a twenty metre distance and the start and endpoint of the profiles in order to avoid values of zero. These points of elevation and their corresponding distance along the stream was then used in the formulas of Hack (1973) and used to plot a simplified stream profile (Fig. 2.15. Knickpoints were identified by calculating and comparison with the profile and then plotted back into ArcGIS (Fig. 2.16).

Due to the small area, climate changes can be excluded from the list of knickpoint origins. All

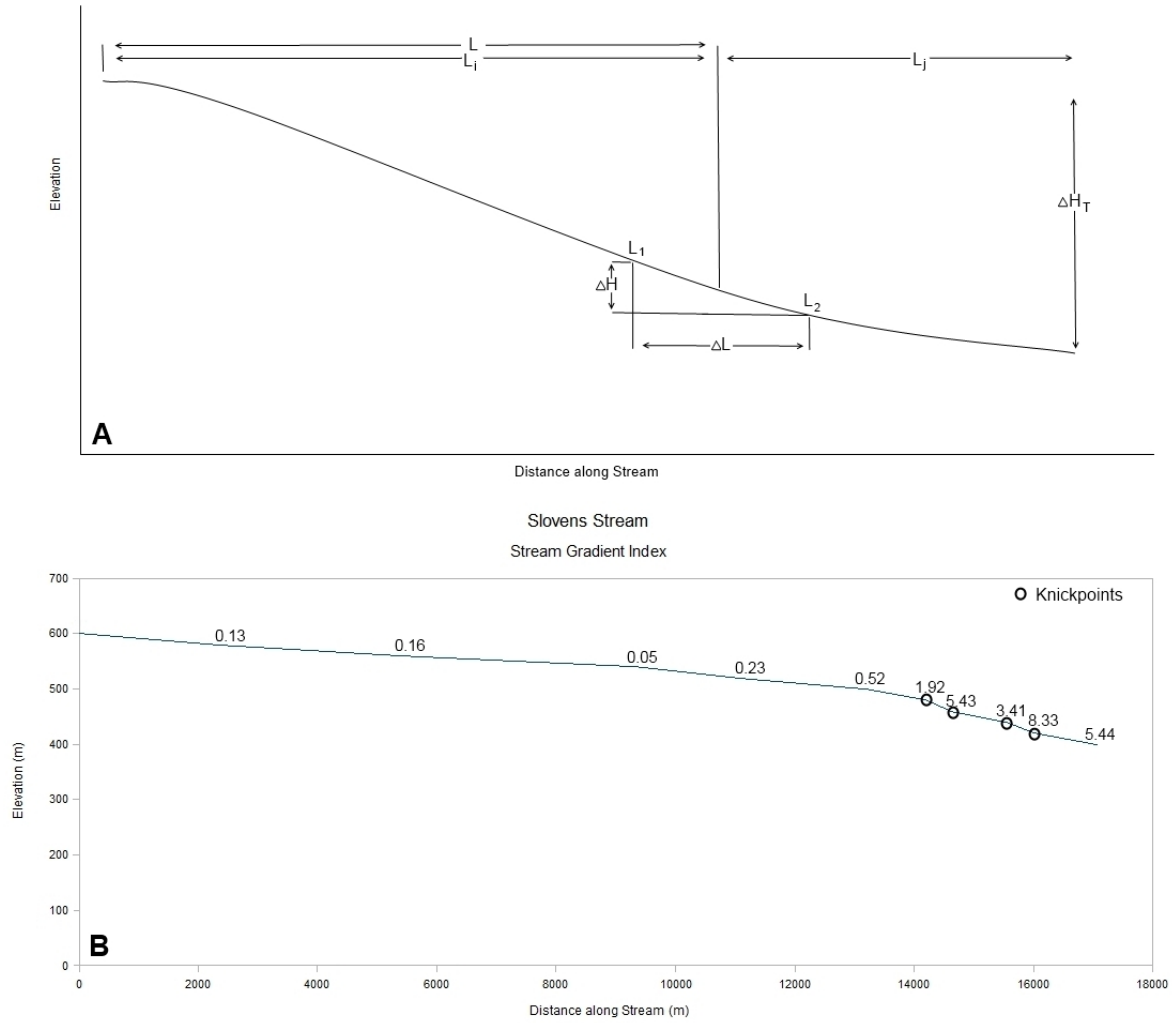

Figure 2.15.: **A** Measured parameters used to calculate the gradient index. Formula and symbol explanation is in the text (after Hack, 1973). **B** The longitudinal profile of the Slovens Stream as an example, labelled with the Stream Gradient Indices of each segments and the identified knickpoints, where sudden changes occurred.

other factors have to be taken into account when looking at each knickpoint. The entry of large tributaries can normally be ignored when it is possible to just use tributaries of the order 3 or less. That would have left the study with five streams instead of nine. Other knickpoint origins are a change in sediment load or lithology. Normally only bedrock rivers are used to rule out the change in sediment load, but that would have reduced the data set. Thus, sediment load and lithology changes are taken into account and checked on a point-to-point basis.

Two knickpoints in this study are situated directly on faults or on projection of faults intersecting with the streams. That does not mean that only these two are related to fault activity. Instead other knickpoints will have migrated upstream after the events that caused them. A necessary prerequisite for a fault related knickpoint origin is, therefore, that a fault has to be located further downstream. Some knickpoints such as the ones in the Broadleaf Stream are downstream from the mapped faults and are either either related to unmapped faults or othere origins such as changes in lithology and sediment load. The full datasets and river profiles can be seen in the appendix.

Waimakariri River: This first order river is 170 km long descending more than 1000 m and

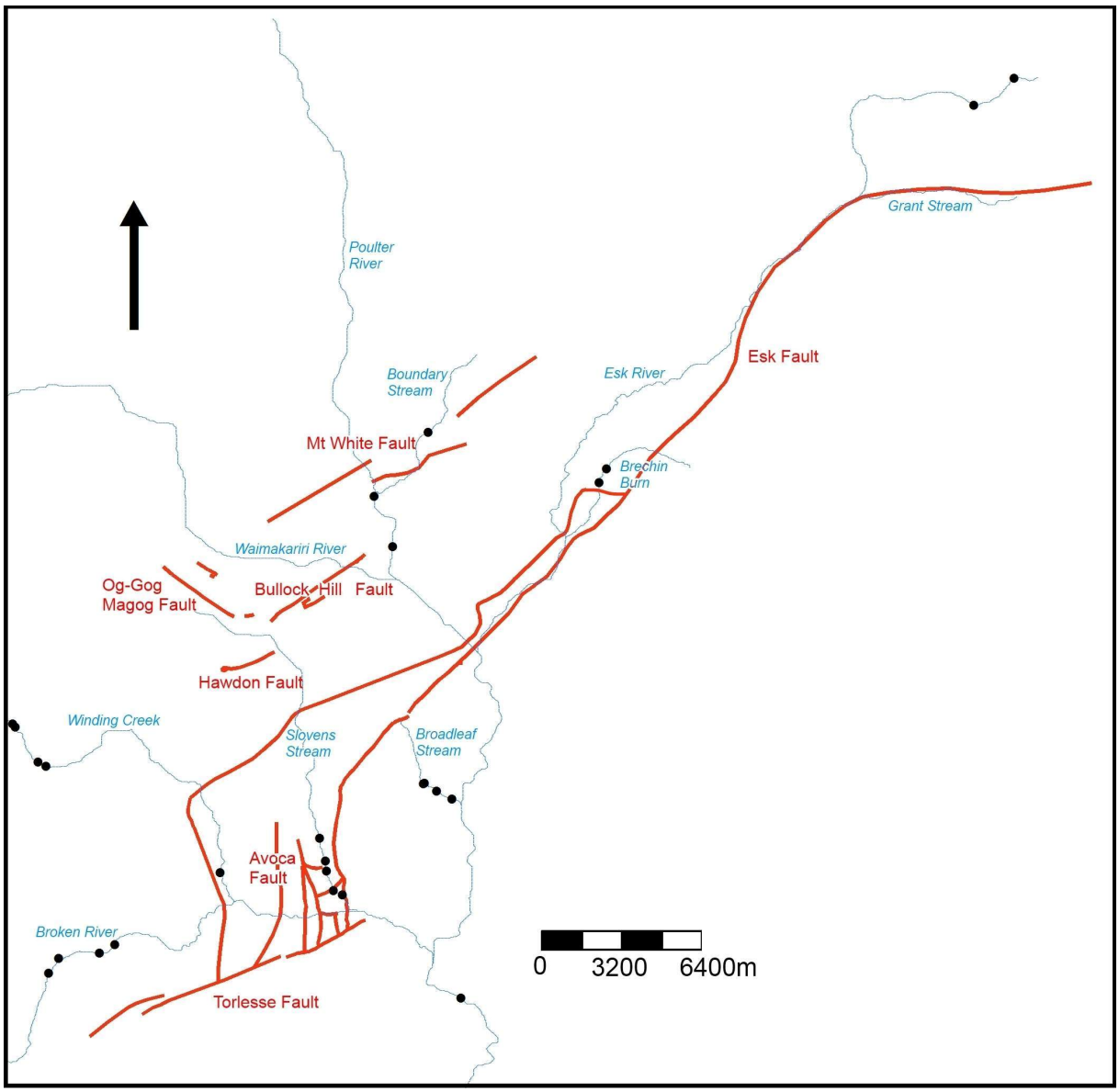

Figure 2.16.: A map showing the knickpoints (black dots) of the examined streams in the study area. Map created by using ArcGIS. No connection has been drawn of the knickpoints as there are too few streams to align them properly. (42°53'S 171°46'E / 43°13'S 172°12'E)

flowing directly into the Pacific Ocean. In this study I only looked at the part that crosses the study area spanning an elevation change of merely 200 m. The stream gradient index has been surprisingly stable despite a number of faults crossing and large tributaries entering. In the field area the Waimakariri is mainly an alluvial river but turns into a bedrock river after crossing the Esk Fault and cutting the Carrington Gorge.

Broken River: The Broken River is a second order river with a normal concave profile flowing from 960 m to 360 m over a length of 32.7 km, where it enters the Waimakariri River. Its knickpoints are in the upper reaches at 900 and 800 m and in the middle of the stream around the 600 m mark. The Broken River is an alluvial river transporting sediment from the extensive fault zone of the Torlesse and Esk faults. The lower knickpoints can be related to the fault zone between the two Esk strands and the smaller faults inbetween such as the Avoca fault, while the upper knickpoints might be from tributaries or the crossing Torlesse fault.

Winding Creek: A third order river, the Winding Creek flows through the Flock Hill Valley

over 17.2 km ranging from 976 to 476 m joining the Broken River. In its upper reaches the Winding Creek runs through glacial gravels having an alluvial character, while in its lower reaches it turns into a bedrock river cutting through Torlesse basement. The Winding Creek is crossed by the western Esk fault. However, its knickpoints are a long way from the fault, which might be a sign, that the fault has been active in early post-glacial times but inactive thereafter or simply a response to the sediment load and unrelated to any fault activity. One knickpoint past the fault is probably related to the change in lithology when the river flows from glacial gravels through bedrock.

Slovens Stream: The Slovens Stream, a third order river flowing into the Broken River, covers a distance of 17.1 km and an elevation change from 600 to 400 m. Not only the length is similar to the Winding Creek but also its change in bed lithology from glacial gravels to Torlesse bedrock. A peculiar thing about the Slovens Stream is its convex form with a very gentle dip at the beginning and increasing steepening at the end. There are no knickpoints in its upper reach where the Hawdon Fault would cross it, instead all knickpoints are concentrated in the fault zone of the Esk Fault, where the river cut in after the glaciers retreated that blocked the way south (Gage, 1958). The knickpoints are likely related to either the change in lithology or the activity of the Esk fault. A fault relation is not favoured as it seems that the main reason for the gradient change is the incision after the glacier retreat.

Broadleaf Stream: The Broadleaf Stream is a short second order river with a length of 5 km and an elevation range from 636 to 399 m. Its path leads almost entirely through glacial deposits before it discharges into the Waimakariri River in the Carrington Gorge. Its knickpoints are downstream of the Esk fault, therefore not related. A possible origin could be a lithology change from the glacial gravels to the Torlesse basement of the Gorge.

Poulter River: The Poulter River is another second order river with a length of 26.5 km and a small elevation difference of 178 m. It is, therefore, a low gradient dipping river running through glacial gravels from the Poulter Advance without cutting into bedrock. Its consistent profile, behaviour and lithology makes the two knickpoints just upstream from the Bullock Hill Fault intriguing. The lower knickpoint could even be on top of the BHF if the fault were to be extrapolated. It is, therefore, very likely that they are of tectonic origin.

Boundary Stream: A tributary from the Poulter River with a length of 8.5 km starts at an elevation of 920 m and enters the Poulter River at 460 m upstream from its knickpoints. The Boundary Stream cuts deep into the glacial gravels and the basement underneath and shows knickpoints in its upper reach which might result from activity on the Mt White Fault which crosses just downstream of the points.

Esk River: The Esk River is a second order river with a length of 42.1 km which descends from 1176 to 419 m. It is another alluvial river and the Esk Fault as well as its western strand run parallel to and through the riverbed. Thus, it is not surprising that the identified knickpoints are in the upper reaches of the river after the fault crossed the river to run along Grant Stream instead of further following the course of the Esk River. Whether the knickpoints result from displacement on the Esk fault or another reason is unclear due to its location far outside the field area.

Grant Stream: The Grant Stream is a third order tributary of the Esk River which has a length of 7.1 km ranging from 998 to 757 m. It flows along the EW striking part of the Esk River and has probably cut into its location due to the fault. The stream profile has a typical

Figure 2.17.: Possibly paired terraces along the Esk River mouth. The Esk Fault runs through the riverbed and is invisible on the surface dipping towards the East (right side in this picture), but the elevation difference suggests post-glacial activity. In this case the eastern terraces would have been uplifted by 20-40m.

shape with no gradient changes and, therefore, no knickpoints.

Brechin Burn: The Brechin Burn is another third order tributary of the Esk River with a length of 7.8 km flowing from 860 to 489 m. The Brechin Burn appears to be a bedrock river but lies outside of the field area. It is crossed by the Esk Fault and the western strand, however, and shows two knickpoints upstream of the western strand which possibly result from tectonic activity.

2.8.2 Terraces

Along the Waimakariri, Poulter, and Esk River fluvial terraces can be found that formed after the retreat of glaciers when the rivers were cutting their way south (Gage, 1958). The terraces at the mouth of the Esk River are on two different sides of the Esk Fault with the eastern terraces on the hanging wall generally higher than the western terraces on the foot wall (Fig. 2.17). Glacial gravels from the second Blackwater Advance, 21-23 ka ago (Fitzsimons, 1997), have been deposited on the upper terraces on both sides of the river, but no dating has been done to constrain the ages of each individual terrace. Elevations of the terrace have been established by use of Google Earth and photos have been used for further characterisation.

Fig. 2.18 shows a cross-section of the terraces and possible pairings based on cliff erosion and surface cover. Terrace 1 and 2 are separated by a 3 m high terrace riser that is less eroded than

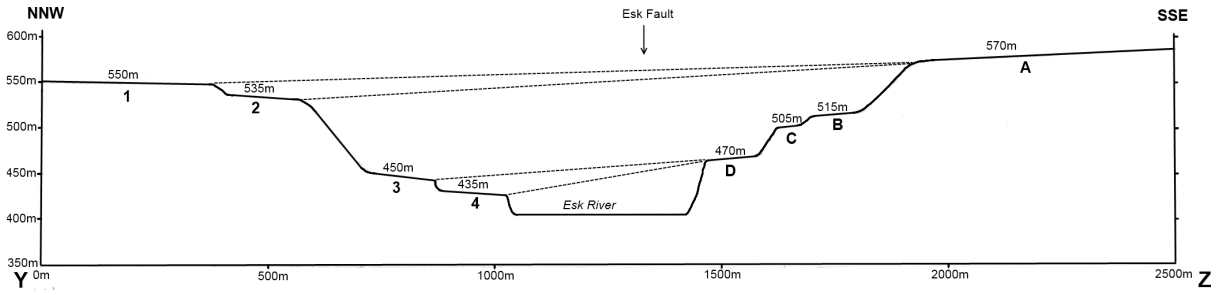

Figure 2.18.: Cross-section YZ of the Esk River from NNW to SSE (YZ in fig. 2.17). Location and extent of the terraces along the profile are extrapolated and are not in accordance with true terrace width or location. Terraces 1 to 4 are on the western shore of the river and terraces A to D are on the eastern side. Possible pairings of terraces are marked with a dashed line: these pairs are 1A, 2A, 3D, and 4D. Terraces B and C seem to be unpaired single terraces. All terraces have been formed after the second Blackwater Advance with material of the advance deposited on both sides of the river (Gage, 1958,Gregg, 1964, Forsyth et al., 2008). Vertical exaggeration 2x

the cliff of terrace 2. The western Esk Fault has been mapped on terrace 2 (Forsyth et al., 2008) and this riser might be a result of faulting. There is a 85 m difference between terrace 2 and terrace 3, and another 15 m difference to terrace 4. The risers of terrace 3 and 4 is a lot less eroded than the terrace 2 riser. On the other side, terrace D shows a similarly edged riser, being a match for either terrace 3 or 4 (3D and 4D in fig. 2.19). Terrace C and D are separated by a 2 m high terrace riser and both show moderate cliff erosion that does not match any terrace on the western side of the river, while terrace A has a well rounded cliff similar to terrace 2 (2A in fig. 2.19). As terrace A and terrace 1 are the highest terraces on their respective sides and assuming no faulting has occurred in terrace 2, they are another possible match (1A in fig. 2.19). In order to prove the proposed pairings, dating needs to be done of the terrace surfaces. However, since this was beyond the scope of this study, I used a logic tree approach to establish faulting data (Fig. 2.19).

Without further field work and dating it is impossible to say whether the terraces are paired and offset or unpaired, therefore, they have been given equal weighting. If they are unpaired, it is impossible to distinguish fault activity in the absence of age dating. In the case of paired, offset terraces, there are essentially four possible scenarios depending on how the terraces 1, 2, and A and 3, 4 and D are paired up. The scenarios with the pair 1A have been given a low weight as the erosion progress of the cliffs do not quite match up as well as 2 and A. Both cliffs of 3 and 4 would be a match with terrace D, so the scenarios have been given equal weight. These pairs lead to the following scenarios: all terraces are offset by 35±5 m (2A, 4D) or by 20±5 m (1A, 3D), or the upper terrace has been displaced by 35±5 m while the lower terrace has been displaced by 20±5 m (2A, 3D). The fourth pairing (1A, 4D) is illogical, as it would feature the upper older terrace being offset less than the lower younger river terrace.

We know from Fitzsimons (1997) that the second Blackwater Advance was between 21 and 23 ka (errors not given in Fitzsimons, 1997). Since the upper terraces all show deposits from that advance they must have formed after the glacial retreat. The larger the total displacement the more likely it has accumulated over a longer timespan. Therefore an older age is favoured for a total vertical displacement of 35±5 m than for a total displacement of only 20±5 m. Assuming an age of 10 ka or less is difficult as there is no apparent reason why the fault did not move for more than 10 ka but still exhibits such a large displacement. Average displacement is mainly

based on the one event measurable at the Blackwater Lake which had a 3.4±0.2 m displacement. Since this might be a large displacement and not representative for average displacement smaller and larger displacements have been taken into account with less weighting.

Using the previous described weighting, the following parameters have been established as the most probable. It does not matter whether the terraces are offset by the same amount (2A-4D) or different amounts (2A-3D). Both have a maximum displacement of 35±5 m since terrace formation. A continuous displacement over 20±2.5 ka then leads to a vertical slip rate of 1.75±0.47 mm/yr (cumulative weight 0.14). Assuming an average displacement of 3.4±0.2 m the recurrence interval is 1944±636 years with either ∼10 events on both terrace pairs (2A-4D) or ∼10 events on the upper terrace and ∼6 events on the lower terrace (2A-3D, cumulative weight 0.06).

For the less likely case of a maximum displacement of 20 m for both terrace pairs, the slip rate would be 1.00±0.38 - 1.33±0.56 mm/year (cumulative weight 0.03), with the same average displacement as above and a recurrence interval of 2551±1215 - 3401±1478 years (cumulative weight 0.01).

2.9 Discussion

2.9.1 The use of geomorphology in assessing the fault activity

Litchfield et al. (2003) used geomorphology and mapping to detect small-scale faults in the Canterbury Plains. Although no additional faults were found in this study using geomophic indices additional supporting data was acquired. Especially in regard to fault displacement geomorphic markers became essential due to the lack of geologic markers. Geomorphic markers are useful to depict recent activity as many landforms have a relatively short lifespan compared to geologic formations. The longest living geomorphic markers are terraces if they are uplifted instead of eroded and if dated they provide an excellent time constraint for tectonic activity. Dating of the terraces along the Esk River combined with the elevation comparisons can eventually prove its activity where the dynamic river bed extinguishes any evidence of the fault itself.

Landslides and alluvial fans are less useful in depicting the activity. Although alluvial fans can be displaced like terraces, the displacement is easily eroded if the fan is still active, while landslides are more in relation to specific events, thus being useful time constraints on single events rather than longtime records of a fault's activity. The other problem with landslides is that landslides are not ubiquitously related to tectonic activity and may occur due to rainfall and progressive slope weakening or undercutting. It is therefore hard to prove if a particular landslide, such as the one on top of the Poulter terraces, is related to rainfall-triggered slope collapse or the fault beneath or next to it.

Rivers, however seem ideal for active tectonic geomorphology since they react almost immediately to any disturbance in the system as shown by the active migration of braided rivers in response to the Darfield earthquake in 2010 (Duffy et al., 2012). In the case of the study area they are even better indicators since their geometry can only be of post-glacial age. Any change is, therefore, attributed to a recent event. This is most visible in the above knickpoint identification. Although the study area is too small to connect knickpoints with each other, which would mimick young faults, as it has been done by Litchfield et al. (2003) they still

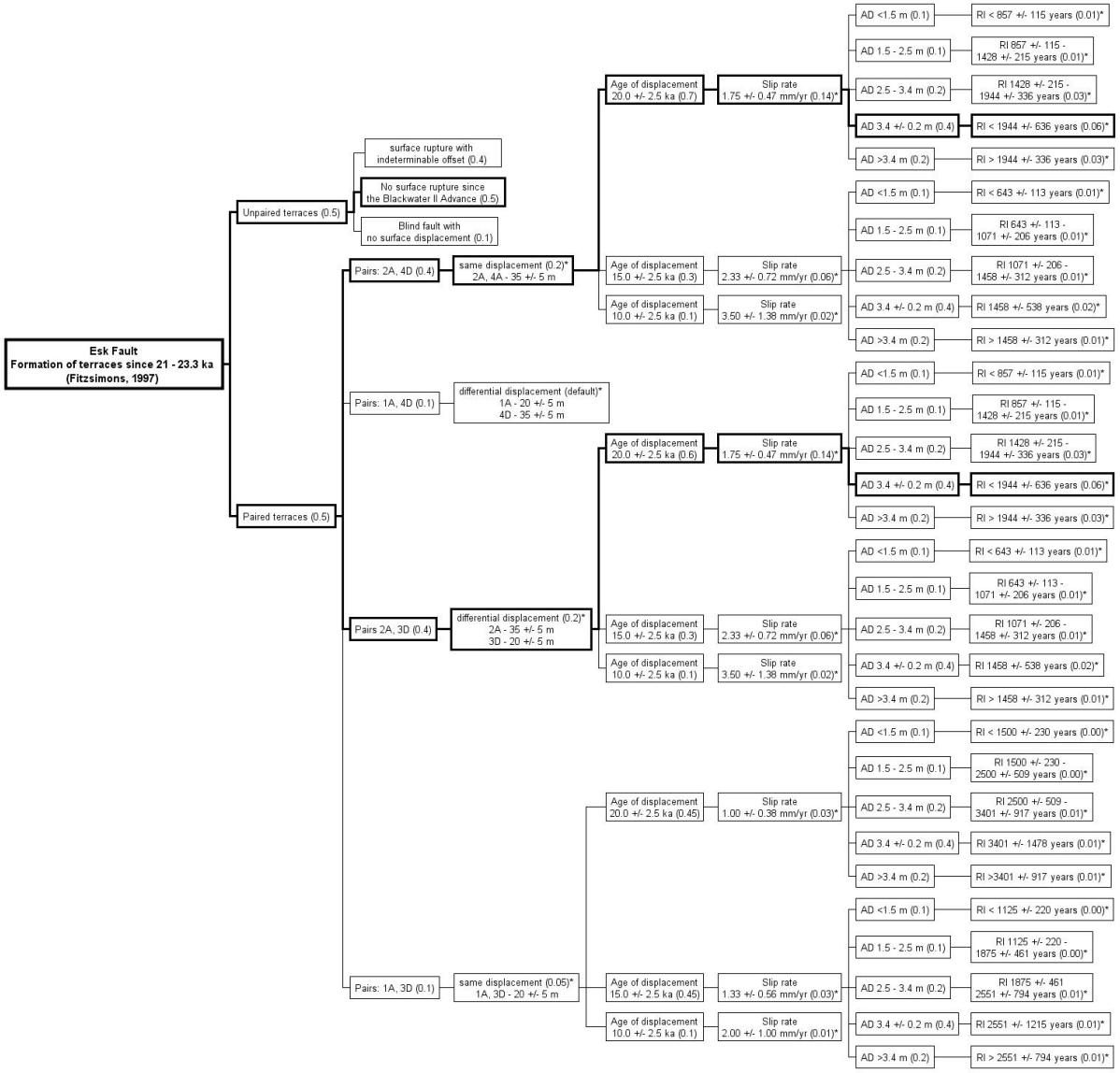

Figure 2.19.: Logic tree for the Esk fault. Weights are in brackets, * for cumulative weights. Parameters which are on the same level and are not subjected to further weighting, such as age and slip rate, and average displacement and recurrence interval show both, individual weighting of the branch and cumulative weight. The most likely scenario is emphasised. Values of 0.00 are possibilities of less than 0.5% probability

strengthen the arguments for fault activity. For example, the knickpoints in the Poulter River suggest that the Bullock Hill Fault extends past the Poulter River besides being not expressed in the alluvial and glacial terraces.

The knickpoints on the Esk River and the possibly offset terraces at the river mouth hint that the Esk Fault is more active than suggested by presently discernable surface ruptures and outcrops. The location of the knickpoints, however, does not help to discern whether the main strand or western strand of the Esk Fault and their connecting faults are active. Since the Slovens Stream does not show an anomalous change in sinuosity where the western strand crosses it and gradient change probably relates to a bed lithology change, it is more likely that activity is still concentrated on the main Esk Fault. The knickpoints on Brechin Burn suggest that at least some activity is occuring on the connecting faults, presumably in order to relief the stress accumulated between the two very close fault strands.

Although the knickpoints of the Slovens Stream might be from activity on the Esk Fault due to their location it is more likely that they result from rapid incision after the retreat of the glaciers. The upper reach of the river has possibly formed earlier, but the incision towards the river mouth did not occur for a while as the way was still blocked, instead a lake has formed. Eventually the stream incised in the bedrock leaving lake deposits at the joint of Slovens and Pufffers Stream. Since the river incised later in this part than its shallow upper reach the profile shows the untypical convex profile and resulting knickpoints.

Geomorphic indices made it possible to detect fault activity where it was not detractable from geologic mapping, such as in the case of the Esk Fault, and strengthen the indication that at least the Bullock Hill Fault is an active fault. However, when the faults are small it can easily happen that no adequate geomorphic markers are applicable to the fault, as is the case for the Hawdon Fault, thus, the markers do not necessarily assist fault assessment. Instead, geomorphic indices are utilised more useful in a wider less localised area with a number of faults than in assessment of a single fault's activity.

2.9.2 Fault activity of the study area

In the classification of New Zealand's faults of van Dissen et al. (2003) the Esk Fault is classified within the lowest class (Class IIb) which equals a recurrence rate of 5000 to 10000 years, with the lowest confidence (4) and based only on subjective comparisons with similar faults. The smaller faults described herein do not appear in the Active Fault Database. In fact, the Esk Fault only crops out in the Mesozoic and Tertiary basement rocks, except at one site, where a more recent event of less than 21 - 23 ka (Fitzsimons, 1997) age could be constrained. Otherwise the fault is covered by glacial gravels or Holocene river beds, when it follows the Esk River and Grant Stream. This coverage gives the impression that the fault is rather inactive, however, the post-glacial event and the possibly offset terraces suggest otherwise. Assuming that the terraces are offset, the recurrence interval of the Esk Fault may be as short as 1944±636 years similar to the recurrence interval of the northern Esk Fault (Noble, 2011) instead of the 5000 to 10000 years suggested by van Dissen et al. (2003). The lack of surface rupture in most parts can be due to the Esk Fault acting as a blind fault in these parts, similar to faults in the Canterbury Plains which are also covered by glacial gravels (Pettinga et al., 2001).

In comparison with the small faults west of the fault line that show apparent slip rates of more than 9 mm/yr, the Esk Fault seems to be less active with a likely slip rate of 1.75±0.47 mm/yr despite being the longest structure in the area. This could be explained by a shift of activity in post-glacial times that led to the smaller faults taking up the sc of activity of the Esk Fault. Another explanation would be that the small faults are expressions of the same fault in depth with energy dissipating through the subsurface. Though this might be true and provides an explanation for the accumulated activity on the Hawdon and Bullock Hill faults, they cannot join the Esk Fault at depth as they dip in opposite directions. Based on the geomorphic and geologic mapping alone, however, it is impossible to make any conclusions about the in-depth nature of the faults.

Irrespective of the source, the amount of activity on the Hawdon Fault and possibly the Bullock Hill Fault is surprising. Both faults show off significant post-glacial displacement which is larger than displacement reported on the active Porters Pass Fault (i.e. Howard et al., 2005). However, the Hawdon Fault does not appear on the recent 1:250k scale geological maps

(Forsyth et al., 2008), although it was mapped by Gregg (1964). The fault shows a clear offset as well as fault planes in the outcropping Torlesse Formation and a defined scarp. In order to achieve 140 m offset in a maximum span of 18000 years, however, implies a slip rate that is almost a quarter of New Zealand's second fastest slipping fault, and up to three times faster than the Porters Pass Fault, in a region believed to be less active and dominated by thrust-faulting instead of strike-slip (Pettinga et al., 2001). Assuming the channels are inherited features that persisted through glacial cover a lower slip rate can be obtained which would be more in line with the sparse expression of the faults. A slip rate similar to the Porters Pass Fault of up to 4.1 mm/year (Howard et al., 2005) would mean that the channels are 34000 years of age. Using the lower end of the Porters Pass Fault slip rate of 0.9 mm/year (Howard et al., 2005) the channels would be over 150 ka old which seems unlikely given the older and more extensive glaciations (Gage, 1958, Fitzsimons, 1997).

One possibility to explain the large offset of ∼140 m is that the scarp formed by gravitational collapse. This would explain why the fault is outcropping only in the hills but not in the glacial outwash plains. In this case, fault activty is still needed to create a sliding plane along which the hanging wall will slide down for substantially more than a fault that scale would produce. However, if that is the case, the offset would be looking like a sinistral movement and not the visible dextral movement which translates the hanging wall uphill against gravitational forces. This does not exclude the possibility that the fault exhibits a combined mechanism of tectonic strike-slip movement and gravitational dip slip moving the hanging wall south, thus, imitating normal movement which does not play into the large dextral offset for previously stated reasons.

Assuming a gravitational origin for the lateral displacement it is more plausible that the movement has occurred at once or over a small time frame instead of 15000 years. A very large sediment influx into the lake would be expected from a sudden movement of that scale. Instead a number of clustered sedimentary events scattered over 15000 years have been identified in the lake core. The sedimentary events identified in the core have been interpreted as earthquake-induced sedimentary movements. Other sources could be rain-fall triggered landslides and flooding events resulting from rock weakening by fault movement and weathering by freeze-thawing. This is a considerable concern since we know that climate change occurred during the Holocene towards a warmer moister climate (McGlone et al., 2004). At the short distance of the coring site from the slope of Mt St Bernard it is not possible to distinguish earthquake-induced from weather-induced landslide deposits, but the lack of surficial landslide deposits leads to favouring the former.

The Waimakariri Valley has a number of Holocene-aged debris fans due to the closely jointed greywacke, high relief and freeze-thaw weathering (McArthur, 1987). Although rain-fall might well be the source for any of the sedimentary events, it seems unusual that there would be a lag time of ∼3000 years before the onset of any landslides. The retreat of the glacier causes changes in the stress field as well as exposes the rock to mechanical and chemical erosion which in turn leads to rock failure in a matter of decades to centuries (Allen et al., 2010).

Another contributing factor to slope stability is the plant cover. According to McGlone et al. (2004) podocarp forest was established by 13600 BP, after replacing a tundra-like grassland-shrubland. The slope was, therefore, likely more prone to failure in the first 4000 years due to the change to sparse plant cover. However, the main cluster of events occurred at a time when the slope would have been more stable due to extensive forest patches of podocarp forest whose

spores have been found in the Lake Hawdon cores by Moar (1971). On the other hand wetter conditions are needed to establish the loose sediment which would be moved in a landslide as the glaciers likely scoured the hill's surface. This would implicate an increase in the volume of the sedimentary disturbances over that period, instead of an increase only a delayed onset of activity can be discerned from the core. Furthermore, it was impossible to correlate the sedimentary events with the changes of plant cover over the entire time span, thus, failing to attribute slope stability changes and in turn rain-fall as a general trigger to the occurrence of sedimentary events in the core.

Another source could be earthquakes on the other major faults in the area such as the Porters Pass Fault. A large enough earthquake on a more distant fault could cause the slope to fail if it was already weakened by continuous fault activity such as is the case on the Hawdon Fault. There is no way to discern whether a sedimentary event in the core has been caused by an earthquake on the fault itself or further away, though it seems unlikely that the majority of the sedimentary events were induced by distant sources. The large displacement of 140 m on the Hawdon Fault itself gives evidence that many earthquakes have originated from the Hawdon Fault and not necessarily other faults. The distance of the Porters Pass Fault to Lake Hawdon makes it more likely that any sedimentary movements from relatively distant earthquakes do not show in the core the same way movements from smaller magnitude events do not seem to be present in the core.

The Bullock Hill Fault, similar to the Hawdon Fault, only crops out in the hillside but not in the outwash plains or post-glacial deposits. Even though the terrace riser is aligned with the projected hillside, the GPR survey did not show the expected fault plane with a vertical displacement of 1.29±0.20 m. Instead signs for a terrace riser with filled channels to both sides of it and possibly one or two little thrust faults can be seen which fits well with the regional stress field. The terrace riser does not reflect the displacement along the fault but only coincides with the fault trace. Furthermore, the RTK profiles across the terrace show backtilting, another sign of fault activity. Another sign for fault activity is the occurence of knickpoints along the Poulter River which are neither lithology nor tributary related but instead lie above the extrapolated fault line of the Bullock Hill Fault. In summary the fault does extend past its trace in the Bullock Hill but the geologic evidence makes it diffcult to get a clear picture of its activity and the constraints upon it.

The Og-Gog-Magog Fault is different to the other faults as it strikes perpendicular to them and does not display significant lateral movement. Nevertheless, itself and the faults parallel to it on the riverside of the faults seem to be active during the Holocence. The fault, however, is less active than the other small faults since no major displacements can be measured, though the complex terrain it crosses makes it difficult to discern fault-related diversions from landform-related ones.

What all of the smaller faults, including the Og-Gog-Magog Fault, have in common is their lack of surface trace in glacial gravels. For instance the Bullock Hill Fault offsets a post-glacial terrace but no signs of fault activity can be found in the older upper terrace resulting from the Poulter Advance. The RTK depicts the hummocky surface without visible backtilting. Nevertheless, post-glacial activity is evident, therefore, evidence of surface rupture has been removed or no surface rupture occurred similar to the blind faults across the Canterbury Plains. The glacial gravels are less compacted than other rock formations, thus, dissipating the seismic energy

instead of rupturing in a single plane during smaller events, while river activity and erosion remove evidence from surface rupture on the gravels more easily than from basement, which is sparse in the study area. In comparison, the northern Esk Fault lies in an area unaffected by glacial advances and can be followed through much more easily. An extensive subsurface study by more GPR lines and trenches would be necessary in order to analyse the behaviour of the faults in glacial gravels and only assumptions can be made here. On the Greendale Fault displacements of >1.5 m were read for slip in areas where no discrete faulting was seen on the surface (Quigley et al., 2012) which might explain the lack of surface rupture here.

2.10 Conclusion

Geologic and geomorphic mapping has revealed a number of small faults west of the southern Esk Fault that show large post-glacial displacements as well as a first assessment of their activity. The initial findings are summarised as follows:

Esk Fault: The Esk Fault is a 30±10 km long steeply East dipping fault that has thrust Mesozoic formations over Miocene to Pliocene rocks but is not visible in the riverbed of the Esk River and the glacial deposits between Slovens Stream and Waimakariri River. One post-glacial offset from a single event appears near the Blackwater Lake. Otherwise the Esk Fault exhibits little evidence for post-glacial displacements beyond a geomorphic analysis that reveals possible activity near Brechin Burn and the upper reach of the Esk River.

Hawdon Fault: The Hawdon Fault is a South dipping dextral strike-slip fault that crops out over a length of only 5 km and displays a post-glacial displacement of 140±10 m, but does not rupture through glacial gravels. There is no evidence of faulting in geomorphic analysis though only few markers are applicable to the fault. A lake at the bottom of the fault provides a timeline of events and shows clustering of activity between 10000 and 15000 BP and between 5000 and 10000 BP. The favoured post-glacial slip rate of the fault is 9.3±2.8 mm/year.

Bullock Hill Fault: The Bullock Hill Fault is another 5 km long, steeply dipping, dextral strike-slip fault with a displacement of either 20 m or 110 m over the last 12000 years since the Poulter Advance. The fault is only displayed in the hillside and two slope failures west of it, but not in the glacial gravels. A straight terrace riser in line with the fault has been shown to be only coincident with the fault but not related to it by GPR and RTK surveys. Knickpoints in the Poulter River suggest that the fault extends past the river.

Og-Gog-Magog Fault: The Og-Gog-Magog Fault is a normal fault perpendicular to the Bullock Hill and Hawdon faults that exhibits minor movement in post-glacial times. It is to small to benefit from geomorphic indices.

Other faults: A number of small-scale faults with minor displacements lie parallel to the Og-Gog-Magog, Hawdon and Bullock Hills faults and appear to be active during the Holocene. Another set of faults crop out in the exposure of basement rocks near Broken River and Waimakariri River and are most likely inactive. The western strand of the Esk Fault is probably as active as the Esk Fault itself, with connections between the faults being more active, as they relieve stress between the two major structures.

3. Paleoseismology

3.1 Introduction

The historic record of earthquakes in New Zealand (∼150 years) is short relative to recurrence intervals for any given fault. Surface ruptures and displacements of geomorphic structures represent paleo-earthquakes whose magnitudes and kinematics can be resolved through paleo-seismic studies and give a more complete picture of the fault and the hazard it poses it for the region. An intrinsic part of paleo-seismic studies is dating in order to establish recurrence intervals and last events. Depending on the suitability ^{14}C, cosmogenic or luminescence dating are used, though in many cases in North Canterbury weathering rinds are used where none of these methods is applicable (i.e. Fitzsimons, 1997). Another part of the paleo-seismic studies are scaling relationships which describe the relationships between rupture length, magnitude and displacement and have been compiled by Wells & Coppersmith (1994) and modified by a number of authors including Stirling et al. (2002) and Stirling et al. (2008) for a New Zealand based data set.

Four of major earthquakes occurred in the field area, including three M_6 events in 1881, 1888, and 1995 (GNS, Gledhill et al., 2000) and a M_7 event in 1929 (Berryman & Villamor, 2004). The 1994 Arthur's Pass earthquake outside of the field area and the 1995 Cass earthquake had no surface rupture and no allocated fault system. Instead their aftershock sequences indicate that the region has a complicated fault structure including blind faults. Thus, a study of the regional seismicity has been undertaken in conclusion with the paleo-seismic study of the previous mapped faults.

Three of the mapped faults in the study region have produced sufficient data for a paleo-seismic investigation: the Esk Fault, the Hawdon Fault, and the Bullock Hill Fault. This chapter describes the results from scaling relationships and comparisons with the regional seismicity based on the data presented in chapter 2 and leads to the conclusion that the surface rupture length of the smaller strike-slip faults do not match with the observed co-seismic slip, thus, indicating fault linkage. Assuming a large fault system instead of two small-scale faults the suggested maximum magnitude for an earthquake in the study area is about 7.6.

3.2 Methods

3.2.1 OSL dating

Optically stimulated luminescence (OSL) dating is an absolute dating method which relies on the trapping and release of energy by electrons within crystals (Aitken, 1998). The emitted light during this process is called luminescence. Exposure to sunlight constantly sets back the electrons restarting the clock. Therefore, the luminescence clock starts as soon as the deposit is sufficiently buried, starting from 30 cm below the surface.

The intensity of the luminescence released is measured as a function of total radiation dose over time. Its relation to the paleodose, which is the quantified past exposure to radiation gives the age of the sample. There are several methods to calculate the paleodose: an additive dose method measuring the luminescence emitted in the laboratory during different levels of irradiation, a regenerative method with several samples being first zeroed out and then exposed to known doses, and the partial bleach method where some samples are measured by the additive method while others are exposed to short bursts of light (Duller, 1996). In this study the paleodose was calculated using the Multiple Aliquot Additive Dose method (MAAD) based on measurements of blue luminescence from the fine grain feldspar produced during infrared stimulation (Murry & Wintle, 2000).

While taking samples in the field one has to evaluate if a bed is a suitable candidate for OSL, e.g. it has been zeroed during transport, therefore, giving a reliable date. Aeolian and suspended sediments are ideal, while sediments in mass movements and transported by bedload are less reliable. The sample is then best taken at a sufficient depth and distance from underlying beds without being exposed to light. We used a metal tube hammered into the sediment and then covered by aluminium foil in order to minimise sunlight exposure. Dating samples were taken from the middle of the tube where they would be least exposed to any light. The samples were sent to the Luminescence Dating Laboratory of the Victoria University in Wellington.

3.2.2 Seismic strain

The New Zealand earthquake catalogue held by GNS Science is complete for M≥4 earthquakes since 1964, for M≥5 since 1940, and M≥6.5 since 1840 (Stirling et al., 2001). M_3 and below earthquakes are only reported post 1990. A Gutenberg-Richter plot (Eq. 3.1) derived from all earthquakes in the study area produces a and b-values (Gutenberg & Richter, 1944) that can be used to establish the seismic moment release rate (Eq. 3.2) and seismic strain rate (Eq. 3.4):

$$\log N = a - bM \tag{3.1}$$

N is the number of events, M the magnitude. The seismic moment release rate, M_0 is derived from Johnston (1996) with t being the time span of the seismic records and M_{max} being the maximum expected magnitude in the region:

$$M_0 \approx \frac{1}{t}\left(\frac{b(10^{(a+d)}}{c-b}\right)(10^{(c-b)}M_{max}) \tag{3.2}$$

Values c and d are factors from the conversion of magnitude scale to seismic moment by Hanks & Kanamori (1979). Stirling et al. (2001) use $c = 1.5$ and $d = 16.05$ for their earthquake source parameters:

$$\log M_0 = 1.5M + 16.05 \tag{3.3}$$

Seismic strain rate, $\dot{\epsilon}_x$, is calculated after Kostrov (1974):

$$\dot{\epsilon}_x = \frac{1}{2\mu\nu}M_0 \tag{3.4}$$

μ is Young's modulus (here: 3 x 10^{11} dyne/cm^2) an ν is the volume of the crust in cm^3. The depth of the seismogenic crust in New Zealand has a maximum depth of 15 km based on

the earthquake catalogue. Calculating the seismic strain rate this way takes into account the uncertainties in a and b values, M_{max}, μ, and ν. The results give an indication of the long-term fault slip, assuming the current seismic strain is representative for the long-term strain.

3.2.3 Seismic scaling relationships

Seismic scaling relationships describe the relationships between various earthquake source parameters and have been derived from an extensive study by Wells & Coppersmith (1994). The fault-scaling regressions from Wells & Coppersmith (1994) have been updated in New Zealand by Terry Webb in unpublished, peer-reviewed studies. The currently used function for moment magnitude, M_W, was developed by Berryman et al. (2002) and published by Stirling et al. (2008):

$$M_W = 4.18 + \frac{2}{3}\log W + \frac{4}{3}\log L \tag{3.5}$$

W is downdip rupture width of the fault in km and L is the subsurface rupture length in km. The subsurface rupture length is in average 15% larger than the surface rupture length, SRL (van Dissen et al., 2003). In case where single event displacement, D, is not measured in the field it is calculated after Aki & Richards (1980), in which case A is measured in cm^2 and D is measured in cm:

$$M_0 = \mu A D \tag{3.6}$$

The relationship between M_W and M_0 was defined by Hanks & Kanamori (1979) as:

$$M_W = \frac{2}{3}\log M_0 - 10.7 \tag{3.7}$$

In order to compare the differences between the earthquake source parameters of New Zealand and other areas fault-scaling regressions were used from Wells & Coppersmith (1994), Stirling et al. (2002), Stirling et al. (2008), and Wesnousky (2008) and plotted in Table 3.1 and Fig. 3.1.

3.3 Regional seismicity

3.3.1 Large earthquakes in historic times

Two well studied earthquakes of magnitude M_W >6 occurred near the study area in 1994 and 1995 respectively. On 19 June 1994 a M_W 6.8 earthquake struck near Arthur's Pass, 25 km southeast of the Alpine Fault (Robinson et al., 1995). The Arthur's Pass earthquake showed a well defined shallow (1-10 km depth) aftershock sequence in a NNW trending zone with the two largest aftershocks (M_W 5.8 and 5.6) within the first 3 days (Fig. 3.2). However, conventional fault plane solutions, body wave and fault kinematics models were contradictory, thus, impeded by the lack of surface rupture and deformation it was impossible to assign the earthquake a fault plane, (Abercrombie et al., 2000). Arnadottir et al. (1995) proposed a sinistral NNW trending 7 km wide, 38 km long steeply WSW dipping fault zone with two deformation modes in a region best known for its right-lateral NE trending faults as their best fit model. The two deformation events suggest the northern 13 km has reverse left-lateral movement and the

Wells & Coppersmith 1994	*SS*	M = 7.04±0.05 + 0.89±0.09 log AD M = 5.16±0.13 + 1.12±0.08 log SRL log AD = -1.70±0.23 + 1.04±0.13 log SRL log SRL = 1.68±0.04 + 0.65±0.18 log AD log MD = -1.69±0.16 + 1.16±0.09 log SRL log SRL = 1.49±0.04 + 0.64±0.05 log MD	A (km^2), SRL (km), AD (m)
	DS	M = 6.64±0.16 + 0.13±0.36 log AD M = 5.00±0.22 + 1.22±0.16 log SRL log AD = -0.60±0.39 + 0.31±0.27 log SRL log SRL = 1.45±0.01 + 0.26±0.23 log AD log MD = -0.44±0.34 + 0.42±0.23 log SRL log SRL = 1.36±0.09 + 0.35±0.19 log MD	
Hanks and Bakun 2002		M_W = 3.98 + log A M_W = 3.07 + 4/3 log A	L<25 km, A (km) L>25 km
Stirling et al. 2002	*All*	M_W = 5.45±0.05 + 0.95±0.06 log L M_W = 5.88±0.12 + 0.80±0.05 log L M_W = 4.54±0.12 + 0.89±0.05 log A log AD = -0.81±0.13 + 0.56±0.08 log L	A (km^2), L (km) L> 50km L (m), AD (m)
Stirling et al. 2008	*All*	M_W = 4.18 + 2/3 log W + 4/3 log L M_W = 5.88 + 0.80 log L	 L>50 km
Wesnousky et al. 2008	*SS*	M_W = 5.56 + 0.87 log SRL log M_0 = 24.47 + 1.31 log A AD = 0.01 SRL MD = 0.03 SRL	A (km^2), SRL (km), AD (m)
	DS	M_W = 4.11 + 1.88 log SRL log M_0 = 22.64 + 2.81 log A AD = 0.06 SRL MD = 0.21 SRL	

Table 3.1.: Scaling relationships from different papers based on New Zealand and global data.

southern 25 km has purely sinistral movement.

Abercrombie et al. (2000) proposed that conversely the earthquake was a mainly reverse event with a complex source, i.e. a second strike-slip source 11 km southwest of the mainshock. It was also impossible to distinguish fault plane and auxiliary plane in the predominantly NE-SW trending focal mechanism solutions. In the case of a two-event model the first event would have been on a NW dipping reverse fault that ruptured from the NE to the SW, triggering a NNW trending strike-slip fault rupturing to the SSE. Another possibility is that the NNW trending fault activated NE trending structures such as the Harper and Bruce fault, as the largest aftershocks occurred at the southern end of the aftershock zone where the Harper Fault lies. Robinson & McGinty (2000) argued that there is no need for a second event and that the dicrepancies result from the complex velocity structure of the Southern Alps. Robinson & McGinty (2000) showed that it was possible that the Arthur's Pass earthquake triggered another event without surface rupture.

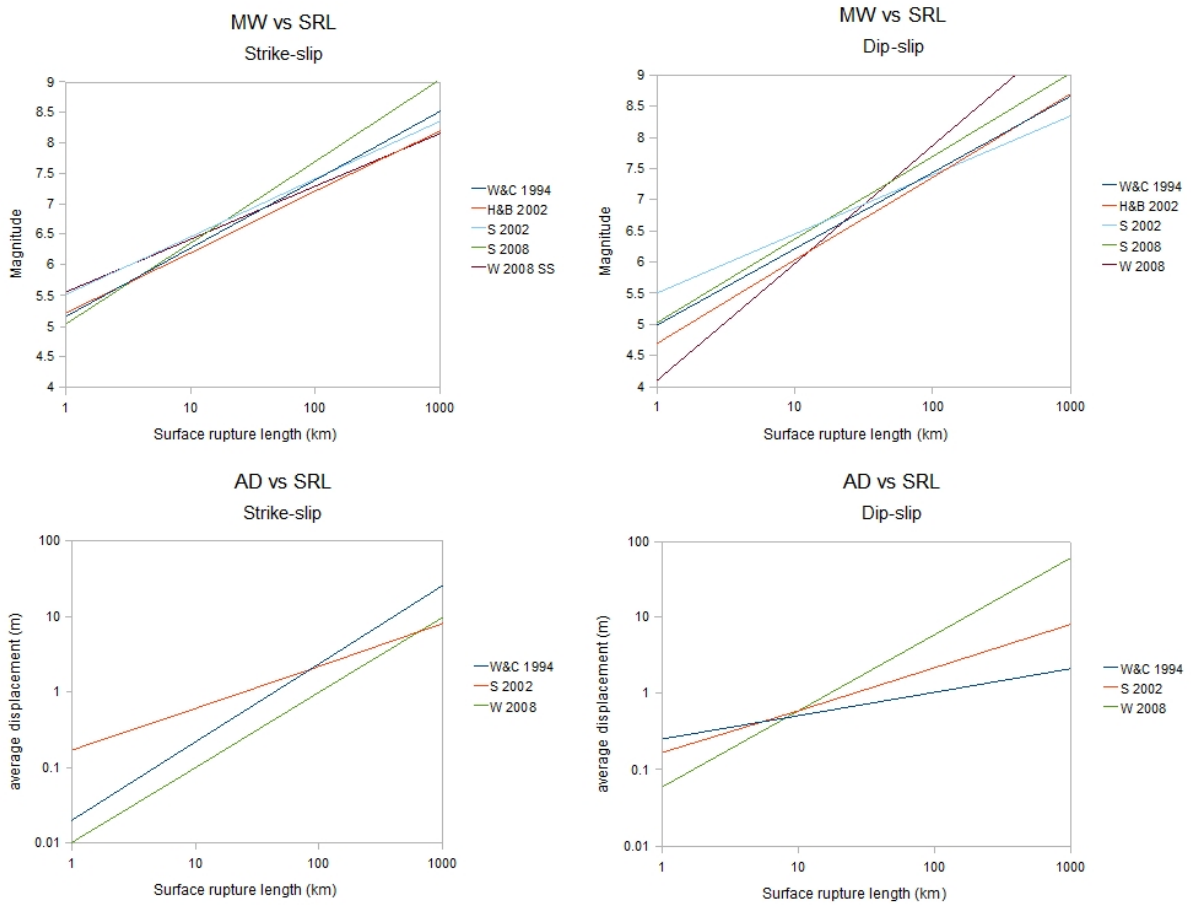

Figure 3.1.: Scaling relationships based on a typical width for the study area of 14.65 m (see Table 3.1 for regressions). W&C 1994 - Wells & Coppersmith (1994), H&B 2002 - Hanks & Bakun (2002), S 2002 - Stirling et al. (2002), S 2008 - Stirling et al. (2008), W 2008 - Wesnousky (2008). Strike-slip data uses the regression from Hanks & Bakun (2002) for faults under 25 km as it applies to the shorter Hawdon and Bullock Hill Fault, while the regression for faults over 25 km length from Hanks & Bakun (2002) is used for dip-slip comparisons.

The M_W 6.2 Cass earthquake occurred on the 24th of November 1995 just at the northwest corner of the field area. In contrast to the Arthur's Pass earthquake the Cass earthquake could be quickly resolved to a oblique reverse focal mechanism (Gledhill et al., 2000). A fault plane with a strike of 176±10° and a dip of 45±5° to the west was proposed, with the auxiliary plane resembling the Hawdon and Bullock Hill faults (fig. 3.2). The aftershock zone had a length of 12 km, a width of 3 km and a depth of up to 10 km, dipping slightly to the west and rupturing south. However, one aftershock group instead follows a band striking NE-SW, and was interpreted by Gledhill et al. (2000) as slip on small faults, possibly the Hawdon and Bullock Hill fault, that were optimally oriented in the combined regional stress field. The aftershock sequence has a b-value of 1.08±0.06, which should be noted in order to compare it to the regional distribution.

Gledhill et al. (2000) noted a peculiar observation: the deeper aftershocks similar to the main event are related to thrust mechanisms but the shallower events showed either normal or strike-slip mechanisms. The proposed theory of Gledhill et al. (2000) was that extensional strains in the hanging wall imposed by the mainshock are released by normal/strike-slip faulting. As both the Arthur's Pass and Cass earthquake ruptured on N and NNW trending faults Gledhill et al. (2000) and Arnadottir et al. (1995) brought up a model of block rotation

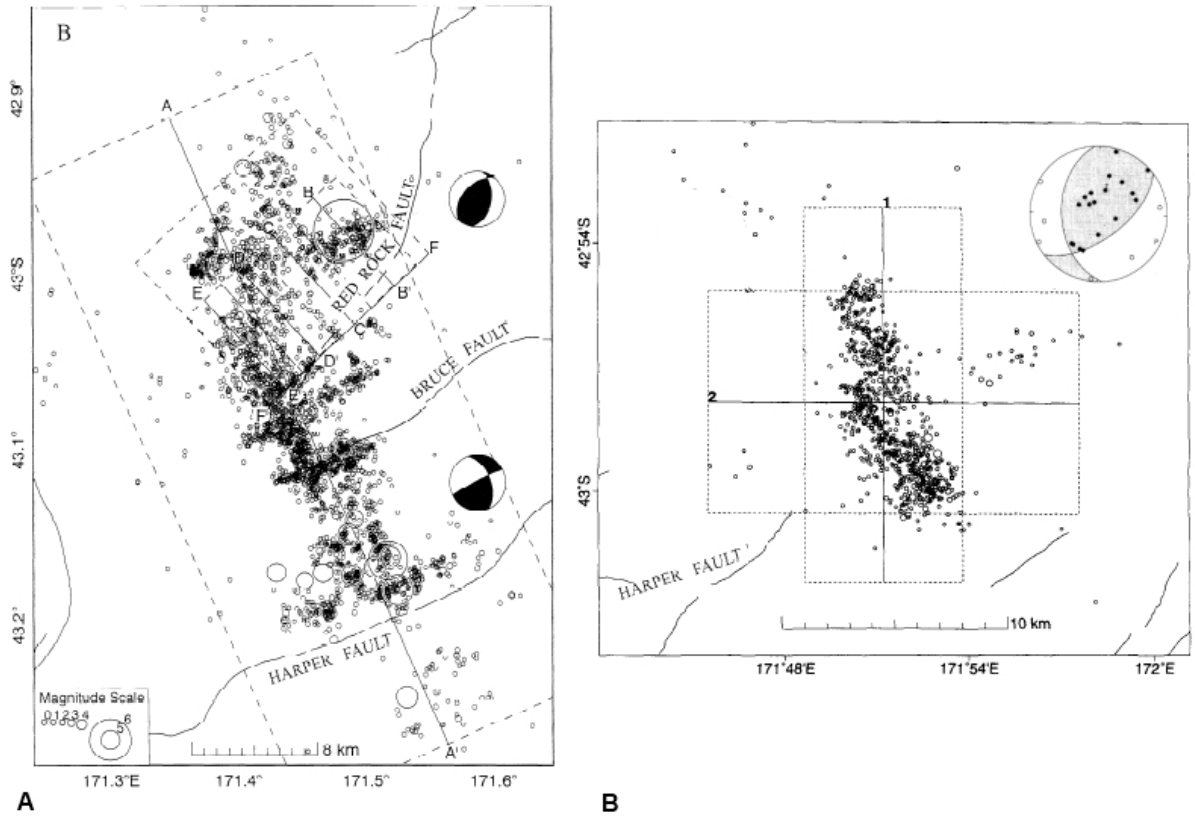

Figure 3.2.: Focal mechanisms and distribution of aftershocks of the 1994 Arthur's Pass (A) and 1995 Cass (B) earthquakes after Abercrombie et al. (2000) and Gledhill et al. (2000). Focal mechanisms are lower hemisphere projections. The faults southeast of the Cass earthquake aftershock zone are the Mt White and Esk faults.

supported by the oblique compression at the plate boundary. Both earthquakes show that the area is a complex transition zone between the northern subduction and the strike-slip of the Alpine Fault with an unknown number of blind faults.

3.3.2 Historical and Instrumental Seismicity

Monitoring of earthquakes since 1990 includes M>2.5 earthquakes with increasing completeness in the greater region encompassing all faults in this study (GNS, GeoNet; Fig. 3.3), allowing Gutenberg-Richter statistics to be derived (Gutenberg & Richter, 1944). The set region includes the Cass earthquake and its aftershock sequence (Fig. 3.3). Earthquakes below $M_{2.25}$ have been omitted from the Gutenberg-Richter plot (Fig. 3.4) and the trendline was fitted to M 2.5-5.25 earthquakes as values beyond are not representative for the time span or sufficiently represented in the earthquake catalogue. The a and b values were established using Eq. 3.1 and a recurrence interval plot was based on the 21 year period (Fig. 3.4, Gutenberg & Richter, 1944). The b-value of the Cass earthquake, 1.08±0.06 is a bit higher, albeit within error, than the b-value of the region, 1.00±0.05.

The Gutenberg-Richter statistics suggest that a M_4 earthquake occurs every year, a M_5 earthquake every 12 years and a M_6 earthquake every 115 years. This is consistent with the historical recurrence of of M>6 earthquakes, the Cass earthquake in 1995 followed 2 M_6 earthquakes

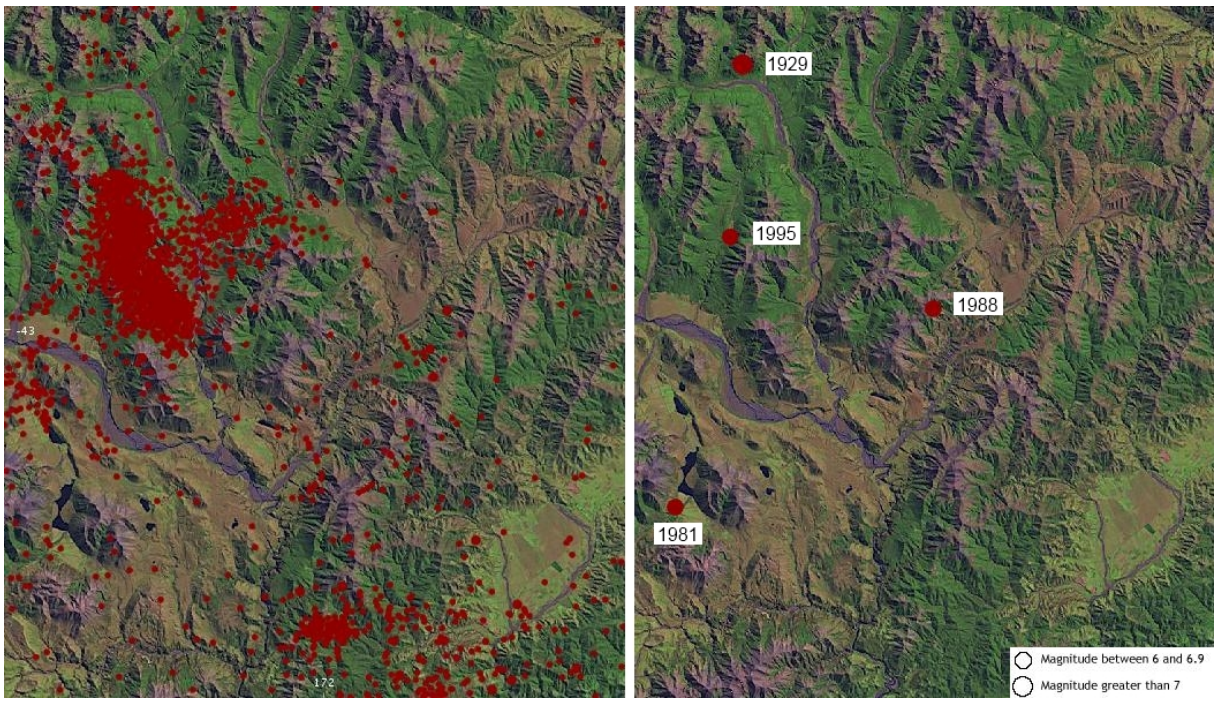

Figure 3.3.: (Left) Locations of all upper crustal earthquakes from 1990 to 11/9/2011. The region spans from 43.255°S and 171.733°E to 42.802°S and 172.253°E. (Right) All M>6 earthquakes and the year they occured in the same region. Map and according data by courtesy of GNS, GeoNet.

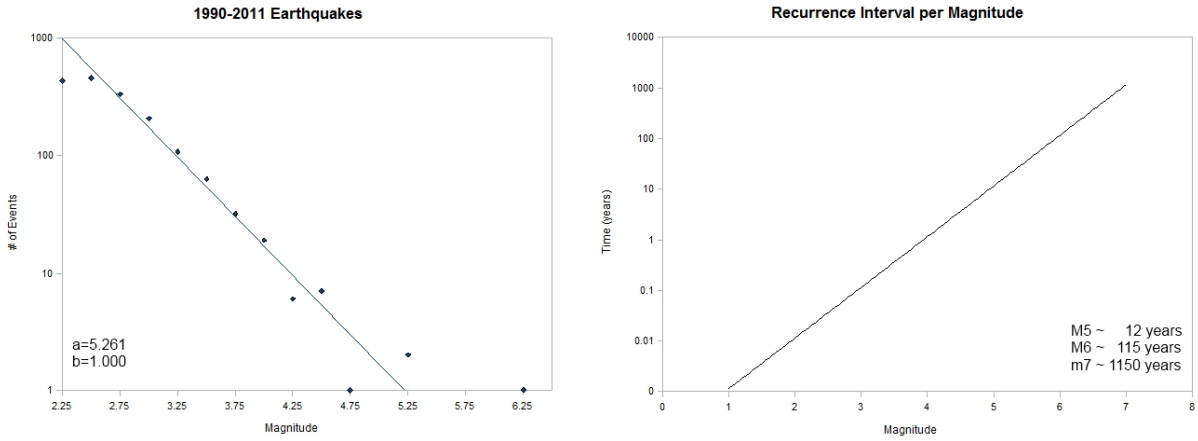

Figure 3.4.: (Left) Gutenberg-Richter plot of earthquakes with magnitudes 2.5-5.25 between 1990 and 2011. (Right) Recurrence interval/magnitude plot resulting from the Gutenberg-Richter plot of events between 1990 and 2011.

in 1881 and 1888. M_7 earthquakes are expected every 1150 years which is a shorter interval than that estimated from the Esk Fault but a longer interval compared to the Bullock Hill and Hawdon faults. The region experienced a $M_{7.1}$ earthquake on the Poulter Fault in March 1929 (Berryman & Villamor, 2004). A M_7 earthquake is therefore of a relatively low probability if these relations are indicative of long term seismicity.

Seismic moment was calculated after Johnston (1996) using c and d values from Hanks & Kanamori (1979) and using 7.2 for maximum magnitude from the national hazard model (Stirling & Gerstenberger, 2010), yielding a value of $4.9*10^{21}$ (Eqs. 3.2, 3.3). Following Kostrov (1974) and assuming a seismogenic zone of 12 km depth as most recorded earthquakes were in 12 km depth or shallower the seismic strain rate for the region, $3.4*10^{-10}$ s^{-1}, was

determined (Eq. 3.4). It is necessary to note that uncertainties in a and b values, M_{max}, μ, and depth of the seismogenic zone lead to greater uncertainties for the seismic strain rate.

The slip rate for the region resulting from the seismic moment rate is calculated over a model fault, which in this case adds up the individual faults to a length of 43 km. The seismicity in the region correlates with a slip rate of 7.9 mm/year comparable to the reported slip rates of the Hawdon and Bullock Hill faults. As these values only reflect seismicity since 1990 and includes two large (M>6) earthquakes discrepancies can be a result of changes in the long-term seismicity of the region.

3.3.3 Focal mechanisms

First motion studies have been undertaken for earthquakes in the field area since 2004. Only four earthquakes had sufficient data to derive fault plane solutions (Fig. 3.5 and 3.6). The focal mechanisms show a strong strike-slip movement along with a reverse motion component.

Event 2655520 from the GNS catalogue occurred on November 18th, 2006 with a magnitude of 4.2 at 5 km depth. The event plots on the southern Esk Fault between Brechin Burn and Grant Stream. One fault plane extracted from the fault plane solution strikes 220° dipping 55° towards the southeast compliant with observations in the field. The event has a oblique reverse motion.

The other three events are located south-west of the Hawdon Fault and occurred on May 13th, 2005 (M 3.1, depth 9 km), April 2nd, 2008 (M 3.9, depth 12 km), and April 3rd, 2008 (M 3.5, depth 5 km) respectively. While event 2403422 shows oblique reverse motion like the event on the Esk Fault, the event on April 2nd has a much stronger reverse component and the April 3rd earthquake is almost purely strike-slip. Since the events do not lie on a recognised fault the fault plane solutions are ambiguous as to whether the fault plane is an EW striking one or a NS striking one. It is possible to project the earthquakes onto the Hawdon Fault, if it is extrapolated to the west, but the either very steep southern dip with 80-90° or northern dip with 55° does not fit with the moderately south dipping fault. All three events have a nodal plane striking NS and dipping towards the east with varying degrees. A NS striking feature is the reverse Castle Hill Fault towards the south but would have to be widely extrapolated to fit the focal mechanisms. It is, thus, more likely that the events lie on an unknown structure that connects between the NS striking reverse faults and the northeast striking dextral strike-slip faults.

3.4 The Esk Fault

Magnitudes from the Esk Fault's paleo-earthquakes are derived from its subsurface rupture length (L) and width (W) using Eq. 3.5 (Stirling et al., 2008). Since there is only a measurement of 30±10 km for the surface rupture length (SRL) a 15% increase is added following Stirling et al. (2008)'s assumption yielding 34.5±11.5 km for L. Using a dip of 50-70° and a depth of 12 km, W ranges between 12.77±0.41 and 15.66±1.14 km. This leads to a typical magnitude for the Esk Fault of M_W 6.97-7.02±0.14.

Eq. 3.7 from Hanks & Kanamori (1979) yields the seismic moment needed for average displacement using eq. 3.6 (Aki & Richards, 1980), thus, average displacement is estimated with 2.34-2.42±0.26 m. This estimate is less than a meter of the single event displacement

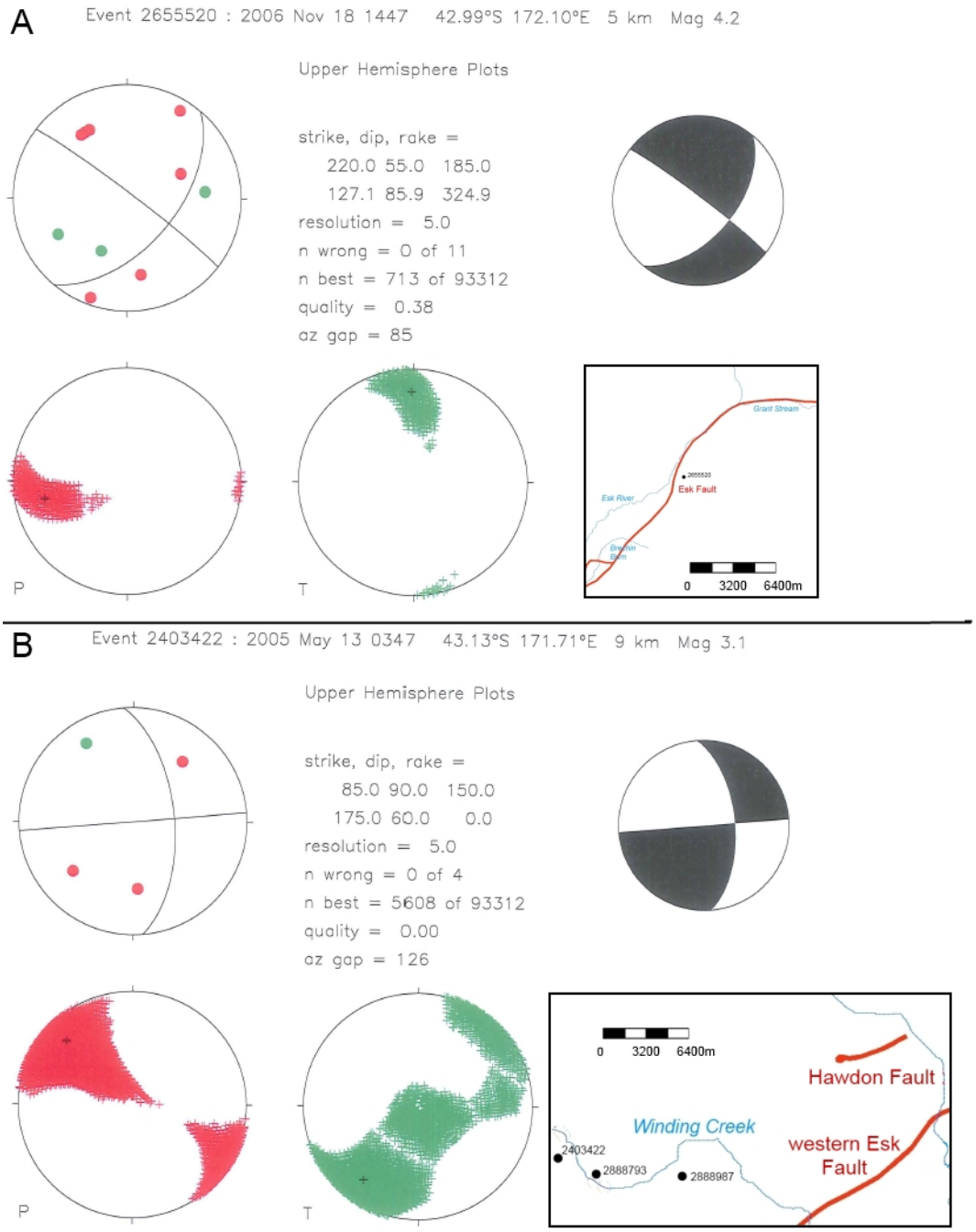

Figure 3.5.: Fault plane solutions for two earthquakes in the field area after 2004 processed by Duncan Noble and GNS. Shown are the stations that received contractional first motion (red) and rarefactional first motion (green) and the resulting nodal planes including the quality of the fault plane solution. Also plotted are the maximum shortening axes (P-Plot), maximum lengthening axes (T-Plot), and the location of the earthquake in the field area. **A** Earthquake no 2655520 occurred on the 18th of November, 2006 at 14:47. It had a magnitude of 4.2 and a focal depth of 5 km. Its fault plane is striking 220° dipping SE with 55°. The likely source of the event is the southern Esk Fault. The fault plane solution exhibits strike-slip movement with a reverse component. **B** Earthquake no 2403422 occurred on the 13th of May, 2005 at 03:47. It had a magnitude of 3.1 and a focal depth of 9 km. It cannot be projected onto a recognised fault with confidence, thus, its fault plane is either striking 85° dipping 90° or striking 175° dipping E with 60°. The fault plane solution exhibits strike-slip movement with a reverse component.

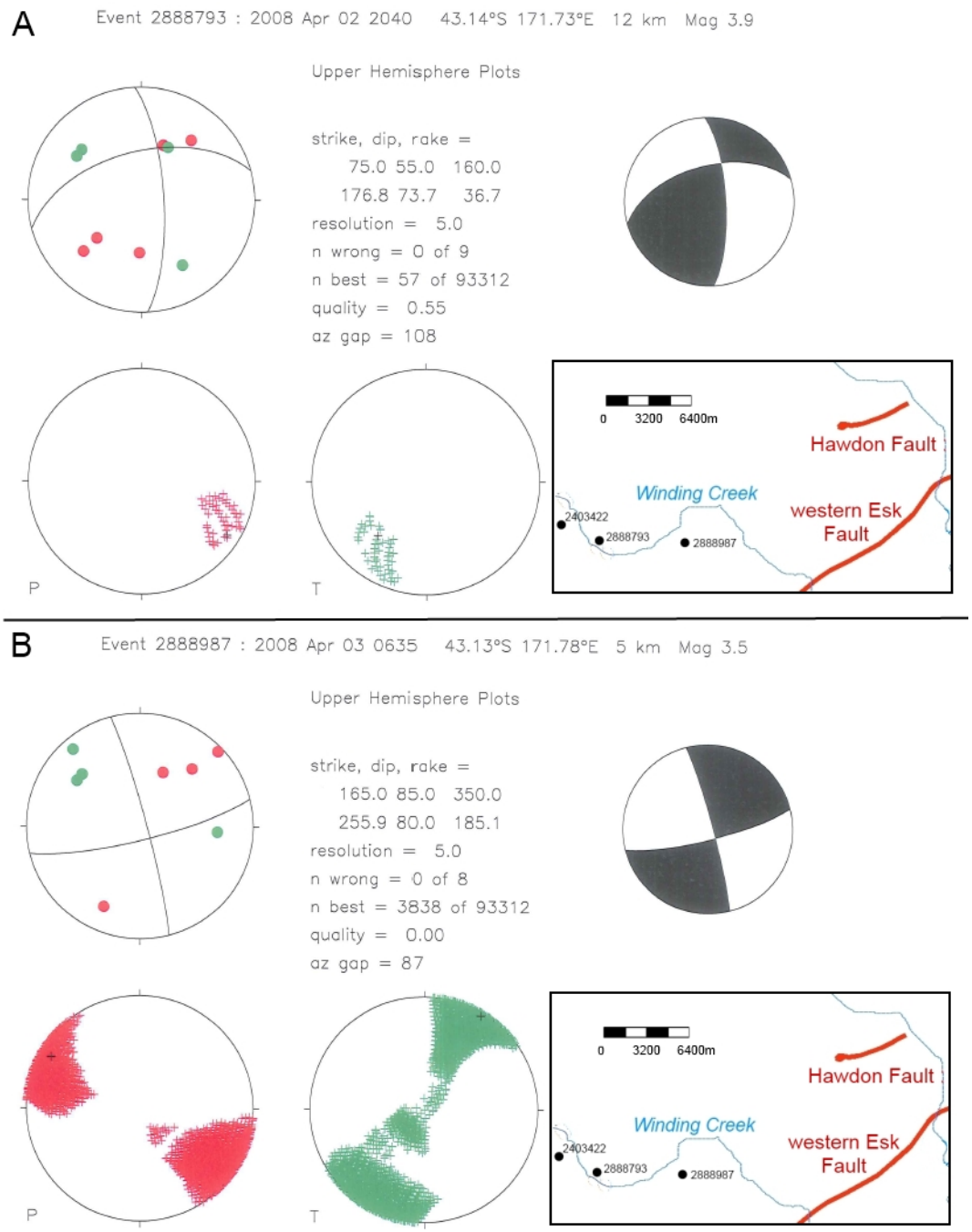

Figure 3.6.: Fault plane solutions for two earthquakes in the field area after 2004 processed by Duncan Noble and GNS. Shown are the stations that received contractional first motion (red) and rarefactional first motion (green) and the resulting nodal planes including the quality of the fault plane solution. Also plotted are the maximum shortening axes (P-Plot), maximum lengthening axes (T-Plot), and the location of the earthquake in the field area. **A** Earthquake no 2888793 occurred on the 2nd of April, 2008 at 20:40. It had a magnitude of 3.9 and a focal depth of 12 km. It cannot be projected onto a recognised fault with confidence, thus, its fault plane is either striking 75° dipping N with 55° or striking 177° dipping E with 74°. The fault plane solution exhibits strike-slip movement with a strong reverse component. **B** Earthquake no 2888987 occurred on the 3rd of April, 2008 at 06:35. It had a magnitude of 3.5 and a focal depth of 5 km. It cannot be projected onto a recognised fault with confidence, thus, its fault plane is either striking 256° dipping S with 80° or striking 165° dipping E with 85°. The fault plane solution exhibits strike-slip movement.

near Blackwater Lake. Either the single event on Lake Blackwater is more like a maximum displacement of the fault, or the estimated average displacement is estimated too low.

In order to resolve this, I used the other scaling relationships from Table 3.1. Earlier work from Stirling et al. (2002) has a direct regression between L and AD which yields an even lower AD for the measured SRL of 1.12±0.21 or a SRL of 211±30 km if using 3.4±0.2 m for an average displacement, which both seem even less likely for the Esk Fault. Better results can be achieved by using the regressions for reverse movement of Wells & Coppersmith (1994) and Wesnousky (2008). If 3.4±0.2 m is used as average displacement Wells & Coppersmith (1994) yields a SRL of 39±13 km and Wesnousky (2008) 57±3 km. Treating the event displacement as an maximum value Wells & Coppersmith (1994) yields a SRL of 35±11 km and Wesnousky (2008) of 16.19±0.95 km. While the SRL value from maximum displacement derived following Wesnousky (2008) is less than the measured length and the SRL from average displacement is more than the measured length, they still enclose the measured value, making the single event displacement a larger than average but not maximum displacement, while the results from Wells & Coppersmith (1994) fit perfectly with the measured surface rupture length.

3.5 The Hawdon Fault

The first approach to establish paleo-magnitudes for the Hawdon Fault uses eq. 3.5 (Stirling et al., 2008), a downdip rupture width of 16.4±3.4 km, derived from a dip of 47±5° and a length of 5.75±1.15 km derived from the measured surface rupture length of 5±1 km. Typical magnitudes for the Hawdon Fault are, thus, of the order of 6.00±0.14. After eq. 3.7 (Hanks & Kanamori, 1979) and eq. 3.6 (Aki & Richards, 1980) the estimated average displacement for each event is 0.40±0.30 m. This value is quite low compared to the overall displacement of a 140±10 m, requiring an improbable number of 350 events in the last 15000 years, which means a M_W 6 earthquake occurs on the Hawdon Fault every 43 years although none has occurred directly on the fault since the establishment of the earthquake catalogue.

350 events have also no relation to the 13±4 events that I identified in the core implying that either most earthquakes on the fault do not cause sedimentary disturbances in the lake despite its proximitiy to the fault line or that there were far less events albeit with a larger magnitude. Therefore, the second approach uses the established events from the core, deducing an average displacement of 10.77±3.31 m for each of the 13±4 events.

Following the second approach, the regression of Stirling et al. (2002) is inadequate for displacements this large resulting in implausible surface rupture lengths of almost 2000 km. Wesnousky (2008) does not give a much better result with such a high average displacement for a strike-slip fault yielding a surface rupture length of a 1000 km. Wells & Coppersmith (1994), however, result in a much lower estimate of 224±67 km. All of these estimates are much longer than the observed fault length, so I assume that only the maximum events show in the core, while the smaller more frequent events are harder to identify due to clustering and insufficient thickness in the core if they even caused surface rupture.

Instead of using 10.77±3.31 m as an average displacement it is inserted as the likely maximum displacement per event. Stirling et al. (2002) do not have a regression for maximum displacement, thus, limiting the approach to the use of regressions from Wells & Coppersmith (1994) and Wesnousky (2008). Regressions from the latter gives a value of 359±126 km, while the

former estimates a surface rupture length of 141±42 km. Again, these exceed the visible trace of the fault of 5±1 km by far. Therefore, the fault must be much longer than initially assumed or link with other similar striking faults north-east and south-west of it.

Based on the fault length derived from Wells & Coppersmith (1994) through the use of maximum displacements, each of the 13±4 events correlates to an earthquake of magnitude 7.62±0.26 with a recurrence rate of 1154±617 years. Taking into account that a large number of smaller events might have gone without evidence in the core, this depicts the maximum magnitude of the fault and minimum recurrence rate. All regressions have been based on the lateral non-gravitational slip. The vertical movement is not part of the regressions here as it is more likely due to topographic collapse than normal faulting.

3.6 The Bullock Hill Fault

3.6.1 Seismicity

Similar to the Hawdon Fault two approaches are being used to establish the paleo-magnitudes of the Bullock Hill Fault. The first one follows eq. 3.5 (Stirling et al., 2008) using a length of 5.75±1.15 km and a width of 12.07-14.65±1.47 km based on the unknown dip that could range from 84° of the minor fault set to 55±10° comparable to the Hawdon Fault. The regression yields a magnitude of 5.91-5.97±0.15 for the fault. Average displacement would be 0.40±0.30 m after eq. 3.6 (Aki & Richards, 1980). To achieve a total displacement of 110±10 275 earthquakes must have occurred on the Bullock Hill Fault during the Holocene, a M 6 earthquake every 43 years, which again is improbable.

Thus, the second approach assumes an average displacement of 5.1±0.5 m displayed by channel D which implies 3 events for channel C, 4 events for channel B and 22 events for channel A (Fig. 2.6, 2.11). Inserting the average displacement into the regression of Stirling et al. (2002) yields a surface rupture length of ∼435 km. Following Wesnousky (2008) a similar length of 510±50 m is given, though both estimates are unlikely. Using the regression for strike-slip faulting of Wells & Coppersmith (1994) another surface rupture length of 136±59 km is estimated, which is similar to the result for the maximum displacement of the Hawdon Fault. The paleo-magnitudes of a fault of that length are of the order of 7.55±0.15 with a recurrence interval of 545±156 years. Again, the large overall displacement leads to the implication that the Bullock Hill Fault is longer than assumed or links with faults such as the Hawdon Fault southeast of it and displacement is amplified by topographical effects.

3.6.2 Dating of the displaced terrace at the Waimakariri-Poulter river junction

To prepare for OSL dating of the last event, assuming the terrace was offset by the Bullock Hill Fault and displays the last rupture, we dug two holes, one in the terrace (Fig. 3.7 A) and one in the meandering channel that cross-cuts this scarp (Fig. 3.7 B). The 80 cm deep terrace hole showed the following sequence: organic horizon (8 cm), sandy silt with isolated pebbles (22 cm), ∼3 mm and ∼2 cm sized gravel in sandy matrix (7 cm), primarily silt with few sand grains (22 cm), a second gravel layer with grainsizes of 4-15 mm (6 cm) and a final light gray sandy layer. The OSL sample (JM01) has been taken at 49 cm depth out of the silt layer.

The 70 cm deep second hole in the meander bend showed an organic horizon (3 cm), a pebble layer (10 cm) followed by a coarse unsorted gravel layer similar to modern river gravels. The

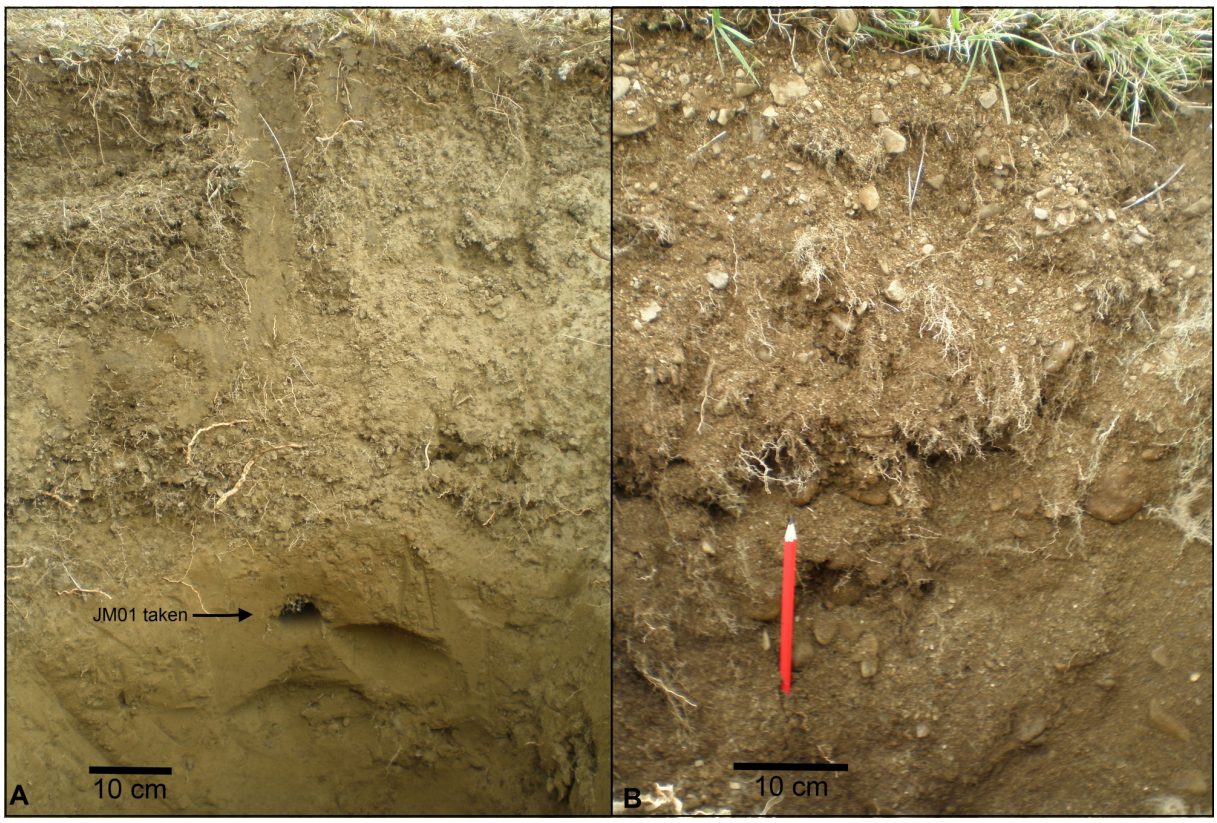

Figure 3.7.: Soil profiles of the faulted terrace (A) and the surrounding meandering channel (B), where the samples for OSL dating have been taken. **A**The OSL sample JM01 has been taken at a depth of 49 cm in a layer of primarily silt with few sand grains. **B**The second OSL sample JM02 has been taken at a depth of 50 cm in a layer of coarse unsorted gravels.

OSL sample (JM02) was taken at 50 cm depth in the pebbly layer. The samples were treated at the Luminescence Dating Laboratory at Victoria University of Wellington and yielded 9.9±1.1 ka for JM01 and 36.4±1.8 for JM02 (see Appendix B). Since the conditions of OSL dating were not optimal, especially for the coarse grained second sample, the second age is discarded as it is too old for a post-glacial fluvial terrace and was probably only partially bleached prior to deposition.

9.9±1.1 ka for the offset terrace seems to be an unlikely age for the last event of the Bullock Hill Fault when presuming that displacement on the fault started after the Poulter advance at 12 ka. Reasons why the dating might have picked up an older age are plenty reaching from the sub-optimal sampling conditions regarding grain size to the bed not being properly zeroed out before deposition. However, it is not an unreasonable age for the river terrace even though the terrace is 150 m below the glacial terrace and only 3 m above the current base level, because incision though the loose glacial gravels would be much faster in the initial stages than at current.

3.7 Discussion

3.7.1 Surface rupture length and Moment magnitude

The paleoseismic studies using the scaling relationships have exposed a major issue in the field area regarding the two smaller faults, Hawdon Fault and Bullock Hill Fault. While the observed surface rupture length and average displacement are acceptable for the reverse Esk Fault, the large post-glacial displacement of the other two faults does not correlate with the exposed

surface trace. There are essentially two possible solutions to the problem. Either, the measured co-seismic slip matches the true slip of the fault implying fewer events, 10-20, and a longer surface rupture length, the measured surface trace corresponds to the surface rupture length of the faults indicating a great number of events, 250-350, and co-seismic displacement of a whole magnitude smaller than measured in the field or the total displacement has been amplified by topographic effects.

I favour the former scenario which correlates much better with my field observations and measurements of coseismic slip as well as the earthquakes on these faults. If the latter scenario would be true it would mean that a M_W 6 earthquake occurs roughly every 40 years on each fault, although only the Cass 1995 earthquake has been recorded in the region in the last 150 years. Instead the regional seismicity correlates well with the recurrence intervals estimated for fewer larger events, estimated M_7 every 1150 years with a recurrence interval of 1154±617 years for the Hawdon Fault. The question is, thus, what fault length is required for magnitudes of this order?

The scaling relationships used in this study scatter quite a bit. Normally, the regressions of Stirling et al. (2002) and later Stirling et al. (2008) are used for New Zealand as they are based on New Zealand data instead of global data which normally leads to an overestimation of the co-seismic slip for small scaled faults (Stirling et al., 2002). They, however, do not work well for the average displacements recorded here yielding fault lengths of more than 1000 km which are implausible. This can be due to the fact that there is no difference made for strike-slip and dip-slip faults compared to Wells & Coppersmith (1994) and Wesnousky (2008) and there are no relationships between maximum co-seismic slip and surface rupture length. Taking the Esk Fault, the regression describes the reverse fault well but underestimates, although still in plausible range, the co-seismic slip that was measured as a single event displacement and might rather relate to a maximum displacement. There is no such relation between the estimates from the regression and measurements from the field with the two strike-slip faults.

Therefore, the scaling relationships of Wells & Coppersmith (1994) and Wesnousky (2008) have been compared. Wesnousky (2008) describes complicated faulting scenarios but has problems with fitting linear relationships between coseismic displacement and fault length of strike-slip events. Again, the relationship describes the Esk Fault well and gives a much lower estimate though still high result of 360-510 km for the fault length of the strike-slip faults. Wells & Coppersmith (1994) is based on global data and tends to overestimate average displacement for small-scale fault (Stirling et al., 2002), but in this case, where the faults require a longer fault length, it yields the best estimate with 141±42 km for the Hawdon Fault and 136±59 km for the Bullock Hill Fault which falls within the range of the Porters Pass Fault, which requires 100-140 km (Howard et al., 2005). These fault lengths are still within reasonable limits as shown by the 2010 El Mayor M_W 7.2 earthquake which had a 120 km long surface rupture length and ∼5 co-seismic lateral slip (Wei et al., 2011).

Given the discrepancies in the scaling relationships all of them have to be considered in order to review the magnitudes of each of the three faults and a hypothetical 140 km long fault. This can be seen in Table 3.2 and is plotted in fig. 3.8. Although the estimated magnitude for a small-scale Hawdon and Bullock Hill fault is around 6, magnitudes for the larger and more probable fault length are more than a magnitude higher, ranging between 7.42±0.12 and 7.90±0.21, and exceed the estimated M7 of the Esk Fault. It is to note that regressions based on New Zealand

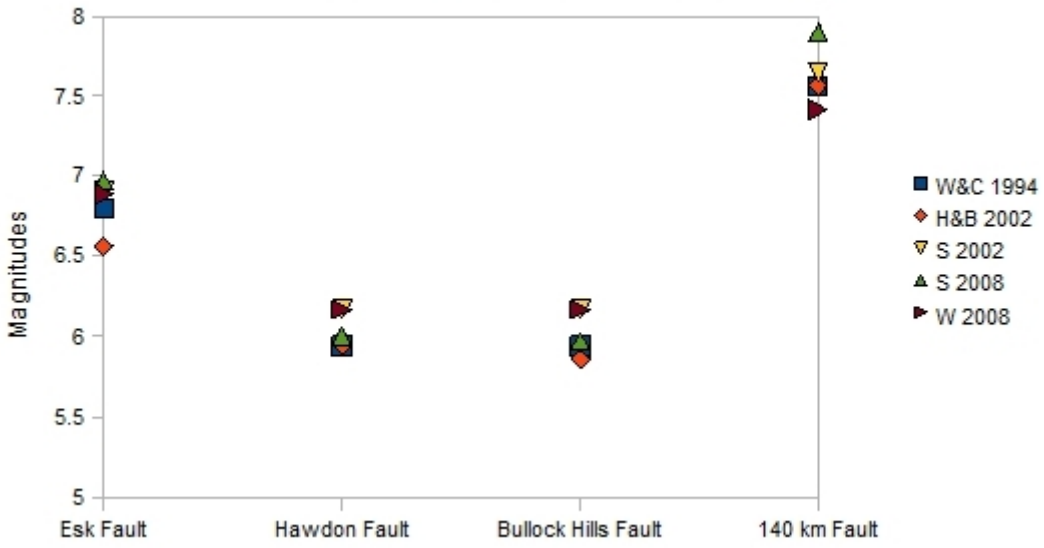

Figure 3.8.: Comparable plot of magnitudes derived from different scaling relationships for the Esk, Hawdon, Bullock Hill Fault and a theoretical 140 km long fault (refer to Table 3.2). Annotations describe regressions from the following authors: W&C 1994 - Wells & Coppersmith (1994), H&B 2002 - Hanks & Bakun (2002), S 2002 - Stirling et al. (2002), S 2008 - Stirling et al. (2008), W 2008 - Wesnousky (2008).

data (Stirling et al., 2002, Stirling et al., 2008) yield generally larger magnitude estimates than the ones derived from global data (Wells & Coppersmith, 1994, Hanks & Bakun, 2002, Wesnousky, 2008).

The Arthur's Pass and Cass earthquake in 1994 and 1995 both show that large magnitude earthquakes can occur without rupturing the surface in the region. Although there is the possibility that surface rupture has been missed in the mountaineous terrain, it is likely that faults in this region do not necessarily rupture the surface or to the full length, which means that faults like the Hawdon and Bullock Hill faults could be potentially longer than observed. The existence of blind or previously unrecognised faults in Canterbury has been previously reported by Pettinga et al. (2001) and demonstrated by the rupture of the hitherto unknown Greendale Fault (Quigley et al., 2010).

	Length (km)	W&C 1994	H&B 2002	S 2002	S 2008	W 2008
Esk Fault	30±10	6.80±0.63	6.56±0.22	6.91±0.28	6.97±0.14	6.89±0.27
Hawdon Fault	5±1	5.94±0.028	5.95±0.12	6.17±0.18	6.00±0.14	6.17±0.08
Bullock Hill Fault	5±1	5.94±0.028	5.86±0.13	6.17±0.18	5.97±0.15	6.17±0.08
140 km Fault	140±45	7.56±0.32	7.57±0.24	7.65±0.34	7.90±0.21	7.42±0.12

Table 3.2.: Comparisons of possible magnitudes for the Esk, Hawdon, and Bullock Hill Fault as well as a theoretical 140 km long fault, derived from scaling relationships in Table 3.1. Annotations describe regressions from the following authors: W&C 1994 - Wells & Coppersmith (1994), H&B 2002 - Hanks & Bakun (2002), S 2002 - Stirling et al. (2002), S 2008 - Stirling et al. (2008), W 2008 - Wesnousky (2008). Refer to fig. 3.8 for visual comparison.

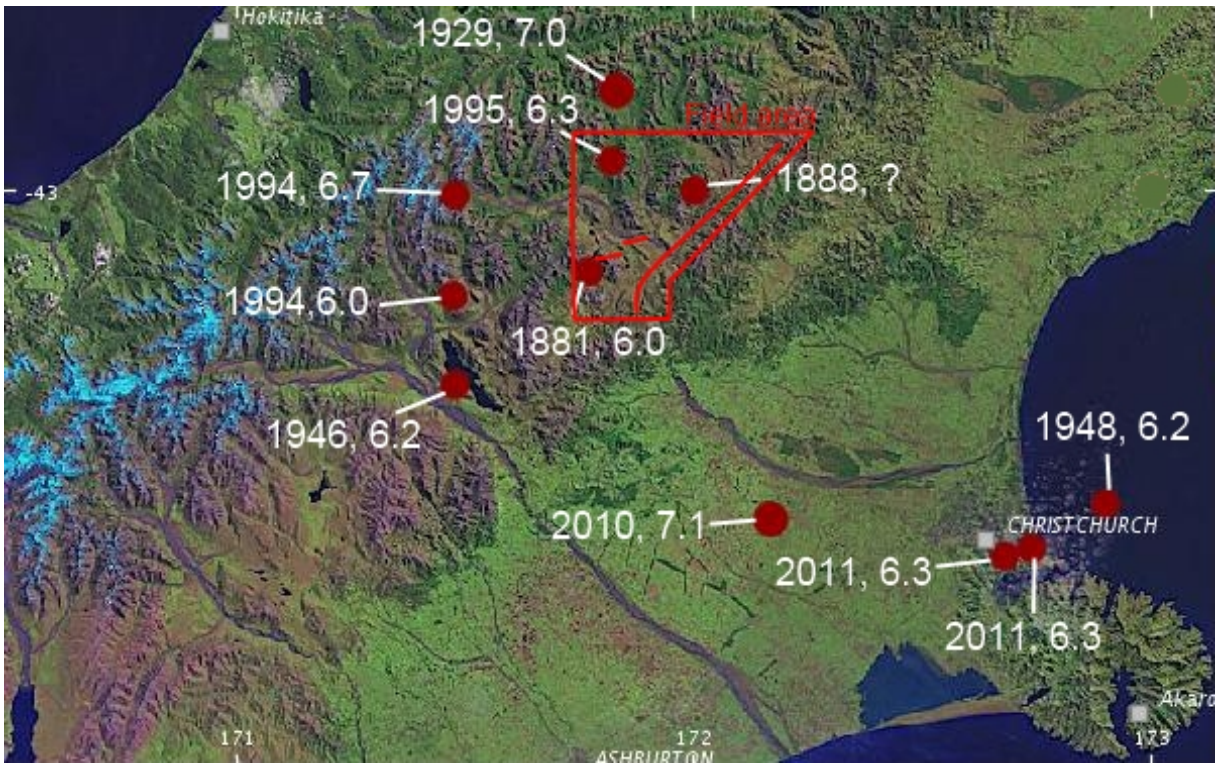

Figure 3.9.: Map showing the location, year and magnitude of all M>6 earthquakes in Canterbury and the study area which might be the location of a M>7 earthquake in the future. Map and according data by courtesy of GNS, GeoNet.

3.7.2 Earthquake hazard

The $M_{7.1}$ Darfield earthquake in 2010 and its aftershock sequence have demonstrated the underlying danger of unrecognised or understudied faults for Canterbury and Christchurch (Quigley et al., 2012). The study area is about 70 km northwest of the city of Christchurch (Fig. 3.9), which is double the distance of the Darfield epicentre. The regional seismicity shows that a M_6 earthquake occurs in that area every 115 years which has been verified by earthquakes in 1881, 1888 and 1995 and a potential M_7 earthquake every 1150 years (e.g. the 1929 M_W 7.1 earthquake on the Poulter Fault; Berryman & Villamor, 2004). The rupture of the Arthur's Pass earthquake in 1994 further to the west caused a large number of landslides, structural damage in the village of Arthur's Pass and the pass road and further damage as far southeast as Christchurch (Abercrombie et al., 2000). An earthquake of the same order of magnitude in the field area which is closer to Christchurch presents a considerable regional hazard and needs to be considered.

The previous ruptures and difficulties of fault plane solutions which indicate a complex structure with an unknown number of blind faults complicate assessment of the hazard the fault region poses for Canterbury. The Esk Fault is capable to produce earthquakes of magnitude 6.97-7.02±0.14 which is only slightly less than the ruptures on the Poulter Fault (1929) and Greendale Fault (2010). The recurrence interval is about every 2000 years but a last event has not been constrained. The only single event displacement seen in the field ruptures gravels from the second Blackwater Advance indicating at least one rupture in the last 20 000 years which is ten times the estimated recurrence interval.

The smaller faults are both capable of M_6 earthquakes which occur every 43 years if their

surface rupture length is as small as observed given the large overall displacement. This activity is not documented by the regional seismicity studies which would either mean that these faults are also overdue or do not rupture in the given recurrence interval which leads back to a larger surface rupture length. Assuming the Hawdon Fault and Bullock Hill Fault are linked with each other and other faults in the region forming a fault structure of 140 km length the expected magnitude would be as large as 7.6.

Although a $M_{7.6}$ earthquake exceeds the estimated maximum magnitude, 7.2 (Stirling et al., 2001), previously allocated to the region, it is a possible magnitude for a large fault as this. An earthquake of that order would definitely be felt in Christchurch and inflict further damage, the extent of which depends on the earthquake magnitude and rupture dynamics. The large displacements on the Hawdon and Bullock Hill faults indicates that the central part of fault rupture could be in close proximity about 80 km northwest of Christchurch.

3.7.3 Glacial loading

Since most of the paleoseismological analysis deals with the post-glacial activity of the study area, there remains the question which effect the glacial advances had on the fault activity. Recent theories proposed by Hampel & Hetzel (2006) and Hampel et al. (2010) try to assess the effect of glacial loading on fault structures and came to the conclusion that slip rate is increased after unloading due to changes in the differential stress. This could explain the high slip rates of 9.3 mm/year for the Hawdon and Bullock Hill Fault. According to Hampel et al. (2010) slip rates increase up to a factor of 10 after a relative quiescence on the fault during glacial cover. Furthermore, there is a lag time between unloading and the reaction of the fault, which is controlled by the viscosity of the Asthenosphere , while the rate of load removal, fault strength, and thickness of the lithosphere are minor factors (Hampel & Hetzel, 2006).

The lake core of the Hawdon Fault shows a lag time of 3000 years until the onset of activity which is followed by clusters of events between 5000 and 15000 years, after which the number of events decreases, suggesting a slow-down of the fault slip rate. Since there is no data recorded of the glacial activity it cannot be said if there was an increase in the slip rate of the Hawdon Fault but its anomalous high nature is suggests a temporary increase. This is backed up by the lack of activity in the last 3000 years which would represent a return to its previous state.

Based on the assumption the glacial unloading led to an increased slip rate of the Hawdon Fault between 5000 and 15000 years BP where the 140 m of displacement occurred, the fault would be currently returning to its pre-glacial activity which would in turn mean a lower slip rate and higher recurrence interval.

3.8 Conclusion

The reconnaissance paleoseismic study of the field area has shown a discrepancy between surface rupture length and fault displacement for the Hawdon and Bullock Hill faults, with the surface rupture length being underestimated for the co-seismic slip. This means that these faults did not rupture along their whole length, have blind segments or link with eachother and other faults.

The Esk Fault exposes good correlation of its vertical displacement and the observed rupture length. The fault is capable of magnitude 6.97-7.02±0.14 earthquakes and presents a risk to the wider Canterbury area and Christchurch.

The Hawdon Fault and Bullock Hill Fault are both capable of M_6 earthquakes if regarded as isolated faults. However, regional seismicity and scaling relationships indicate, that the two faults are part of a larger fault system that has a length of $140_{\pm}55$ km, which is not unfeasibly long (e.g. El Mayor 2010) and collectively capable of producing earthquakes of up to magnitude 7.6. An earthquake of that order in that location poses a major risk to Christchurch and the Canterbury region. Given the relative quiescence of the Hawdon Fault shown by the formation of a new undisrupted channel the risk has either decreased through return to a slower slip rate of the fault or increased due to stress accumulation.

4. Fault linkage and blind faults in North Canterbury

4.1 Introduction

The paleo-seismic and geomorphic studies of the field area have shown that the previously unstudied Hawdon and Bullock Hill fault have unexpectedly high slip rates and co-seismic displacements for their observed rupture length. Instead of their 5 km a surface rupture of 140±55 km has been correlated from scaling relationships, which coincides with the correlation of 100-140 km for the co-seismic offset reported on the Porters Pass Fault (Howard et al., 2005). Furthermore, following the prevalent NE strike of the strike slip faults an accommodation space of ∼140 km is available between the western tip of the Porters Pass Fault and the Hope Fault, the youngest fault of the Marlborough Fault System (Cowan et al., 1996).

In this chapter I examine the factors indicating linkage between the faults in this study and previous studied faults as well as propose which recognised but unstudied faults may be part of the fault system. Part of the faults pass through glacial outwash and till without any surface expression and previous large earthquakes such as the Arthur's Pass and Cass earthquakes have had no surface rupture. The resulting complexity of the rupture patterns can best be explained by acknowledging blind faults. Combining blind faults with fault linkage results in a major fault of the same scale of the Marlborough Fault System which may account for the reported fault slip deficit in North Canterbury revealed in comparisons of geologic with GPS data (Wallace et al., 2007). Contrary to existing interpretations, I suggest that most fault-slip deformation in North Canterbury does not occur at the tip of the PPAFZ but further north-east in the centre along the Hawdon and Bullock Hill faults.

4.2 Blind faulting in the field area

Several signs of blind faulting have been found in the area. Many of the observed faults do not show a continuous surface trace despite being tectonically active in the Holocene. Lettis et al. (1997) discern between blind faults, that do not rupture the surface, and buried faults, whose surface rupture has been obscured by sedimentation and erosion. Both mechanisms are potentially applicable in the field area. Fig.4.1 shows which parts of the mapped faults are potentially blind.

4.2.1 The Esk Fault

The trace of the Esk Fault travels through Torlesse bedrock, glacial gravels, and riverbeds. Despite two exposures in Torlesse bedrock only a single event displaces the glacial gravels from the second Blackwater Advance near Blackwater Lake that covers most of the fault trace. This is the only sign of post-glacial activity. The deformation, however, is rather limited to the small

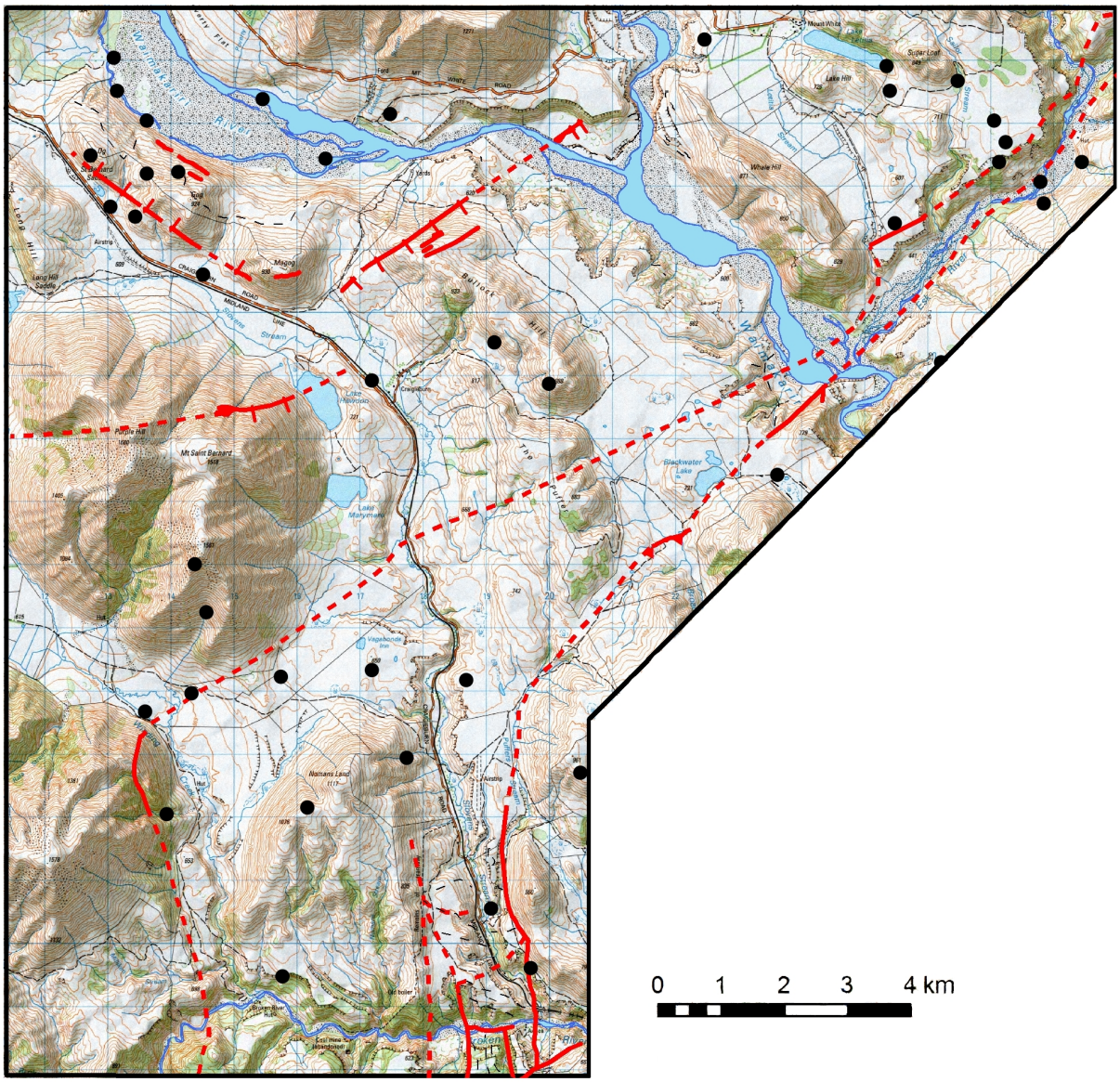

Figure 4.1.: This map compiled in ArcGIS shows the faults in the field area highlighting the parts that are blind faults (dashed red line). Earthquakes from the GNS earthquake catalague are also shown, error for the location is 3-8 km. (43°03'S 171°47'E / 43°12'S 172°01'E)

area south of the Blackwater Lake and no correlatable displacements along the fault have been found.

A large part of the fault runs through the riverbed of the Esk River. In here, sedimentation and erosion processes are too fast to see a displacement making it possible to bury the Esk Fault during phases of inactivity. The terraces on both sides of the river, however, should preserve the deformation. The analysis of the terraces near the Esk River mouth suggests that 20-35 m of displacement may have occurred on the Esk Fault since the formation of the terraces assuming the terraces are paired. This shows that the Esk Fault, at least in this part, is not truly blind but a buried fault (Lettis et al., 1997) although it cannot be buried very deep to have displacement over such a short time frame.

4.2.2 The Hawdon and Bullock Hill faults

The Hawdon Fault and Bullock Hill Fault have both been shown to be highly active faults. Both faults are practically invisible in glacial gravels. The Hawdon Fault is well exposed in the hillside and bedrock outcrops. It runs through Lake Hawdon and crops out again in the little bedrock ridge on the other side, where the fault apparently terminates. Northeast of the bedrock ridge the valley floor is covered in glacial outwash gravels that show no disruption. The western tip of the fault is buried under alluvial fans. It is unclear if it runs through Lake Pearson and further, however, there is no surface rupture in the glacial gravels west of the lake.

The Bullock Hill Fault is plainly visible in the Bullock Hill Fault but cannot be traced through the morainic deposits at the foot of the hill nor on the other side of the Waimakariri River. The rupture of the Holocene river terrace is uncertain, although RTK has shown backtilting and GPR profiles have picked up a northward dipping fault. The same RTK does not show backtilting on the older upper terrace which is made of 40 m of morainic material thus leading to the assumption that the glacial gravels are refracting and dissipating the seismic energy leading making the fault truly blind when running through glacial gravels.

4.2.3 Earthquake sources

Fig. 4.1 shows the location of larger earthquakes in relation to the known faults. Most of these earthquakes do not occur on the proposed fault planes, most prominently the Cass earthquake in 1994. The fault plane solution of the Cass earthquake is a NS trending fault dipping 45±5° to the west with one aftershock sequence following a NE-SW band (Gledhill et al., 2000). While the NE-SW trending band can be attributed to either the Bullock Hill Fault, Hawdon Fault or similar striking but further north lying Mt White Fault, there is no fault that has a NS strike.

In the same manner, the earthquakes shown in fig. 3.5 and 3.6 cannot be attributed directly to one fault or the other. They seem to lie in between the NE striking Hawdon Fault and the N striking Castle Hill Fault. It is quite possible that these events occurred on blind faults connecting the two faults.

4.3 Fault linkage scenarios

4.3.1 Derivation of a fitting fault system

The main issue in the dataset is that in order to achieve a maximum displacement of 10.77±3.31 m (Hawdon Fault) or an average displacement of 5.1±0.5 m (Bullock Hill Fault) a surface rupture length of at least 140±55 km is required. I approach this problem from the Hawdon Fault considering all possibilities. Assuming part of the Hawdon Fault is hidden underneath glacial gravels, such as is the case for the Bullock Hill Fault, there is a maximum space of 25 km before the fault reaches the larger NE-SW trending reverse faults, the Esk and Harper faults. This distance is only partly covered by glacial gravels and shows no further offset along strike. This possibility is, therefore, discarded.

Since there is not enough space between the binding faults to the east and west to accommodate for 140 km, the fault needs to be extended by other means such as connecting it to similar striking and proximal faults. The closest fitting fault is the Bullock Hill Fault, which lies ∼1 km to the north, strikes NE and has an equal length and the same dextral displacement as the

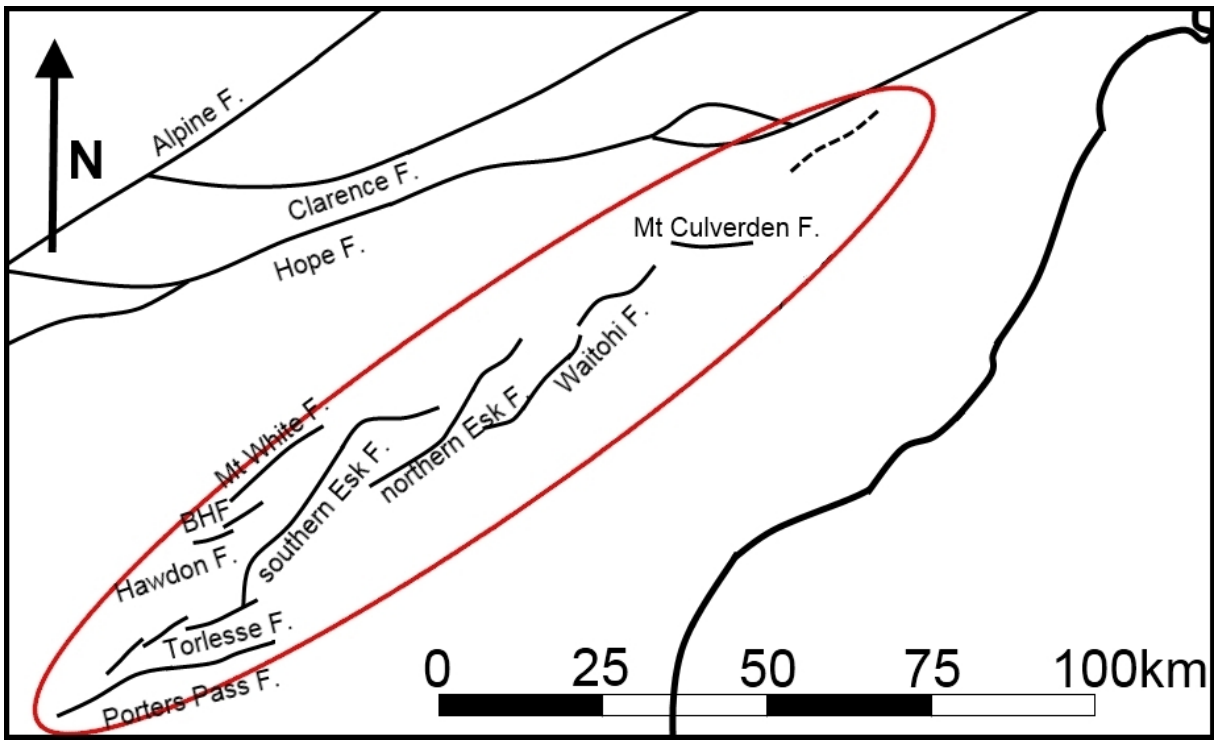

Figure 4.2.: Map view of the proposed fault zone extending from the Porters Pass Fault to the Hope Fault east of Hanmer Springs over a length of 140±10 km. Faults, excluding the Hawdon Fault and Bullock Hill Fault (BHF), as mapped by Nathan et al. (2002), Rattenbury et al. (2006), Cox & Barrell (2007), and Forsyth et al. (2008).

Hawdon Fault. The next fault 2.1 km north is the Mt White Fault, striking 050° with a length of ∼15 km. These faults are all within 3-4 km of eachother which is the maximum distance faults to kinematically interact defined by Wesnousky (2008), but no similar faults can be found within that reach northeast or southwest. The total length of the three faults equals ∼25 km which is already as long as the 25 km the binding faults accommodate for an unsegmented Hawdon Fault and equally short of the required 140±55 km.

A similar situation occurs at the Porters Pass Fault, that slips with 3.2-4.1 mm/year at its eastern end and 0.3-0.9 mm/year at its western end and requires 100-140 km of surface rupture length while only displaying 40 km (Howard et al., 2005). Both, the Hawdon Fault and the Porters Pass Fault show displacement that requires a fault length of ∼140 km. Hence, it seems likely that they are both part of a larger fault system that stretches from the western end of the Porters Pass Fault to the Hope Fault, striking NE-SW (Fig. 4.2). This accommodation space is roughly 140±10 km long, equalling the required surface rupture length for both faults.

Other NE-SW striking faults in the reach are the Torlesse Fault, the southern, western and northern Esk faults, the Waitohi Downs Fault and an unnamed fault near Hanmer Springs (Fig. 4.2). The Mt Culverden Fault is striking E-W. Noble (2011) studied the northern Esk Fault and found it to be a dextral strike-slip fault with a reverse component fitting with the overall dextral movement of the proposed fault system. The southern Esk Fault exhibits no lateral displacement and its length is well correlated by the vertical displacement. Thus, it might not be part of the fault system. The fault system is bound on its northeastern end by the Hope Fault and on its southwestern end by the Redcliffe Fault (Howard et al., 2005).

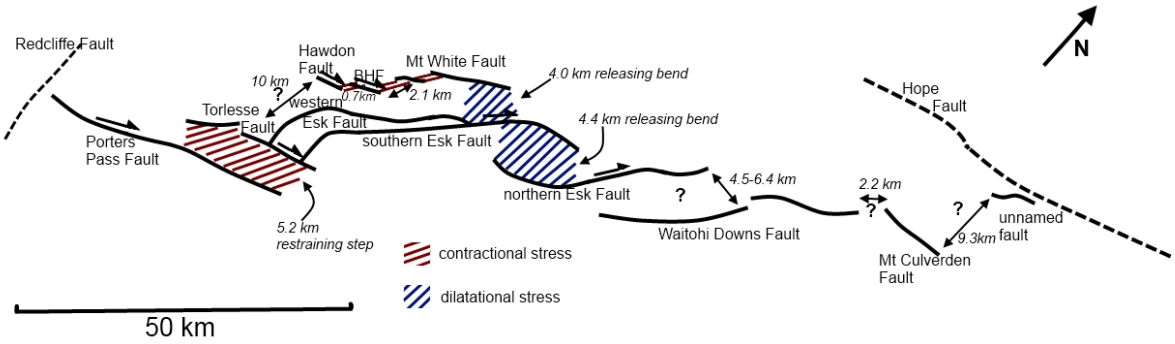

Figure 4.3.: Map view of the proposed fault system displaying fault traces and step-over widths. Zones of expected contractional (red) and dilatational (blue) stress are identified. Abbreviations are: PPF - Porters Pass Fault, TF - Torlesse Fault, HF - Hawdon Fault, BHF - Bullock Hill Fault, MWF - Mt White Fault, wEF - western Esk Fault, sEF - southern Esk Fault, nEF - northern Esk Fault, WDF - Waitohi Downs Fault, MCF - Mt Culverden Fault, u.f. - unnamed fault near Hanmer Springs.

4.3.2 Linkage and interaction of the fault segments

I start off with a map view of the faults that are part of the proposed fault system (Fig. 4.3). Fault traces within the fault system that are not primarily dextral slipping like the western and southern Esk faults are also included. The location and dimensions of fault steps are shown to scale and the distance between overlapping features are annotated. The separation distance is usually measured perpendicular to the average strike of two compared fault segments. The fault steps are also labelled restraining steps and releasing bends depending on whether fault slip would cause contractional or dilatational stress within the fault step (Segall & Pollard, 1980). In general, the left-stepping links are causing contractional stresses in the overlap zone, while the right-stepping links cause dilatational stress leading to complicated fault geometries.

The Porters Pass Fault and Torlesse Fault, Torlesse Fault and Hawdon Fault, Hawdon Fault and Bullock Hill Fault, Mt White Fault and southern Esk Fault, southern Esk Fault and northern Esk Fault, and northern Esk Fault and Waitohi Downs Fault overlap in various degrees, while the Bullock Hill Fault and Mt White Fault, Waitohi Downs Fault and Mt Culverden Fault, and Mt Culverden Fault and the unnamed fault do not. The southern and northern Esk faults show the diagnostic hook-shape of advanced linkage (Acocella et al., 2000). According to Gupta & Scholz (2000) underlapping faults propagate towards each other while overlapping faults are retarded.

Here I distinguish between hard fault linkage and soft linkage. Hard linkage describes physically linked, a state that does only occur between the Torlesse Fault and southern Esk Fault. When the faults are linked throughout their stress fields it is called soft linkage. Most faults in this fault system are currently soft linked if at all. A general tool to examine fault interaction is the separation overlap ratio (Table 4.1) used by Aydin & Schultz (1990) and Huggins et al. (1996), although Gupta & Scholz (2000) prefer using displacement gradients which require an extensive data set that is not available for this study. I acknowledge that the separation overlap ratio is not good enough to define the state of interaction and can exhibit a wide range. For the overlapping faults in this study excluding the Torlesse Fault and Hawdon Fault and the Hawdon Fault and Bullock Hill Fault step the separation overlap ratio is 0.30-0.45. The Torlesse Fault and Hawdon Fault has a high value of 2.27 due to the wide separation, and the Hawdon Fault

and Bullock Hill Fault has a high value of 3.5 due to its small overlap.

Wesnousky (2008) describes that there is no kinematic interaction between faults that are more than 3-4 km separated, although Gupta & Scholz (2000) notes that the distance of possible linkage for strike-slip faults is dependant on the dominant fault length and generally does not exceed 15%. I have, therefore, classified the steps after both approaches (Table 4.1). I have found that most faults exceed the separation of 4 km and only the three core faults (Hawdon Fault, Bullock Hill Fault, and Mt White Fault) and the Waitohi Downs and Mt Culverden fault step are close enough for interaction. Following Gupta & Scholz (2000) all fault steps between the Hawdon Fault and Mt Culverden Fault are below the threshold.

	Separation (km)	**Separation/Overlap**	**<4 km**	**Separation/Length**
PPF - TF	5.2	0.39	no	33%
TF - HF	10.0	2.27	no	62%
HF - BHF	0.7	3.50	yes	14%
BHF - MWF	2.1	underlapping	yes	14%
MWF - SEF	4.0	0.30	no	13%
SEF - NEF	4.4	0.45	no	14%
NEF - WDF	4.5-6.4	0.36-0.51	no	15-21%
WDF - MCF	2.2	underlapping	yes	7%
MCF - u.f.	9.3	underlapping	no	130%

Table 4.1.: Interaction between faults. The separation is measured perpendicular to the average strike. Separation overlap ratios follow the approach of Aydin & Schultz (1990), Huggins et al. (1996), and Gupta & Scholz (2000). Wesnousky (2008) defined that faults beyond 4 km of separation do not rupture co-seismically, while Gupta & Scholz (2000) use a separation length ratio of 15% as threshold value. Abbreviations are: PPF - Porters Pass Fault, TF - Torlesse Fault, HF - Hawdon Fault, BHF - Bullock Hill Fault, MWF - Mt White Fault, SEF - southern Esk Fault, NEF - northern Esk Fault, WDF - Waitohi Downs Fault, MCF - Mt Culverden Fault, u.f. - unnamed fault near Hanmer Springs.

4.3.3 Displacement and slip rate

I used data of dextral single event displacement from the Porters Pass Fault (Howard et al., 2005), the Hawdon Fault and Bullock Hill Fault (this study) and the northern Esk Fault (Noble, 2011) to show the slip distribution along the fault length (Fig. 4.4). The different data curves of the individual fault segments overlapped and formed one asymmetric curve for the slip distribution of the whole system. The average co-seismic slip of the system is 5 m with maximum slip on the Hawdon Fault. No slip data is available for the north part of the system and might be considerably less.

The lateral slip rate follows a similar asymmetric pattern with its peak of 9.3±2.8 mm/yr on the Hawdon and Bullock Hill Fault. The fault system slows down towards the southwestern end to 0.3-0.9 mm/year (Howard et al., 2005). The slip rate of 0.82±0.06 mm/year on the northern Esk Fault (Noble, 2011) indicates a similar trend for the northeastern end.

4.3.4 Fault source parameter

The previous results show that linkage is not yet complete and the fault system is in an incipient stage. Dawers & Anders (1995) states that during the time of fault linkage, the whole system can deform as a single fault with co-seismic slip along the fault. However, ruptures on one fault

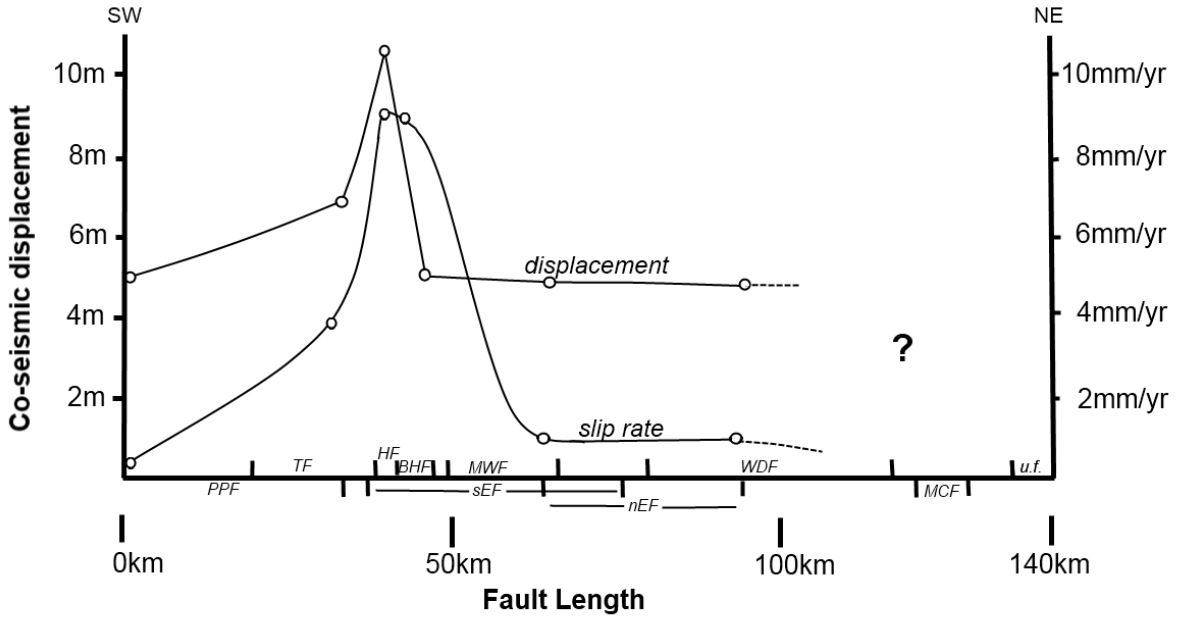

Figure 4.4.: Lateral Single event displacement and slip rate along the fault system including the location and extent of the individual fault traces. Displacement data from this study, Howard et al. (2005), and Noble (2011). Slip data is indicated by a circle. Abbreviations are: PPF - Porters Pass Fault, TF - Torlesse Fault, HF - Hawdon Fault, BHF - Bullock Hill Fault, MWF - Mt White Fault, sEF - southern Esk Fault, nEF - northern Esk Fault, WDF - Waitohi Downs Fault, MCF - Mt Culverden Fault, u.f. - unnamed fault near Hanmer Springs.

will not propagate to others in the system if the separation is larger than 4 km which it is in most cases (Wesnousky, 2008). Although this is a simplification and the interaction also depends on fault orientation and geometry, i.e. whether the faults dip to each other and connect in depth or not, this would be in favour of a segmented rupture. In both cases blind faults need to be considered which could make up for the lack of step-overs in some parts of the system.

I used a logic tree approach to describe the source parameters of the fault if it ruptures the entire length (Fig. 4.5). The first parameter is fault length which is the total span between the Redcliffe Fault and Hope Fault. Dip of the fault is unknown but should be steeper than 45°. The Hawdon Fault and the northern Esk Fault have a dip of ∼50° which gets the most weighting. The Bullock Hill Fault and Porters Pass Fault are steeper and could be more representative of the overall fault system. Seismogenic depth is 12 km as it was for the field area, therefore the downdip rupture width depends on the dip only. Fault area depends on the width of the fault and uses the same length for all approaches.

The next weighting step involves the seismic moment, M_0, and moment magnitude, M_W. The moment magnitude is calculated with different scaling relationships. Most weight is given to the New Zealand based regression from Stirling et al. (2008). Seismic moment is subsequently calculated after Hanks & Kanamori (1979). Co-seismic average displacement results of the formula used by Aki & Richards (1980) and depends on the calculated seismic moment and area.

Faulting scenario	Segment name	Length (km)	wt	Dip	Width (km)	Area (km²)	wt	Scaling relation	MW	M0	AD (m)	wt	Slip rate (mm/yr)	RI (yr)	wt	wt*
whole fault ruptures	-	140	1.0	*50°*	*15.66*	*2192.4*	*0.5*	*Stirling et al. 2008*	*7.64*	*3.2*10^27*	*4.87*	*0.7*	9.20	530	0.1	0.04
													4.10	*1190*	*0.7*	*0.25*
													0.82	5939	0.2	0.07
								Wesnousky 2008	7.43	1.6*10^27	2.43	0.1	9.20	264	0.1	0.01
													4.10	593	0.7	0.04
													0.82	2963	0.2	0.01
								WC 1994	7.56	2.5*10^27	3.80	0.1	9.20	413	0.1	0.01
													4.10	927	0.7	0.04
													0.82	4634	0.2	0.01
								HB 2002	7.52	2.1*10^27	3.19	0.1	9.20	347	0.1	0.01
													4.10	778	0.7	0.04
													0.82	3890	0.2	0.01
				60°	13.86	1940.4	0.3	*Stirling et al. 2008*	*7.64*	*3.2*10^27*	*5.50*	*0.7*	9.20	598	0.1	0.02
													4.10	*1341*	*0.7*	*0.15*
													0.82	6707	0.2	0.04
								Wesnousky 2008	7.43	1.6*10^27	2.75	0.1	9.20	299	0.1	0.00
													4.10	671	0.7	0.02
													0.82	3354	0.2	0.01
								WC 1994	7.56	2.5*10^27	4.29	0.1	9.20	466	0.1	0.00
													4.10	1046	0.7	0.02
													0.82	5232	0.2	0.01
								HB 2002	7.45	1.7*10^27	2.92	0.1	9.20	317	0.1	0.00
													4.10	712	0.7	0.02
													0.82	3561	0.2	0.01
				70°	12.77	1787.8	0.2	*Stirling et al. 2008*	*7.64*	*3.2*10^27*	*5.96*	*0.7*	9.20	648	0.1	0.01
													4.10	*1454*	*0.7*	*0.10*
													0.82	7268	0.2	0.03
								Wesnousky 2008	7.43	1.6*10^27	2.98	0.1	9.20	324	0.1	0.00
													4.10	727	0.7	0.01
													0.82	3634	0.2	0.00
								WC 1994	7.56	2.5*10^27	4.66	0.1	9.20	507	0.1	0.00
													4.10	1137	0.7	0.01
													0.82	5683	0.2	0.00
								HB 2002	7.41	1.5*10^27	2.80	0.1	9.20	304	0.1	0.00
													4.10	683	0.7	0.01
													0.82	3414	0.2	0.00

Figure 4.5.: Logic tree approach for a whole fault rupture. Most likely scenario is highlighted in italic. Scaling relationships from Stirling et al. (2008), Wesnousky (2008), Wells & Coppersmith (1994), and Hanks & Bakun (2002).

Faulting scenario	Segment name	Length (km)	Dip	MW	M0	AD (m)	Slip rate (mm/yr)	RI (yr)
Segmented rupture	Porters Pass Fault	40	60-80°	7.4	1.67*10^27	8	0.3-4.1	1500
	Porters Pass Fault – western segment		60-80°	N/A	N/A	N/A	0.3-0.9	9000
	Porters Pass Fault – eastern segment		60-80°	7.1	5.76*10^26	4	3.2-4.1	1500
	Torlesse Fault	20	N/A	N/A	N/A	N/A	N/A	N/A
	Hawdon Fault	5	47°	6	1.1*10^25	>5	9.3	42
	Bullock Hill Fault	5	55-85°	5.9	7.9*10^24	5	9.2	43
	Mt White Fault	15	N/A	N/A	N/A	N/A	N/A	N/A
	Southern Esk Fault	30	55-75°	7	3.2*10^27	N/A	N/A	N/A
	Northern Esk Fault	20	50°	N/A	N/A	5	0.82	6000
	Waitohi Downs Fault	30	N/A	N/A	N/A	N/A	N/A	N/A
	Mt Culverden Fault	7	N/A	N/A	N/A	N/A	N/A	N/A
	unnamed Fault	5	N/A	N/A	N/A	N/A	N/A	N/A

Figure 4.6.: Fault rupture parameters for the individual segments (Howard et al., 2005, Noble, 2011).

The last step deals with the slip rate of the fault. Peak velocity is the 9.3 mm/year at the Hawdon Fault, while a low estimate is given by Noble (2011) for the northern Esk Fault with 0.82 mm/year. I gave the most weight to an intermediate slip rate which was reported by Howard et al. (2005) at the Porters Pass Fault, 4.1 mm/year. From slip rate and average displacement results the recurrence interval of the fault is calculated.

One of the most likely fault scenarios is a 140 km long fault with an average displacement of 4.87 m. It is capable of earthquakes of maximum magnitude 7.64 with a recurrence interval of 530 years. Another option involves an average displacement of 5.50 m and M_W 7.64 earthquakes every 598 years.

If the fault is not rupturing as a whole a segmented fault scenario for the dextral movement is proposed (Fig. 4.6). This scenario includes the reported displacements and slip rates of the Porters Pass Fault (Howard et al., 2005) and northern Esk Fault (Noble, 2011). The lateral displacement for the Hawdon Fault, Bullock Hill Fault, and southern Esk Fault are from this study. In case of the Hawdon and Bullock Hill fault recurrence rate and moment magnitude are derived from the 5 km fault length these faults show in the field.

4.4 Discussion

4.4.1 Blind faults

Several clearly delineated fault traces in North Canterbury seem to 'disappear' when they encounter thick glacial-fluvial sedimentary sequences. The Bullock Hill fault trace runs through the hills, disappears in the Poulter advance gravels without a trace, and potentially reappears in line with a younger alluvial terrace before disappearing again under older glacial gravels. Glacial gravels also obscure the expression of fault displacement along the Esk faults. A very clear trace can be found in the northern part, where there is no glacial cover sequence while the southern part is barely exposed anywhere but along bedrock.

Thick, poorly consolidated glacial gravels cause significant seismic refraction and dissipation of seismic energy during earthquakes. This prevents the underlying fault from rupturing the surface in a discrete plane. Instead the displacement may be very subtle or completely unrecognisable. A second explanation is that post-rupture erosion and deposition removes the observable rupture trace relatively fast. While this is a process that has to be considered when dealing with other faults in more level terrain, here we favour the former explanation. There is no sign of surface processes such as paleo-stream-channels on the glacial gravels that do not also affect the lower lying river terrace.

The disappearance and reappearance of the fault traces along strike suggests that they are continuous faults at depth with discontinuous surface traces (e.g. blind fault segments). Blind faults present a considerable hazard in urban centres around the world, e.g. the Puente Hills blind thrust under Los Angeles, California, with at least four MW = 7.2-7.5 earthquakes in the last 11000 years (Dolan et al., 2003), a blind normal fault in the Taipei Basin under Taipei, Taiwan, causing 3 smaller earthquakes (M = 3.8, 3.2, 3.7) since 2004 (Chen et al., 2010) and the Biwako-seigan fault zone under Kyoto, Japan, which last ruptured in 1185 with M = 7.4 (Kaneda et al., 2008), but the absence of a surface expression makes the hazard potential difficult to assess. The Stuoragurra fault in Norway has about 10 m of total displacement identified in trench studies, but there is no surface expression in the overlying glacial materials (Dehls et al., 2000) comparable to the faults examined in this study.

Folding of the cover sequence often accompanies the blind thrust faults but it is less likely along simple, linear segments of strike-slip faults (e.g. Parsons et al., 2005, Giménez et al., 2009). This agrees with the observation of anticlinal folding on the reverse Esk fault with no folding on the other two dextral faults. Lettis et al. (1997) argue that most blind thrust faults can be detected by geomorphic and paleo-seismic studies, however, this is not the case in blind strike-slip faulting as seen in the Bam earthquake in Iran (Talebian et al., 2004).

If some segments of the Hawdon, Bullock Hill and Esk faults are blind, other active blind faults are likely to exist in North Canterbury as argued by Pettinga et al. (2001). Instrumentally recorded seismicity shows that the Canterbury Plains are tectonically active, although only a few active structures (e.g. Racecourse Hill) are geomorphically expressed (Pettinga et al., 2001). That these blind faults pose a major hazard to the city of Christchurch is demonstrated by the previously undetected Greendale fault (Quigley et al., 2010). Since no previous surface expression indicated the fault's presence the fault has either not ruptured since the Last Glacial Maximum (LGM) or behaved as a blind fault whose previous post-LGM ruptures were not preserved in the Quaternary river gravels. The latter is possible considering the subtle expression of the recent surface rupture could easily be removed with modification of the surface by farming.

Lettis et al. (1997) report a magnitude dependance for surface rupture. While only 40% of earthquakes at magnitude 5.9 rupture the surface and show co-seismic displacement more than 90% do so at magnitude 7.2. Given the fact that co-seismic displacement of the Hawdon and Bullock Hill Fault is caused by M>7.2 a failure to rupture the glacial gravels means either their part of the 10% that do not rupture the surface or had a long enough quiet period for surface processes to obscur and bury the fault trace and could be overdue for another large earthquake.

The presence of blind faults in Canterbury that have not yet been identified or investigated is possibly one of the major contributing factors to the slip deficit reported by Wallace et al. (2007).

4.4.2 Fault linkage

The similar length (5 km) of the Bullock Hill and Hawdon faults, their overlapping tips, their proximity to each other, and their comparable deformation pattern makes linkage between these faults feasible. The Mt White Fault is close enough according to Wesnousky (2008) to be ruptured co-seismically in an event on the two smaller faults. The other faults in the system appear to too far for direct linkage, but this discounts the presence of blind faults in the area. Most of the area is covered by glacial gravels as can be seen by the discontinuous trace of the

southern Esk Fault. There could be any number of blind faults lying under these gravels as demonstrated by the Arthurs's Pass and Cass earthquakes, that occurred on unknown faults (Robinson et al., 1995, Abercrombie et al., 2000, Robinson & McGinty, 2000, Gledhill et al., 2000).

The southern Esk Fault is different from the other two faults as it shows primarily reverse movement and less activity. Looking at the configuration of the fault system (Fig. 4.3) the southern Esk Fault also does not quite fit in the overlapping. Fault strike indicates the Torlesse Fault and Hawdon Fault overlap, while the Esk fault lies in the stress shadow. Assuming the southern Esk Fault is not part of the system does not fit well with the other end of the fault, where it overlaps in a diagnostic hook-shape with the northern Esk Fault indicating advanced linkage (Acocella et al., 2000). Thus, similar to the description by Gupta et al. (1998) the southern Esk Fault is part of the system having already linked with the Torlesse Fault. I propose that activity has moved westwards to the Hawdon, Bullock Hill and Mt White faults.

The highest slip rates in the fault system occurs on the Hawdon and Bullock Hill faults with slip rates of ∼9 mm/year. This is not unusual as slip during fault linkage is generally greater in the central segments of the fault system (Willemse et al., 1996, Xu et al., 2006). Further, the Porters Pass fault slips at 0.3-0.9 mm/year at its western end, the tip of the fault system, and 3.2-4.1 mm/year at its eastern end, which is 40 km closer to the centre of our proposed fault system (Howard et al., 2005) as well as possibly interacting with other fault segments of the system which promotes a higher displacement rate (Gupta et al., 1998, Xu et al., 2006). Likewise at the other end of the system, the slip rate on the northern part of the Esk fault decreases to 0.82 mm/year. By linking these faults, and summing up their slip rates, a closer match is found with the aseismic deformation measured by GPS data (Wallace et al., 2007). Following that asymmetric patter, I predict that the Waitohi Downs Fault, Mt Culverden Fault and the unnamed little fault at the end of the system have very low slip rates of less than 0.5 mm/year. As the tips of the active faults propagate slip rate on these segments will increase.

The main question remains if the fault system ruptures at a whole or if rupture is segmented. Given the maximum displacement at the Hawdon Fault and Bullock Hill Fault, these only make sense in a whole fault rupture. However, the southern Esk Fault can be well described by a segment rupture as seems to happen for the northern Esk Fault and Porters Pass Fault (Howard et al., 2005, Noble, 2011) though these two show lateral co-seismic displacement suggestive of a larger fault. As this fault system is incipient I propose a complicated rupture pattern, where segments can rupture without triggering rupture on the other fault, but the fault system occasionally ruptures as a whole. A comparison of the timing of paleoseismic events needs to be done to distinguish between segmented rupture and unsegmented one.

If the fault ruptures as a whole, the hypocentre does not have to be at the source of maximum displacement, i.e. the Hawdon Fault and Bullock Hill Fault (Gupta & Scholz, 2000, Wesnousky, 2008). Gupta & Scholz (2000) showed that there is no correlation between the hypocentresource of the earthquake and the maximum displacement. This means the earthquake does not necessarily have to initiate near the Hawdon Fault or Bullock Hill Fault but could do so anywhere near in the system.

If I compare the proposed fault system to the Marlborough Faults, several similarities stand out. The length of the system is comparable to the northern faults, accompanied by the same overall dextral deformation mechanism and similar northeastern strike. The temporal relation-

ships amongst fault initiation ages of the Marlborough Fault System suggest that a new fault initiates every 1.4-1.9 Ma further south (Wallace et al., 2007). The Hope Fault has started activity a reported ∼1 Ma ago (Wood et al., 1994), it is thus feasible that another system is initiating further south. The current incipient state of the proposed fault system fits these requirements surprisingly well.

4.5 Conclusion

Geomorphologic and paleoseismic data from the Waimakariri valley and other parts of North Canterbury supports the notion that the Hawdon fault and Bullocks Hills fault, are the centre of a major regional fault zone spanning a length of 140 km and extending from the western tip of the Porters Pass fault to the Hope fault, east of Hanmer Springs. Both, the Hawdon and Bullock Hill faults exhibit a slip rate of over 9 mm/year, twice as much as the Porters Pass fault, with post-glacial channel offsets of more than 100 m. Mapping of these faults has revealed significant blind faulting in North Canterbury caused when faults cross glacial gravels and this may help explain the observed slip deficit in the region.

Along a NE strike from the south-west tip of the Porters Pass fault to the Hope fault east of Hanmer Springs, which presents a northern binding fault for this incipient fault system, an accommodation space of ∼140 km can be established, exactly the required fault length for the observed co-seismic displacements on the Hawdon and Bullock Hill Fault. Although the known faults in this area do not total in length to this accommodation space, I expect that there are yet more blind faults in North Canterbury still to be discovered that will fill the missing links. The missing links will also be filled as the existing faults' tips continue to propagate and it is possible that entirely new sections may form before the fault system reaches the maturity of the Marlborough Fault System and forms a continuous structure. Therefore, I propose the existence of a 140 km long dextral fault system stretching from the Porters Pass to the Hope fault of a similar scale to the Marlborough Fault System faults. The location, comparable strike and dextral deformation mode makes this developing fault system the southernmost extension of the Marlborough Fault System.

5. Conclusions and future work

- Geological and geomorphical mapping revealed a series of very active small-scaled faults and blind faulting in the Waimakariri Valley.
- The Esk Fault has been previously recognised but unstudied. In contrary to first impressions the fault has been active in post-glacial times showing a Holocene vertical offset of 3.4±0.2 m near Lake Blackwater.
- The Esk Fault does not rupture the surface in many places and surface rupture is removed in others as is the case on the Esk River mouth where post-glacial terraces seem offset by 20-35 m but no fault trace can be seen in the fast eroding river bed.
- The average displacement of the Esk Fault correlates well with the observed rupture length of 30±10 km. The fault is capable of M_W 6.97-7.02±0.14 earthquakes with a recurrence rate of approximately 2000 years.
- The Hawdon Fault is a 5±1 km long NE trending fault with a post-glacial dextral offset of 140±10 m that crops out in the Mt St Bernard hill but does not rupture through the glacial gravels that cover the valley floor. The favoured slip rate for the fault is 9.3±2.8 mm/year.
- From a lake core a seismic record can be established for the Hawdon Fault showing 13±4 sedimentary events that implicate a maximum displacement of 10.77±3.31 m.
- The Bullock Hill Fault is another 5±1 km long NE trending fault with a potential post-glacial dextral offset of 110±10 m and an average displacement of 5±0.5 m. The fault crops out in the northern hillside of the Bullock Hill and probably extends on to an alluvial terrace on the other side of the Waimakariri River and beyond as indicated by a knickpoint on the Poulter River.
- The post-glacial lateral slip rate of the Bullock Hill Fault is 9.2±1.8 mm/year. The fault has also minor vertical movement.
- The Og-Gog-Magog Fault is a 1 km long NW trending fault that is exposed in the southern flanks of the three hills and has normal movement indicative of the regional shortening direction.
- Both, the Hawdon Fault and Bullock Hill Fault have estimated surface rupture length from their co-seismic slip that extend to 140 km, surpassing the exposed surface traces by far. Both faults would generate earthquakes of M_W 6 on a frequent basis if treated as isolated small faults but could generate M_W 7.6 events if derived from their estimated rupture length.

- The inconsistency between exposed fault trace and estimated rupture length for the Hawdon Fault and Bullock Hill Fault in conjunction with a similar discrepancy reported for the Porters Pass Fault led to the hypothesis of a new incipient dextral NE trending fault system that extends from the western tip of the Porters Pass Fault to the Hope Fault near Hanmer Springs over a length of 140 km.
- The new fault system shows various degrees of fault linkage and includes a number of blind faults as well as the following faults: Porters Pass Fault, Torlesse Fault, Hawdon Fault, Bullock Hill Fault, Mt White Fault, southern and northern Esk Fault, Waitohi Downs Fault, Mt Culverden Fault and an unnamed fault.
- As an incipient fault system the whole system can evolve as own fault but also on separate segments with no kinematic interaction. The whole system is capable of generating M_W 7.64 earthquakes every 530 years with a co-seismic average displacement of 4.87 m.
- The strike and dextral deformation of the incipient fault system are similar to the Marlborough Fault system and its southern location implicates that this system is the southernmost extension of the Marlborough Fault System.

Future work will include:

- Cosmogenic surface exposure dating of abandoned river channel might provide minimum channel ages that will help to further define the activity of the studied faults.
- Paleoseismology needs to be established for the Torlesse Fault, Mt White, Waitohi Downs Fault, Mt Culverden Fault, and the unnamed fault.
- Geomorphic mapping needs to be done not only in areas of unstudied faults but an areas where no surface rupture is present lest there are currently undetected blind faults.
- Modelling will give an impression of how the fault system ruptures in an event and how it will evolve in the future.
- To further test if the fault system is capable of rupturing as a whole or even rupture adjacent segments at the same time, paleo-earthquakes need to be checked for synchronity.

Bibliography

Abercrombie, R., Webb, T., Robinson, R. & McGinty, P. (2000): The enigma of the Arthur's Pass, New Zealand, earthquake: 1. Reconciling a variety of data for an unusual earthquake sequence. *Journal of Geophysical Research*, **105** (B7).

Acocella, V., Gudmundsson, A. & Funiciello, R. (2000): Interaction and linkage of extension fractures and normal faults: examples from the rift zone of Iceland. *Journal of Structural Geology*, **22**, 1233–1246.

Aitken, M. J. (1998): *An introduction to optical dating: the dating of Quaternary sediments by the use of photon-stimulated luminescence* (Oxford University Press, Oxford).

Aki, K. & Richards, P. G. (1980): *Quantitative Seismology: Theory and methods* (W. H. Freeman, San Francisco, California).

Allen, S. K., Cox, S. C. & Owens, I. F. (2010): Rock avalanches and other landslides in the central Southern Alps of New Zealand: a regional study considering possible climate change impacts. *Landslides*.

Arnadottir, T., Beavan, J. & Pearson, C. (1995): Deformation associated with the 18 June 1994 Arthur's Pass earthquake New Zealand. *New Zealand Journal of Geology and Geophysics*, **38** (553-558).

Aydin, A. & Schultz, R. A. (1990): Effect of mechanical interaction on the development of strike-slip faults with échelon patterns. *Journal of Structural Geology*, **12**, 123–129.

Beck, C., Manalt, F., Chapron, E., van Rensbergen, P. & Batist, M. d. (1996): Enhanced seismicity in the early post-glacial period: evidence from the post-Würm sediments of Lake Annecy, Northwestern Alps. *Journal of Geodynamics*, **22** (1), 155–171.

Begg, J. G. & Johnston, M. R. (2000): Geology of the Wellington area. 1:250,000 Geological Map.

Berryman, K. & Villamor, P. (2004): Surface rupture of the Poulter Fault in the 1929 March 9 Arthur's Pass earthquake, and redefinition of the Kakapo Fault, New Zealand. *New Zealand Journal of Geology and Geophysics*, **47** (2), 341–351.

Berryman, K., Webb, T., Hill, N., Stirling, M., Rhoades, D., Beavan, J. & Darby, D. (2002): Seismic Loads on Dams - Waitaki System: Earthquake Source Characterisation - Main Report.

Browne, G. H. (1992): The northeastern portion of the Clarence Fault: tectonic implications for late Neogene evolution of Marlborough, New Zealand. *New Zealand Journal of Geology and Geophysics*, **35**, 437–445.

Bull, W. B. (1991): *Geomorphic Responses to Climate Change* (Oxford University Press, New York).

Burchfiel, B. C. & Royden, L. H. (1985): North-south extension within the convergent Himalayand region. *Geology*, **13** (10), 679–682.

Campbell, J. (1973): Displacement data from the Alpine fault at Lake Rotoiti and its relevance to glacial chronology and the tempo of tectonism. *IXth Congress INQUA (International Union for Quaternary Research) Abstracts Volume 57-58*.

Cartwright, J. A., Trudgill, B. D. & Mansfield, C. S. (1995): Fault growth by segment linkage: an explanation for scatter in maximum displacement and trace length data from the Canyonlands Grabens of SE Utah. *Journal of Structural Geology*, **17** (9), 1319–1326.

Chen, K. C., Huang, B. S., Huang, W. G., Wang, J. H., Kim, K. H., Lee, S. J., Lai, Y. C., Tsao, S. & Chen, C. H. (2010): A Blind Normal Fault beneath the Taipei Basin in Northern Taiwan. *Terrestrial Atmospheric and Oceanic Sciences*, **21** (3), 495–502.

Cowan, H. (1990): Late Quaternary displacements on the Hope fault at Glynn Wye, North Canterbury. *New Zealand Journal of Geology and Geophysics*, **33**, 285–293.

Cowan, H., Nicol, A. & Tonkin, P. (1996): A comparison of historical and paleoseismicity in a newly formed fault zone and a mature fault zone, North Canterbury, New Zealand. *Journal of Geophysical Research*, **101** (B3), 6021–6036.

Cox, S. C. & Barrell, D. J. A. (2007): Geology of the Aoraki area. 1:250,000 Geological Map.

Dalmayrac, B. & Molnar, P. (1981): Parallel thrust and normal faulting in Peru and constraints on the state of stress. *Earth and Planetary Science Letters*, **55** (3), 473–481, doi: 10.1016/0012-821X(81)90174-6.

Davis, J. L. & Annan, A. P. (1989): Ground penetrating radar for high-resolution of soil and rock stratigraphy. *Geophysical Prospecting*, **37**, 531–551.

Dawers, N. H. & Anders, M. H. (1995): Displacement-length scaling and fault linkage. *Journal of Structural Geology*, **17** (5), 607–614.

Dehls, J. F., Olesen, O., Olsen, L. & Blikra, L. H. (2000): Neotectonic faulting in northern Norway; the Stuoragurra and Nordmannvikdalen postglacial faults. *Quaternary Science Reviews*, **19**, 1447–1460.

van Dissen, R. J., Berryman, K., Webb, T., Stirling, M., Villamor, P., Wood, P. R., Nathan, S., Nicol, A., Begg, D., Barrel, D., McVerry, G., Langridge, R., Litchfield, N. & Pace, B. (2003): An interim classification of New Zealand's active faults for the mitigation of surface rupture hazard. *2003 Pacific Conference on Earthquake Engineering*.

van Dissen, R. J. & Nicol, A. (1998): Paleoseismicity of the middle Clarence Valley section of the Clarence fault, Marlborough, New Zealand. *Geological Society of NZ Miscellaneous Publications*, **101 A**, 233.

Dolan, J. F., Christofferson, S. A. & Shaw, J. H. (2003): Recognition of Paleoearthquakes on the Puente Hills Blind Thrust Fault, California. *Science*, **300**, 115–118.

Duffy, B., Quigley, M., van Dissen, R. J., Stahl, T., Leprince, S., McInnes, C., Barrell, D. & Bilderback, E. (2012): Earthquake dynamics at a releasing fault bend from multi-temporal LiDAR. *submitted*.

Duller, G. A. T. (1996): Recent developments in luminescence dating of Quaternary sediments. *Progress in Physical Geography*, **20**, 127–145.

Fitzsimons, S. J. (1997): Late-glacial and early holocene glacier activity in the Southern Alps, New Zealand. *Quaternary International*, **38/39**, 69–76.

Forsyth, P. J., Barrel, D. J. A. & Jongens, R. (2008): Geology of the Christchurch area. 1:250000 Geological Map.

Gage, M. (1958): Late Pleistocene glaciation of the Waimakariri Valley, Canterbury. *New Zealand Journal of Geology and Geophysics*, **1**, 103–122.

Gage, M. (1970): Late Cretaceous and Tertiary rocks of Broken River, Canterbury. *New Zealand Journal of Geology and Geophysics*, **13**, 507–559.

Gage, M. & Suggate, R. P. (1958): Glacial Chronology of the New Zealand Pleistocene. *Bulletin of the Geological Society of America*, **69**, 589–598.

Giménez, J., Borque, M. J., Gil, A. J., Alfaro, P., Estévez, A. & Suriñach, E. (2009): Comparison of long-term and short-term uplift rates along an active blind reverse fault zone (Bajo Segura, SE Spain). *Studia Geophysica et Geodaetica*, **53**, 81–98.

Gledhill, K., Robinson, R., Webb, T., Abercrombie, R., Beavan, J., Cousins, J. & Eberhart-Phillips, D. (2000): The Mw 6.2 Cass, New Zealand, earthquake of 24 November 1995: Reverse faulting in a strike-slip region. *New Zealand Journal of Geology and Geophysics*, **43** (2), 255–269.

GNS Science (03/06/2011b): Investigations reveal previously unknown fault structures in Canterbury region. URL `http://www.gns.cri.nz/Home/News-and-Events/Media-Releases/Fault-structures-revealed`.

GNS Science (06/09/2011a): Graphic shows two main Christchurch fault ruptures. URL `http://www.gns.cri.nz/Home/News-and-Events/Media-Releases/Two-main-faults`.

Gregg, D. R. (1964): Sheet 18 Hurunui (1st ed.)., Geological Map of N.Z. 1: 250000.

Gupta, A. & Scholz, C. H. (2000): A model of normal fault interaction based on observations and theory. *Journal of Structural Geology*, **22**, 865–879.

Gupta, S., Cowie, P. A., Dawers, N. H. & Underhill, J. R. (1998): A mechanism to explain rift-basin subsidence and stratigraphic patterns through fault-array evolution. *Geology*, **26** (5), 595–598.

Gutenberg, B. & Richter, C. F. (1944): Earthquake study in southern California. *Eos, Transaction AGU*, **26**, 313–314.

Hack, J. T. (1973): Stream-Profile Analysis and Stream-Gradient Index. *Jour. Research U.S. Geol. Survey*, **1** (4), 421–429.

Hampel, A. & Hetzel, R. (2006): Response of normal faults to glacial-interglacial fluctuations of ice and water masses on Earth's surface. *Journal of Geophysical Research*, **111** (B06406).

Hampel, A., Hetzel, R. & Maniatis, G. (2010): Response of faults to climate-driven changes in ice and water volumes on Earth's surface. *Philosophical Transactions of the Royal Society A: Mathematical, Physical and Engineering Sciences*, **368** (1919), 2501–2517.

Hanks, T. C. & Bakun, W. H. (2002): A bilinear source-scaling model for M-log A observations of continental earthquakes. *Bulletin of the Seismological Society of America*, **92** (5), 1841–1846.

Hanks, T. C. & Kanamori, H. (1979): Hanks, T.C., Kanamori, H. 1979. A moment magnitude scale. Journal of Geophysical Research 84. 2348-2350. *Journal of Geophysical Research*, **84**, 2348–2350.

Howard, M., Nicol, A., Campbell, J. & Pettinga, J. (2005): Holocene paleoearthquakes on the strike-slip Porters Pass Fault, Canterbury, New Zealand. *New Zealand Journal of Geology and Geophysics*, **48**, 59–74.

Huggins, P., Watterson, J., Walsh, J. J. & Childs, C. (1996): Relay zone geometry and displacement transfer between normal faults recorded in coal-mine plans. *Journal of Structural Geology*, **17**, 1741–1755.

Johnston, A. C. (1996): Seismic moment assessment of earthquakes in stable continental regions-II, Historical seismicity. *Geophysical Journal International*, **125**, 639–678.

Kaneda, H., Kinoshita, H. & Komatsubara, T. (2008): An 18,000-year record of recurrent folding inferred from sediment slices and cores across a blind segment of the Biwako-seigan fault zone, central Japan. *Journal of Geophysical Research*, **113**, B05 401.

Keller, E. A. & Pinter, N. (2000): *Active Tectonics: Earthquakes, Uplift, and Landscape*. 2 ed. (Prentice Hall).

Knuepfer, P. L. K. (1992): Temporal variations in latest Quaternary slip across the Australian-Pacific plate boundary, northeastern South Island, New Zealand. *Tectonics*, **11** (3), 449–464.

Kostrov, V. V. (1974): Seismic moment and energy of earthquakes, and seismic flow of rock. *Physics of the Solid Earth*, **1**, 13–21.

Lettis, W. R., Wells, D. L. & Baldwin, J. N. (1997): Empirical observations regarding reverse earthquakes, blind thrust faults, and Quaternary deformation: Are blind thrust faults truly blind? *Bulletin of the Geological Society of America*, **87** (5), 1171–1198.

Litchfield, N., Campbell, J. & Nicol, A. (2003): Recognition of active reverse faults and folds in North Canterbury, New Zealand, using structural mapping and geomorphic analysis. *New Zealand Journal of Geology and Geophysics*, **46**, 563–579.

Little, T. A., Grapes, R. H. & Berger, G. W. (1998): Late Quaternary strike-slip on the eastern part of the Awatere fault, South Island, New Zealand. *Bulletin of the Geological Society of America*, **110**, 2–23.

Little, T. A. & Jones, A. (1998): Seven million years of strike-slip and related off-fault deformation, northeastern Marlborough fault system, South Island, New Zealand. *Tectonics*, **17** (2), 285–302.

McArthur, J. L. (1987): The characteristics, classification and origin of late Pleistocene fan deposits in the Cass Basin, Canterbury, New Zealand. *Sedimentology*, **34**, 459–471.

McGlone, M. S., Turney, C. S. M. & Wilmshurst, J. M. (2004): Late-glacial and Holocene vegetation and climatic history of the Cass Basin, central South Island, New Zealand. *Quaternary Research*, **62**, 267–279.

Moar, N. T. (1971): Aranuian Pollen Diagrams from Canterbury, Nelson, and North Westland, South Island. *New Zealand Journal of Botany*, **9**, 80–145.

Murry, A. S. & Wintle, A. G. (2000): Luminescence dating of quartz using an improved single aliquot regenerative dose protocol. *Radiation Measurements*, **32**, 57–73.

Nathan, S., Rattenbury, M. S. & Suggate, R. P. (2002): Geology of the Greymouth area. 1:250,000 Geological Map.

Nobes, D. C. (2011): Ground penetrating radar measurements over glaciers. In: Singh, V. P., Singh, P. & Haritashya, U. K. (Hrsgs.), *Encyclopedia of Snow, Ice and Glaciers*, pp. 490–504 (Springer Verlag, Heidelberg).

Noble, D. (2011): *Tectonic geomorphology of the northern Esk Fault*. PhD thesis, University of Canterbury, Christchurch.

Parsons, B., Wright, T., Rowe, P., Andrews, J., Jackson, J., Walke, R., Khatib, M., Talebian, M., Berman, E. & Engdahl, E. R. (2005): The 1994 Sefidabeh (eastern Iran) earthquakes revisited: new evidence from satellite radar interferometry and carbonate dating about the growth of an active fold above a blind thrust fault. *Geophysical Journal International*, **164**, 202–217.

Pettinga, J., Yetton, M. D., van Dissen, R. J. & Downes, G. (2001): Earthquake source identification and characterisation for the Canterbury region, South Island, New Zealand. *Bulletin of the New Zealand Society for Earthquake Engineering*, **34** (4), 282–317.

Prescott, J. R. & Hutton, J. T. (1994): Cosmic ray contributions to dose rates for luminescence and ESR dating: Large depths and long-term time variations. *Radiation Measurements*, **23** (2/3), 497–500.

Quigley, M., van Dissen, R., Villamor, P., Litchfield, N., Barrell, D., Furlong, K., Stahl, T., Duffy, B., Bilderback, E., Noble, D., Townsend, D., Begg, J., Jongens, R., Ries, W., Claridge, J., Klahn, A., Mackenzie, H., Smith, A., Hornblow, S., Nicol, R., Cox, S., Langridge, R. & Pedley, K. (2010): Surface rupture of the Greendale Fault during the Mw 7.1 Darfield (Canterbury) earthquake, New Zealand: Initial Findings. *Bulletin of the New Zealand Society for Earthquake Engineering*, **43** (4).

Quigley, M., van Dissen, R. J., Litchfield, N., Villamor, P., Duffy, B., Barrell, D., Furlong, K., Stahl, T., Bilderback, E. & Noble, D. (2012): Surface rupture during the 2010 M_W 7.1 Darfield (Canterbury) earthquake: Implications for fault rupter dynamics and seismic-hazard analysis. *Geology*, **40** (1).

Rattenbury, M. S., Cooper, R. A. & Johnston, M. R. (1998): Geology of the Nelson area. 1:250,000 Geological Map.

Rattenbury, M. S., Townsend, D. & Johnston, M. R. (2006): Geology of the Kaikoura area. 1:250,000 Geological Map.

Robinson, R. & McGinty, P. (2000): The enigma of the Arthur's Pass, New Zealand, earthquake 2. The aftershock distribution and its relation to regional and induced stress fields. *Journal of Geophysical Research*, **105** (B7), 16 139–16 150.

Robinson, R., Reyners, M., Webb, T., Arnadottir, T., Beavan, J., Cousins, J., van Dissen, R. & Pearson, C. (1995): The M_W 6.7 Arthur's Pass Earthquake in the Southern Alps, New Zealand, June 18, 1994. *Seismological Research Letters*, **66** (2).

Rother, H. (2006): *Late Pleistocene Glacial Geology of the Hope-Waiau Valley System in North Canterbury, New Zealand*. PhD thesis, University of Canterbury.

Segall, P. & Pollard, D. D. (1980): Mechanics of discontinuous faults. *Journal of Geophysical Research*, **85** (B8), 4337–4350.

Sibson, R., Ghisetti, F. & Crookbain, R. (2011): 'Andersonian' wrench faulting in a regional stress field during the 2010–2011 Canterbury, New Zealand, earthquake sequence. *Faulting, Fracturing and Igneous Intrusion in the Earth's Crust*, **Geological Society of London Special Volume (in press)**.

Speight, R. (1938): Morainic deposits of the Waimakariri Valley. *Transactions and Proceedings of the Royal Society of New Zealand*, **68**, 143–160.

Stirling, M. & Gerstenberger, M. (2010): Ground Motion-Based Testing of Seismic Hazard Models in New Zealand. *Bulletin of the Seismological Society of America*, **100** (4), 1407–1414, doi:10.1785/0120090336.

Stirling, M., Gerstenberger, M., Litchfield, N., McVerry, G., Smith, W., Pettinga, J. & Barnes, P. (2008): Seismic hazard of the Canterbury Region, New Zealand: New eathquake source model and methodology. *Bulletin of the New Zealand Society for Earthquake Engineering*, **41** (2), 51–67.

Stirling, M., Pettinga, J., Berryman, K. & Yetton, M. D. (2001): Probabilistic seismic hazard assessment of the Canterbury region, New Zealand. *Bulletin of the New Zealand Society for Earthquake Engineering*, **34** (4), 318–334.

Stirling, M., Rhoades, D. & Berryman, K. (2002): Comparison of Earthquake Scaling Relations Derived from Data of the Instrumental and Preinstrumental Era. *Bulletin of the Seismological Society of America*, **92** (2), 812–830.

Suggate, R. P. (1990): Late Pliocene and Quaternary glaciations of New Zealand. *Quaternary Science Reviews*, **9**, 175–197.

Talebian, M., Fielding, E. J., Funning, G. J., Ghorashi, M., Jackson, J., Nazari, H., Parsons, B., Priestley, K., Rosen, P. A., Walker, R. & Wright, T. (2004): The 2003 Bam (Iran) earthquake: Rupture of a blind strike-slip fault. *Geophysical Research Letters*, **31** (L11611).

Walcott, R. I. (1998): Modes of oblique compression: Late Cenozoic tectonics of the South Island, New Zealand. *Reviews of Geophysics*, **36** (1), 1–26.

Wallace, L. M., Beavan, J., McCaffrey, R., Berryman, K. & Denys, P. (2007): Balancing the plate motion budget in the South Island, New Zealand using GPS, geological and seismological data. *Geophysical Journal International*, **168**, 332–352.

Wannamaker, P. E., Caldwell, T. G., Jiracek, G. R., Maris, V., Hill, G. J. & Ogawa, Y. (2009): Fluid and deformation regime of an advancing subduction system at Marlborough, New Zealand. *Nature*, **460**, 733–737.

Wei, S., Fielding, E., Leprince, S., Sladen, A., Avouac, J.-P., Helmberger, D., Hauksson, E., Chu, R., Simons, M., Hudnut, K., Herring, T. & Briggs, R. (2011): Superficial simplicity of the 2010 El Mayor–Cucapah earthquake of Baja California in Mexico. *Nature Geoscience*, **4** (9), 615–618.

Wells, D. L. & Coppersmith, K. J. (1994): New Empirical Relationships among Magnitude, Rupture Length, Rupture Width, Rupture Area, and Surface Displacement. *Bulletin of the Seismological Society of America*, **84** (4), 974–1002.

Wesnousky, S. G. (2008): Displacement and Geometrical Characteristics of Earthquake Surface Ruptures: Issues and Implications for Seismic-Hazard Analysis and the Process of Earthquake Rupture. *Bulletin of the Seismological Society of America*, **98** (4), 1609–1632.

Willemse, E. J. M., Pollard, D. D. & Aydin, A. (1996): Three-dimensional analyses of slip distributions on normal fault arrays with consequences for fault scaling. *Journal of Structural Geology*, **18** (2&3), 295–309.

Wood, R. A., Pettinga, J., Bannister, S., Lamarche, G. & McMorran, T. J. (1994): Structure of the Hanmer strike-slip basin, Hope fault, New Zealand. *Bulletin of the Geological Society of America*, **106**, 1459–1473.

Xu, S.-S., Nieto-Samaniego, A. F., Alaniz-Álvarez, S. A. & Velasquillo-Martínez, L. G. (2006): Effect of sampling and linkage on fault length and length–displacement relationship. *International Journal of Earth Science (Geologische Rundschau)*, **95**.

A. Stream Gradient Indices

Elevation (m)	Length (m)	GI	K	Stream Gradient Index
960	0			
940	450	10	120.65	0.08
920	900	30	155.43	0.19
900	1175	75.45	175.48	0.43
880	1700	54.76	194.79	0.28
860	2300	66.67	219.62	0.3
840	2825	97.62	243.35	0.4
820	3275	135.56	263.72	0.51
800	3650	184.67	281.12	0.66
780	4300	122.31	303.24	0.4
760	5000	132.86	333.7	0.4
740	5700	152.86	367.53	0.42
720	6500	152.5	407.18	0.37
700	7625	125.56	465.03	0.27
680	8600	166.41	540.61	0.31
660	9550	191.05	626.41	0.3
640	10700	176.09	747.25	0.24
620	12225	150.33	971.09	0.15
600	13075	297.65	1299.21	0.23
580	14800	161.59	2009.32	0.08
560	15675	348.29	4356.45	0.08
540	17575	175	-18698.4	0.01
520	18800	296.94	-2678.54	0.11
500	20225	273.86	-1538.89	0.18
480	21600	304.18	-1050.44	0.29
460	22975	324.18	-790.91	0.41
440	24650	284.33	-610.53	0.47
420	25975	382.08	-488.55	0.78
400	28350	228.74	-378.36	0.6
380	30650	256.52	-271.07	0.95
360	32725	305.42	-175.48	1.74

Table A.1.: Broken River

Elevation (m)	Length (m)	GI	K	Stream Gradient Index
976	0			
960	250	8	101.72	0.08
940	475	32.22	130.32	0.25
920	650	64.29	147.69	0.44
900	750	140	158.3	0.88
880	950	85	169.19	0.5
860	1100	136.67	181.34	0.75
840	1300	120	193.15	0.62
820	1500	140	206.44	0.68
800	1750	130	221.38	0.59
780	2125	103.33	242.44	0.43
760	2575	104.44	271.46	0.38
740	2875	181.67	299.72	0.61
720	3250	163.33	327.26	0.5
700	3750	140	366.89	0.38
680	4475	113.45	432.63	0.26
660	5375	109.44	548.73	0.2
640	6200	140.3	738.75	0.19
620	7450	109.2	1200.79	0.09
600	9800	73.4	-57249.64	0
580	11800	108	-948.47	0.11
560	13725	132.6	-470.78	0.28
540	14925	238.75	-309.66	0.77
520	15725	383.13	-236.48	1.62
500	16200	672.11	-193.98	3.46
480	16875	490	-153.57	3.19
476	17175	227	-105.67	2.15

Table A.2.: Winding Creek

Elevation (m)	Length (m)	GI	K	Stream Gradient Index
600	0			
580	2375	10	77.11	0.13
560	5425	25.57	164.29	0.16
540	9325	37.82	729.85	0.05
520	11100	115.07	-503.09	0.23
500	13200	115.71	-221.48	0.52
480	14200	274	-142.76	1.92
460	14650	641.11	-118.04	5.43
440	15550	335.56	-98.32	3.41
420	16025	664.74	-79.79	8.33
400	17075	315.24	-57.96	5.44

Table A.3.: Slovens Stream

Elevation (m)	Length (m)	GI	K	Stream Gradient Index
615	0			
600	1275	7.5	48.07	0.16
580	4050	19.19	81.2	0.24
560	6700	40.57	130.05	0.31
540	9200	63.6	210.08	0.3
520	12075	74	445.48	0.17
500	15050	91.18	-3772.9	0.02
480	18575	95.39	-322.88	0.3
460	22350	108.41	-145.83	0.74
440	25000	178.68	-83.73	2.13
437	26500	51.5	-50.34	1.02

Table A.4.: Poulter River

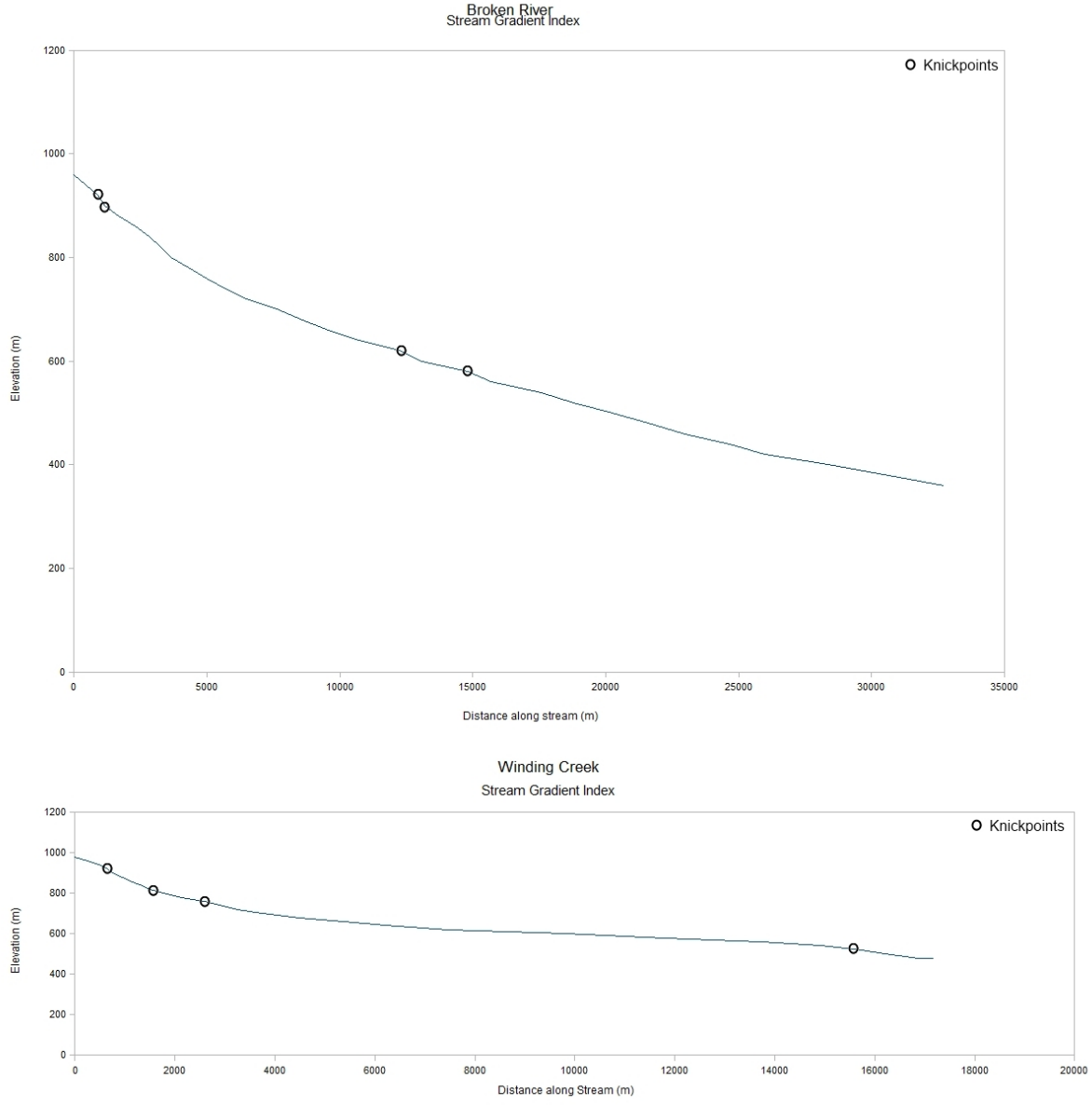

Figure A.1.: Stream profile of the Broken River and Winding Creek

Elevation (m)	Length (m)	GI	K	Stream Gradient Index
1176	0			
1160	325	8	136.33	0.06
1140	675	28.57	171.24	0.17
1120	875	77.5	190.4	0.41
1100	1075	97.5	202.33	0.48
1080	1725	43.08	224.69	0.19
1060	2325	67.5	253.64	0.27
1040	2750	119.41	275.67	0.43
1020	3225	125.79	294.4	0.43
1000	3500	244.55	309.8	0.79
980	3900	185	323.63	0.57
960	4325	193.53	340.6	0.57
940	4875	167.27	360.89	0.46
920	5425	187.27	384.29	0.49
900	6175	154.67	412.92	0.37
880	6800	207.6	444.74	0.47
860	7700	161.11	482.37	0.33
840	8575	186	530.1	0.35
820	9400	217.88	580.82	0.38
800	10150	260.67	633.35	0.41
780	10950	263.75	691.54	0.38
760	12150	192.5	778.92	0.25
740	13525	186.73	919.71	0.2
720	15325	160.28	1163.43	0.14
700	16925	201.56	1591	0.13
680	18850	185.84	2508.83	0.07
660	19925	360.7	4815.96	0.07
640	21600	247.91	28953.6	0.01
620	23175	284.29	-5890.19	0.05
600	25150	244.68	-2529.21	0.1
580	26700	334.52	-1599.45	0.21
560	28650	283.85	-1158.73	0.24
540	30700	289.51	-867.51	0.33
520	32175	426.27	-698.59	0.61
500	33850	394.18	-585.58	0.67
480	35650	386.11	-486.23	0.79
460	37350	429.41	-402.87	1.07
440	39450	365.71	-322.61	1.13
420	41725	356.81	-228.95	1.56
419	42075	119.71	-138.18	0.87

Table A.5.: Esk River

Elevation (m)	Length (m)	GI	K	Stream Gradient Index
560	31600			
540	34625	218.93	183.48	1.19
520	39100	164.75	202.82	0.81
500	42400	246.97	225.7	1.09
480	46875	199.5	252.37	0.79
460	50100	300.7	283.77	1.06
440	54325	247.16	320.59	0.77
420	60200	194.94	385.33	0.51
400	66150	212.35	497.64	0.43
380	71950	238.1	689.99	0.35
360	76450	329.78	1030.27	0.32
340	80000	440.7	1661.59	0.27
320	86425	259.03	6735.35	0.04
300	92875	277.98	-2295.57	0.12

Table A.6.: Waimakariri River

Elevation (m)	Length (m)	GI	K	Stream Gradient Index
860	0			
840	150	10	43.18	0.23
820	450	20	62.2	0.32
800	900	30	84.99	0.35
780	1350	50	112.56	0.44
760	2000	51.54	154.74	0.33
740	2475	94.21	220.71	0.43
720	3075	92.5	339.68	0.27
700	3375	215	581.07	0.37
680	3700	217.69	1107.71	0.2
660	3975	279.09	7774.57	0.04
640	4150	464.29	-2219.93	0.21
620	4275	674	-1193.36	0.56
600	4450	498.57	-814.33	0.61
580	4850	232.5	-503.23	0.46
560	5100	398	-347.94	1.14
540	5550	236.67	-257.62	0.92
520	6225	174.44	-175.81	0.99
500	7000	170.65	-115.05	1.48
489	7775	104.85	-67.85	1.55

Table A.7.: Brechin Burn

Elevation (m)	Length (m)	GI	K	Stream Gradient Index
636	0			
620	750	8	94.34	0.08
600	1750	25	215.73	0.12
580	2200	87.78	555.89	0.16
560	2650	107.78	3948.81	0.03
540	2975	173.08	-943.04	0.18
520	3050	803.33	-569.86	1.41
500	3250	315	-445.31	0.71
480	3525	246.36	-319.28	0.77
460	3800	266.36	-235.27	1.13
440	4000	390	-187.25	2.08
420	4275	300.91	-151.15	1.99
400	4525	352	-118.95	2.96
399	5000	10.03	-79.04	0.13

Table A.8.: Broadleaf Stream

Elevation (m)	Length (m)	GI	K	Stream Gradient Index
998	0			
980	400	9	67.99	0.13
960	1125	21.03	113.59	0.19
940	1475	74.29	160.69	0.46
920	1975	69	211.19	0.33
900	2325	122.86	287.26	0.43
880	2900	90.87	440.95	0.21
860	3375	132.11	1005.26	0.13
840	3825	160	-11447.08	0.01
820	4475	127.69	-724.02	0.18
800	5075	159.17	-339.93	0.47
780	5650	186.52	-216.59	0.86
760	6550	135.56	-135.12	1
757	7125	35.67	-76.05	0.47

Table A.9.: Grant Stream

Elevation (m)	Length (m)	GI	K	Stream Gradient Index
920	0			
900	225	10	106.62	0.09
880	525	25	149.41	0.17
860	750	56.67	182.87	0.31
840	1175	45.29	223.15	0.2
820	1625	62.22	282.71	0.22
800	2450	49.39	397.18	0.12
780	2800	150	567.99	0.26
760	3000	290	694.33	0.42
740	3350	181.43	881.58	0.21
720	3650	233.33	1271.9	0.18
700	4175	149.05	2794.76	0.05
680	4400	381.11	-39214.55	0.01
660	4500	890	-5225.29	0.17
640	4750	370	-2697.95	0.14
620	5100	281.43	-1467.82	0.19
600	5300	520	-1028.65	0.51
580	5525	481.11	-831.4	0.58
560	5825	378.33	-667.88	0.57
540	6175	342.86	-531.47	0.65
520	6600	300.59	-420.2	0.72
500	7150	250	-322.33	0.78
480	7675	282.38	-242.54	1.16
460	8525	190.59	-156.06	1.22

Table A.10.: Boundary Stream

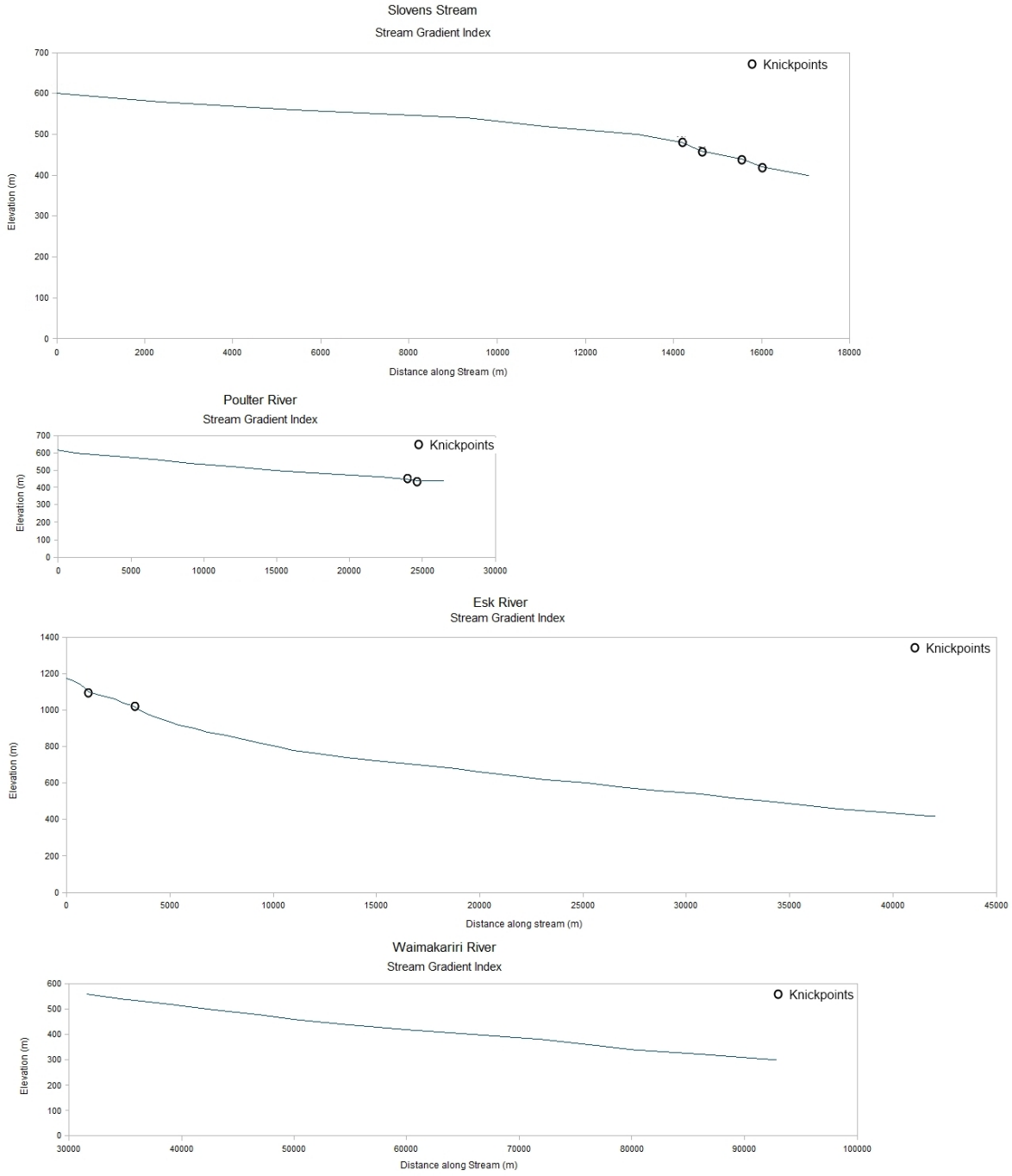

Figure A.2.: Stream profile of the Slovens Stream, Poulter River, Esk River, and Waimakariri River

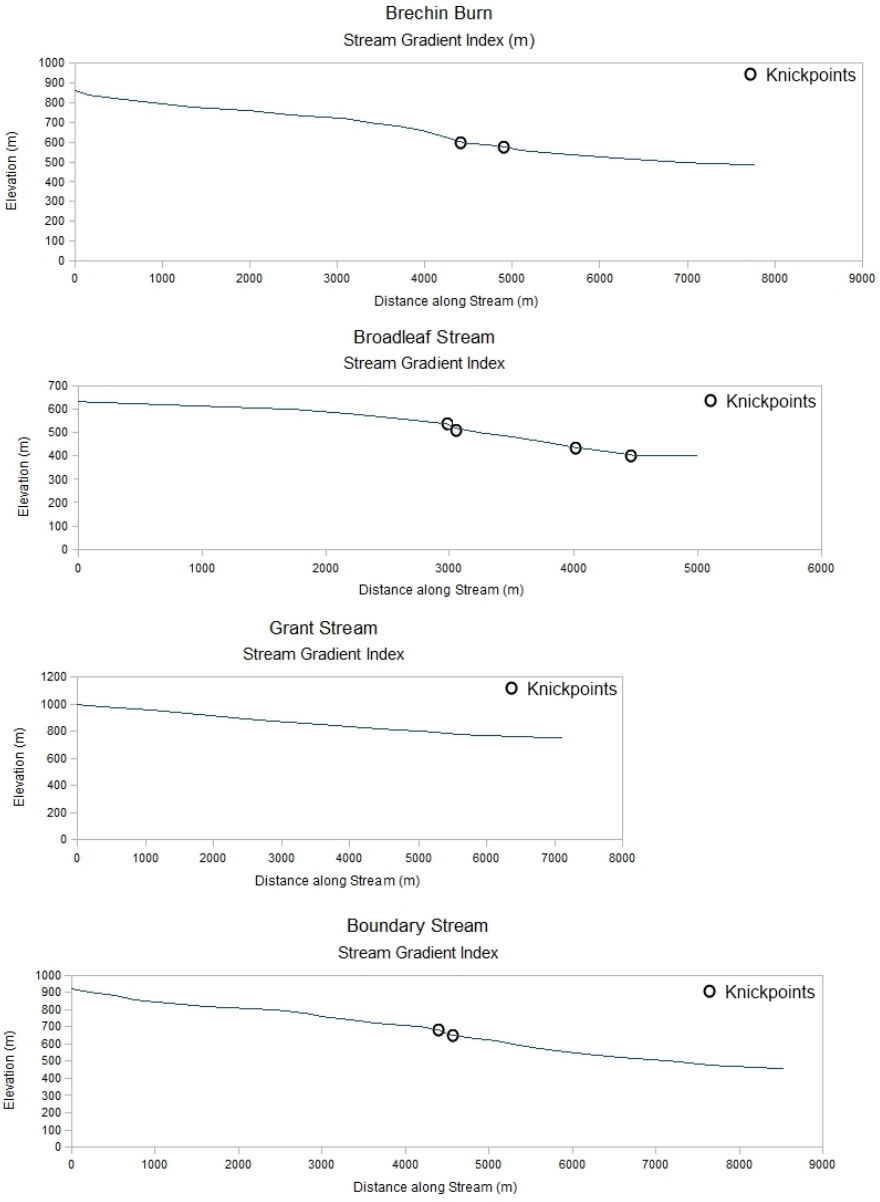

Figure A.3.: Stream profile of the Brechin Burn, Broadleaf Stream, Grant Stream, and Boundary Stream

B. OSL dating

Optically stimulated luminescence (OSL) dating is an absolute dating method which relies on the trapping and release of energy by electrons within crystals (Aitken, 1998). The usability of the method is dependent on the decay of radioisotopes within the deposit, which adds energy to the electrons and causes them to move to higher energy levels. Without radiation no absolute zero for the luminescence clock is given. On their way to higher energy bands the electrons get trapped by crystal defects where they can drop back to their lower level upon the addition of small amounts of energy. The emitted light during this process is called luminescence. Exposure to sunlight constantly sets back the electrons restarting the clock. Therefore, the luminescence clock starts as soon as the deposit is sufficiently buried, starting from 30 cm below the surface. In the laboratory the luminescence and subsequent zeroing of the sample is caused by the addition of light, thus optically stimulated.

The intensity of the luminescence released is measured as a function of total radiation dose over time. Its relation to the paleodose, which is the quantified past exposure to radiation gives the age of the sample. There are several methods to calculate the paleodose: an additive dose method measuring the luminescence emitted in the laboratory during different levels of irradiation, a regenerative method with several samples being first zeroed out and then exposed to known doses, and the partial bleach method where some samples are measured by the additive method while others are exposed to short bursts of light (Duller, 1996). In this study the paleodose was calculated using the Multiple Aliquot Additive Dose method (MAAD) based on measurements of blue luminescence from the fine grain feldspar produced during infrared stimulation.

While taking samples in the field one has to evaluate if a bed is a suitable candidate for OSL, e.g. it has been zeroed during transport, therefore, giving a reliable date. Aeolian and suspended sediments are ideal, while sediments in mass movements and transported by bedload are less reliable. The sample is then best taken at a sufficient depth and distance from underlying beds without being exposed to light. We used a metaltube shoved in the sediment and then covered by aluminium foil in order to minimise sunlight exposure. Dating samples were taken from the middle of the tube where they would be least exposed to any light. The samples were sent to the Luminescence Dating Laboratory of the Victoria University in Wellington. Optically stimulated luminescence (OSL) dating is an absolute dating method which relies on the trapping and release of energy by electrons within crystals (Aitken, 1998). The usability of the method is dependent on the decay of radioisotopes within the deposit, which adds energy to the electrons and causes them to move to higher energy levels. Without radiation no absolute zero for the luminescence clock is given. On their way to higher energy bands the electrons get trapped by crystal defects where they can drop back to their lower level upon the addition of small amounts of energy. The emitted light during this process is called luminescence. Exposure to sunlight constantly sets back the electrons restarting the clock. Therefore, the luminescence clock starts as soon as the deposit is sufficiently buried, starting from 30 cm below the surface. In the laboratory

the luminescence and subsequent zeroing of the sample is caused by the addition of light, thus optically stimulated.

In the laboratory the samples were prepared by physically removing their outer surfaces, and chemically removing all carbonates, organic matter, and iron oxide coatings. The fine grains, 4-11 μm, were separated, suspended in ethanole and acetone, and evenly deposited on aluminium discs. The samples where then dried in an oven, milled, weighed, sealed in air tight perspex containers, and stored for at least four weeks. The remaining sediments were filled into a plastic cube for water content measurements.

All discs were normalised before equivalent dose measurements by MAAD since luminescence can vary between the discs. Therefore, 0.1 second infrared measurements were taken before irradiation. Beta irradiation was done on the Riso TL-DA-15 ^{90}Sr/^{90}Y β irradiator, calibrated against ^{60}Co gamma source, SFU, Vancouver, Canada with about 3% uncertainty. Alpha irradiation was carried out on a ^{241}Am irradiatior, calibrated by ELSEC Littlemore, UK. Of the total 48 discs, 30 were subjected to β irradiation, 9 to α irradiation, and 9 were not-irradiated. All discs were stored for another four weeks to relax the crystal lattice. After that, they were measured using the Riso TL-DA-15 reader with infrared diodes at 880 nm for 100 s detecting the blue luminescence at 410 nm emitted from feldspar. The first 10 seconds of the shine down curves, substracted by the average of the last 20 seconds and the so called late light, were used or the luminescence growth curve. Through extrapolation to the dose axis the paleodose was established. For dose rate calculations the α efficiency was obtained by a similar plot from the α irradiated discs.

The dose rate consists of dose rate from the sample's burial environment and the dose rate from cosmic rays. The dose rate from the burial environment was derived from radionuclide contents ^{238}U, ^{232}Th and ^{40}K, water content and the a-value measured by comparing the luminescence from α irradiation and β irradiation. The radionuclide content was obtained by counting the produced gamma rays of the sample over a minimum of 24 hours and comparing them to standard samples. Water content was derived from the ratio of water weight to the dry weight of the sample with a 10% uncertainty. The dose rate from cosmic rays was calculated by the depth of the sample, its longitude, latitude, and altitude using the convention formula and factors published by Prescott & Hutton (1994). The results of the cosmic dose rates, water contents, radionuclide contents, and luminescence dating ages are as follows:

	JM01	JM02
Depth below surface (m)	0.49	0.5
Cosmic Dose Rate (Gy/ka)	0.2107±0.0105	0.2104±0.0105

Table B.1.: Cosmic dose rates

	JM01	JM02
Water Content %	16.75	4.8
U (ppm) from ^{234}Th	3.50±0.37	2.63±0.20
U (ppm) from ^{226}Ra, ^{214}Pb, ^{214}Bi	2.82±0.21	2.72±0.12
U (ppm) from ^{210}Pb	2.86±0.29	2.33±0.15
Th (ppm) from ^{208}Tl, ^{212}Pb, ^{228}Ac	11.65±0.17	10.54±0.11
K %	2.29±0.05	2.29±0.04

Table B.2.: Water contents, radionuclide contents

	JM01	JM02
a-Value	0.096±0.012	0.074±0.004
Equivalent Dose (Gy)	45.04±4.65	172.40±7.97
Dose Rate (Gy/ka)	4.55±0.18	4.73±0.08
OSL age (ka)	9.9±1.1	36.4±1.8

Table B.3.: a-values, equivalent doses, dose rates and luminescence dating ages

C. Earthquake data 1990-2011

ID	Latitude	Longitude	Day	Month	Year	Magnitude	Depth
125506	-43.18	172.08	11	5	1990	2.64	8.28
133119	-43.15	171.75	29	5	1990	2.77	5
133356	-43.05	171.8	2	6	1990	2.94	6.32
138308	-42.96	172.17	25	6	1990	2.47	5
140268	-43.18	172.02	7	7	1990	2.8	5
150831	-43.17	172.16	22	8	1990	4.18	12
153388	-43.18	172.17	22	8	1990	3.03	12
152686	-43.19	172.11	22	8	1990	2.22	5
154821	-43.04	171.76	9	9	1990	2.72	5
155523	-43.03	171.76	9	9	1990	4.32	5
154824	-43.05	171.74	9	9	1990	2.46	0.71
154825	-43.02	171.76	9	9	1990	2.32	5
155024	-43.02	171.76	9	9	1990	2.45	12
154828	-43.04	171.74	9	9	1990	2.53	5
153251	-43.04	171.76	9	9	1990	2.87	5
155031	-43.01	171.77	10	9	1990	2.3	12
153268	-43.05	171.75	10	9	1990	2.82	5
155041	-43.03	171.75	11	9	1990	2.33	5
155043	-43.01	171.76	11	9	1990	2.11	12
155045	-42.90	171.77	11	9	1990	2.23	33
155128	-43.04	171.76	15	9	1990	2.81	5
155144	-43.04	171.76	16	9	1990	2.68	5
155145	-43.04	171.77	16	9	1990	2.42	5
155146	-43.04	171.77	16	9	1990	2.81	5
159168	-43.04	171.76	25	9	1990	2.24	5
159506	-43.03	171.74	26	9	1990	2.28	5
166768	-43.06	171.73	17	10	1990	2.55	0
166771	-43.06	171.75	17	10	1990	2.38	0
166785	-43.03	171.74	18	10	1990	2.2	5
171854	-43.19	172.14	2	11	1990	2.5	5
170975	-43.03	171.74	2	11	1990	2.66	0.18
170976	-43.02	171.80	3	11	1990	2.49	3.93
173778	-42.83	172.01	13	11	1990	2.78	5
179989	-43.22	171.89	3	12	1990	3.16	19.33
189418	-43.03	172.09	9	1	1991	4.39	6.01
192414	-43.03	172.04	9	1	1991	2.95	0.06
193156	-43.01	172.07	10	1	1991	3.42	6.94
206831	-43.11	172.12	24	2	1991	2.41	31.12
214949	-42.90	171.77	24	3	1991	2.36	35.43
220531	-43.16	171.86	17	4	1991	2.48	31.84
220313	-43.01	172.08	17	4	1991	2.6	5.49
225996	-43.08	171.81	12	5	1991	3.4	2.49
227421	-43.07	171.82	12	5	1991	2.59	5
229388	-43.18	172.19	19	5	1991	3.09	6.63
231485	-43.06	171.81	27	5	1991	2.89	5.65
233661	-42.95	171.85	3	6	1991	2.13	32.81
232752	-43.08	171.81	3	6	1991	3.02	1.29
236853	-42.82	172.25	14	6	1991	2.32	5
240049	-43.06	171.84	2	7	1991	2.59	36.59
245190	-43.00	172.11	17	7	1991	2.04	5

ID	Latitude	Longitude	Day	Month	Year	Magnitude	Depth
245191	-43.00	172.06	17	7	1991	2.55	5
250367	-42.97	172.20	6	8	1991	2.74	31.77
254007	-43.14	171.83	20	8	1991	2.86	5
255704	-43.06	171.77	1	9	1991	2.97	5
255175	-43.05	171.77	1	9	1991	3.56	3.75
253742	-43.04	171.77	1	9	1991	4.61	5.86
253743	-43.04	171.77	1	9	1991	3.76	5.84
258270	-43.06	171.77	1	9	1991	3.36	2.2
258463	-43.01	171.83	1	9	1991	2.67	12
255710	-43.05	171.77	1	9	1991	2.66	2.55
255711	-43.02	171.77	1	9	1991	2.65	8.57
255718	-43.05	171.76	1	9	1991	3.06	0
255178	-43.05	171.76	1	9	1991	3.18	2.52
255722	-43.04	171.77	1	9	1991	2.59	5
258523	-43.04	171.77	1	9	1991	2.83	5
253755	-43.06	171.77	1	9	1991	3.76	2.98
258774	-43.05	171.84	1	9	1991	2.08	5
255656	-43.04	171.75	2	9	1991	2.75	5
257447	-43.01	171.76	4	9	1991	2.52	11.26
257546	-43.03	171.74	5	9	1991	2.53	5
257450	-43.06	171.75	6	9	1991	2.95	5
256244	-43.05	171.75	6	9	1991	3.27	5
257451	-43.04	171.75	6	9	1991	3.13	5.2
256115	-43.02	171.76	7	9	1991	2.65	12
259705	-43.03	171.74	7	9	1991	2.99	5
255326	-43.04	171.77	8	9	1991	2.8	5
260140	-43.02	171.74	8	9	1991	3.11	5
257605	-43.04	171.76	8	9	1991	2.36	5
255351	-42.93	171.78	9	9	1991	2.26	32.95
258240	-43.04	171.78	9	9	1991	2.01	5
258650	-43.04	171.76	11	9	1991	2.79	5
259101	-43.04	171.75	16	9	1991	3.12	5
261158	-42.88	171.77	20	9	1991	2.55	33
268327	-43.09	172.07	18	10	1991	3.01	12
266078	-43.08	171.75	19	10	1991	3.64	21.39
274200	-43.16	172.02	9	11	1991	2.95	9.41
278708	-43.16	171.90	9	11	1991	2.4	12
279835	-42.97	172.24	26	11	1991	2.39	36.56
285208	-43.18	172.25	1	12	1991	3.79	33
282912	-43.16	172.21	12	12	1991	2.81	18.17
294995	-43.02	172.10	23	1	1992	2.52	5
302740	-42.96	172.03	7	2	1992	2.57	16.08
309042	-42.99	171.79	3	3	1992	2.18	33
337820	-42.94	171.79	29	5	1992	2.26	31.48
341709	-42.99	171.75	30	5	1992	1.94	33
339303	-43.18	172.17	4	6	1992	2.68	32.84
340468	-42.88	171.75	8	6	1992	2.59	1.27
375897	-42.93	171.89	7	10	1992	2.6	5
378478	-43.17	172.05	22	10	1992	2.91	12
380037	-43.18	172.24	31	10	1992	2.68	5
379163	-43.21	172.15	1	11	1992	3.86	14.38
385535	-43.07	172.10	7	11	1992	2.66	6.32
386954	-43.20	172.17	20	11	1992	2.72	12
389702	-43.06	172.07	4	12	1992	2.92	5.26
396488	-43.18	172.07	24	12	1992	2.56	5
403068	-42.80	171.84	14	1	1993	2.44	33
403858	-43.08	172.07	21	1	1993	3.1	5
425544	-42.90	172.23	6	4	1993	2.49	3.48
480521	-43.21	172.15	28	8	1993	2.92	12
497468	-43.21	171.93	14	10	1993	2.64	12

ID	Latitude	Longitude	Day	Month	Year	Magnitude	Depth
503869	-43.19	172.09	31	10	1993	2.34	5
514306	-43.07	172.07	3	11	1993	2.16	5
517854	-43.06	171.77	17	11	1993	2.72	5
519179	-43.20	172.08	27	11	1993	2.42	5
529516	-42.99	171.93	11	12	1993	2.6	5
530903	-43.03	172.14	21	12	1993	2.86	12
566871	-43.21	172.04	21	2	1994	2.28	5
569188	-43.03	172.09	25	2	1994	2.6	5
577899	-42.82	172.23	11	3	1994	1.68	39.58
579137	-43.12	171.74	17	3	1994	2.39	12
599244	-43.20	172.01	11	5	1994	3.03	12
610103	-42.99	171.77	16	6	1994	2.88	12
1008054	-43.12	171.77	18	6	1994	3.51	10
1004171	-43.01	171.79	18	6	1994	2.82	10
1004540	-43.21	171.83	18	6	1994	2.69	10
1005667	-43.20	171.77	18	6	1994	2.03	10
1007723	-43.15	171.84	19	6	1994	3.06	5
1007740	-42.91	171.95	19	6	1994	2.89	5
1009657	-42.90	171.83	19	6	1994	2.86	5
1009742	-43.13	171.94	19	6	1994	2.32	10
1011739	-43.17	171.81	20	6	1994	2.06	5
1010887	-43.02	171.75	20	6	1994	1.24	5
1018909	-43.09	171.74	20	6	1994	1.54	5
1011609	-43.13	171.77	20	6	1994	1.67	5
610786	-42.94	171.83	29	6	1994	2.05	10.64
615010	-43.05	171.74	2	7	1994	2.4	5
623345	-42.81	171.87	2	7	1994	2.34	5
635372	-42.93	172.22	26	7	1994	3	11.26
665034	-42.88	171.77	3	10	1994	3.15	5
665035	-42.88	171.78	3	10	1994	2.67	6.37
696553	-43.14	172.21	29	11	1994	2.44	12
696566	-42.87	171.78	29	11	1994	2.47	12
709244	-42.94	171.9	15	12	1994	2.64	5
710894	-42.87	171.74	22	12	1994	2.92	5
711184	-42.88	171.79	1	1	1995	2.84	12
716978	-43.05	171.8	3	1	1995	2.28	12
723534	-42.82	172.06	18	1	1995	2.92	12
732215	-42.84	172.09	18	1	1995	2.89	12
786520	-43.17	172.17	13	4	1995	2.52	12
806164	-42.96	171.94	9	5	1995	2.79	12
819558	-43.09	171.83	7	6	1995	2.49	39.51
820098	-43.06	171.87	14	6	1995	2.7	33
904303	-43.15	172.18	12	7	1995	3.28	5
904499	-43.17	172.21	13	7	1995	2.66	12
830804	-42.98	172.17	18	7	1995	2.66	5
843183	-43.00	171.84	4	9	1995	2.31	12
853948	-43.21	172.15	4	10	1995	3.38	12
853975	-43.21	172.13	7	10	1995	2.49	12
872721	-43.05	171.88	1	11	1995	2	33
771641	-43.07	172.05	23	11	1995	3.14	3.92
788939	-42.92	171.95	23	11	1995	1.86	5
771645	-42.95	171.82	24	11	1995	6.29	7.26
783820	-42.95	171.83	24	11	1995	3.89	5
785186	-42.98	171.85	24	11	1995	3.95	5
785314	-42.98	171.87	24	11	1995	3.69	5
785384	-42.97	171.84	24	11	1995	3.43	5
785385	-42.98	171.86	24	11	1995	3.67	5
785581	-42.99	171.84	24	11	1995	2.92	5
785580	-42.95	171.82	24	11	1995	3.04	5
785582	-42.97	171.85	24	11	1995	2.94	5

ID	Latitude	Longitude	Day	Month	Year	Magnitude	Depth
785585	-42.96	171.82	24	11	1995	3.1	5
785592	-42.99	171.74	24	11	1995	3.22	5
785595	-42.99	171.85	24	11	1995	3.78	5
788786	-42.94	171.84	24	11	1995	3.56	5
788986	-42.98	171.85	24	11	1995	3.43	5
788912	-42.95	171.82	24	11	1995	3.13	5
788988	-42.95	171.86	24	11	1995	3.28	5
788984	-42.98	171.85	24	11	1995	3.19	5
788987	-42.98	171.87	24	11	1995	3.21	5
789024	-43.02	171.84	24	11	1995	2.62	5
790666	-43.00	171.81	24	11	1995	2.49	5
790664	-42.98	171.86	24	11	1995	3.17	5
791881	-42.96	171.82	24	11	1995	2.61	5
791999	-42.95	171.83	24	11	1995	2.55	5
792125	-42.81	171.85	24	11	1995	2.24	5
791893	-42.94	171.83	24	11	1995	2.49	5
792503	-42.94	171.84	24	11	1995	2.56	5
792955	-42.91	171.81	24	11	1995	2.05	5
792959	-42.96	171.85	24	11	1995	3.19	5
792969	-42.97	171.82	24	11	1995	2.75	5
792968	-42.93	171.82	24	11	1995	2.41	5
792981	-42.93	171.81	24	11	1995	2.13	5
792986	-42.98	171.84	24	11	1995	2.3	5
792988	-42.96	171.83	24	11	1995	3.19	5
792993	-42.95	171.83	24	11	1995	3.19	5
792991	-42.98	171.85	24	11	1995	3.53	5
793027	-42.96	171.83	24	11	1995	3	5
792990	-42.98	171.86	24	11	1995	2.75	5
793028	-42.82	171.87	24	11	1995	2.68	5
793067	-42.95	171.84	24	11	1995	2.3	5
793071	-42.94	171.8	24	11	1995	2.38	5
793069	-42.99	171.84	24	11	1995	2.42	5
793073	-42.98	171.82	24	11	1995	2.52	5
793074	-42.98	171.85	24	11	1995	2.25	5
793072	-42.99	171.85	24	11	1995	2.6	5
794866	-42.97	171.84	24	11	1995	2.28	5
794885	-42.96	171.84	24	11	1995	3.17	5
794887	-42.96	171.85	24	11	1995	2.3	5
794888	-43.01	171.87	24	11	1995	2.55	5
794891	-43.02	171.84	24	11	1995	2.92	5
794892	-42.97	171.84	24	11	1995	2.63	5
794893	-43.00	171.86	24	11	1995	2.91	5
794894	-42.95	171.84	24	11	1995	2.79	5
794895	-42.96	171.84	24	11	1995	2.83	5
794912	-43.16	171.75	24	11	1995	2.42	5
794938	-43.00	171.83	24	11	1995	2.61	5
794943	-43.01	171.82	24	11	1995	2.41	5
794945	-42.98	171.85	24	11	1995	2.56	5
771554	-42.98	171.87	24	11	1995	4.04	3.66
783838	-42.95	171.83	24	11	1995	3.34	5
783986	-42.99	171.84	24	11	1995	3.23	5
785597	-42.93	171.84	24	11	1995	3.02	5
785149	-42.86	171.89	24	11	1995	3.43	5
775356	-42.97	171.86	24	11	1995	3.03	6.43
771648	-42.97	171.86	24	11	1995	3.73	4.86
785150	-42.99	171.86	24	11	1995	3.97	3.75
785165	-42.95	171.83	24	11	1995	3.14	6.12
785187	-42.95	171.85	24	11	1995	3.32	5.35
785250	-42.95	171.83	24	11	1995	3.39	6
785598	-42.92	171.83	24	11	1995	2.64	5

ID	Latitude	Longitude	Day	Month	Year	Magnitude	Depth
785251	-42.98	171.87	24	11	1995	2.67	5
785583	-42.96	171.82	24	11	1995	3.56	5.66
785584	-42.95	171.83	24	11	1995	2.13	5
785599	-42.98	171.85	24	11	1995	2.39	5
785600	-42.97	171.86	24	11	1995	2.6	5
773218	-43.18	172.13	24	11	1995	2.14	5
785609	-42.95	171.85	24	11	1995	2.45	5
785610	-42.98	171.87	24	11	1995	2.96	5
770625	-42.99	171.86	24	11	1995	2.81	5
785612	-43.00	171.85	24	11	1995	3.67	5
785621	-42.96	171.84	24	11	1995	2.6	5
785622	-42.93	171.83	24	11	1995	2.76	4.24
785623	-42.97	171.84	24	11	1995	2.26	5
785624	-42.99	171.82	24	11	1995	2.46	5
785625	-42.99	171.84	24	11	1995	2.39	5
785626	-42.99	171.91	24	11	1995	2.26	5
785627	-42.85	171.84	24	11	1995	1.96	5
773698	-42.95	171.83	24	11	1995	2.84	5.94
785637	-42.98	171.86	24	11	1995	3.13	5
785638	-42.95	171.83	24	11	1995	2.42	5
785639	-42.99	171.85	24	11	1995	3.32	5
785640	-42.99	171.86	24	11	1995	3.48	2.51
785641	-42.97	171.82	24	11	1995	3.39	5
776558	-42.94	171.86	24	11	1995	2.42	7.43
785643	-42.97	171.86	24	11	1995	2.66	5
785644	-43.00	171.87	24	11	1995	2.82	5
785645	-42.97	171.83	24	11	1995	2.95	4.45
785646	-42.95	171.82	24	11	1995	3.09	5
785647	-42.96	171.83	24	11	1995	3.5	5
785648	-42.97	171.84	24	11	1995	3.1	5
785649	-42.89	171.78	24	11	1995	2.29	5
785650	-42.99	171.84	24	11	1995	2.67	5
785651	-42.96	171.83	24	11	1995	2.6	5
785657	-42.86	171.78	24	11	1995	2.28	5
785659	-42.97	171.83	24	11	1995	2.88	5.36
785660	-42.94	171.83	24	11	1995	2.97	5.57
785662	-42.95	171.85	24	11	1995	2.44	3.62
785664	-42.98	171.86	24	11	1995	2.02	5
771454	-42.94	171.84	24	11	1995	2.49	5
785666	-42.93	171.83	24	11	1995	3.25	4.14
785677	-42.97	171.86	24	11	1995	3.45	2.78
785679	-42.98	171.84	24	11	1995	2.7	5
787171	-42.96	171.81	24	11	1995	2.34	5
787361	-42.94	171.82	24	11	1995	2.22	5
787396	-42.95	171.82	24	11	1995	1.99	5
787509	-42.98	171.86	24	11	1995	2.87	5
788914	-42.97	171.84	24	11	1995	2.81	5
788915	-42.98	171.86	24	11	1995	2.66	4.03
788916	-42.98	171.83	24	11	1995	2.07	5
788917	-42.96	171.86	24	11	1995	3.01	5
788918	-42.95	171.82	24	11	1995	2.78	4.83
788919	-42.98	171.87	24	11	1995	3.46	2.99
788920	-42.96	171.84	24	11	1995	3.75	6.02
788924	-42.97	171.85	24	11	1995	2.87	3.63
788925	-42.97	171.85	24	11	1995	2.81	5
772971	-42.92	171.75	24	11	1995	2.41	5
788927	-42.98	171.84	24	11	1995	2.5	5
788928	-42.98	171.83	24	11	1995	2.32	5
788929	-42.98	171.87	24	11	1995	2.49	5
773702	-42.98	171.87	24	11	1995	2.34	5

ID	Latitude	Longitude	Day	Month	Year	Magnitude	Depth
788930	-42.91	171.83	24	11	1995	2.39	5
771651	-42.93	171.83	24	11	1995	2.46	5
788931	-42.95	171.86	24	11	1995	2.51	5
788932	-42.98	171.84	24	11	1995	2.18	5
788933	-42.96	171.85	24	11	1995	2.9	5
772972	-43.00	171.86	24	11	1995	2.66	4.12
781910	-42.97	171.84	24	11	1995	2.45	5
788935	-42.97	171.86	24	11	1995	2.35	5
788940	-42.95	171.83	24	11	1995	1.9	5
788941	-42.95	171.84	24	11	1995	2.76	5
788943	-42.99	171.86	24	11	1995	2.18	5
788944	-42.96	171.83	24	11	1995	2.33	5
788945	-42.93	171.84	24	11	1995	3.21	5
788989	-42.84	171.77	24	11	1995	2.53	5
771652	-42.95	171.83	24	11	1995	2.99	4.75
788947	-42.99	171.84	24	11	1995	2.17	5
788970	-42.91	171.86	24	11	1995	1.98	5
788969	-42.97	171.86	24	11	1995	2.19	5
770630	-42.94	171.84	24	11	1995	3.47	3.98
788972	-42.92	171.82	24	11	1995	2.23	5
788971	-42.96	171.84	24	11	1995	2.85	4.99
788974	-42.98	171.87	24	11	1995	2.81	5
788980	-42.95	171.82	24	11	1995	2.03	5
788981	-42.99	171.85	24	11	1995	2.7	5
788982	-42.96	171.84	24	11	1995	3.83	6.03
788983	-42.96	171.81	24	11	1995	2.45	5
773704	-42.93	171.84	24	11	1995	2.15	5
788991	-42.99	171.86	24	11	1995	2.98	4.22
788992	-42.98	171.87	24	11	1995	3.36	3.53
788993	-42.95	171.84	24	11	1995	2.31	5
788994	-42.94	171.82	24	11	1995	1.77	5
788996	-42.97	171.84	24	11	1995	2.44	5
789043	-42.98	171.83	24	11	1995	2.63	5
789045	-42.98	171.85	24	11	1995	2.84	5
789046	-42.96	171.83	24	11	1995	2.77	5
772978	-42.95	171.86	24	11	1995	2.42	5
789049	-43.00	171.83	24	11	1995	2.13	5
772979	-42.97	171.81	24	11	1995	2.39	5
789053	-42.98	171.86	24	11	1995	2.81	5
789054	-42.98	171.86	24	11	1995	2.57	5
789740	-42.94	171.83	24	11	1995	2.77	5
789741	-42.91	171.81	24	11	1995	2.75	5
790056	-42.97	171.85	24	11	1995	2.34	5
790058	-42.95	171.83	24	11	1995	2.7	5
790060	-42.99	171.85	24	11	1995	4.09	5
776564	-42.96	171.85	24	11	1995	2.48	7.09
791700	-42.93	171.85	24	11	1995	3.01	4.73
791702	-42.98	171.85	24	11	1995	2.47	5
791703	-42.95	171.90	24	11	1995	2.56	5
771655	-42.96	171.86	24	11	1995	2.47	5
792001	-42.98	171.86	24	11	1995	3.07	5
792003	-42.98	171.86	24	11	1995	2.54	5
771656	-42.97	171.86	24	11	1995	2.27	4.2
792947	-42.94	171.84	24	11	1995	2.86	4.75
792950	-42.98	171.87	24	11	1995	2.17	5
792951	-42.89	171.79	24	11	1995	1.92	5
792952	-42.97	171.84	24	11	1995	3	4.39
792953	-42.98	171.85	24	11	1995	2.75	4.47
792954	-42.92	171.81	24	11	1995	2.12	5
792960	-42.88	171.86	24	11	1995	2.23	5

ID	Latitude	Longitude	Day	Month	Year	Magnitude	Depth
772987	-42.97	171.85	24	11	1995	2.42	5
792962	-42.99	171.89	24	11	1995	2.89	5.51
792963	-42.97	171.84	24	11	1995	2.31	5
792964	-42.99	171.86	24	11	1995	2.78	5
792965	-42.97	171.84	24	11	1995	2.07	5
771555	-42.94	171.82	24	11	1995	3.67	5.53
775358	-42.85	171.77	24	11	1995	2.1	5
792996	-42.98	171.86	24	11	1995	2.02	5
792997	-42.97	171.81	24	11	1995	1.71	5
792998	-42.96	171.81	24	11	1995	2.12	5
792999	-42.97	171.84	24	11	1995	2.38	5
793000	-42.98	171.87	24	11	1995	2.25	5
793001	-42.98	171.86	24	11	1995	2.48	5
771455	-42.95	171.85	24	11	1995	2.65	5
793003	-42.97	171.84	24	11	1995	1.91	5
793004	-42.94	171.85	24	11	1995	2.21	5
793005	-43.00	171.85	24	11	1995	1.91	5
776568	-42.95	171.84	24	11	1995	2.47	5
772990	-42.94	171.83	24	11	1995	2.15	5
793030	-42.94	171.82	24	11	1995	2.13	5
793031	-42.97	171.83	24	11	1995	2.46	5
793032	-42.94	171.83	24	11	1995	2.44	5
793033	-42.92	171.83	24	11	1995	1.84	5
771658	-42.96	171.83	24	11	1995	3.07	4.96
793035	-42.94	171.84	24	11	1995	2.93	5
793037	-42.94	171.81	24	11	1995	1.89	5
776570	-42.90	171.84	24	11	1995	2.04	5
772991	-42.93	171.84	24	11	1995	2.26	5
793051	-42.99	171.86	24	11	1995	2.69	5
793052	-42.93	171.81	24	11	1995	2.08	5
793053	-42.97	171.83	24	11	1995	2.18	5
775360	-42.95	171.83	24	11	1995	2.54	5
771659	-42.98	171.88	24	11	1995	2.59	5
793055	-42.95	171.83	24	11	1995	3.16	5
772993	-42.98	171.85	24	11	1995	2.74	5
793057	-42.96	171.83	24	11	1995	1.96	5
793058	-42.98	171.85	24	11	1995	1.98	5
772994	-42.98	171.87	24	11	1995	2.45	5
793060	-42.97	171.85	24	11	1995	2.36	5
793062	-42.99	171.86	24	11	1995	2.35	5
793063	-42.93	171.83	24	11	1995	2.98	5
772995	-42.92	171.83	24	11	1995	2.98	5
793066	-42.92	171.82	24	11	1995	2.64	5
771456	-42.92	171.83	24	11	1995	2.41	5
792971	-43.00	171.85	24	11	1995	3.07	5
792972	-42.99	171.86	24	11	1995	2.86	5
792973	-42.99	171.84	24	11	1995	2.18	5
792974	-42.95	171.83	24	11	1995	2.11	5
792976	-42.96	171.82	24	11	1995	1.85	5
773706	-42.95	171.83	24	11	1995	1.98	5
773219	-42.98	171.87	24	11	1995	2.23	5
775363	-42.94	171.83	24	11	1995	2.14	5
776581	-42.94	171.84	24	11	1995	2.58	5
792978	-42.98	171.85	24	11	1995	1.91	5
779106	-42.97	171.85	24	11	1995	3.39	5
773707	-42.98	171.84	24	11	1995	2.14	5
793007	-42.96	171.81	24	11	1995	2.39	5
775364	-42.95	171.83	24	11	1995	2.41	5
793049	-42.95	171.84	24	11	1995	2.11	5
793008	-42.94	171.85	24	11	1995	2.48	5

ID	Latitude	Longitude	Day	Month	Year	Magnitude	Depth
793009	-42.98	171.85	24	11	1995	2.54	5
776587	-42.94	171.91	24	11	1995	2.09	5
775367	-42.97	171.83	24	11	1995	2.19	5
793010	-42.98	171.85	24	11	1995	2.18	5
775368	-42.96	171.82	24	11	1995	3.19	5
793013	-42.97	171.83	24	11	1995	2.63	5
776588	-42.97	171.85	24	11	1995	2.38	5
772862	-42.96	171.87	24	11	1995	2.32	5
793034	-42.91	171.81	24	11	1995	2.41	5
793016	-42.98	171.85	24	11	1995	3.3	5
793036	-42.99	171.86	24	11	1995	3.22	5
793038	-42.95	171.85	24	11	1995	3.6	5
793039	-42.99	171.86	24	11	1995	2.73	5
776593	-42.95	171.84	24	11	1995	2.36	5
776597	-42.98	171.86	24	11	1995	2.15	5
773001	-42.98	171.85	24	11	1995	2.08	5
793040	-42.97	171.84	24	11	1995	2.46	5
776598	-42.98	171.85	24	11	1995	2.26	5
773003	-42.92	171.82	24	11	1995	2.27	5
793042	-42.99	171.88	24	11	1995	2.77	5
793043	-42.98	171.86	24	11	1995	2.69	5
776599	-42.94	171.83	24	11	1995	2.13	5
794873	-42.93	171.84	24	11	1995	2.53	5
775371	-42.98	171.85	24	11	1995	2.89	5
794874	-42.97	171.84	24	11	1995	2.51	5
773709	-42.99	171.85	24	11	1995	2.19	5
773006	-42.99	171.87	24	11	1995	2.62	5
794876	-42.96	171.84	24	11	1995	1.98	5
775372	-42.93	171.84	24	11	1995	2.11	5
773007	-42.98	171.86	24	11	1995	3.3	5
794878	-42.93	171.84	24	11	1995	2.64	5
794879	-42.88	171.77	24	11	1995	2.15	5
775373	-42.98	171.87	24	11	1995	2.29	5
794880	-42.93	171.85	24	11	1995	2.68	5
776600	-42.98	171.86	24	11	1995	1.99	5
776601	-42.98	171.86	24	11	1995	2.38	5
794882	-42.96	171.83	24	11	1995	2.49	5
776603	-42.96	171.83	24	11	1995	3.92	5
793078	-42.95	171.84	24	11	1995	2.46	5
793079	-42.99	171.85	24	11	1995	2.82	5
776604	-42.98	171.86	24	11	1995	1.83	5
776611	-42.94	171.83	24	11	1995	1.85	5
775374	-42.94	171.83	24	11	1995	2.19	5
793085	-42.98	171.85	24	11	1995	2.34	5
793086	-42.98	171.88	24	11	1995	2.16	5
776613	-42.93	171.84	24	11	1995	2.13	5
776616	-42.95	171.84	24	11	1995	2.65	5
793087	-43.00	171.87	24	11	1995	1.91	5
773014	-42.93	171.85	24	11	1995	2.69	5
793088	-42.91	171.79	24	11	1995	2.04	5
794853	-42.99	171.87	24	11	1995	1.99	5
775377	-42.95	171.86	24	11	1995	2.63	5
794855	-42.93	171.84	24	11	1995	2.17	5
794856	-42.97	171.87	24	11	1995	2.14	5
773891	-42.91	171.82	24	11	1995	2.14	5
772863	-42.96	171.84	24	11	1995	2.6	5
794857	-42.98	171.86	24	11	1995	2.46	5
794858	-42.98	171.85	24	11	1995	1.99	5
775378	-42.95	171.81	24	11	1995	2.16	5
794860	-42.99	171.85	24	11	1995	2.12	5

ID	Latitude	Longitude	Day	Month	Year	Magnitude	Depth
773016	-42.97	171.87	24	11	1995	2.67	5
794883	-42.97	171.86	24	11	1995	2.69	5
776621	-42.99	171.89	24	11	1995	1.99	5
794884	-42.94	171.85	24	11	1995	1.96	5
773892	-42.96	171.84	24	11	1995	2.42	5
794896	-42.92	171.82	24	11	1995	2.13	5
794898	-42.97	171.85	24	11	1995	2.19	5
776626	-42.99	171.85	24	11	1995	2.73	5
773220	-42.96	171.83	24	11	1995	2.03	5
794900	-42.97	171.86	24	11	1995	2.32	5
776627	-42.95	171.86	24	11	1995	2.39	4.96
773894	-42.88	171.78	24	11	1995	1.92	5
794901	-42.98	171.84	24	11	1995	2.29	5
794902	-43.00	171.82	24	11	1995	2.19	5
794903	-42.98	171.82	24	11	1995	2.1	5
773019	-42.98	171.85	24	11	1995	2.52	5
776630	-42.97	171.86	24	11	1995	1.85	5
773021	-42.97	171.86	24	11	1995	2.36	5
794905	-42.99	171.86	24	11	1995	3.08	5
794906	-42.97	171.84	24	11	1995	2.22	5
794921	-42.96	171.84	24	11	1995	2.5	5
794922	-42.94	171.84	24	11	1995	2.34	5
794923	-42.96	171.85	24	11	1995	2.76	5
794946	-42.95	171.81	24	11	1995	2.03	5
794947	-42.97	171.81	24	11	1995	2.05	5
776637	-42.99	171.87	24	11	1995	2.45	5
776638	-42.95	171.84	24	11	1995	2.52	5
776639	-42.98	171.84	24	11	1995	2.3	5
794948	-42.97	171.84	24	11	1995	3.46	5
773023	-42.90	171.83	24	11	1995	2.25	5
776640	-42.91	171.82	24	11	1995	2.72	5
775382	-43.00	171.89	24	11	1995	1.75	5
794951	-42.99	171.81	24	11	1995	1.92	5
794952	-42.98	171.86	24	11	1995	1.82	5
795265	-42.95	171.82	24	11	1995	2.35	5
794950	-42.93	171.84	24	11	1995	2.96	4.12
773025	-42.96	171.83	24	11	1995	2.93	5.26
773026	-42.99	171.88	24	11	1995	2.15	7.5
776644	-42.94	171.84	24	11	1995	2.65	7.22
794956	-42.97	171.84	24	11	1995	2.05	6.75
775383	-42.98	171.86	24	11	1995	1.78	5
794957	-42.93	171.85	24	11	1995	1.85	5
794959	-42.97	171.87	24	11	1995	2.39	5
775384	-42.99	171.86	24	11	1995	2.55	5
794960	-42.97	171.82	24	11	1995	2.35	5
794961	-42.94	171.84	24	11	1995	2.02	5
794962	-42.96	171.83	24	11	1995	2.77	5
795681	-42.95	171.84	24	11	1995	2.63	5
795682	-43.00	171.84	24	11	1995	1.71	5
795683	-42.93	171.82	24	11	1995	2.18	5
795391	-43.00	171.89	24	11	1995	1.79	5
776649	-42.96	171.85	24	11	1995	2.67	5
776651	-42.98	171.87	24	11	1995	2.51	5
775386	-42.93	171.83	24	11	1995	1.95	5
771672	-42.96	171.84	24	11	1995	2.52	5
795680	-42.95	171.86	24	11	1995	1.71	5
795685	-42.93	171.84	24	11	1995	1.78	5
795612	-42.95	171.86	24	11	1995	2.88	5
795686	-42.96	171.84	24	11	1995	2.67	5
776656	-42.97	171.88	24	11	1995	2.32	5

ID	Latitude	Longitude	Day	Month	Year	Magnitude	Depth
773034	-42.99	171.88	24	11	1995	2.49	5
795684	-42.96	171.84	24	11	1995	1.98	5
773035	-42.98	171.86	24	11	1995	2.65	5
795687	-42.98	171.87	24	11	1995	2.77	4.85
773719	-42.98	171.87	24	11	1995	2.28	5
795688	-42.99	171.85	24	11	1995	2.37	5
773720	-42.95	171.85	24	11	1995	2.46	5
795689	-42.97	171.86	24	11	1995	2.2	5
773037	-42.98	171.87	24	11	1995	2.92	5
773038	-42.96	171.84	24	11	1995	2.57	5
795690	-42.98	171.85	24	11	1995	2.22	5
776663	-42.91	171.83	24	11	1995	2.07	5
797285	-42.94	171.85	24	11	1995	1.99	5
797286	-42.93	171.78	24	11	1995	1.99	5
771463	-42.99	171.86	24	11	1995	2.98	5
773041	-42.98	171.87	24	11	1995	2.76	5
776667	-42.92	171.83	24	11	1995	1.93	5
795693	-42.97	171.86	24	11	1995	3.2	5
770636	-42.95	171.90	24	11	1995	3.8	5
773043	-42.99	171.87	24	11	1995	2.51	5
795694	-42.97	171.85	24	11	1995	2.29	5
773044	-42.93	171.83	24	11	1995	2.02	5
776672	-42.87	171.78	24	11	1995	1.96	5
795706	-42.93	171.85	24	11	1995	2.3	5
773047	-42.93	171.85	24	11	1995	2.35	5
775387	-42.98	171.85	24	11	1995	2.13	5
795699	-42.86	171.80	24	11	1995	2.09	5
795700	-43.00	171.88	24	11	1995	2.33	5
771675	-42.98	171.88	24	11	1995	2.46	5
795701	-42.98	171.84	24	11	1995	2.53	5
795702	-42.94	171.81	24	11	1995	1.9	5
773050	-42.93	171.85	24	11	1995	2.51	5
773722	-42.95	171.83	24	11	1995	1.92	5
795703	-42.96	171.83	24	11	1995	1.86	5
773051	-42.98	171.85	24	11	1995	2.08	5
795707	-42.92	171.83	24	11	1995	2.28	5
773052	-42.98	171.88	24	11	1995	2.18	5
776675	-42.95	171.85	24	11	1995	2.44	5
795710	-42.92	171.82	24	11	1995	1.8	5
776677	-42.98	171.87	24	11	1995	2.55	5
776679	-42.97	171.85	24	11	1995	1.89	5
775388	-42.97	171.84	24	11	1995	2.04	5
773054	-42.94	171.85	24	11	1995	2.43	5
771466	-42.92	171.82	24	11	1995	1.83	5
775389	-42.91	171.83	24	11	1995	2.19	5
795711	-42.95	171.90	24	11	1995	3.37	5
795712	-42.93	171.85	24	11	1995	2.24	5
773056	-42.93	171.85	24	11	1995	2.49	5
795714	-42.95	171.83	24	11	1995	1.99	5
776686	-42.98	171.85	24	11	1995	2.09	5
795713	-42.93	171.85	24	11	1995	3.07	5
773723	-42.98	171.85	24	11	1995	2.83	5
795715	-43.01	171.79	24	11	1995	2.03	5
776688	-42.89	171.78	24	11	1995	2.02	5
776691	-42.98	171.87	24	11	1995	2.64	5
795716	-42.95	171.82	24	11	1995	2.3	5
771676	-42.95	171.85	24	11	1995	2.76	5
773061	-42.91	171.84	24	11	1995	2.57	5
776697	-42.95	171.86	24	11	1995	2.69	5
776700	-42.99	171.86	24	11	1995	2.7	5

ID	Latitude	Longitude	Day	Month	Year	Magnitude	Depth
776706	-42.99	171.89	24	11	1995	1.68	5
773064	-42.92	171.84	24	11	1995	2.31	5
776707	-42.94	171.84	24	11	1995	2.09	5
795718	-42.97	171.87	24	11	1995	2.46	5
795719	-42.91	171.83	24	11	1995	2.81	5
773066	-42.92	171.83	24	11	1995	2.05	5
795721	-42.94	171.83	24	11	1995	1.7	5
795722	-42.96	171.83	24	11	1995	2.16	5
795720	-42.97	171.84	24	11	1995	3.44	5
795723	-42.97	171.83	24	11	1995	2.43	5
795724	-42.96	171.80	24	11	1995	1.88	5
773067	-42.94	171.84	24	11	1995	2.71	5
795726	-42.96	171.84	24	11	1995	2.06	5
776708	-42.94	171.82	24	11	1995	2.62	5
795727	-42.97	171.84	24	11	1995	2.24	5
771680	-42.97	171.86	24	11	1995	3.27	5
776710	-42.96	171.84	24	11	1995	1.44	5
795728	-42.93	171.81	24	11	1995	2.08	5
795729	-42.96	171.83	24	11	1995	2.47	5
776712	-42.98	171.83	24	11	1995	2.27	5
776713	-43.00	171.88	24	11	1995	1.91	5
795731	-42.93	171.85	24	11	1995	2.24	5
795732	-42.95	171.80	24	11	1995	1.53	5
795734	-42.97	171.85	24	11	1995	1.86	5
795737	-42.92	171.83	24	11	1995	3.33	5
795739	-42.96	171.82	24	11	1995	2.38	5
775391	-42.93	171.81	24	11	1995	2.1	5
795740	-42.94	171.81	24	11	1995	2.06	5
795741	-42.97	171.87	24	11	1995	2	5
775392	-42.97	171.84	24	11	1995	2.8	5
776714	-42.97	171.83	24	11	1995	1.54	5
776715	-42.97	171.84	24	11	1995	2.16	5
776718	-42.93	171.84	24	11	1995	2.28	5
772868	-42.91	171.84	24	11	1995	2.49	5
776719	-42.96	171.84	24	11	1995	2.35	5
776721	-42.98	171.88	24	11	1995	2.36	5
775393	-42.95	171.82	24	11	1995	1.93	5
776724	-42.98	171.85	24	11	1995	2.05	5
775394	-42.91	171.83	24	11	1995	1.94	5
773073	-42.95	171.87	24	11	1995	2.18	5
773726	-42.96	171.86	24	11	1995	2.06	5
775395	-42.96	171.85	24	11	1995	2.48	5
771683	-42.99	171.85	24	11	1995	3.42	5
795735	-42.98	171.87	24	11	1995	2.72	5
795736	-42.91	171.83	24	11	1995	3.12	5
775397	-42.91	171.83	24	11	1995	1.85	5
795738	-42.99	171.89	24	11	1995	2.09	5
795744	-42.98	171.87	24	11	1995	2.29	5
776731	-42.91	171.83	24	11	1995	2.43	5
773076	-42.99	171.88	24	11	1995	2.53	5
776732	-42.94	171.91	24	11	1995	2.53	5
776733	-42.96	171.83	24	11	1995	1.81	5
795746	-43.00	171.87	24	11	1995	3.06	5
795747	-42.93	171.84	24	11	1995	2.61	5
773078	-42.97	171.86	24	11	1995	2.07	5
775398	-42.99	171.86	24	11	1995	2.25	5
773079	-42.93	171.83	24	11	1995	2.1	5
776735	-42.95	171.84	24	11	1995	2.32	5
773080	-42.99	171.87	24	11	1995	2.29	5
776737	-42.88	171.81	24	11	1995	2.11	5

ID	Latitude	Longitude	Day	Month	Year	Magnitude	Depth
776739	-42.92	171.82	24	11	1995	2.07	5
795750	-42.95	171.81	24	11	1995	2.03	5
776740	-43.00	171.91	24	11	1995	1.57	5
773081	-42.91	171.84	24	11	1995	2.36	5
795758	-42.94	171.85	24	11	1995	2.71	5
776741	-42.90	171.83	24	11	1995	2.31	5
795748	-42.99	171.87	24	11	1995	2.21	5
795749	-42.95	171.84	24	11	1995	2.81	5
795752	-42.98	171.86	24	11	1995	2.93	5
773083	-42.95	171.81	24	11	1995	2.06	5
795753	-42.99	171.87	24	11	1995	2.48	5
795754	-42.93	171.83	24	11	1995	2.22	5
773085	-42.93	171.81	24	11	1995	2.4	5
776742	-42.95	171.85	24	11	1995	1.97	5
773087	-42.91	171.83	24	11	1995	2.34	5
776746	-42.98	171.87	24	11	1995	1.95	5
775400	-42.97	171.82	24	11	1995	2.31	5
771470	-42.96	171.84	24	11	1995	2.2	5
795759	-42.98	171.86	24	11	1995	1.91	5
773088	-42.98	171.86	24	11	1995	2.93	5
795760	-42.99	171.87	24	11	1995	2.72	5
776748	-42.92	171.82	24	11	1995	2.01	5
773090	-42.99	171.89	24	11	1995	2.81	5
773091	-42.98	171.87	24	11	1995	2.41	5
776751	-42.95	171.86	24	11	1995	2.43	5
773728	-42.99	171.89	24	11	1995	2.03	5
775402	-42.97	171.86	24	11	1995	1.79	5
795762	-42.92	171.83	24	11	1995	2	5
773093	-42.94	171.84	25	11	1995	2.17	5
773838	-42.90	171.85	25	11	1995	2.01	15.2
776764	-42.94	171.82	25	11	1995	2.32	5
788964	-42.94	171.84	25	11	1995	2.6	5
788965	-42.99	171.87	25	11	1995	2.69	5
776766	-42.95	171.83	25	11	1995	3	5
782477	-42.93	171.84	25	11	1995	2.38	5
773097	-42.97	171.84	25	11	1995	2.56	5
773596	-42.95	171.82	25	11	1995	1.99	5
773597	-42.97	171.84	25	11	1995	1.88	5
771473	-42.99	171.89	25	11	1995	2.04	5
788997	-42.98	171.87	25	11	1995	2.03	5
771686	-43.00	171.87	25	11	1995	1.88	5
788998	-42.95	171.83	25	11	1995	2.69	5
773101	-42.86	171.78	25	11	1995	1.94	5
788999	-42.99	171.89	25	11	1995	2.26	5
789001	-42.94	171.85	25	11	1995	2.22	5
776774	-42.89	171.80	25	11	1995	1.79	5
776775	-42.96	171.84	25	11	1995	2.28	5
773104	-42.86	171.75	25	11	1995	2	5
773323	-42.98	171.85	25	11	1995	1.98	5
789006	-42.98	171.86	25	11	1995	2.03	5
773324	-42.98	171.87	25	11	1995	2.3	5
773221	-42.97	171.87	25	11	1995	2.36	5
773731	-42.94	171.85	25	11	1995	2.18	5
789007	-42.98	171.85	25	11	1995	2.39	5
770644	-42.97	171.84	25	11	1995	1.87	5
789009	-42.98	171.87	25	11	1995	2.35	5
773222	-42.92	171.84	25	11	1995	2.44	5
773407	-43.00	171.89	25	11	1995	2.02	5
773105	-42.94	171.83	25	11	1995	2.58	5
789013	-42.95	171.84	25	11	1995	2.61	5

ID	Latitude	Longitude	Day	Month	Year	Magnitude	Depth
789014	-42.99	171.87	25	11	1995	3.25	4.95
775406	-42.98	171.86	25	11	1995	2.22	5
789017	-42.98	171.88	25	11	1995	3	5
789463	-42.96	171.84	25	11	1995	2.17	5
773106	-42.98	171.86	25	11	1995	2.78	5
770649	-42.98	171.86	25	11	1995	2.08	5
789023	-42.98	171.82	25	11	1995	1.77	5
773223	-42.95	171.84	25	11	1995	2.12	5
776789	-42.98	171.86	25	11	1995	1.66	5
776791	-42.97	171.75	25	11	1995	2.11	5
773733	-42.95	171.83	25	11	1995	2.46	5
773734	-42.95	171.83	25	11	1995	2.18	5
773224	-42.99	171.86	25	11	1995	2.59	5
776793	-42.98	171.88	25	11	1995	1.76	5
776794	-42.96	171.86	25	11	1995	2.43	5
789026	-42.96	171.85	25	11	1995	2.32	5
773739	-42.98	171.88	25	11	1995	2.35	5
776799	-42.98	171.85	25	11	1995	2.05	5
789041	-42.96	171.82	25	11	1995	2.89	5
775448	-42.93	171.84	25	11	1995	1.87	5
773740	-42.93	171.83	25	11	1995	1.86	5
789047	-42.96	171.84	25	11	1995	2.48	5
789042	-42.91	171.83	25	11	1995	2.19	5
789044	-42.93	171.90	25	11	1995	2.51	5
779153	-42.95	171.85	25	11	1995	1.85	5
773226	-42.94	171.84	25	11	1995	2.45	5
776189	-42.96	171.81	25	11	1995	2.2	5
789355	-43.00	171.88	25	11	1995	1.21	5
773408	-42.98	171.86	25	11	1995	2.23	5
770654	-42.93	171.84	25	11	1995	5.19	5.59
776190	-42.92	171.83	25	11	1995	2.16	5
790057	-42.93	171.83	25	11	1995	2.33	5
776192	-42.97	171.84	25	11	1995	2.13	5
790059	-42.99	171.87	25	11	1995	2.42	5
771558	-42.92	171.81	25	11	1995	1.84	5
790663	-42.95	171.85	25	11	1995	2.46	5
773744	-42.97	171.86	25	11	1995	2.28	5
781917	-42.91	171.81	25	11	1995	2.03	5
773745	-42.96	171.84	25	11	1995	2.46	5
776194	-42.88	171.76	25	11	1995	1.97	5
779154	-42.97	171.86	25	11	1995	1.97	5
794862	-42.99	171.89	25	11	1995	1.85	5
794864	-42.99	171.89	25	11	1995	2.15	5
790665	-42.98	171.88	25	11	1995	2.99	5
792936	-42.91	171.83	25	11	1995	4.25	5.23
790703	-42.91	171.83	25	11	1995	2.02	5
771688	-42.99	171.86	25	11	1995	3.01	5
771477	-42.98	171.87	25	11	1995	2.45	5
792506	-42.93	171.82	25	11	1995	1.92	5
773107	-42.92	171.83	25	11	1995	2.99	5
773900	-42.91	171.83	25	11	1995	2.29	5
773228	-42.91	171.83	25	11	1995	2.66	5
793023	-42.94	171.85	25	11	1995	2.1	5
776195	-42.91	171.82	25	11	1995	2.19	5
771478	-42.92	171.83	25	11	1995	2.12	5
772869	-42.95	171.82	25	11	1995	1.97	5
771480	-42.95	171.86	25	11	1995	2.98	5
776196	-42.95	171.85	25	11	1995	2.24	5
792937	-42.99	171.87	25	11	1995	2.31	5
773749	-42.94	171.85	25	11	1995	2.53	5

ID	Latitude	Longitude	Day	Month	Year	Magnitude	Depth
792942	-42.95	171.82	25	11	1995	1.91	5
781920	-42.91	171.82	25	11	1995	2.04	5
773108	-42.93	171.83	25	11	1995	2.67	5
773750	-42.91	171.82	25	11	1995	2.22	5
773751	-43.00	171.89	25	11	1995	2	5
792945	-42.91	171.83	25	11	1995	2.27	5
773230	-42.91	171.82	25	11	1995	2.22	5
792946	-42.91	171.82	25	11	1995	2.42	5
781921	-42.95	171.83	25	11	1995	1.9	5
776197	-42.91	171.82	25	11	1995	2.01	5
773753	-42.99	171.85	25	11	1995	2.07	5
776198	-42.93	171.83	25	11	1995	2.07	5
781922	-42.95	171.84	25	11	1995	1.91	5
773754	-42.99	171.86	25	11	1995	2.04	5
773231	-42.91	171.83	25	11	1995	2.76	5
792958	-42.91	171.83	25	11	1995	2.14	5
773755	-42.97	171.86	25	11	1995	2.22	5
776200	-42.91	171.84	25	11	1995	2.33	5
771483	-42.98	171.85	25	11	1995	3.32	5
773756	-43.00	171.87	25	11	1995	1.88	5
776201	-42.91	171.83	25	11	1995	2.03	5
773233	-42.91	171.82	25	11	1995	2	5
773234	-43.00	171.88	25	11	1995	2.05	5
792983	-43.00	171.88	25	11	1995	2.39	5
779156	-42.91	171.83	25	11	1995	2.57	5
773235	-42.98	171.87	25	11	1995	2.35	5
773236	-42.98	171.87	25	11	1995	2.65	5
779175	-42.98	171.87	25	11	1995	2.09	5
792994	-42.98	171.86	25	11	1995	2.91	4.08
776203	-42.90	171.82	25	11	1995	1.96	5
773759	-42.93	171.84	25	11	1995	2.28	5
776205	-42.94	171.82	25	11	1995	2.24	5
792995	-42.93	171.85	25	11	1995	2.39	5
779205	-42.97	171.84	25	11	1995	2.43	5
779207	-42.97	171.87	25	11	1995	2.04	5
779213	-42.99	171.86	25	11	1995	1.75	5
776206	-42.94	171.90	25	11	1995	1.93	5
773413	-42.96	171.86	25	11	1995	2.27	5
771690	-42.97	171.85	25	11	1995	2.84	5
793020	-42.90	171.83	25	11	1995	2.3	5
773762	-42.98	171.77	25	11	1995	2.09	5
779257	-43.00	171.84	25	11	1995	2.2	5
793021	-42.98	171.88	25	11	1995	2.02	5
773111	-42.99	171.86	25	11	1995	2.59	5
773240	-42.96	171.85	25	11	1995	1.94	5
773112	-42.95	171.86	25	11	1995	2.52	5
773764	-42.92	171.82	25	11	1995	2.13	5
771691	-42.93	171.84	25	11	1995	2.78	5
779272	-42.95	171.83	25	11	1995	1.9	5
770663	-42.95	171.84	25	11	1995	2.54	5
773241	-42.97	171.86	25	11	1995	2.29	5
779277	-42.95	171.84	25	11	1995	3.2	5
773242	-42.97	171.85	25	11	1995	2.51	5
793046	-42.96	171.86	25	11	1995	2.36	5
776207	-42.91	171.82	25	11	1995	2.13	5
773602	-42.98	171.86	25	11	1995	2	5
776209	-42.95	171.84	25	11	1995	2.15	5
773952	-42.94	171.82	25	11	1995	2.31	5
773114	-42.94	171.84	25	11	1995	2.32	5
773115	-42.98	171.87	25	11	1995	2.94	5

ID	Latitude	Longitude	Day	Month	Year	Magnitude	Depth
773116	-42.98	171.87	25	11	1995	2.86	5
776211	-42.97	171.85	25	11	1995	2.21	5
781925	-42.92	171.82	25	11	1995	2.07	5
773839	-42.98	171.87	25	11	1995	1.71	5
776212	-42.97	171.84	25	11	1995	1.91	5
779309	-42.91	171.81	25	11	1995	2.15	5
776213	-42.93	171.83	25	11	1995	2.61	5
776214	-42.93	171.82	25	11	1995	1.93	5
771692	-42.91	171.83	25	11	1995	3.8	5
793084	-42.94	171.81	25	11	1995	2.12	5
772873	-42.93	171.89	25	11	1995	2.52	5
773244	-42.97	171.85	25	11	1995	2.23	5
771562	-42.97	171.87	25	11	1995	4.07	5
776215	-42.94	171.81	25	11	1995	2.22	5
781926	-42.94	171.83	25	11	1995	2.01	5
773117	-42.90	171.83	25	11	1995	2.91	5
771693	-42.94	171.85	25	11	1995	2.63	5
772874	-42.98	171.86	25	11	1995	3.26	5
794917	-42.97	171.85	25	11	1995	2.59	5
773767	-42.96	171.85	26	11	1995	2.52	5
773768	-42.91	171.83	26	11	1995	2.28	5
779346	-43.00	171.89	26	11	1995	1.45	5
794868	-42.99	171.86	26	11	1995	2.49	7.29
780540	-42.98	171.86	26	11	1995	2.24	4.17
771497	-42.96	171.82	26	11	1995	2.47	7.86
779351	-42.91	171.84	26	11	1995	2.02	7.06
773118	-42.97	171.87	26	11	1995	2.77	5
779352	-42.92	171.83	26	11	1995	1.93	5
780555	-42.92	171.83	26	11	1995	2.88	4.62
770670	-42.93	171.84	26	11	1995	2.25	6.84
780563	-42.98	171.86	26	11	1995	2.89	2.78
776217	-42.97	171.82	26	11	1995	1.94	5
794877	-42.92	171.80	26	11	1995	2.03	5
773245	-42.91	171.83	26	11	1995	2.21	4.5
771566	-42.99	171.87	26	11	1995	3.91	6.79
773418	-42.97	171.84	26	11	1995	2.04	5
780573	-43.10	172.03	26	11	1995	2.09	5
780577	-43.07	171.99	26	11	1995	1.63	5
780578	-43.09	172.00	26	11	1995	1.89	5
780583	-43.09	172.00	26	11	1995	1.67	5
780589	-42.98	171.86	26	11	1995	2.06	5
794918	-43.10	171.98	26	11	1995	1.83	5
780590	-42.99	171.89	26	11	1995	2.89	4.9
780591	-43.01	171.87	26	11	1995	1.98	5
775055	-43.10	171.97	26	11	1995	2.36	5
780596	-42.94	171.85	26	11	1995	2.11	5
773122	-42.99	171.87	26	11	1995	3.26	5.79
780610	-42.98	171.87	26	11	1995	2.28	5.59
770680	-42.95	171.85	26	11	1995	3.85	8.37
773123	-42.96	171.83	26	11	1995	2.74	7.14
773771	-42.93	171.83	26	11	1995	2.17	4.91
780613	-42.94	171.81	26	11	1995	2.57	6.3
782291	-43.02	172.03	26	11	1995	1.81	5
794910	-42.93	171.84	26	11	1995	1.93	5
773124	-42.91	171.84	26	11	1995	2.39	5
780622	-43.07	172.00	26	11	1995	1.86	5
771698	-43.00	171.86	26	11	1995	3.76	6.76
776219	-42.92	171.92	26	11	1995	2.08	5
780625	-43.08	171.99	26	11	1995	1.63	5
794913	-42.98	171.86	26	11	1995	2.17	5

ID	Latitude	Longitude	Day	Month	Year	Magnitude	Depth
771699	-42.99	171.88	26	11	1995	3.63	6.3
773772	-42.97	171.86	26	11	1995	2.36	5
794914	-42.98	171.86	26	11	1995	2.26	4.28
780631	-42.98	171.83	26	11	1995	2.21	11.48
794915	-43.06	171.97	26	11	1995	1.68	5
780634	-43.08	172.06	26	11	1995	1.53	5
780635	-43.09	172.08	26	11	1995	1.75	5
773126	-42.94	171.86	26	11	1995	2.9	5.3
780640	-42.98	171.87	26	11	1995	2.45	7.27
780643	-42.98	171.85	26	11	1995	1.96	5
780644	-42.94	171.81	26	11	1995	1.97	6.56
771700	-43.08	172.05	26	11	1995	1.83	5
773128	-42.92	171.82	26	11	1995	2.77	5.01
773773	-42.97	171.83	26	11	1995	2.46	8.19
773774	-42.99	171.87	26	11	1995	2.36	4.8
794953	-43.00	171.88	26	11	1995	2.25	8.69
773869	-42.98	171.86	26	11	1995	2.35	6.84
780656	-42.94	171.83	26	11	1995	1.9	5
794954	-42.93	171.84	26	11	1995	2.07	7.14
780657	-42.98	171.84	26	11	1995	2.21	8.66
780659	-43.01	171.90	26	11	1995	1.9	9.08
780660	-42.99	171.87	26	11	1995	2.33	4.95
771701	-42.99	171.88	26	11	1995	3.06	5.6
780661	-43.07	171.99	26	11	1995	1.75	5
773252	-42.92	171.83	26	11	1995	2.02	5
780662	-43.09	171.99	26	11	1995	1.84	5
773130	-42.99	171.87	26	11	1995	3.17	4.2
773131	-42.91	171.83	26	11	1995	3.14	4.82
794958	-43.05	171.98	26	11	1995	1.81	5
780672	-42.97	171.85	26	11	1995	2.47	6.64
773776	-43.06	171.96	26	11	1995	1.94	5
780677	-42.93	171.83	26	11	1995	1.97	5
780685	-42.93	171.84	26	11	1995	1.93	5
780687	-42.91	171.81	26	11	1995	1.84	5
776220	-42.91	171.82	26	11	1995	1.99	5
773132	-42.96	171.84	26	11	1995	2.31	8.31
795697	-42.93	171.83	26	11	1995	2.6	7.32
776221	-42.92	171.83	26	11	1995	1.99	5
779367	-43.05	171.95	26	11	1995	2.16	5
780700	-43.16	172.06	26	11	1995	2.01	5
795698	-42.99	171.87	26	11	1995	2.81	6.06
780704	-43.13	172.04	26	11	1995	1.98	5
780711	-43.10	172.05	26	11	1995	1.82	5
780712	-43.04	171.99	26	11	1995	1.98	5
780717	-42.95	171.81	26	11	1995	1.94	5
770683	-43.08	171.99	26	11	1995	1.9	5
770685	-42.92	171.83	26	11	1995	2.55	4.35
795705	-43.00	171.87	26	11	1995	2.42	4.24
775056	-43.10	172.03	26	11	1995	2.22	5
773777	-42.99	171.89	26	11	1995	2.54	4.37
780734	-43.07	171.99	26	11	1995	1.84	5
780736	-42.99	171.88	26	11	1995	2.53	4.81
771508	-42.94	171.83	26	11	1995	2.56	9.13
770686	-42.97	171.85	26	11	1995	1.83	8.58
795708	-42.95	171.83	26	11	1995	2.23	8.37
779375	-42.97	171.86	26	11	1995	2.08	6.64
780744	-43.09	172.04	26	11	1995	1.67	5
795717	-42.99	171.87	26	11	1995	2.25	6.89
780753	-42.97	171.87	26	11	1995	2.16	5.36
773257	-42.97	171.84	26	11	1995	2.49	7.43

ID	Latitude	Longitude	Day	Month	Year	Magnitude	Depth
780761	-43.01	171.86	26	11	1995	2.33	4.06
773810	-42.98	171.87	26	11	1995	2.87	8.31
772882	-42.91	171.83	26	11	1995	2.17	5
780773	-42.99	171.88	26	11	1995	2.99	6.67
780775	-42.98	171.87	26	11	1995	2.78	5.16
795764	-42.91	171.84	26	11	1995	2.63	5
771702	-42.99	171.87	26	11	1995	3.1	6.69
779388	-42.95	171.84	26	11	1995	2.25	5
779395	-42.92	171.82	26	11	1995	2	5
772830	-42.96	171.85	26	11	1995	2.37	8.03
779398	-42.99	171.87	26	11	1995	3.16	6.59
773139	-42.95	171.87	26	11	1995	2.64	3.71
780811	-42.97	171.83	27	11	1995	2.63	5
793082	-42.98	171.83	27	11	1995	2.91	5
793083	-42.97	171.82	27	11	1995	1.71	5
780816	-42.93	171.83	27	11	1995	2.56	3.65
773141	-42.93	171.84	27	11	1995	2.75	7.41
780830	-42.98	171.77	27	11	1995	2.2	5
775064	-43.08	171.97	27	11	1995	1.82	8.44
773143	-42.94	171.84	27	11	1995	3.26	4.93
775066	-43.10	172.04	27	11	1995	1.99	9.38
775067	-42.98	171.88	27	11	1995	2.38	6.97
771569	-42.93	171.84	27	11	1995	2.39	3.78
780847	-42.97	171.86	27	11	1995	3.27	8.13
795770	-42.97	171.87	27	11	1995	2.55	5
776224	-42.95	171.84	27	11	1995	2.42	9.19
776225	-42.97	171.85	27	11	1995	2.31	8.31
773147	-42.98	171.86	27	11	1995	2.93	3.53
780873	-42.99	171.88	27	11	1995	2.64	4.65
776226	-42.93	171.90	27	11	1995	2.38	8.6
770708	-42.94	171.85	27	11	1995	2.58	4.53
773151	-42.98	171.86	27	11	1995	2.56	5
771706	-42.95	171.84	27	11	1995	2.58	7.9
795774	-42.93	171.85	27	11	1995	3.02	6.58
773153	-42.93	171.83	27	11	1995	2.1	6.05
771521	-42.94	171.86	27	11	1995	2.37	4.44
780930	-42.98	171.86	27	11	1995	3.13	2.83
773156	-42.97	171.87	27	11	1995	2.47	8.63
795775	-42.98	171.87	27	11	1995	2.48	6.25
772889	-42.92	171.92	27	11	1995	2.56	5.69
795776	-42.91	171.84	27	11	1995	2.64	4.68
770764	-42.92	171.92	27	11	1995	2.6	5.85
773160	-42.91	171.84	27	11	1995	2.22	5
776227	-42.98	171.89	27	11	1995	2.42	6.87
773162	-42.93	171.93	27	11	1995	3.37	5.45
771525	-42.95	171.84	27	11	1995	3.07	7.8
795778	-42.98	171.87	27	11	1995	1.9	3.05
773163	-42.93	171.85	27	11	1995	2.75	4.37
779405	-43.11	171.89	27	11	1995	1.28	5
771707	-42.98	171.85	27	11	1995	3.1	7.82
773164	-42.97	171.87	27	11	1995	2.41	3.13
779408	-42.93	171.84	27	11	1995	2.17	5.94
776228	-42.92	171.85	27	11	1995	1.9	7.16
781015	-42.93	171.84	27	11	1995	2.76	3.57
779409	-42.92	171.83	27	11	1995	2.11	4.28
795781	-42.97	171.87	27	11	1995	2.52	3.65
771708	-42.96	171.84	27	11	1995	1.92	10.18
770771	-42.97	171.86	27	11	1995	4.29	6.56
779410	-42.96	171.88	27	11	1995	1.97	3.42
773265	-42.99	171.87	27	11	1995	2.24	9.58

ID	Latitude	Longitude	Day	Month	Year	Magnitude	Depth
773433	-42.99	171.88	27	11	1995	2.35	4.51
773269	-42.92	171.84	28	11	1995	2.29	3.79
774742	-42.99	171.88	28	11	1995	2.56	4.92
773270	-42.91	171.85	28	11	1995	2.78	4.75
773272	-42.95	171.87	28	11	1995	3.08	5
774711	-43.06	171.96	28	11	1995	2.29	9.31
774746	-42.93	171.83	28	11	1995	2.22	2.46
773273	-42.94	171.84	28	11	1995	2.35	3.7
796519	-42.93	171.84	28	11	1995	1.63	3.53
773277	-42.99	171.88	28	11	1995	3.12	4.62
795792	-42.94	171.84	28	11	1995	2.33	6.96
773279	-42.95	171.87	28	11	1995	2.66	3.13
775148	-42.92	171.99	28	11	1995	2.09	8.63
775149	-42.95	171.85	28	11	1995	2.4	9.3
795793	-42.97	171.85	28	11	1995	2.7	5.34
771709	-42.93	171.84	28	11	1995	3.5	5.99
795794	-42.93	171.83	28	11	1995	2.89	3.46
774747	-42.98	171.87	28	11	1995	2.12	5.59
773281	-42.91	171.82	28	11	1995	2.2	4.34
771710	-42.96	171.85	28	11	1995	2.68	7.35
771711	-42.96	171.84	28	11	1995	3.23	8.62
795795	-42.96	171.84	28	11	1995	2.95	7.75
781211	-42.97	171.84	28	11	1995	2.47	8.01
773285	-42.94	171.92	28	11	1995	2	4.36
795797	-42.92	171.83	28	11	1995	2.56	3.36
773286	-42.94	171.84	28	11	1995	2.67	8.23
795799	-42.92	171.83	28	11	1995	2.06	3.37
773287	-42.92	171.83	28	11	1995	2.48	3.83
779414	-43.10	171.86	28	11	1995	1.7	5
773443	-42.98	171.87	28	11	1995	2.12	5
773288	-42.94	171.84	28	11	1995	2.43	8.88
795800	-42.92	171.83	28	11	1995	2.29	5.24
779416	-42.96	171.86	28	11	1995	2.46	5.26
773291	-42.91	171.85	28	11	1995	2.35	3.65
776233	-42.98	171.89	28	11	1995	2.08	8.34
773292	-43.00	171.87	28	11	1995	2.33	3.19
773293	-42.98	171.87	28	11	1995	2.44	5.35
771712	-42.95	171.86	28	11	1995	2.97	5.86
773294	-42.91	171.84	28	11	1995	2.13	3.72
773295	-42.92	171.84	28	11	1995	2.17	4.78
773296	-42.93	171.85	29	11	1995	2.66	4.5
795806	-43.10	171.99	29	11	1995	2.05	5
773298	-42.99	171.88	29	11	1995	2.9	4.33
771570	-42.98	171.87	29	11	1995	3.52	5.45
795815	-43.10	171.99	29	11	1995	2.08	5
795816	-42.94	171.93	29	11	1995	1.69	5
795817	-42.93	171.83	29	11	1995	2.06	5
795818	-43.10	171.99	29	11	1995	1.96	5
795801	-42.93	171.82	29	11	1995	1.99	5
774761	-42.99	171.87	29	11	1995	2.32	4.8
795820	-42.94	171.91	29	11	1995	2.15	5
779438	-42.99	171.89	29	11	1995	2.77	4.91
781368	-43.00	171.86	29	11	1995	3.02	6.23
774765	-42.97	171.86	29	11	1995	2.42	5.81
795832	-42.97	171.82	29	11	1995	1.94	5
795836	-42.97	171.81	29	11	1995	2.52	5
795839	-42.97	171.83	29	11	1995	2.05	5
795840	-42.94	171.81	29	11	1995	2.16	5
795844	-42.95	171.89	29	11	1995	2.01	5
774768	-42.96	171.86	29	11	1995	1.95	8.93

ID	Latitude	Longitude	Day	Month	Year	Magnitude	Depth
774769	-42.93	171.84	29	11	1995	1.86	5
771715	-42.99	171.86	29	11	1995	2.89	5.66
774770	-42.93	171.85	29	11	1995	2.18	5
774771	-42.99	171.86	29	11	1995	2.72	5.99
770724	-42.99	171.87	29	11	1995	2.58	5.76
774774	-42.88	171.77	29	11	1995	1.82	5
774779	-42.94	171.83	29	11	1995	2.21	4.92
795865	-42.98	171.84	29	11	1995	1.81	5
774780	-42.94	171.85	29	11	1995	2.46	6.11
774912	-42.96	171.84	29	11	1995	2.44	7.86
775151	-42.96	171.80	29	11	1995	2.04	5
770728	-43.00	171.86	30	11	1995	2.28	9.14
770734	-42.88	171.78	30	11	1995	1.95	5
796522	-42.97	171.87	30	11	1995	2.2	6.96
779541	-42.93	171.86	30	11	1995	2.32	5
774785	-42.94	171.83	30	11	1995	1.85	5
776234	-42.93	171.82	30	11	1995	1.82	5
774786	-42.99	171.83	30	11	1995	2.11	5
796647	-42.86	171.75	30	11	1995	1.73	5
776235	-42.93	171.91	30	11	1995	2.13	5
795924	-43.05	171.93	30	11	1995	1.83	6.59
795925	-42.96	171.83	30	11	1995	2.01	6.33
774790	-42.98	171.85	30	11	1995	2.33	5
779623	-43.10	171.99	30	11	1995	2.08	5
781549	-42.95	171.89	30	11	1995	2.34	8.75
776237	-42.98	171.85	30	11	1995	1.8	5
774918	-43.10	172.00	30	11	1995	2.15	5
774792	-42.99	171.86	30	11	1995	2.38	4.89
779629	-42.93	171.84	30	11	1995	1.84	5
774794	-42.97	171.84	30	11	1995	2.74	6.11
779640	-42.94	171.83	30	11	1995	2.3	5
796528	-42.96	171.83	30	11	1995	2.13	5
774919	-42.93	171.84	30	11	1995	2.37	4.33
774798	-42.99	171.86	30	11	1995	2.79	4.47
796527	-42.97	171.82	30	11	1995	2.34	7.97
796529	-42.99	171.86	30	11	1995	2.28	7.14
776239	-42.95	171.83	30	11	1995	1.98	6.63
775152	-42.99	171.86	30	11	1995	2.15	5.33
774801	-42.88	171.76	30	11	1995	2.11	5
774802	-42.88	171.77	30	11	1995	2.03	3.95
774803	-42.99	171.86	30	11	1995	2.63	6.6
796535	-43.00	171.88	30	11	1995	2.15	9.88
776241	-42.93	171.81	30	11	1995	2.16	8.19
773472	-42.94	171.90	30	11	1995	3.03	4.42
774804	-42.94	171.85	30	11	1995	2.34	6.91
774806	-42.95	171.82	30	11	1995	2.29	7.84
773476	-42.92	171.82	30	11	1995	2.19	5
774807	-42.98	171.77	30	11	1995	2.12	5
774808	-42.96	171.83	1	12	1995	2.01	5
774810	-42.93	171.92	1	12	1995	2.13	5
774811	-42.93	171.83	1	12	1995	1.8	5
796540	-42.92	171.83	1	12	1995	2.15	5
775153	-42.96	171.82	1	12	1995	2.25	5
774815	-42.98	171.87	1	12	1995	2.69	3.28
773485	-42.91	171.82	1	12	1995	2.86	4.25
781683	-42.95	171.83	1	12	1995	2.31	9.28
773486	-42.99	171.88	1	12	1995	2.85	5.39
779696	-42.94	171.86	1	12	1995	2.06	9.16
773487	-42.99	171.87	1	12	1995	2.78	4.54
774822	-42.95	171.90	1	12	1995	2.24	5

ID	Latitude	Longitude	Day	Month	Year	Magnitude	Depth
774824	-42.93	171.83	1	12	1995	2.08	4.57
771717	-42.98	171.77	1	12	1995	3.24	5.89
781720	-42.99	171.87	1	12	1995	3.05	3.71
773493	-42.94	171.84	1	12	1995	3.17	5.84
771718	-42.98	171.86	1	12	1995	2.46	6.28
796639	-42.95	171.80	1	12	1995	2.19	5
774827	-42.95	171.84	1	12	1995	2.88	8.46
775167	-42.96	171.85	1	12	1995	2.38	14.63
773499	-42.96	171.84	1	12	1995	2.86	4.49
773501	-42.94	171.88	1	12	1995	2.65	21.96
773505	-42.94	171.85	1	12	1995	2.75	4.51
774833	-42.95	171.84	1	12	1995	2.75	9
774836	-42.98	171.86	2	12	1995	2.18	5
774839	-42.95	171.84	2	12	1995	2	4.98
774670	-42.97	171.86	2	12	1995	2.34	5
774844	-42.88	171.77	2	12	1995	2.25	4.21
774846	-42.88	171.77	2	12	1995	2.19	4.25
796766	-42.97	171.82	2	12	1995	2.38	5
774847	-42.96	171.88	2	12	1995	2.31	12
775184	-42.95	171.85	2	12	1995	2.17	5
774848	-42.93	171.83	2	12	1995	1.92	5
774850	-42.92	171.83	2	12	1995	2.75	5
775185	-42.97	171.87	2	12	1995	2.23	16.53
776245	-42.96	171.83	2	12	1995	2.37	12
796774	-42.92	171.84	2	12	1995	2.43	5.22
771723	-43.00	171.87	2	12	1995	2.56	5
774856	-42.96	171.86	2	12	1995	2.48	5
773516	-42.93	171.83	2	12	1995	2.9	5
774857	-42.93	171.83	2	12	1995	2.21	5
774866	-42.98	171.85	3	12	1995	2.41	5
774875	-42.92	171.83	3	12	1995	2.49	5
774876	-42.92	171.84	3	12	1995	2.63	4.76
774879	-42.97	171.84	3	12	1995	2.12	5
773529	-42.94	171.92	3	12	1995	2.66	5
796996	-42.94	171.91	3	12	1995	2.09	5
771726	-42.92	171.82	3	12	1995	2.87	5
774881	-42.99	171.87	3	12	1995	2.3	5
774887	-42.97	171.85	3	12	1995	2.34	5
776248	-42.93	171.84	3	12	1995	2.19	12
775192	-42.99	171.87	4	12	1995	2.23	5
771728	-42.96	171.83	4	12	1995	3.34	5
774904	-42.91	171.82	4	12	1995	2.09	5
774905	-42.91	171.82	4	12	1995	2.01	5
775197	-42.96	171.87	4	12	1995	2.18	12
770820	-42.88	171.76	4	12	1995	2.11	5
776254	-42.91	171.82	5	12	1995	2.3	5
774952	-42.96	171.84	5	12	1995	2.55	6.68
775499	-43.00	171.87	5	12	1995	2.41	5
797229	-42.94	171.82	5	12	1995	2.53	5
776255	-42.96	171.84	5	12	1995	2.51	6.58
775508	-42.97	171.79	5	12	1995	2.05	5
775509	-42.96	171.82	5	12	1995	2.02	5
774961	-42.96	171.80	5	12	1995	2.18	5
770847	-42.99	171.86	5	12	1995	2.43	5
774964	-42.93	171.83	5	12	1995	2.67	3.63
770850	-43.00	171.86	5	12	1995	3.97	6.04
775520	-42.96	171.82	5	12	1995	2.2	5
776259	-42.92	171.91	5	12	1995	2.22	12
776084	-42.95	171.88	5	12	1995	2.22	4.75
775525	-42.85	171.77	5	12	1995	2.26	5

ID	Latitude	Longitude	Day	Month	Year	Magnitude	Depth
776086	-42.91	171.81	6	12	1995	2.04	5
774978	-42.98	171.84	6	12	1995	2.85	4.25
775531	-42.96	171.82	6	12	1995	2.19	5
775540	-42.96	171.82	6	12	1995	1.98	5
776147	-42.93	171.85	6	12	1995	2.24	22.87
774983	-42.94	171.92	6	12	1995	2.47	5
775542	-42.94	171.83	6	12	1995	2.14	5
776262	-42.93	171.83	6	12	1995	2.08	5
775553	-42.99	171.87	7	12	1995	2.16	5
775557	-42.98	171.87	7	12	1995	2.19	5
776264	-42.94	171.80	7	12	1995	2.06	5
775564	-42.98	171.85	7	12	1995	3.09	5
775565	-42.94	171.91	7	12	1995	1.83	5.89
775569	-42.99	171.86	7	12	1995	2.52	5
770912	-42.91	171.84	7	12	1995	2.99	5
775572	-42.92	171.81	7	12	1995	2.19	5
776266	-42.88	171.76	7	12	1995	2.14	5
775577	-42.93	171.84	7	12	1995	2.74	5
770921	-42.98	171.87	7	12	1995	3.57	5
770935	-42.91	171.84	7	12	1995	2.62	5
770946	-42.86	171.78	7	12	1995	2.12	5
775589	-42.94	171.96	8	12	1995	2.47	5
775593	-42.89	171.78	8	12	1995	2.87	5
770960	-42.96	171.87	8	12	1995	1.88	12
775595	-42.94	171.83	8	12	1995	2.15	5
775599	-42.90	171.85	8	12	1995	2.05	12
775601	-43.00	171.85	8	12	1995	2.26	5
775608	-42.84	171.83	9	12	1995	1.79	5
776026	-42.99	171.83	9	12	1995	2.47	5
775611	-42.92	171.83	9	12	1995	2.03	5
775612	-42.99	171.87	9	12	1995	2.73	5
775613	-42.96	171.82	9	12	1995	3.27	5
776275	-43.00	171.83	9	12	1995	2.08	5
776277	-43.00	171.84	9	12	1995	2.23	5
775614	-42.99	171.84	9	12	1995	2.78	5
775617	-42.94	171.83	9	12	1995	2.94	5
775619	-43.00	171.84	9	12	1995	2.47	5
775623	-43.00	171.83	9	12	1995	2.17	5
775629	-43.00	171.87	10	12	1995	2.7	5
775630	-42.97	171.85	10	12	1995	2.04	5
775631	-42.94	171.85	10	12	1995	3.13	5
775634	-43.00	171.85	10	12	1995	2.86	5
775638	-42.92	171.83	10	12	1995	2.3	5
775786	-42.92	171.83	10	12	1995	2.2	5
775641	-42.99	171.83	10	12	1995	2.32	5
775642	-42.95	171.82	10	12	1995	2.28	5
771016	-42.93	171.83	10	12	1995	3.91	5
775789	-42.95	171.90	10	12	1995	2.4	5
798150	-42.81	171.82	10	12	1995	3.54	5
798151	-42.81	171.83	10	12	1995	2.83	5
775645	-42.99	171.88	10	12	1995	2.7	5
776153	-42.97	171.80	11	12	1995	2.27	5
771034	-42.94	171.88	11	12	1995	2.45	12
775646	-42.99	171.77	11	12	1995	2.81	5
775661	-42.91	171.84	11	12	1995	3.07	5
775663	-42.93	171.84	11	12	1995	3.1	5
776155	-42.90	171.94	11	12	1995	2	31.18
775687	-42.96	171.84	11	12	1995	2.99	5
776287	-42.98	171.86	12	12	1995	2.76	5
775692	-42.99	171.86	12	12	1995	2.67	5

ID	Latitude	Longitude	Day	Month	Year	Magnitude	Depth
800217	-42.96	171.88	12	12	1995	2.52	5
775729	-42.95	171.86	12	12	1995	3.48	5
776828	-42.99	171.87	13	12	1995	2.96	12
777636	-43.10	171.74	13	12	1995	2.53	33
800562	-42.94	171.88	13	12	1995	3.2	12
777645	-42.92	171.85	14	12	1995	2.41	5
777646	-42.99	171.87	14	12	1995	3.3	12
800575	-42.98	171.88	15	12	1995	2.79	7.59
777654	-42.80	171.82	15	12	1995	2.71	5
871983	-42.81	171.82	17	12	1995	3.08	5
872256	-42.94	171.85	17	12	1995	2.56	5
872266	-42.93	171.93	18	12	1995	2.94	5
872272	-42.99	171.88	18	12	1995	2.91	5
872089	-42.81	171.81	18	12	1995	3.96	5
872287	-42.94	171.86	18	12	1995	2.66	5
872312	-42.97	171.88	19	12	1995	2.59	12
872411	-42.98	171.86	20	12	1995	3.02	12
872766	-42.98	171.87	20	12	1995	2.46	5
874066	-43.00	171.86	21	12	1995	4.1	5
872782	-43.04	172.06	22	12	1995	3.11	5
872784	-42.99	171.84	22	12	1995	3.69	5
872785	-42.99	171.91	22	12	1995	2.82	12
872788	-42.95	171.90	22	12	1995	2.84	5
892886	-42.91	171.87	23	12	1995	2.73	12
872797	-42.95	171.82	23	12	1995	3.54	5
872799	-42.99	171.83	23	12	1995	2.24	5
872803	-43.00	171.87	24	12	1995	2.61	7.5
874526	-42.90	171.87	24	12	1995	2.45	12
872808	-42.99	171.86	24	12	1995	3.01	5
874089	-42.96	171.86	24	12	1995	2.21	5
874091	-42.99	171.87	24	12	1995	2.48	5
873605	-42.90	171.97	25	12	1995	2.31	12
872818	-42.96	171.89	25	12	1995	2.19	5
872819	-42.97	171.87	26	12	1995	2.52	5
872838	-42.93	171.93	27	12	1995	2.57	5
875513	-42.99	171.85	28	12	1995	2.74	5
874196	-42.99	171.84	29	12	1995	3.37	5
874198	-42.95	171.87	29	12	1995	2.17	12
873993	-42.96	171.91	29	12	1995	2.68	12
874225	-43.00	171.87	30	12	1995	3.26	4.79
874228	-43.00	171.87	30	12	1995	2.29	5
877449	-42.93	172.09	30	12	1995	3.03	5
874272	-42.94	171.85	31	12	1995	2.56	5
874315	-42.92	171.84	1	1	1996	2.94	5
874320	-42.98	171.87	1	1	1996	3.11	5
874363	-42.84	171.90	2	1	1996	1.84	33
874372	-43.02	171.87	2	1	1996	2.7	8.09
874398	-42.96	171.84	3	1	1996	3.76	5
874408	-42.93	171.83	3	1	1996	2.7	5
874409	-42.94	171.83	3	1	1996	2.59	5
874440	-43.00	171.89	4	1	1996	2.27	5
901365	-43.01	171.88	4	1	1996	2.46	5
874452	-43.00	171.90	4	1	1996	2.09	8.8
874460	-42.95	171.82	4	1	1996	2.71	5
901375	-42.93	172.09	5	1	1996	2.27	5
901377	-43.02	171.98	5	1	1996	2.36	21.65
874494	-42.99	171.87	5	1	1996	2.7	5
874038	-42.94	171.93	6	1	1996	2.39	5
901385	-42.98	171.85	6	1	1996	3.13	9.02
877074	-43.00	171.84	6	1	1996	3.83	5

ID	Latitude	Longitude	Day	Month	Year	Magnitude	Depth
878217	-43.18	172.18	7	1	1996	3.12	5
878218	-43.00	171.87	7	1	1996	2.78	5
879658	-42.92	171.98	8	1	1996	2.63	8.68
879241	-43.00	171.85	9	1	1996	2.67	5
879667	-43.01	171.87	9	1	1996	2.58	5
875865	-42.88	171.77	9	1	1996	2.5	5
901688	-42.93	171.85	10	1	1996	2.25	5
886656	-42.93	171.84	11	1	1996	3.42	5
886665	-43.01	171.87	12	1	1996	3.38	5
897069	-43.00	171.87	12	1	1996	2.68	5
897073	-42.93	171.85	13	1	1996	2.31	5
896864	-42.93	171.96	15	1	1996	2.37	5
902619	-43.03	172.03	17	1	1996	2.38	25.32
898947	-42.97	171.78	17	1	1996	2.27	5
896882	-42.97	171.80	17	1	1996	2.54	4.96
896901	-42.92	171.84	18	1	1996	2.49	12
895877	-43.00	171.87	18	1	1996	2.52	6.76
896907	-43.07	172.22	19	1	1996	2.09	33
896909	-42.95	171.98	19	1	1996	2.47	5
896924	-43.00	171.89	20	1	1996	2.32	5
898640	-42.94	171.83	20	1	1996	2.57	5
896925	-42.92	171.99	20	1	1996	2.59	12
896125	-42.99	171.76	21	1	1996	2.32	5
896928	-42.92	171.86	21	1	1996	2.71	9.45
896935	-42.93	171.92	22	1	1996	2.48	5
896942	-42.98	171.86	23	1	1996	2.49	5
896943	-42.99	171.76	23	1	1996	2.99	5
896964	-42.93	171.84	25	1	1996	2.47	5
896373	-42.93	171.83	26	1	1996	2.39	5
896978	-42.95	171.85	26	1	1996	2.53	12
896614	-42.98	171.86	27	1	1996	2.82	12
908653	-42.94	171.84	31	1	1996	2.23	5
909804	-42.93	171.94	31	1	1996	2.4	5
909806	-42.92	171.83	31	1	1996	3.19	5
909823	-42.97	171.91	1	2	1996	2.23	12
909824	-42.97	171.88	1	2	1996	2.58	8.3
908017	-42.98	171.86	2	2	1996	2.5	5
909908	-42.99	171.88	4	2	1996	2.4	12
911912	-42.93	171.93	7	2	1996	2.73	5
912093	-43.01	171.88	7	2	1996	2.16	5
911913	-43.01	171.88	7	2	1996	2.68	5
911916	-42.92	171.91	7	2	1996	2.41	5
936676	-42.98	171.89	9	2	1996	2.18	12
909684	-42.93	171.85	10	2	1996	3.03	12
936686	-42.82	171.88	10	2	1996	1.87	12
911965	-42.93	171.84	10	2	1996	2.31	5
909713	-42.92	171.88	11	2	1996	2.59	12
912041	-42.99	171.87	12	2	1996	2.57	5
922374	-42.99	171.85	15	2	1996	2.49	5
948449	-43.00	171.83	16	2	1996	2.57	12
950417	-43.02	171.88	18	2	1996	2.74	5
922414	-42.93	171.91	18	2	1996	2.44	5
922758	-42.96	171.83	20	2	1996	2.95	5
926129	-43.20	172.20	21	2	1996	2.62	12
926132	-43.01	171.87	21	2	1996	2.96	5
921909	-43.01	171.88	22	2	1996	2.7	5
926921	-42.94	171.82	23	2	1996	3.01	5
926939	-43.00	171.85	24	2	1996	2.05	5
927014	-42.96	171.83	28	2	1996	2.72	5
948834	-42.97	171.85	29	2	1996	2.35	5

ID	Latitude	Longitude	Day	Month	Year	Magnitude	Depth
926670	-43.00	171.89	1	3	1996	2.2	5
948851	-42.91	171.87	1	3	1996	1.97	17.49
926554	-43.03	171.85	2	3	1996	3.68	5
926560	-42.98	171.84	4	3	1996	3.64	5
957799	-43.01	171.88	5	3	1996	3.15	5
948182	-43.01	171.88	5	3	1996	2.27	5
948914	-43.04	171.85	6	3	1996	2.36	5
936805	-43.04	171.99	9	3	1996	2.12	19.57
936884	-42.94	171.86	10	3	1996	3.21	5
949476	-42.98	171.87	11	3	1996	3.16	5
950796	-42.96	171.88	12	3	1996	1.98	5
952338	-43.01	171.90	12	3	1996	2.26	12
951977	-42.97	171.84	13	3	1996	2.97	5
951052	-42.98	171.88	13	3	1996	2.74	5
951188	-42.99	171.84	14	3	1996	3.03	5
955007	-43.06	172.11	15	3	1996	2.62	12
954980	-43.03	171.91	15	3	1996	3.16	12
959580	-42.96	171.87	18	3	1996	2.79	12
956216	-42.92	171.93	24	3	1996	2.39	12
954488	-42.99	171.88	24	3	1996	4.06	5
955731	-43.00	171.83	24	3	1996	2.82	12
956574	-42.93	171.94	27	3	1996	2.27	12
956234	-42.93	171.93	27	3	1996	2.71	12
956249	-42.94	171.89	28	3	1996	2.53	12
957569	-42.99	171.87	28	3	1996	2.17	12
956253	-42.93	171.84	28	3	1996	3.24	12
957585	-42.96	171.89	30	3	1996	2.59	12
958495	-42.95	171.85	2	4	1996	3.05	12
961033	-42.96	171.83	4	4	1996	2.52	12
961226	-42.98	171.86	8	4	1996	2.86	5
980213	-42.93	171.94	10	4	1996	3.13	12
963188	-43.21	171.98	10	4	1996	3.57	12
964438	-42.91	172.01	10	4	1996	2.62	5
960749	-43.03	171.86	11	4	1996	3.44	12
981076	-42.95	171.88	12	4	1996	4.28	12
963720	-42.92	171.94	12	4	1996	2.63	12
964454	-42.94	171.92	12	4	1996	2.6	5
963299	-42.95	171.91	12	4	1996	2.52	12
964256	-42.92	171.92	12	4	1996	2.32	5
963206	-42.94	171.93	13	4	1996	2.41	12
962657	-42.92	171.92	15	4	1996	2.64	12
964709	-42.92	171.93	16	4	1996	2.52	12
964845	-43.01	171.77	16	4	1996	2.47	12
982958	-42.96	171.92	17	4	1996	3.09	12
966075	-42.92	171.94	17	4	1996	2.5	12
962745	-42.97	171.89	18	4	1996	3.29	12
966245	-42.95	171.85	19	4	1996	2.51	12
966257	-43.02	171.87	20	4	1996	2.53	12
966339	-43.01	171.94	23	4	1996	2.64	12
978954	-42.93	171.93	24	4	1996	2.52	12
978955	-43.01	171.87	25	4	1996	2.8	12
966498	-42.95	171.84	25	4	1996	2.46	5
978962	-42.98	171.87	25	4	1996	2.48	5
984364	-42.94	171.85	3	5	1996	2.42	12
966583	-42.95	171.83	3	5	1996	3.29	12
966586	-42.94	171.84	3	5	1996	2.82	5
979443	-42.94	171.91	4	5	1996	2.66	12
966609	-42.94	171.93	4	5	1996	3.11	12
966634	-42.94	171.92	5	5	1996	3.39	12
966635	-42.94	171.92	5	5	1996	2.9	12

ID	Latitude	Longitude	Day	Month	Year	Magnitude	Depth
966637	-42.97	171.92	5	5	1996	2.87	12
983841	-42.94	171.93	10	5	1996	3.23	12
990257	-42.81	171.80	10	5	1996	3.6	12
986265	-42.96	171.84	15	5	1996	3.16	12
987723	-42.83	171.83	17	5	1996	2.7	12
987726	-42.91	171.77	18	5	1996	2.9	12
989398	-43.11	172.10	27	5	1996	2.82	12
988847	-42.96	171.92	3	6	1996	4.45	12
1000163	-43.04	171.86	21	6	1996	2.59	12
1000074	-42.93	171.92	21	6	1996	2.58	12
997080	-42.96	171.95	22	6	1996	2.75	5
1000539	-42.98	171.84	23	6	1996	2.6	12
1002669	-42.97	171.90	3	7	1996	2.51	12
1004787	-43.14	172.24	5	7	1996	2.38	12
1004797	-42.98	171.89	6	7	1996	2.63	12
1003084	-42.93	171.85	6	7	1996	3.14	5
1005851	-42.98	171.85	9	7	1996	2.4	12
1003689	-42.91	171.85	10	7	1996	2.86	12
1017613	-42.95	171.88	13	7	1996	2.83	5
882731	-43.01	171.87	28	7	1996	2.82	5
882734	-42.96	171.86	28	7	1996	2.57	12
882655	-43.01	171.88	29	7	1996	2.89	5
1023644	-42.92	171.87	6	8	1996	2.59	5
1023648	-43.09	172.22	8	8	1996	2.07	12
1027718	-43.01	171.87	17	8	1996	2.41	5
1023709	-42.95	171.84	29	8	1996	2.73	5
1035599	-43.02	171.85	18	9	1996	4.11	5
1036247	-42.93	171.87	19	9	1996	2.27	5
1038750	-42.96	171.84	24	9	1996	3	5
1037801	-42.94	171.85	25	9	1996	2.37	5
1041948	-42.92	171.96	3	10	1996	2.54	12
1044163	-42.91	171.94	14	10	1996	2.38	12
1070064	-42.93	171.85	29	10	1996	2.66	12
1052608	-43.00	171.89	7	11	1996	2.78	12
1054394	-42.98	171.89	9	11	1996	2.81	12
1052650	-42.94	171.87	11	11	1996	3.28	5
1053959	-42.94	172.00	18	11	1996	3.04	12
1065050	-42.97	171.89	11	12	1996	3.24	12
1065055	-42.96	171.91	11	12	1996	2.5	12
1061180	-42.93	171.91	22	12	1996	4.71	5
1066990	-42.94	171.94	22	12	1996	2.7	5
1066992	-42.93	171.93	22	12	1996	2.22	5
1061184	-42.93	171.92	22	12	1996	2.99	5
1066002	-42.93	171.93	22	12	1996	2.75	5
1066995	-42.93	171.95	23	12	1996	2.42	5
1068336	-42.94	171.94	23	12	1996	2.8	12
1066042	-42.93	171.92	24	12	1996	2.78	5
1066044	-42.93	171.93	24	12	1996	2.43	5
1067512	-42.94	171.94	24	12	1996	2.52	5
1067699	-43.03	171.85	27	12	1996	2.73	12
1067709	-42.93	171.93	27	12	1996	2.71	5
1066088	-42.93	171.91	27	12	1996	2.81	5
1072803	-42.97	171.82	2	1	1997	3.01	5
1071017	-42.93	171.93	12	1	1997	3.53	5
1073405	-42.91	171.79	13	1	1997	2.89	12
1089600	-43.19	172.16	14	1	1997	2.54	5
1073467	-43.18	172.03	16	1	1997	3.13	5
1080473	-42.94	171.89	24	1	1997	3.41	5
1090323	-42.95	171.95	14	2	1997	2.09	5
1090443	-43.01	171.89	19	2	1997	2.6	5

ID	Latitude	Longitude	Day	Month	Year	Magnitude	Depth
1090639	-42.96	171.90	1	3	1997	2.36	5
1090665	-42.99	171.88	2	3	1997	2.8	12
1092069	-42.92	171.88	4	3	1997	2.72	12
1101300	-42.92	171.86	11	3	1997	2.33	12
1100297	-42.94	171.92	14	3	1997	2.72	5
1100343	-42.92	171.83	16	3	1997	3.04	5
1100374	-43.20	172.14	18	3	1997	3.36	5
1100416	-42.99	171.87	20	3	1997	3.46	5
1108751	-42.97	171.90	21	3	1997	2.52	5
1116761	-42.96	171.89	12	4	1997	3.73	12
1129607	-43.13	172.02	4	5	1997	2.37	12
1136106	-43.22	172.01	29	5	1997	3.18	12
1138931	-43.00	171.87	5	6	1997	3.07	5
1147577	-42.85	171.98	18	6	1997	2.61	25.47
1147399	-42.94	171.84	23	6	1997	3.35	5
1150939	-42.99	171.88	2	7	1997	3.25	12
1154408	-42.98	171.88	13	7	1997	2.3	12
1154580	-43.00	171.87	18	7	1997	2.86	5
1154594	-42.94	171.93	21	7	1997	2.49	5
1162944	-43.00	171.86	15	8	1997	2.7	5
1161624	-43.01	171.78	18	8	1997	2.58	5
1175657	-42.93	171.94	5	9	1997	2.33	5
1174507	-43.00	171.88	9	9	1997	2.85	5
1174578	-42.88	171.81	16	9	1997	2.56	5
1177005	-42.96	171.90	20	9	1997	2.62	9.58
1179337	-43.05	172.13	27	9	1997	2.72	33
1188135	-42.90	171.79	16	10	1997	2.73	12
1212300	-42.93	171.97	23	12	1997	2.66	12
1221920	-42.96	171.89	6	1	1998	2.7	12
1222489	-42.97	171.87	10	1	1998	2.41	12
1229372	-42.81	172.06	23	1	1998	2.61	30.23
1229414	-42.97	171.90	2	2	1998	3.38	12
1232194	-42.93	171.92	5	2	1998	3.52	5
1204341	-43.01	171.87	29	3	1998	2.96	5
1253997	-42.89	171.76	12	4	1998	2.78	12
1218419	-42.98	171.81	18	4	1998	2.15	12
1276210	-42.92	171.86	29	5	1998	2.47	12
1297754	-43.17	171.74	13	6	1998	2.93	12
1284234	-42.99	171.87	19	6	1998	2.61	5
1266410	-42.93	172.20	10	7	1998	2.9	12
1284889	-42.94	171.87	25	8	1998	2.78	12
1309554	-43.14	172.25	2	9	1998	2.46	12
1290883	-42.96	171.89	6	9	1998	3.39	12
1323196	-43.05	171.77	20	10	1998	2.65	33
1329371	-43.13	172.11	28	10	1998	2.86	12
1324553	-42.95	171.89	1	11	1998	3.49	12
1329387	-42.95	171.89	1	11	1998	2.68	12
1325655	-42.93	171.81	4	11	1998	3.49	5
1326323	-42.95	171.98	9	11	1998	3.17	12
1332140	-42.92	171.84	22	11	1998	2.58	5
1353737	-43.05	171.77	22	11	1998	2.1	5
1337596	-42.96	171.86	3	12	1998	2.14	5
1337711	-43.00	172.01	4	12	1998	2.04	12
1337758	-42.93	171.83	4	12	1998	3.43	5
1337944	-42.93	171.84	6	12	1998	3.02	5
1343963	-42.99	171.87	12	12	1998	2.15	5
1353745	-43.00	171.87	15	1	1999	3.16	9.05
1372962	-43.20	172.05	11	3	1999	2.88	5
1378589	-42.93	171.92	27	3	1999	3.59	12
1388086	-42.97	171.85	27	4	1999	2.65	7.63

ID	Latitude	Longitude	Day	Month	Year	Magnitude	Depth
1388172	-43.20	172.05	29	4	1999	3.54	12
1406780	-43.01	171.92	17	6	1999	2.59	12
1408670	-43.17	172.02	23	6	1999	2.36	5
1409311	-42.99	171.76	28	6	1999	2.8	5
1414462	-42.92	171.82	17	7	1999	2.92	5
1429044	-43.17	172.23	23	7	1999	2.84	12
1415186	-42.89	171.77	24	7	1999	2.45	5
1422057	-42.95	171.92	15	8	1999	2.72	5
1428554	-42.94	171.91	10	9	1999	2.59	5
1429254	-42.93	171.83	14	9	1999	4.49	12
1429255	-42.93	171.82	14	9	1999	2.86	5
1429256	-42.93	171.82	14	9	1999	3.45	5
1429290	-42.93	171.82	15	9	1999	3.03	5
1444297	-42.99	171.94	21	9	1999	2.66	12
1431833	-42.93	171.82	23	9	1999	2.99	5
1444534	-42.93	171.82	22	10	1999	3.04	5
1447357	-42.92	172.07	2	11	1999	2.82	5
1448899	-42.95	171.83	11	11	1999	2.72	5
1455210	-42.94	171.81	21	11	1999	3.58	5
1455426	-42.89	172.22	24	11	1999	2.51	9.88
1457309	-42.95	171.96	5	12	1999	3.31	5
1465904	-43.02	171.79	21	12	1999	2.81	12
1470775	-42.94	171.97	7	1	2000	3.03	5
1470978	-42.94	171.96	10	1	2000	2.61	12
1489427	-42.92	171.83	14	2	2000	2.83	5
1493900	-43.17	172.15	2	3	2000	2.84	12
1495534	-42.94	171.93	7	3	2000	2.84	18.01
1504113	-42.93	171.84	31	3	2000	3.14	5
1507403	-42.91	171.86	12	4	2000	2.8	12
1515300	-42.95	171.92	25	4	2000	2.66	12
1518336	-42.94	171.99	6	5	2000	2.52	12
1519026	-43.03	171.92	8	5	2000	2.62	12
1536118	-42.91	171.94	21	6	2000	2.08	8.19
1568883	-42.92	171.87	12	7	2000	2.52	12
1597203	-42.93	171.83	8	8	2000	2.66	5
1597221	-42.93	171.82	8	8	2000	3.51	5
1605819	-42.92	171.85	5	9	2000	3.43	12
1607911	-42.92	171.91	14	9	2000	2.27	12
1614416	-42.99	171.79	3	10	2000	3.29	12
1614452	-43.00	171.78	3	10	2000	2.93	5
1616581	-42.93	171.91	9	10	2000	2.9	5
1634893	-42.95	171.89	31	10	2000	2.73	5
1635631	-42.92	171.84	2	11	2000	2.87	5.38
1638069	-42.97	171.86	11	11	2000	2.54	5
1638569	-43.02	171.87	14	11	2000	2.58	5
1654496	-42.97	171.90	10	12	2000	2.57	12
1661689	-42.92	171.86	25	12	2000	2.93	12
1664044	-42.96	171.86	3	1	2001	2.36	5
1722967	-42.96	172.04	21	1	2001	3.23	12
1689940	-43.22	172.10	6	2	2001	2.52	12
1690521	-43.10	172.14	7	2	2001	2.18	33
1760752	-42.98	171.83	20	2	2001	2.76	5
1697812	-42.96	171.95	1	3	2001	3.78	5
1705333	-42.86	172.21	20	3	2001	2.67	5
1709544	-42.96	171.86	25	3	2001	2.95	5
1711805	-43.12	172.15	31	3	2001	2.66	33
1712849	-42.93	171.83	3	4	2001	3.98	5
1712950	-42.93	171.92	4	4	2001	3.06	5
1743882	-43.16	172.05	10	6	2001	1.97	12
1847179	-43.16	172.12	1	7	2001	2.58	12

ID	Latitude	Longitude	Day	Month	Year	Magnitude	Depth
1768407	-42.92	171.83	31	7	2001	3.03	5
1779645	-42.93	171.89	18	8	2001	2.93	10.38
1779946	-42.93	171.88	19	8	2001	2.74	12
1780058	-42.93	171.86	20	8	2001	2.85	5
1780944	-42.93	171.88	22	8	2001	2.91	12
1782974	-42.93	171.96	28	8	2001	2.54	12
1793575	-42.85	171.85	23	9	2001	2.18	12
1794417	-42.93	171.9	27	9	2001	2.75	12
1883859	-42.91	171.86	7	10	2001	2.68	12
1807300	-42.93	171.95	17	10	2001	2.53	12
1811850	-43.00	171.90	1	11	2001	2.31	12
1823637	-42.94	171.84	30	11	2001	3.07	5
1824034	-43.19	172.06	2	12	2001	3.03	5
1825773	-43.13	172.04	9	12	2001	2.53	33
1830583	-43.07	171.83	2	1	2002	2.32	17.31
1835233	-42.93	171.84	18	1	2002	3.08	12
1835584	-42.93	171.86	20	1	2002	3.08	12
1837734	-42.83	171.80	24	1	2002	2.33	5
1844091	-42.84	171.84	8	2	2002	2.74	12
1844620	-42.91	171.85	12	2	2002	2.1	5
1846943	-42.93	171.93	17	2	2002	2.74	5
1853774	-42.93	171.97	15	3	2002	2.6	12
1855083	-42.98	171.87	20	3	2002	3.42	12
1879843	-43.15	171.81	21	5	2002	2.22	12
1883254	-43.14	172.02	29	5	2002	2.59	12
1883588	-43.02	172.24	30	5	2002	2.77	12
1885093	-42.93	171.98	4	6	2002	2.97	12
1888275	-42.95	171.95	13	6	2002	3.03	12
1896522	-42.96	171.80	8	7	2002	2.43	12
1896532	-42.96	171.77	8	7	2002	2.46	5
1896555	-43.19	172.06	9	7	2002	2.51	12
1896679	-42.95	171.90	9	7	2002	2.44	12
2024840	-43.15	172.13	21	7	2002	2.6	27.48
1902733	-42.97	171.90	27	7	2002	2.96	5
2031454	-42.92	171.82	14	8	2002	2.8	12
1917597	-43.15	172.22	3	9	2002	2.72	33
1926611	-43.01	171.92	20	9	2002	2.98	5
1983737	-42.93	171.95	19	10	2002	2.12	5
1988397	-42.97	171.81	31	10	2002	2.94	5
1992433	-42.89	171.84	9	11	2002	3.02	5
2006470	-42.83	171.82	17	12	2002	2.21	12
2025932	-43.04	171.87	16	2	2003	2.36	12
2026372	-42.95	171.93	17	2	2003	2.27	5
2030239	-42.95	171.90	25	2	2003	2.65	12
2031439	-43.17	172.16	26	2	2003	2.73	12
2102220	-42.94	171.86	29	4	2003	2.62	12
2058848	-43.05	171.83	3	5	2003	2.53	12
2063105	-43.21	171.87	14	5	2003	2.38	12
2084241	-42.89	171.78	7	7	2003	2.53	33
2084566	-43.18	172.16	8	7	2003	2.93	12
2084630	-43.17	172.08	8	7	2003	2.44	29.11
2089962	-43.18	171.88	20	7	2003	2.98	32.19
2090578	-42.89	171.81	22	7	2003	2.5	12
2091063	-42.99	171.87	23	7	2003	2.6	5
2094171	-42.94	171.98	31	7	2003	2.87	5
2094813	-42.94	171.96	1	8	2003	2.61	5
2096174	-43.00	171.88	4	8	2003	2.26	5
2107552	-43.00	171.87	29	8	2003	2.94	12
2122904	-42.95	171.89	29	9	2003	2.55	12
2123971	-43.00	171.79	2	10	2003	2.4	5

ID	Latitude	Longitude	Day	Month	Year	Magnitude	Depth
2152500	-42.89	171.76	29	11	2003	3.06	5
2153324	-42.97	171.86	2	12	2003	2.15	12
2153488	-42.91	171.92	2	12	2003	2.22	12
2161136	-42.98	171.84	22	12	2003	2.19	5
2161543	-42.93	171.96	23	12	2003	2.4	7.48
2179877	-42.95	171.93	1	2	2004	3.25	12
2179879	-42.93	171.92	1	2	2004	2.22	12
2185858	-42.92	172.23	15	2	2004	2.36	28.57
2194083	-43.22	172.12	3	3	2004	2.79	28.8
2202598	-42.93	171.92	21	3	2004	2.55	5
2203504	-42.94	171.88	23	3	2004	2.64	5
2217018	-42.98	172.22	20	4	2004	2.13	9.97
2218677	-42.94	171.88	23	4	2004	2	5
2218770	-42.93	171.84	23	4	2004	1.96	5
2225550	-43.18	172.20	5	5	2004	2.36	33
2225573	-42.80	171.99	5	5	2004	2.36	12
2230727	-42.90	171.85	15	5	2004	2.15	5
2236102	-42.96	171.88	24	5	2004	2.02	33
2258243	-42.91	171.82	4	7	2004	2.9	5
2265416	-43.17	172.17	16	7	2004	2.64	5
2272353	-42.96	171.95	30	7	2004	2.23	5
2277314	-43.18	172.07	8	8	2004	2.56	5
2281707	-42.96	171.89	17	8	2004	2.36	12
2281968	-43.13	172.01	17	8	2004	2.58	5
2305255	-42.97	171.83	9	10	2004	2.14	5
2315087	-43.07	172.04	31	10	2004	3.05	5
2323429	-42.94	171.83	17	11	2004	2.2	5
2341105	-42.96	171.89	20	12	2004	2.13	5
2345994	-42.95	171.89	1	1	2005	2.88	5
2346036	-42.95	171.89	1	1	2005	2.5	5
2346816	-42.95	171.95	3	1	2005	2.55	12
2351456	-42.99	171.84	14	1	2005	2.18	12
2351892	-42.80	171.92	15	1	2005	2.6	5
2576340	-42.93	171.82	5	2	2005	2.07	5
2365912	-43.18	172.05	16	2	2005	3.86	10.68
2367010	-42.92	171.89	19	2	2005	2.04	5
2370956	-43.13	172.04	28	2	2005	2.37	32.11
2371819	-42.91	171.94	2	3	2005	2.25	5
2372302	-42.92	172.05	3	3	2005	2.09	12
2375513	-42.95	171.96	11	3	2005	3.2	5
2385546	-42.91	171.92	3	4	2005	2.87	5
2389361	-42.92	171.93	12	4	2005	2.29	5
2390873	-42.98	172.20	15	4	2005	2.16	5
2392220	-43.16	172.23	18	4	2005	2.44	9.63
2414949	-42.95	171.93	7	6	2005	2.46	5
2421841	-42.96	171.91	23	6	2005	2.3	5
2424244	-43.22	172.09	28	6	2005	3.12	12
2430981	-42.89	171.79	11	7	2005	2.11	5
2438402	-43.13	172.20	27	7	2005	2.55	12
2448069	-43.05	171.74	18	8	2005	3.33	5
2452410	-43.19	172.15	28	8	2005	2.26	33
2453727	-42.94	171.91	31	8	2005	2.2	5
2464953	-43.13	172.20	26	9	2005	2.09	12
2465684	-42.95	171.84	28	9	2005	2.3	5
2465781	-43.17	172.09	28	9	2005	2.82	12
2465992	-42.93	171.84	29	9	2005	2.57	12
2470023	-43.00	171.88	7	10	2005	2.94	5
2476559	-42.96	171.92	22	10	2005	2.8	12
2479808	-43.13	172.02	30	10	2005	2.5	12
2486081	-43.18	172.05	13	11	2005	2.69	12

ID	Latitude	Longitude	Day	Month	Year	Magnitude	Depth
2490979	-42.93	171.96	24	11	2005	2.4	5
2491152	-43.18	172.05	24	11	2005	2.69	12
2498896	-42.96	171.92	12	12	2005	2.47	5
2498926	-42.91	171.83	12	12	2005	2.79	5
2504945	-42.87	171.78	26	12	2005	2.22	5
2515444	-43.20	172.20	19	1	2006	2.62	12
2519359	-42.99	171.79	28	1	2006	3.84	5
2530304	-42.95	171.94	24	2	2006	2.19	5
2530743	-43.20	172.12	25	2	2006	2.35	12
2532897	-42.80	171.86	2	3	2006	2.15	5
2532900	-42.90	171.85	2	3	2006	1.98	5
2556538	-42.91	171.84	20	4	2006	3.29	5
2564371	-43.14	172.12	6	5	2006	2.27	33
2568376	-42.99	171.87	15	5	2006	2.54	5
2573100	-42.95	171.89	26	5	2006	3.41	5
2811965	-43.17	172.17	28	5	2006	2.66	5
2575800	-42.95	171.97	31	5	2006	2.86	5
2576269	-42.94	171.92	2	6	2006	2.29	5
2582386	-42.91	171.83	14	6	2006	2.44	5
2583517	-42.90	171.84	16	6	2006	2.08	5
2591207	-42.94	171.83	3	7	2006	2.58	5
2601060	-42.95	171.93	25	7	2006	3.32	5
2604347	-42.99	171.94	1	8	2006	2.06	5
2611280	-42.95	171.93	15	8	2006	2.01	5
2625955	-42.92	171.83	17	9	2006	2.55	5
2631633	-42.81	171.90	29	9	2006	1.97	12
2634607	-42.92	172.01	5	10	2006	2.16	12
2648582	-42.92	171.82	4	11	2006	2.49	5
2655520	-42.99	172.10	18	11	2006	4.22	5
2666841	-42.80	171.90	12	12	2006	2.43	5
2671309	-42.91	171.95	20	12	2006	2.3	12
2673583	-43.01	172.07	25	12	2006	2.14	5
2679176	-43.00	171.88	6	1	2007	2.41	5
2680808	-42.84	171.81	10	1	2007	1.87	5
2683401	-42.99	171.88	16	1	2007	3	5
2684839	-42.97	171.78	19	1	2007	2.12	12
2686315	-42.92	171.83	22	1	2007	2.89	5
2692842	-42.93	171.86	6	2	2007	3.31	5
2696604	-42.93	171.93	14	2	2007	2.97	5
2720407	-42.94	171.85	5	4	2007	2.17	5
2723537	-43.10	172.07	10	4	2007	2.93	12
2726626	-42.98	171.91	18	4	2007	1.97	5
2727788	-42.92	171.90	20	4	2007	2.07	5
2747593	-42.91	171.83	3	6	2007	2.38	5
3168546	-42.99	171.86	16	6	2007	2.06	5
2773651	-43.22	172.04	31	7	2007	3.42	5
2775719	-42.99	171.87	5	8	2007	2.57	5
3553636	-43.07	171.85	21	9	2007	2.63	5
2820754	-42.93	171.86	12	11	2007	2.36	5
2831273	-42.92	171.99	4	12	2007	3.02	6.75
2845659	-43.14	172.00	3	1	2008	2.24	5
2885752	-43.13	171.77	27	3	2008	3.19	0
2888987	-43.13	171.78	3	4	2008	3.63	5
2888996	-43.16	171.75	3	4	2008	2.24	5
2889009	-43.15	171.74	3	4	2008	2.55	5
2893829	-43.05	171.77	13	4	2008	1.91	33
2893868	-43.02	172.06	13	4	2008	1.86	12
2898422	-43.17	172.05	22	4	2008	2.13	12
2898892	-43.14	171.75	24	4	2008	2.19	12
2899573	-43.14	171.77	25	4	2008	2.62	5

ID	Latitude	Longitude	Day	Month	Year	Magnitude	Depth
2947720	-42.91	171.81	2	8	2008	2.71	5
2955632	-42.94	171.98	19	8	2008	3.06	5
3003189	-42.83	171.81	21	11	2008	2.35	5
3015037	-43.22	172.11	7	12	2008	2.6	12
3054325	-43.21	172.16	4	3	2009	4.09	5
3054326	-43.21	172.17	4	3	2009	3.33	5
3060111	-42.98	171.87	15	3	2009	2.14	5
3062772	-43.02	172.06	21	3	2009	2.68	5
3069947	-42.84	171.80	3	4	2009	2.29	5
3100573	-42.88	171.83	31	5	2009	2.46	5
3113694	-42.89	171.83	24	6	2009	2.33	5
3120431	-42.94	171.88	6	7	2009	2.11	5
3124060	-43.00	171.87	13	7	2009	3.51	5
3132937	-43.06	172.22	1	8	2009	2.03	12
3140246	-42.91	171.83	2	8	2009	1.98	5
3145922	-42.89	171.85	29	8	2009	2.77	5
3153282	-43.18	172.06	13	9	2009	3.25	12
3158426	-43.19	171.99	16	9	2009	2.26	12
3159720	-43.18	172.04	18	9	2009	2.09	9.96
3158471	-43.18	172.06	24	9	2009	3.43	9.28
3171521	-43.19	171.99	20	10	2009	2.28	12
3173948	-42.93	171.91	25	10	2009	2.1	5
3176331	-43.10	172.10	30	10	2009	2.11	5
3177164	-43.20	172.23	1	11	2009	2.06	29.39
3186317	-43.18	172.06	19	11	2009	2.1	9.11
3202889	-43.09	172.21	2	12	2009	1.97	5
3216922	-43.19	172.13	18	12	2009	1.92	5
3214793	-43.16	172.01	27	12	2009	2.18	12
3249166	-43.17	172.06	29	1	2010	2.21	5
3268223	-42.95	171.96	28	2	2010	2.62	12
3271255	-42.94	171.98	6	3	2010	2.53	5
3275912	-42.93	171.82	16	3	2010	2.56	3
3280067	-42.92	171.92	24	3	2010	1.67	8.63
3280191	-42.94	171.93	24	3	2010	1.98	3
3284030	-42.94	172.00	1	4	2010	2.33	5
3287777	-43.22	172.23	8	4	2010	2.19	5
3318565	-43.20	171.97	5	6	2010	2.33	11.19
3320118	-42.94	171.87	8	6	2010	2.14	6.3
3328246	-43.18	171.98	23	6	2010	2.51	2
3336807	-43.07	171.80	9	7	2010	2.52	5
3343701	-42.94	171.89	12	7	2010	1.65	5
3345930	-42.94	171.93	18	7	2010	1.71	5
3345466	-42.92	171.81	26	7	2010	1.78	5
3346843	-42.90	172.06	28	7	2010	2.91	5
3348491	-43.18	172.03	31	7	2010	2.64	9.67
3356067	-43.07	171.82	2	8	2010	2.88	5
3349729	-43.21	172.08	3	8	2010	2.74	9.72
3350404	-43.06	171.81	4	8	2010	2.11	5
3351476	-42.87	171.84	6	8	2010	2.07	5
3352720	-42.94	171.90	8	8	2010	2.66	5
3358599	-42.83	171.81	20	8	2010	3.71	5
3358575	-42.83	171.80	20	8	2010	2.25	5
3358578	-42.84	171.82	20	8	2010	2.33	12
3358959	-42.88	171.95	21	8	2010	2.67	12
3362156	-43.21	171.99	27	8	2010	3.26	5
3362167	-43.21	172.02	27	8	2010	2.67	5
3362380	-43.20	171.99	27	8	2010	2.67	7.53
3371451	-43.22	172.08	13	9	2010	2.99	9.07
3371867	-43.20	172.08	14	9	2010	3.17	10.32
3375067	-43.01	172.09	19	9	2010	4.1	5

ID	Latitude	Longitude	Day	Month	Year	Magnitude	Depth
3375072	-43.01	172.08	20	9	2010	2.59	5
3376440	-43.22	172.02	22	9	2010	2.8	6.99
3377634	-43.17	172.11	24	9	2010	3.57	5
3377655	-43.17	172.12	24	9	2010	3.36	5
3377713	-43.18	172.11	24	9	2010	2.88	5
3377903	-43.17	172.11	24	9	2010	2.5	5
3379823	-43.17	172.12	28	9	2010	2.91	5
3380030	-43.17	172.11	29	9	2010	2.71	5
3380345	-43.17	172.02	29	9	2010	2.8	11.21
3388737	-43.21	172.21	2	10	2010	2.57	5
3382124	-43.18	172.10	3	10	2010	2.99	5
3383704	-43.22	171.96	6	10	2010	2.24	5
3383717	-43.17	172.04	6	10	2010	2.29	5
3384384	-43.19	172.06	7	10	2010	2.19	5
3388485	-43.17	172.04	13	10	2010	3.7	5
3388797	-43.22	172.10	14	10	2010	3.35	6.83
3389045	-43.16	172.07	14	10	2010	2.48	5
3389506	-43.17	172.03	15	10	2010	2.87	5
3389523	-43.21	172.14	15	10	2010	2.86	5
3394012	-43.20	172.19	22	10	2010	2.38	5
3394034	-43.19	172.10	22	10	2010	2.75	5
3394035	-43.18	172.09	22	10	2010	2.68	5
3394126	-43.21	172.10	23	10	2010	3.09	5
3394382	-43.17	172.07	23	10	2010	2.46	5
3395024	-43.20	172.13	25	10	2010	3.38	5
3395815	-43.16	172.04	26	10	2010	2.66	6.38
3396054	-43.16	172.07	27	10	2010	2.4	5
3400435	-42.90	171.84	31	10	2010	3.71	5
3401298	-43.21	172.25	2	11	2010	2.37	12
3403219	-43.21	172.06	6	11	2010	4.6	8.72
3403230	-43.22	172.08	6	11	2010	2.01	5
3403256	-43.22	172.09	6	11	2010	3.54	5
3403264	-43.22	172.10	6	11	2010	2.45	5
3403382	-43.22	172.10	6	11	2010	2.64	5
3403941	-43.22	172.08	8	11	2010	2.38	5
3405904	-43.20	172.11	11	11	2010	3.76	7.51
3406520	-43.21	172.21	13	11	2010	2.43	5
3406605	-43.19	171.89	13	11	2010	3.16	12
3407140	-43.22	172.10	14	11	2010	4.05	7.62
3407710	-43.22	172.05	15	11	2010	3.36	7.28
3435310	-43.22	172.04	15	11	2010	3.04	7.86
3408589	-43.21	172.20	17	11	2010	2.72	5
3408821	-43.21	172.12	17	11	2010	2.59	5.79
3414100	-43.22	172.04	28	11	2010	2.32	5
3421817	-43.22	172.09	1	12	2010	2.9	5
3416006	-42.89	171.83	2	12	2010	2.42	5
3416928	-43.22	172.10	4	12	2010	3.36	8.98
3440546	-43.09	172.18	2	1	2011	2.85	12
3446049	-43.22	172.09	11	1	2011	2.48	5
3453410	-43.15	171.86	21	1	2011	2.45	12
3454087	-43.19	172.06	23	1	2011	2.38	5
3458090	-43.18	172.08	31	1	2011	2.47	5
3459803	-43.16	172.02	3	2	2011	4.45	8.45
3459804	-43.19	172.03	3	2	2011	3.43	10.07
3459810	-43.18	172.00	3	2	2011	2.85	8.95
3459812	-43.19	172.00	3	2	2011	2.48	12
3459872	-43.18	172.02	3	2	2011	2.79	10.66
3460334	-43.18	172.02	4	2	2011	3.21	9.33
3460335	-43.17	172.03	4	2	2011	2.99	8.65
3461525	-43.19	172.02	7	2	2011	2.62	12

ID	Latitude	Longitude	Day	Month	Year	Magnitude	Depth
3463096	-43.16	171.95	10	2	2011	2.21	5
3463124	-43.16	171.95	10	2	2011	2.38	5
3463472	-43.02	172.08	11	2	2011	2.53	5
3464455	-43.17	171.97	13	2	2011	2.81	5
3467001	-43.08	172.14	18	2	2011	2.48	5
3468010	-43.19	172.01	20	2	2011	2.78	10.18
3470570	-43.18	172.01	25	2	2011	3.14	9.26
3472328	-42.82	171.92	1	3	2011	2.35	5
3473915	-43.21	172.06	4	3	2011	2.57	5
3474836	-43.20	172.08	6	3	2011	3.41	5
3478208	-42.87	171.86	13	3	2011	2.51	5
3481433	-43.19	172.02	20	3	2011	2.77	8.14
3482215	-43.18	172.02	21	3	2011	2.37	9.65
3485826	-43.22	172.12	26	3	2011	2.43	5
3486092	-43.08	172.06	26	3	2011	2.12	5
3489399	-43.20	172.00	30	3	2011	2.57	5
3492537	-43.18	172.01	6	4	2011	2.7	9.66
3493607	-43.22	172.06	7	4	2011	2.25	7.91
3496096	-43.17	172.02	12	4	2011	2.8	12.68
3496315	-43.21	172.00	13	4	2011	2.58	10.36
3496544	-43.21	172.10	13	4	2011	3.63	8.22
3496695	-43.21	172.08	14	4	2011	2.99	5
3496724	-43.21	172.09	14	4	2011	2.6	7.09
3499257	-43.22	172.11	18	4	2011	2.04	5
3499916	-43.21	172.07	20	4	2011	3.02	7.11
3499934	-43.17	172.06	20	4	2011	2.47	9.03
3499964	-43.21	172.09	20	4	2011	3.05	7
3502786	-43.21	172.06	25	4	2011	2.83	8.88
3504411	-42.86	171.92	29	4	2011	2.61	28.74
3505099	-43.18	171.99	29	4	2011	5.22	10.72
3542406	-43.18	171.98	29	4	2011	2.69	9.32
3544184	-43.19	172.00	29	4	2011	2.79	8.92
3505111	-43.19	171.98	29	4	2011	2.23	10.15
3544189	-43.18	172.00	29	4	2011	2.26	9.73
3544193	-43.19	171.99	29	4	2011	2.47	10.12
3505114	-43.19	172.02	29	4	2011	2.51	8.06
3505115	-43.17	171.99	29	4	2011	2.32	5
3505116	-43.18	172.01	29	4	2011	2.6	8.96
3544202	-43.19	172.01	29	4	2011	2.68	8.43
3544206	-43.18	172.00	29	4	2011	2.93	8.38
3544208	-43.19	171.99	29	4	2011	2.68	10.07
3505126	-43.18	171.99	29	4	2011	2.71	5
3544219	-43.18	172.01	29	4	2011	2.51	8.53
3544225	-43.18	172.00	29	4	2011	2.95	8.62
3505142	-43.18	172.01	29	4	2011	2.16	8.62
3505144	-43.18	172.01	29	4	2011	2.17	8.17
3546450	-43.18	172.01	29	4	2011	2.17	8.88
3505156	-43.18	172.02	29	4	2011	2.06	8.64
3546460	-43.19	172.02	29	4	2011	1.83	8.94
3505199	-43.16	171.97	30	4	2011	2.56	5
3505214	-43.18	172.01	30	4	2011	2.12	9.25
3505226	-43.18	172.00	30	4	2011	2.3	9.59
3505274	-43.19	171.98	30	4	2011	2.42	9.91
3505275	-43.18	172.02	30	4	2011	2.47	8.69
3505277	-43.19	172.01	30	4	2011	2.51	8.89
3505308	-43.18	172.00	30	4	2011	2.25	9.06
3505309	-43.18	172.01	30	4	2011	2.37	8.48
3542391	-43.18	171.99	30	4	2011	2.46	5
3505341	-43.18	172.01	30	4	2011	1.95	9.45
3505347	-43.19	171.98	30	4	2011	2.43	9.74

ID	Latitude	Longitude	Day	Month	Year	Magnitude	Depth
3505408	-43.19	172.00	30	4	2011	1.91	9.45
3505453	-43.19	172.00	30	4	2011	2.44	8.91
3548903	-43.18	172.00	30	4	2011	3.13	5
3548907	-43.18	172.00	30	4	2011	2.93	5
3505462	-43.19	171.97	30	4	2011	2.03	9.99
3505473	-43.19	171.91	30	4	2011	1.91	10.61
3505474	-43.19	172.06	30	4	2011	2.49	5
3548926	-43.21	171.97	30	4	2011	2.46	11.49
3505492	-43.16	172.03	30	4	2011	2.15	5
3505495	-43.18	172.01	30	4	2011	2.39	9.71
3505503	-43.18	172.02	30	4	2011	2.45	9.19
3505505	-43.18	172.02	30	4	2011	2.21	12
3505549	-43.19	171.99	30	4	2011	1.89	9.6
3505609	-43.18	172.08	30	4	2011	1.85	5
3549371	-43.19	171.94	30	4	2011	2.21	10.24
3549385	-43.18	171.99	30	4	2011	2.13	8.72
3553808	-43.19	171.96	1	5	2011	2.06	10.27
3553825	-43.18	171.98	1	5	2011	2.86	5
3506146	-43.18	172.01	1	5	2011	2.45	5
3506474	-43.18	172.00	2	5	2011	2.53	8.49
3506483	-43.18	171.99	2	5	2011	2.26	5
3506617	-43.19	172.00	2	5	2011	2.36	9.54
3506628	-43.17	171.99	3	5	2011	2.68	5
3506927	-43.19	171.97	3	5	2011	2.34	10.43
3506971	-43.18	172.00	3	5	2011	2.92	5
3507213	-43.20	171.94	4	5	2011	2.21	12
3507307	-43.16	172.03	4	5	2011	3.25	5
3507311	-43.20	172.01	4	5	2011	3.14	9.13
3507358	-43.18	171.99	4	5	2011	2.54	9.03
3507702	-43.18	172.01	5	5	2011	2.32	8.54
3555748	-43.18	172.01	5	5	2011	2.56	9.31
3555771	-43.19	171.99	5	5	2011	2.33	10.09
3508615	-43.19	172.01	7	5	2011	2.75	8.47
3509156	-43.19	172.00	8	5	2011	3	5
3510042	-43.20	171.98	9	5	2011	2.58	12
3510142	-43.18	172.00	10	5	2011	2.64	10.03
3510308	-42.90	171.79	10	5	2011	2.5	5
3559970	-43.18	171.99	11	5	2011	2.74	9.49
3559574	-43.19	172.00	12	5	2011	2.38	9.29
3511425	-43.21	172.09	12	5	2011	2.78	5
3511890	-43.19	172.00	13	5	2011	2.47	9.25
3512735	-43.19	172.01	14	5	2011	2.46	8.6
3512985	-43.18	172.00	15	5	2011	2.84	5
3516371	-43.20	171.99	20	5	2011	2.37	9.32
3517129	-43.18	172.01	22	5	2011	2.51	8.53
3517813	-43.19	172.00	23	5	2011	2.22	9.65
3518642	-43.20	172.12	25	5	2011	1.83	5
3518932	-43.21	172.10	25	5	2011	3.23	5
3518982	-43.19	171.99	25	5	2011	3.12	9.12
3518995	-43.20	172.10	25	5	2011	2.53	5
3519202	-43.18	172.01	26	5	2011	2.58	8.67
3519383	-43.19	172.00	26	5	2011	3.01	12
3519535	-43.18	171.96	26	5	2011	2.65	10.44
3520025	-43.18	172.02	27	5	2011	2.35	8.94
3520637	-43.19	172.10	28	5	2011	2.68	9.24
3522187	-43.18	172.01	31	5	2011	2.53	9.16
3552277	-43.18	171.99	31	5	2011	2.23	9.35
3522331	-43.18	171.99	31	5	2011	2.1	9.63
3522573	-43.19	172.03	31	5	2011	1.99	8.74
3523885	-43.22	172.01	3	6	2011	3.07	5

ID	Latitude	Longitude	Day	Month	Year	Magnitude	Depth
3524103	-43.22	172.08	3	6	2011	2.86	5
3526507	-43.02	172.08	8	6	2011	2.95	5
3527476	-43.22	172.08	10	6	2011	3.43	7.41
3528243	-43.18	172.02	11	6	2011	2.56	9.6
3530464	-43.21	172.10	16	6	2011	2.75	10
3535332	-43.01	171.75	24	6	2011	2.48	5
3535862	-42.96	171.92	25	6	2011	2.51	2.22
3540538	-43.00	171.76	4	7	2011	3.91	5
3540553	-43.02	171.75	4	7	2011	2.61	5
3540653	-43.01	171.76	5	7	2011	2.76	5
3540922	-43.01	171.77	5	7	2011	3	5
3541483	-43.17	172.05	6	7	2011	3.08	9.55
3541921	-43.21	172.21	7	7	2011	4.41	11.72
3542473	-43.18	172.00	8	7	2011	3.02	7.64
3543442	-43.20	172.01	9	7	2011	3.18	7.6
3544468	-43.13	172.02	11	7	2011	2.86	6.9
3546286	-43.01	171.75	14	7	2011	3.19	5
3546715	-43.18	172.02	15	7	2011	2.27	7.03
3546813	-43.17	172.07	15	7	2011	2.5	5.18
3550640	-43.18	172.01	22	7	2011	1.99	5
3559270	-43.19	172.02	8	8	2011	2.31	8.83
3569578	-43.17	172.02	28	8	2011	3.59	7.94
3571597	-43.18	172.02	31	8	2011	2.41	8.99
3572955	-43.20	172.05	3	9	2011	2.51	9.12
3575125	-43.19	172.01	7	9	2011	1.86	12

Table C.1.: Earthquakes from 1965 to 2011. Extract from the New Zealand earthquake catalogue for the area defined in Fig. 3.3 (GNS, GeoNet).